

University of South Wales



2059383

Bound by **Abbey**  
**Bookbinding Co.,**  
Cardiff, South Wales  
Tel: (01 222) 395882



**NAILFOLD CAPILLARY LOOP SHAPE  
ANALYSIS AND CLASSIFICATION BY  
USING IMAGE PROCESSING AND PATTERN  
RECOGNITION TECHNIQUES**



**MUSTAFA ORAL**

**A thesis submitted in partial fulfillment of the requirements of the University of Glamorgan/Prifysgol Morgannwg for the degree of Doctor of Philosophy**

**February 1998**

## **ABSTRACT**

Nailfold capillaroscopy is a useful tool to diagnose endocrine, cardiovascular, neuropsychiatric, rheumatic and other diseases. Diagnoses are made on the presence or absence of certain types of capillary loops which are classified according to their shape. We have surveyed six clinicians, asking them to classify 217 capillary loops, in order to establish quantitative nailfold capillary loop classification criteria. The participating clinicians were not unanimous about the classification of any capillary, and there was no consensus about the class of 17% of the capillary loops. Some of the clinicians classified two occurrences of the same shape differently. This clearly demonstrates the need for well established classification criteria.

Nailfold capillary loop classes can be divided into two major groups: Descriptive Classes (DC); "cuticulis", "open", "tortuous", "crossed", "bizarre" and "bushy", and Label Classes; "enlarged", "elongated" and "giant". Furthermore label classes can be divided into two groups, Width Anomaly Classes (WAC); "enlarged" and "giant", and Length Anomaly Class (LAC), "elongated". While descriptive classes give information about the shape of a loop, label classes emphasise dimensional anomalies of a loop. Assignment of a loop with one the descriptive or label classes causes information loss about the dimensions or shape, respectively. In order to preserve as much information as possible within a class, we propose a new class system that contains 17 classes which are the combination of WAC, LAC and DC.


We propose quantitative classification criteria for commonly used classes: "cuticulis", "open", "tortuous", "elongated" and "giant". Although the class "enlarged" can be expressed quantitatively, inappropriate assignments of "enlarged" by the participating clinicians have not allowed us to set quantitative classification criteria. While definition of the class "crossed" is purely qualitative, a classification mechanism that is neither qualitative nor quantitative is proposed for "bizarre" and "bushy" loops.

We propose the use of pattern recognition algorithms that are based on the evaluation of the capillary shape parameters such as loop length, loop width, limb width, the curvature, orientation, etc., to classify capillaries. By the use of mathematical morphology, skeletonization, topological relations, feature vectors, in an hierarchical structure, the software TANCCAS (The Automated Nailfold Capillary Classification and Analysis System) has been developed to calculate the shape parameters and to classify the capillary loops. These algorithms have been implemented on a Pentium PC and have resulted in an 88% accuracy level which is compared to participating clinicians' overall classifications of the test images.

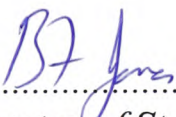
## ***Certificate of Research***

*This is to certify that, except where specific reference is made, the work described in this thesis is the result of the candidate. Neither this thesis, nor any part of it, has been presented, or is currently submitted, in candidature for any degree at any other University.*

***Signed***

  
.....  
*Candidate*

***Signed***

  
.....  
*Director of Studies*

***Date***

*26th February, 1998.*

## **TABLE OF CONTENTS**

### **ABSTRACT**

Acknowledgements	I
List of Figures	II
List of Tables	VIII
List of Terms	X

### **CHAPTER 1 INTRODUCTION**

1.1 The Problem and Problem Approach	1-1
1.2 The Aims and Objectives	1-4
1.3 Contribution to Existing Knowledge	1-5
1.4 Main Findings of the Research	1-6
1.5 The Structure of the Thesis	1-7

### **CHAPTER 2 NAILFOLD CAPILLARY MICROSCOPY**

2.1 Introduction	2-1
2.2 Capillary Microscopy	2-1
2.2.1 Introduction to Capillaroscopy	2-1
2.2.2 The Developments of Capillary Microscopy	2-2
2.2.3 Classical Capillaroscopy Techniques	2-4
2.3 Nailfold Capillaroscopy	2-5
2.3.1 The Structure of a Healthy Nailfold Capillary Loop	2-5
2.3.2 Diagnostic Importance of Nailfold Capillaroscopy	2-6
2.3.3 Nailfold Capillary Morphology Alterations	2-8
2.3.4 Nailfold Capillary Morphology Pattern Classification, A Literature Review	2-9
2.3.5 Quantitative Nailfold Capillary Microscopy	2-14

## **CHAPTER 3 PROPOSING THE CAPILLARY LOOP PATTERN CLASSIFICATION CRITERIA**

3.1	Introduction	3-1
3.2	A Discussion on The Nailfold Capillary Loop Patterns Described By Previous Researchers	3-1
3.3	An Experimental Study: The Classifications of the Test Images By Practitioners	3-3
3.4	The Classification Criteria	3-6
3.4.1	Classification Criteria of CuticulisType	3-8
3.4.2	Classification Criteria of Open and Tortuous Type	3-11
3.4.3	Classification Criteria of Crossed Pattern	3-17
3.4.4	Classification Criteria of Bushy and Bizarre Patterns	3-18
3.4.5	Classification Criteria of Enlarged Loops	3-21
3.4.6	Classification Criteria of Giant Loops	3-22
3.4.7	Classification Criteria of Elongated Loops	3-24

## **CHAPTER 4 IMAGE PROCESSING LIBRARY OF TANCCAS**

4.1	Automation Strategy of The Classification Criteria	4-1
4.1.1	Atypical Loops	4-2
4.1.2	Crossed Loops	4-3
4.1.3	Open and Tortuous Loops	4-3
4.1.4	Cuticulis Loops	4-4
4.2	Introduction to Image Processing Library of TANCCAS	4-5
4.2.1	Thresholding	4-7
4.2.2	Mathematical Morphology Operations	4-7
4.2.2.1	Boundary Extraction	4-8
4.2.2.2	Skeletonization	4-9
4.2.2.3	Pruning	4-14

4.2.3	Labelling	4-16
4.2.4	Polygonal Approximation	4-19
4.2.5	Scalar Descriptors	4-19
4.2.5.1	Area	4-19
4.2.5.2	Length	4-19
4.2.5.3	Width	4-20
4.2.5.4	Orientation	4-21
4.2.5.5	Compactness	4-21
4.2.5.6	Circular Arc Approximation	4-22

## **CHAPTER 5 THE AUTOMATED CLASSIFICATION AND ANALYSIS OF NAILFOLD CAPILLARIES**

5.1	Structure of The Automated Nailfold Capillary Classification and Analysis System (TANCCAS)	5-1
5.2	Development Methodology	5-2
5.3	Data Acquisition	5-4
5.4	Implementation of The Classification Criteria	5-5
5.4.1	Pre-processing Module Part I (PPM-I)	5-8
5.4.1.1	The Chain Regulator	5-12
5.4.1.2	The Capillary Loop Cropper	5-17
5.4.2	Pre-Processing Module Part-II (PPM-II)	5-18
5.4.2.1	Transformer Unit (TU)	5-23
5.4.2.2	Auxiliary Classification Unit (ACU)	5-25
5.4.3	Main Classification Module (MCM)	5-35
5.4.3.1	Open-Tortuous Classification Unit (OTCU)	5-36
5.4.3.2	Tortuosity Analyzer	5-39
5.4.3.3	Bizarre-Bushy Clasification Unit (BBCU)	5-40
5.4.4	Class Decision Unit	5-42



## **CHAPTER 6 SELECTION OF THE CRITICAL VALUES**

6.1	Introduction	6-1
6.2	Selection of Exclusive-Curvature Angle	6-1
6.2.1	Preparation of Data Sets	6-1
6.2.1.1	Arrangements of Sub-Data Sets	6-2
6.2.2	The Critical Values Selection Methods	6-5
6.2.2.1	Calculation of $OPTIMAL_{\theta}$	6-5
6.2.2.2	Fat Pencil Method	6-11
6.2.2.3	Calculation of Suggested $\theta_{CUTICULIS\ ND_{\theta}}$ from Normal Distribution Functions	6-12
6.3	Selection of Critical Segmental Curvature Angles $\beta_{OPEN}$ and $\beta_{TORTUOUS}$	6-15
6.4	Selection of Critical Length $Length_{ELONGATED}$	6-21
6.4.1	Formal Detection of Elongated Capillary Loops in Overall Data Set	6-22
6.4.2	Informal Detection of Elongated Capillary Loops in Overall Data Set	6-23
6.5	Selection of Critical Limb Width $LimbWidth_{GIANT}$	6-27

## **CHAPTER 7 VALIDATION OF THE SYSTEM**

7.1	Introduction	7-1
7.2	The Analysis Criteria	7-1
7.3	Justification of Proposed Combinational Class Set	7-5
7.4	Classification Performance of TANCCAS	7-6
7.4.1	Class Identification Performance of TANCCAS	7-8
7.4.2	TANCCAS's Agreement With Individuals	7-9
7.4.3	Validation of Capillary Loop Analysis Capability of TANCCAS	7-9
7-5	Summary	

## **CHAPTER 8 GENERAL CONCLUSIONS AND RECOMMENDATIONS FOR FUTURE RESEARCH**

<b>8.1</b>	<b>The Strengths and The Weaknesses of the Proposed Classification System and TANCCAS</b>	<b>8-1</b>
<b>8.2</b>	<b>General Conclusions</b>	<b>8-5</b>
8.2.1	Proposing A New Class Set	8-5
8.2.2	Proposing The Classification Criteria	8-6
8.2.2.1	Descriptive Class Definitions	8-6
8.2.2.1.1	Non-Parametrical Classes Definition (Crossed, Bushy, Bizarre)	8-6
8.2.2.1.2	Parametrical Classes Definition (Cuticulis, Open, Tortuous)	8-7
8.2.2.2	Anomaly Classes Definitions (Enlarged Giant and Elongated)	8-8
<b>8.3</b>	<b>Recommendations For Future Research</b>	<b>8-9</b>

<b>REFERENCES</b>	<b>R</b>
-------------------	----------

### **APPENDICES**

Appendix A	The Nailfold Capillary Loop Test Images	AA
Appendix B	The Synthetic Capillary Loop Images	AB
Appendix C	The Classification Results of the Practitioners and TANCCAS for the Test Images	AC
Appendix D	The Tables that Display TANCCAS's Agreements with the Practitioners	AD

## **ACKNOWLEDGEMENTS**

I wish to thank the following people:

My supervisors, Prof. B.F. Jones Mr. C. Morris,

The collaborating institution, Royal National Hospital for Rheumatic Diseases, Bath, UK, and Prof. F. Ring,

The Mustafa Kemal University, Turkey (for providing the postgraduate education grant),

The technical and secretarial staff of the Computer Studies Department,

The Student Services staff Amanda Evans for guiding me to the light when I lost in total darkness,

Mary and Stephen Mason for being a mum and big brother through out my stay in this magical country, Wales.

Special thanks to Emel Laptali and Nilhan Alptekin for their friendship, support and patience to my endless tortures.

Finally I would like to dedicate this dissertation to my wife Dr. Emel Oral (Laptali) who gave me life and thought me love.

## LIST OF FIGURES

### Chapter 2

- Figure 2.1 Schematic diagrams of the skin(a) structure of skin capillaries  
(b) angle of capillary loops at different places on the finger. 2-6
- Figure 2.2. Ten basic morphological capillary loop patterns of Gibson et al.  
[56] 2-10
- Figure-2.3 The capillary morphology of the nailfold by Norris and  
Chowning[63] 2-11
- Figure 2.4 Different patterns of nailfold capillary loops by [Houtman et al. 86] 2-13

### Chapter 3

- Figure 3.1 (a) Some of the cuticulis type capillary loops in the test images  
(b) a collection of cuticulis loops mis-classified as open pattern (by  
the practitioners).(c) The cuticulis loop (i2:N2) is longer several  
than open type loops of the test images. 3-9
- Figure 3.2 A capillary loop and its morphological parameters. 3-10
- Figure 3.3 Demonstration of dividing the capillary limbs into their segments  
and calculating the segmental curvature angles  $\beta_{ij}$ . (indices i and j  
represents the limb and the segment number, respectively) for  
(Image 2 capillary no 35) 3-13
- Figure 3.4 A collection of open type capillary loops 3-15
- Figure 3.5 A collection of tortuous capillary loops 3-16
- Figure 3.6 Crossed capillary loops of the test images 3-18
- Figure 3.7 Atypical capillary structures in the test images 3-19
- Figure 3.8 Illustration of the classification mechanism of bushy and bizarre  
structures 3-20
- Figure 3.9 Giant capillary loops of the test images. 3-23

## Chapter 4

- Figure 4.1 The structural elements that used in Skeleton() function. X denotes “don’t care” condition 4-10
- Figure 4.2 (a) Thinning() operation on an artificial binary image by sequential logical and arithmetical operations. The function is insensitive to boundary corners and noise. 4-12
- (b) Skeleton() operation on the artificial binary image by using sequential mathematical morphology operation thinning (structural element  $B^8$  is given in figure 4.1). The function is sensitive to boundary corners and noise. 4-13
- Figure 4.3 Prunning by labelling (a) binary image to be pruned by 3 pixels (b) labelling of chains' end points (3+1 iteration) (c) Deletion of the pixels labelled 4 that has not got a neighbour that is labelled by 5, and restoration of pixels labelled 5 (in the next iteration deletion will be made on the pixels labelled 3 and restorations on the pixels labelled 4) (d) Prune() output of image (a) 4-16
- Figure 4.4 The stages of the labelling algorithm; (a) Original image (b) After raw labelling (c) Labeled image(d) Equality list 4-18
- Figure 4.5 Calculation of loop width by (a) 'slicing' method, (b) rectangular approximation 4-21
- Figure 4.6 Approximation of Cuticulis Capillaries to an Arc of Circle. 4-22
- Figure 4.7 An Arc With Central Angle  $\beta > \pi/2$  4-24
- Figure 4.8 (a) A capillary loop with  $\Delta l$  long limbs (b) Its circular approximation 4-25
- Figure 6.6 The plot of the function  $f(\theta, \Delta l/\text{base})$  4-26

## Chapter 5

- Figure 5.1 The structure of TANCCAS 5-2
- Figure 5.2 Development Methodology of the TANCCAS 5-3

Figure 5.3	The block diagram of the mechanism which takes images in the microvascular area.	5-4
Figure 5.4	(a) The original image of Image-1 of Appendix A (For better print quality, the original file is histogram equalized). (b) Histogram of the original image	5-6
Figure 5.5	The test file "collect.tif" and its histogram	5-8
Figure 5.6	The block diagram of Pre-Processing Module (Part I)	5-9
Figure 5.7	(a) The Output of Thresholding function. (b) The labelled image. (c) The final image after removing the small objects and the objects that touch the picture borders	5-11
Figure 5.8	(a) The output of skeletonization algorithm. (b)The input of Long Branch Remover (LBR). (c) Artificially created blob (The area of interest is magnified.)	5-11
Figure 5.9	The Block Diagram of Chain Regulator (CR)	5-13
Figure 5.10	(a) The output of Flood Fill algorithm, (b) Conversion to binary (c) Output of Logical NOT operation for 'b'. (d) The output of FCR Labelling. (The area of interest is magnified).	5-14
Figure 5.11	(a) The output of OR operation (b) The input of Long Branch Remover (LBR) for artificially defected image "collect.asc".	5-14
Figure 5.12	(a) The output of RS Labelling for the loop T11. (b) The area of interest (c) The vectors of the chain segments.	5-15
Figure 5.13	(a) The output of RS Labelling for the image "collect.asc", (Area of interest is magnified). (b) The output of Chain Regulator for the image "collect asc".	5-15
Figure 5.14	The block diagram of Capillary Loop Cropper	5-17
Figure 5.15	The processing steps of Capillary Loop Cropper (CRC). (a) The input image (from LBR's output). (b) The output of End Point Connector, (c) Flood Fill operation, (d) Inversion output (e) Object Labelling output (f) The output of Masking operation.	5-19
Figure 5.16	Pre-processing module part II (PPM-II)	5-21
Figure 5.17	The block diagram of Transformer Unit (TU)	5-22

Figure 5.18	(a) The input image to be transformed (b) The RS Labelled image (c) The output of end point connector (d) Flood Filled background (brown) and background controlled the most outer enclosed area filling (gray) (e) Thresholding output (f) Binary object edge detecting output (g) Object Labelling and (h) RS Labelling outputs.	5-23
Figure 5.19	Processing steps to find number of enclosed areas ( $N^{Enclosed}$ ) for the loop T14 (a) Output of Flood Fil (b)Output of FCR Labelling	5-25
Figure 5.20	A problematic capillary loop	5-26
Figure 5.21	The objects to be classified one of the classes; Circular, Rectangular and Triangular.	5-26
Figure 5.22	Typical examples of case (1,1), (a) "Normal" capillary loop (b) "Enlarged" capillary loop.	5-27
Figure 5.23	Analysis steps of the loop (i3:N21) (a) the loop (b) its skeleton (c) Orientation line (red) (d) detected loop tip points (circled) (e) disclosed chain loop.	5-28
Figure 5.24	(a) The GOP loop of "collect.asc", (b) Labelled and enclosed loop chains (c) Flood Filling of limbs surface (d) the output of ACU for the loop	5-29
Figure 5.25	(a) The BSH loop of "collect.asc" as input image of ACU (b) The output of AUC for the loop	5-30
Figure 5.26	The morphological variations of the capillary loops that have (2,2) control pair.	5-30
Figure 5.27	The analysis mechanism of CASE (2,2)	5-32
Figure 5.28	(a) Crossed capillary loop of "collect.asc" and its orientation line. (b) The skeleton of the area encircled by outer chain and the perpendicular line (yellow) (c) the skeleton part that passes through the inner chains area (red).	5-33
Figure 5.29	The possible inputs of CASE ( $N^{Chains}>2, N^{Enclosed}$ ) (The numbers in parenthesis are ( $N^{Chains}, N^{Enclosed}$ ) control pair for the loop)	5-33
Figure 5.30	The block diagram of Main Classification Module (MCM)	5-35
Figure 5.31	The block diagram of Open-Tortuous Classification Unit (OTCU)	5-37

<b>Figure 5.32</b>	The processing steps of MCM (a) The input image (The loop NET of "collect.asc", (b) Output of Enclose, (c) The loop's silhouette (d) Skeletal chain of the loop, (e) Polygonally approximated skeletal chain (f) Stretched skeletal chain tip segments (yellow lines) (g) The loop's side chains (h) Tortuosity analysis, (the detected concavities and convexities of chain 2, are flood filled for display purposes.) (i) Analysis result (given $\beta_{ij}$ angle value belongs to the concave/convex that has got the same base line colour)	5-38
<b>Figure 5.33</b>	Detection of concaves and convexes on a side chain.	5-39
<b>Figure 5.34</b>	The syntetic bushy (a) and bizarre (b) structures that had been used to test the efficiency of compactness as a delimiter of atypical structures and open/tortuous loops in early development stages of TANCCAS.	5-41
<b>Figure 5.35</b>	(a) The skeletal chain of (b) the capillary loop BSH of "collect.asc", (c) the silhouette of the loop's rough sketch, (d) the skeleton of the silhouette.	5-42
<b>Figure 5.36</b>	(a) The sub-image of the loop T17 as input to MCM (b) The loop 17's skeleton, (c) The rough sketch silhouette of the loop (d) The silhouette's skeleton (e) Detected and connected skeletal branch end points. (f) Output of Masking operation.	5-43
<b>Figure 5.37</b>	Class Decision Mechanism of CDU	5-45

## **Chapter 6**

<b>Figure 6.1</b>	Distribution of exclusive curvature angles ( $\theta$ ) (a) for cuticulis population and (b) for OP-TO population.	6-4
<b>Figure 6.2</b>	(a) Probability mass distribution of cuticulis population (b) cumulative frequency distribution of cuticulis population.	6-7
<b>Figure-6.3</b>	(a) Probability mass distribution of OP-TO population (b) Cumulative frequency distribution of OP-TO population	6-8



Figure 6.4	Cumulative and reverse cumulative frequency distribution functions in continuous space.	6-9
Figure 6.5	Cumulative and reverse cumulative frequency distribution functions and their relative regression lines for Cuticulis and OP-TO Populations in discrete space.	6-9
Figure 6.6	Powered Bi-Cumulative Distributions of Cuticulis and Op-TO populations	6-10
Figure-6.7	OPTIMAL $\theta$ calculation from PB-CDFs of cuticulis and OP-TO populations	6-11
Figure-6.8	Normal Distributions of Cuticulis and OP-TO Populations.	6-13
Figure 6.9	A capillary loop and its side chains.	6-16
Figure 6.10	A capillary segment and its properties	6-16
Figure 6.11	Normal Distributions of Open and Tortuous Segmental Curvature Angles $\beta$ for Overall Population.	6-18
Figure 6.12	Powered Bi-Cumulative Distribution of Open and Tortuous Segmental Curvature Angles $\beta$ for Overall Population	6-19
Figure 6.13	Segment size pair distributions of open and tortuous populations in overall data sets	6-19
Figure 6.14	Hypothesized distribution selection of the populations.	6-25
Figure 6.15	Cumulative Frequency Distribution of Open and Tortuous Capillary Loop Lengths in Overall Agreement Data Set	6-26
Figure 6.16	Cumulative Frequency Distribution of Enlarged Capillary Population with Outliers that Possible Giant Entries	6-29
Figure 6.17	Cumulative Frequency Distribution of Enlarged and Giant capillary Loop Populations.	6-29

## **Chapter 7**

Figure 7.1	The class distributions of the capillary loops in six test images by the practitioners	7-4
------------	--	-----

## LIST OF TABLES

### Chapter 2

Table 2.1	Some clinical conditions previously correlated with capillaroscopic abnormalities.	2-7
-----------	--	-----

### Chapter 5

Table 5.1	The conditions of being an open or tortuous loop by checking ( $n_1$ , $n_2$ ) control pair. ( $n_i$ number of curves on side chain- $i$ , $\beta_{ij}$ curvature angle, $pO_i$ , $pT_i$ possibility of being Open or Tortuous for side chain- $i$ , respectively)	5-40
-----------	--	------

### Chapter 6

Table 6.1	The effects on the overall class agreement in the cases of absence of each practitioner	6-4
Table 6.2	The analysis results to choose a $\theta_{\text{CUTICULIS}}$ critical angle for the classification of cuticulis type capillaries.	6-14
Table 6.3	The analyses results to select a $\beta_{\text{OPEN}}$ critical segmental curvature angle.	6-20
Table 6.4	Detection of the outliers by using formal method.	6-22
Table 6.5	Informal detection of outliers by using $1.5 \cdot \text{IQR}$ whisker.	6-23
Table 6.6	Informal detection of outliers by using $0.84 \cdot \text{IQR}$ whisker	6-24
Table 6.7	Detection of outliers by using $1.5 \cdot \text{IQR}$ whisker.	6-28

### Chapter 7

Table 7.1	Consensus class(es) distribution of the capillary loops	7-5
Table 7.2	Consensus Value Distributions for the practitioners and	7-6

<b>Table 7.3</b>	<b>Classification Success Rates for the practitioners and TANCCAS</b>	<b>7-7</b>
<b>Table 7.4</b>	<b>Descriptive or label classes usage rates of the practitioners</b>	<b>7-7</b>
<b>Table 7.5</b>	<b>Class Identification Success Rates of TANCCAS</b>	<b>7-8</b>
<b>Table 7-6</b>	<b>Capillary morphometry (Mean <math>\pm</math> SD), comparisons with the literature</b>	<b>7-10</b>

## LIST OF TERMS

**Suggested Class:** The capillary loop class that is assigned by the participating clinician.

**Consensus Class:** The majority of the classes that are assigned by the participating clinicians. In the case of not acquiring the majority, the capillary loop is assigned to more than one consensus class that are the joint consensus classes.

**Consensus Value:** The number of clinicians that acquire the majority on the consensus of a capillary loop.

**Preliminary Class:** The class that is assigned to a capillary loop in Pre-Processing Module-Part II (PPM-II) by TANCCAS. The preliminary class will be either confirmed or rejected in Main Classification Module (MCM) and Class Decision Unit.

**Actual Class:** The class that is assigned to a capillary loop by TANCCAS, after rejecting or accepting the preliminary classes that are identified in PPM-II or MCM.

# **CHAPTER 1**

# **Chapter1 Introduction**

## **1.1 The Problem and Problem Approach**

Pattern recognition is used for object recognition. Recognition is not possible without knowledge, and decisions about classes or groups into which recognized objects are classified are based on such knowledge. Knowledge about objects and their classes gives the necessary information for object classification. Good knowledge representation design is the most important part of solving the image understanding problem. Furthermore, a small number of relatively simple control strategies, or in another words a well structured representation of a priori data and hypothesis is often sufficient for intelligent systems to solve even complex problems. Therefore the first step for object recognition is to accumulate enough knowledge about the object.

Although capillaroscopy continues to fascinate the researchers since the early days of the invention of the microscope, it has gained a great deal of importance in clinical research and practice since the late 1950s. Because of allowing easy access to view capillary loops by using non-invasive in-vivo techniques, nailfold capillaroscopy has been a very active research area. Many attempts have been made to find a correlation between the patterns of the nailfold vascular bed and the diseases. Capillary morphology analysis is one of the tools to enrich the capillaroscopic readings. The literature review showed that there is not an established protocol for either terminology nor quantitative nailfold capillary pattern classification, despite the valuable efforts of Houtman et al., [86]. Apart from a few so-called loop patterns ("enlarged", "elongated", "giant"), definitions of the capillary loop patterns are purely qualitatively defined by previous researchers. As has been stated earlier, these definitions display great deviations from one research group to another, and, even within a research group.

By evaluating the literature findings about capillary loop patterns, basic characteristics of the classes can be obtained. Of course, by using these definitions, only the loops that are typical examples of their classes, can be identified. Since the loops'

patterns within a class display variations, for the loops near to class borders, these definitions are not sufficient. In such cases, the clinicians classify the loops arbitrarily. Quantitative definitions of class borders, on the other hand, prevent arbitrary classifications, and unifies the classification criteria used by different researchers. Therefore establishment of quantitative nailfold capillary morphology pattern classification criteria will be beneficial for the clinicians, even with no experience in the field. Since there is no available information to propose the classification criteria, by evaluating several clinicians' classifications of a sample group of capillary loops, and combining these findings with the ones obtained from literature review, quantitative classification criteria can be proposed. Thereupon, this study aims to fulfill the urgent need to propose quantitative nailfold capillary loop classification criteria.

We propose quantitative classification criteria for "cuticulis", "open", "tortuous", "elongated" and "giant" loops. A critical ratio between loop length and width is defined as a delimiter of "cuticulis" loops. "open" and "tortuous" loops can be classified quantitatively by dividing the capillary loop into convex subsets and measuring each convex's tortuosity and its significance on overall appearance. Tortuosity of a convex segment can be determined by the ratio between convex depth/convex base length. Quantifications of "elongated" and "giant" types are achieved by setting a critical loop length and limb width, respectively. While classification criteria of crossed capillaries remained qualitative, a semi-quantitative classification mechanism is proposed for "bizarre" and "bushy" loops. The mechanism uses geometric relations rather than numerical calculations for the classifications. Since, the classification criteria based on measurements, we used the term semi-quantitative.

The proposed nailfold classification criteria can be automated by employing image processing and pattern recognition techniques. Unlike some recognition problems; tree leaves, cell classifications [Meyer 79, Smeulders 80, Dayhoff and Dayhoff 88, Arman and Pearce 90, Shiotani et al. 94], plankton [Simpson et al.], algae [Thiel 94], aircraft, character recognition [Cash and Hatamian 87, Wang and Pavlidis 93], i.e., nailfold capillary loops do not have a constant shape within a class. In such

classifications, of course, there are some problems that make the recognition difficult such as; different viewing angles [Tanaka et al. 85], deformation and overlapping of the objects [Knoll and Jain 86] as well as the undesired effects of the pre-processing and segmentation processes. Internal scalar transform methods; moments of the area [Savini 88], 2D Fourier transformation [Simpson et al.], chord distribution, use mathematical properties derived from the area within a complete shape contour. Such descriptors usually take the form of numerical measures of the shape rather than representing symbolic properties. External scalar transformation methods; polar, rectangular and curvature representation, Fourier coefficients as shape descriptors [Kiryati and Maydan 89], autoregressive models [Sekita et al. 92], bending energy [Yang et al.74], can be used for coding of the object boundary. Space domain techniques, on the other hand, describe the structural and relational properties of a shape. The descriptions usually involve the translation of numerical data for example boundary path coordinates into semantic information such as descriptive tree structures or boundary primitives. Medial axis transform (MAT), thinning [Meyer 79], polygonal approximation [Gupta et al. 93], signatures [Bruckstein et al. 93], Hough transformation are among the most commonly used space domain shape coding techniques. Additionally, a complex shape can be decomposed into a set of simpler shapes, by using primary convex subsets (PCS) technique [Pavlidis 72] .

Shape variations of crossed, "bizarre" and "bushy", are so large that class borders cannot be drawn with a single numerical value by using scalar transform techniques. However, by reducing their shape information using thinning operation and evaluating their skeletal properties relative to object boundaries, they can be recognized. The classification of crossed capillary loops, requires special attention, since their outer boundaries are no different from those "open" and "tortuous" loops. The number of skeletal chain segments, their relative positioning to the loop's center of gravity and finally number of inner boundary chains and their relation to the loop's skeleton are the key factors for crossed capillary loop classification. On the other hand, the classes; "cuticulis", "open" and "tortuous", can be efficiently classified by combining scalar transformation and scale domain techniques. A single numerical value *exclusive-*



**curvature angle** that is a property of circular arc approximation of capillary loop boundary, can be used as a delimiter of "cuticulis" loops classifications. "open" and "tortuous" loops can be decomposed to a single line by using thinning operation. Furthermore the loop's *outer* boundary can be represented with convex subsets. By using polygonal approximation followed by the so-called circular arc approximation, the feature vectors [Cromwell and Kak, Dori 95] *side1(number of convexities (n), the curvature angle of convex<sub>1</sub>,...convex<sub>n</sub>)*, *side2(number of convexities (n), the curvature angle of convex<sub>1</sub>,...convex<sub>n</sub>)* can be produced. (Note that the feature vector's dimensions are variable (relative to the number of convexities of a *side*.) By measuring tortuosity of each convex and its significancy on overall appearance, recognition of "open" and "tortuous" loops can be achieved.

The number of boundary chains, loop length and loop limb width are the numerical values that are used for recognition of the classes "enlarged", "elongated" and "giant", respectively.

Taking a different action at a time according to the information extracted from the object, a hierarchical classification mechanism can be used for the classification of nailfold capillary loops. Of course, this is not the only way to solve the classification problem. However it proved to be an efficient method by achieving 88% classification accuracy rate compared to participating clinicians' classifications results.

## **1.2 The Aims and Objectives**

It is the aim of this study to propose a quantitative criteria for the classification of nailfold capillary loops, and create an automated system to classify the nailfold capillaries into 17 different types; "open", "enlarged open", "giant open", "elongated open", "enlarged elongated open", "giant elongated open", "tortuous", "enlarged tortuous", "giant tortuous", "elongated tortuous", "enlarged elongated tortuous", "giant elongated tortuous", "cuticulis", "enlarged cuticulis", "crossed", "bizarre" and "bushy", and analyze their morphological parameters; length, width, limb width, number of loops and class distributions. This involves the following objectives;

- 1) To identify the most commonly used nailfold capillary classes and to acquire the classification criteria to identify these classes by reviewing the literature.
- 2) To carry out a classification experiment with the clinicians
  - a) to identify practical handicaps of the existing qualitative classification criteria
  - b) to test the responses of the clinicians to the same capillary loop
  - c) to derive information to propose a quantitative classification criteria
  - d) to validate the automated system's performance by comparing its classification results with the clinicians.
- 3) To propose the quantitative classification criteria by combining the literature findings and the clinicians evaluations of the test images.
- 4) To review the literature to acquire knowledge about image processing and pattern recognition methods.
- 5) To combine the existing techniques in an intelligent way to develop an automated system that solves the recognition problem.

Unlike other pattern recognition problems, the object class definitions are not available before hand, in other words, apart from typical examples of the classes, there are uncertainties about the classes of some capillary loops that deviate from being typical, even amongst the clinicians that are in the same research group. Developing a system that recognizes only the typical loops will not have a practical use. Therefore proposal of quantitative nailfold capillary loop classification criteria is essential as well as developing an automated system within this study.

### **1.3 Contribution to Existing Knowledge**

*Proposal of the classification criteria for nailfold capillary loops is the main contribution of this research to the existing knowledge.* Quantitative classification criteria for "cuticulis", "open" and "tortuous", and so-called semi-quantitative classification criteria for "bizarre" and "bushy" loops are proposed for the first time with study.

A new class system that contains 17 classes, has been proposed by combining the most commonly used capillary classes that are Width Anomaly Classes (WAC); "enlarged" and "giant", Length Anomaly Class(LAC), "elongated", and Descriptive Classes (DC); "cuticulis", "open", "tortuous", crossed, "bizarre", and "bushy", in the order of *WAC-LAC-DC*. Apart from the classes crossed, "bizarre" and "bushy", **fourteen new classes** that provides richer information than their component classes, have been **suggested** for the first time for the classification of nailfold capillary loops.

Automated classification of nailfold capillary loops is achieved for the first time by the development of The Automated Nailfold Capillary Classification and Analysis System (TANCCAS) using image processing and pattern recognition methods.

#### **1.4 Main Findings of the Research**

The literature review and evaluations on the clinicians' classifications of the test images produced the following findings:

- 1) Lack of a well established nailfold capillary loop classification criteria
- 2) Lack of nailfold capillary loop class terminology
- 3) The researchers' interpretation differences of the existing qualitative classification criteria
- 4) Practical problems of using qualitative classification criteria
- 5) Classification errors of the clinicians due to human perception weaknesses
- 6) Lack of information provided by the existing classes
- 7) To be able propose quantitative classification criteria for "cuticulis", "open", "tortuous", semi-quantitative classification criteria for "bizarre" and "bushy" loops
- 8) To be able to increase the information, provided by the classes, by creating combinational classes using the most common classes
- 9) Efficiency of space domain shape coding techniques to represent the loops pattern information

- 10) Efficiency of using a simple new scalar measure the so-called curvature angle, that is product of the circular arc approximation, to code the loops
- 11) Development of an automated system that has flexible structural control mechanism to allow future improvements.

### **1.5 The Structure of the Thesis**

A background about capillaroscopy; the techniques, its importance as a diagnostic tool, and a literature review about existing nailfold capillary classification criteria is given in Chapter 2. A discussion about the nailfold capillary loop patterns described by previous researchers, and about the experimental study that were carried out with participant clinicians, as well as the proposed classification criteria, form the Chapter 3. Introduction of the image library functions of the automated system TANCCAS together with literature surveys on the functions can be found in Chapter 4. The structure of the TANCCAS, development methodology, and implementation steps of solving the recognition problem given in detail in Chapter 5. The selection of critical values that forms the border lines of classes given in Chapter 6. Justifications of the suggested classes and the developed system TANCCAS are addressed in Chapter 7. Finally the strengths and weaknesses and future developments of the developed system, general conclusions and recommendations are outlined in Chapter 8.

# **CHAPTER 2**

## Chapter 2 Nailfold Capillary Microscopy

### 2.1 Introduction

This chapter aims to give a general overview of the studies of capillary microscopy, nailfold capillaroscopy in particular. The importance of nailfold capillaroscopy as a non-invasive diagnostic tool and its clinical use will be emphasized. Qualitative and semiquantitative capillary pattern classification systems of previous researchers will be discussed in detail in order to obtain basic morphological patterns of nailfold capillary loops. Finally, an overview will be given for quantitative analysis of limited morphological parameters of nailfold capillary loops.

### 2.2 Capillary Microscopy

#### 2.2.1 Introduction to Capillaroscopy

Capillary microscopy is a simple non-invasive method for examining the *microcirculation* in living beings, both in health and disease. In all of the diseases involving the microcirculation, capillaroscopy gives remarkable information from both clinical and diagnostic points of view. Microcirculation is the collective name for the smallest components of the cardiovascular network; the arterioles, capillaries, and venules. They are the site of control of tissue perfusion, blood-tissue exchange and tissue blood volume. A major fraction of total pressure dissipation occurs in *the arterioles*. A change in arteriolar structure or function affects local tissue perfusion, and systemic arterial blood pressure control. *The capillaries* are the major exchange vessels. The nutrients required to sustain the cells in a tissue flow across capillary walls. Finally, *venules* are important capacitance vessels that localize most of the tissue blood volume.

Present knowledge on the structure and functions of microcirculation in humans is mainly formed by the studies of optical and electron microscopy, classical and dynamic capillaroscopy with and without fluorescent dyes, laser Doppler fluxmetry, and

transcutaneous oxygen tension measurements (tcpO<sub>2</sub>). By using different combinations of these capillaroscopy techniques, valuable information on pathophysiological phenomena of the microcirculation can be obtained in many diseases, for example, vascular disorders, collagenosis, Raynaud's phenomenon, diabetes and hypertension.

### 2.2.2 The Developments of Capillary Microscopy

William Harvey described the blood circulation for the first time in 1628, but was unaware at that time of the capillary microcirculation. However, the 17<sup>th</sup> century Italian scientist Marcello Malpighi recognized the microvessels linking the arterial and venous system in frogs' lungs, in 1661. Discovery of capillaries around the nail was achieved by Johan Christophorus Kolhaus in 1663. As microscope technology steadily improved in the following century, major progress was made; Marshall Hall distinguished between precapillary, capillary, and postcapillary vessels, in 1831. Different body sites, such as ocular conjunctivae, lip's malleoli, *nailfold*, and fingertips allow direct access to viewing the capillaries in human body.

The essence of *skin capillaroscopy* is to examine the *morphology* and *function* of dermal papillary capillaries. The skin capillaries can be viewed and studied directly with an ordinary optical microscope. Many different viewing set-ups have been developed since 1919; Basler, for example, described a sophisticated mechanical set-up for the actual measurement of the velocity of the blood cells in human nailfold capillaries <sup>[Basler 19]</sup>. In 1964, Zimmer and Demis [64] developed a microscope-television system to study dynamic blood flow noninvasively in human skin capillaries. At about the same time, Brånemark [63, 64] introduced an invasive technique to study the dynamics of the skin capillaries in 1964, by inserting a modified titanium chamber in a skin tube of the upper arm. In 1974, Bollinger et al., [74] refined Zimmer and Demis's method and adopted a frame to frame analysis to measure blood flow velocity and vessel diameters in nailfold capillaries. Fagrell et al., [77a, 77b, 77c] further refined Bollinger and his co-workers' technique to be used in clinical practice.

Some years later, Bollinger and Fagrell introduced dynamic capillaroscopy with fluorescent dyes (Fluorescence Video Microscopy) [Bollinger 82, Bollinger and Fagrell 90]. The use of intravital fluorescent dyes, Na-fluorescein(NAF) and indocyanine green (ICG) has enhanced the image contrast and made possible to visualize previously invisible microvascular and interstitial compartments such as pericapillary halo, plasma skimming, etc. [Bollinger et al. 79, 82, 86, Jager et al. 80, Zauggvesti et al. 95] The technique has, also, allowed analysis of transcapillary diffusion of sodium fluorescein [Bollinger et al. 79, 82, Jager et al. 80]. The determination of blood cell velocity was automated by novel procedures based on computer aided densitometry and image analysis [Bollinger et al. 79, Jager et al. 80, Pries 88, Baer-Suryadinata and Bollinger 85]. However, some patients may develop side effects to the dyes used in fluorescence video microscopy [Carski et al. 78, Enzmann and Ruprecht 82, Waldhausen et al. 81] therefore precautions must be taken whenever the traces are injected intravenously.

Two other techniques, laser Doppler Fluxmetry and transcutaneous measurement of oxygen pressure have enriched the clinical capillaroscopy. The blood flow in thermoregulatory vascular bed, i.e. the subpapillary arterial and venous plexa dominates the signal recording of the laser Doppler flowmetry [Fagrell 90]. Although it is easy to use in clinical practice [Arvesen et al. 94, Netten et al. 96, Jorneskog and Fagrell 96], the interpretation of the recordings, some times, proved to be difficult. Transcutaneous oxygen pressure reflects primarily the function of the nutritive skin capillaries. The technique is only an indirect measure of the amount of oxygen that is delivered from the blood in the total skin microcirculation out to the skin surface.

Presently, capillaroscopy is the only method to evaluate blood flow in the nutritional capillaries with certainty, and is the best choice for studying the nutritional status of a certain skin area. The monograph edited by Bollinger and Fagrell [90] gives an excellent overview of the developments in clinical capillary microscopy research.



### **2.2.3 Classical Capillaroscopy Techniques**

The skin capillaries can be studied directly with an ordinary light, preferably stereo, microscope with a total magnification from 10-100x [Bollinger and Fagrell 90]. In the early 20<sup>th</sup> century, many investigators used high magnifications(100 to 300 times) that could provide detailed images of a few loops in a narrow microscopic field. In 1955, Wertheimer and Wertheimer [55] introduced capillaroscopy with smaller magnification (25 to 50 times). With small magnification power, the microvascular landscape can be observed. It was Maricq [81] who recognized and established the advantages of the wide-field capillary microscopy [Andrade et al. 90],with 12 to 14X magnifications.

The skin surface should be illuminated with a cold light source that is directed to the skin surface at an angle of approximately 45° for optimal view. The area should be focused on an area of approximately 1 cm<sup>2</sup>. An AC powered 15W microscope lamp or fiber optic illuminator is suitable for this purpose. In order to minimize the reflections from the skin surface, as well as making the skin transparent, some kind of oil, such as, immersion or paraffin oil, has to be applied to the skin. In some patients, the skin surface may be less transparent, possibly because of structural changes in the epidermis, or presence of interfering substances on the skin surface. In such cases, the horny layer of the skin should be peeled off. Applying an ordinary adhesive tape to the skin several times or peeling off the horny layer with the sharp end of an injection needle, the papillary layer should be exposed.

The microscopic observations can be recorded on ordinary photographs, and several photographic procedures [Gibson et al. 56, Wertheimer and Wertheimer 55, Lefford and Edwards 86, Maricq 81] have been reported in the literature. In order to achieve optimal contrast between the capillaries and the surrounding tissue, a blue filter should be placed in front of the illuminator. Depending on the light source, sometimes a green filter [Lefford and Edwards 86] may give better contrast than blue one. Nowadays, microscope and video are coupled and recordings have been made on video tapes

[Fagrell et al. 88, Carpentier and Maricq 90, Yu et al. 95, Haenggi et al. 95]. With a color picture, the capillaries often became indistinct [Bollinger and Fagrell 90]. Therefore, the documentation should be in black and white, in order to obtain best contrast between the capillary loops and surrounding tissue.

## **2.3 Nailfold Capillaroscopy**

### **2.3.1 The Structure of a Healthy Nailfold Capillary Loop**

A schematic cross-section of the skin is shown in Figure 2.1(a). The two main layers, the epidermis and corium originate from ectodermal and mesodermal tissue, respectively. The vessels of the subpapillary plexus, the arterial and the venous vessels, lie at the tunica propria. The vessels of the subpapillary plexus run more or less horizontally to the skin surface, and the capillary loops grow vertically up from these vessels into the corpus papillare. Each papillae shelters one capillary loop, which appears at capillaroscopy as a tiny red point corresponding to the top of the capillary loop. In the nailfold area, the capillary loops become progressively more parallel to the skin surface. In the last row they can be visualized in their full length. (Figure 2.1(b)).

Normally, subpapillary vascular plexus cannot be observed in the nailfold area, but in about 30% of the healthy individuals it is visible<sup>[Bollinger and Fagrell 90]</sup>. A capillary loop is built up by an arterial and a venous limb, and the apical part that connects these two limbs together. Usually, the arterial limb of the capillary loop is narrower than the venous one. The average diameters of the arteriolar and venular limbs are given as  $15.0 \pm 2.5\mu\text{m}$  and  $16.7 \pm 3.0\mu\text{m}$ , respectively, and by employing fluorescein isothiocyanat-human albumin (FITC-HA) mean thickness of capillary wall can be calculated as 2-2.25 $\mu\text{m}$ . The ratio of veno/arterial diameter is given as 1.2 to 1.5X (The numerical measurements of the capillary loops are taken from [Bollinger and Fagrell 90]). The morphological pattern of a specific capillary in a finger of an individual can be observed for years with the same appearance [Norris and Chowning 63]. The capillaries might become slightly tortuous and also dilated with age. The nailfold capillaries can be classified according to their morphology and distribution, and different classification

systems have been used [Norris and Chowning 63, Gibson et al. 56, Andrade et al. 90, Houtman et al. 86]. The discussions on these classification systems are given in section 2.3.4.

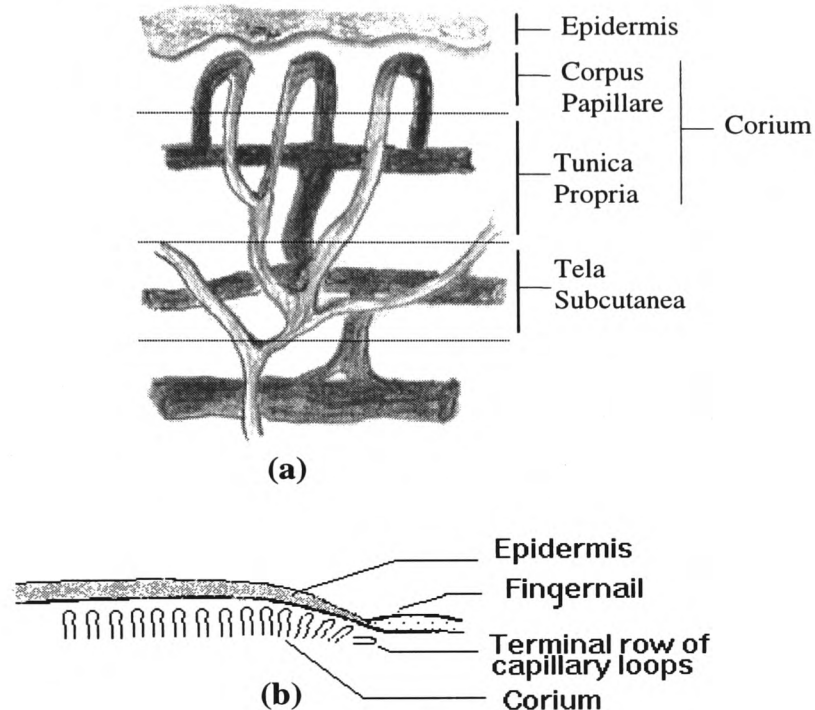


**Figure 2.1:** Schematic diagrams of the skin. (a) structure of skin capillaries (b) angle of capillary loops at different places on the finger.

### 2.3.2 Diagnostic Importance of Nailfold Capillaroscopy

Nailfold Capillaroscopy (NFC) has achieved considerable popularity as an in vivo and non invasive diagnostic tool that allows to study capillary **morphological abnormalities**, capillary blood cell velocity, and the diffusion of dye through the capillary wall. A wide range of pathological conditions have been correlated with capillaroscopic abnormalities. A list of many of these clinical conditions is given in Table 2.1. A diagnostic criterion for a disease can be derived from the data that is accumulated by the capillaroscopic measurements e.g. capillary shape alterations, capillary loop distribution, blood cell velocity, diffusion of fluorescent dyes through the capillary wall.

The normal capillary landscape is a uniform palisade formed by loops of homogenous size and morphology. This pattern is entirely disorganized in a few rheumatic diseases such as scleroderma [Studer et al. 91, Lefford and Edwards 86] , dermatomyositis, and mixed connective disease [Andrade et al. 90, Kabasakal et al. 96, Houtman et al. 86, Maricq and LeRoy 73]. In connective tissue disease, capillary abnormalities seem to appear earlier in the nailfold area than other sites of the skin of the finger [Houtman et al. 86]. The earliest abnormalities almost always appear in the distal row of nailfold capillaries in scleroderma-related Raynaud's phenomenon [Carpentier and Maricq 90]. Carpentier and Maricq [90] report that the changes are usually more prominent in the ring finger and occur rarely in the thumb [Maricq 81, Maricq et al. 80].

<b>Neuropsychiatric Diseases</b>	<b>Cardiovascular Diseases</b>
Multiple Sclerosis	Arterial Hypertension <sup>5,6</sup>
Schizophrenia	Congestive Heart Failure.
Manic Depressive Psychosis	
Epilepsy	
Oligophrenia	<b>Rheumatic Diseases</b>
Nocturnal Enuresis	Rheumatic Fever
Hemiplegia.	Rheumatic Arthritis
	Systemic Lupus Erythematosus
<b>Endocrine Diseases:</b>	Scleroderma <sup>7</sup>
Hypothyroidism	Dermatomyositis <sup>8,9</sup>
Addison's Disease	Mixed connective tissue disease
Diabetes Mellitus <sup>1,2,3,4</sup>	
1 [Chang et al 97]	<b>Miscellaneous Diseases</b>
2 [Zauggvesti et al. 95]	Digital Clubbing
3 [Jorneskog and Fagrell 96]	Glomerulonephritis
4 [Netten et al. 96]	Polycythemia Vera
5 [Bonacci et al. 96]	
6 [Prasad et al 95]	
7 [Maeda et al. 95]	
8 [Klyszcz et al 96]	
9 [Leteurtre et al 94]	

**Table 2.1:** Some clinical conditions previously correlated with capillaroscopic abnormalities.

Capillary morphology of the nailfold in mentally ill patients particularly in schizophrenia, differs from healthy controls by having decreased number of capillaries, a smaller size, a decreased color value, and the presence of many bizarre shapes [Norris and Chowning 63, Wertheimer and Wertheimer 55]. A well-documented work of Bollinger and Fagrell [90] emphasis the diagnostic importance of capillaroscopy in ischemia, diabetes mellitus, chronic venous incompetence, lymphedema, primary Raynaud's phenomenon, progressive systemic sclerosis, mixed connective tissue disease, dermatomyositis, rheumatoid arthritis and vibration disease.

The diagnostic criteria of nailfold capillary morphology alterations in disease can be found in the addressed studies. Discussions of these classification criteria are beyond the scope of this study. The main interest is to review the classification protocols of the shape alterations of individual capillary loops.

### **2.3.3 Nailfold Capillary Morphology Alterations**

The high degree of control needed to ensure optimal microvascular function is met by a range of control mechanisms. These include very rapidly acting local metabolic and myogenic mechanisms, endothelium-dependent mechanisms of release of vasoactive substances, nervous and hormonal influences, as well as slowly acting structural mechanisms [Struijker-Boudier et al. 96]. The microcirculation has an impressive ability to remodel the deployment of its vascular components, to change vessel length and number and to alter structural features of the vessel wall. These long term structural changes are increasingly recognised as important features of many diseases. The pathology of the microcirculation in disease reflects visible manifestations of long term control mechanisms of diameter change as well as structural damage, including wall thickening, vessel tortuosity, growth and rarefaction.

The visible nature of the changes in pathology has for a long time determined the mainly qualitative approach in microcirculation research [Wertheimer and Wertheimer 55, Norris and Chowning 63, Gibson et al. 56, Maricq 81]. In order to study possible

clinical capillaroscopic correlations, scale systems were developed to grade the extensions of the microangiopathic picture. Although qualitative and semiquantitative approaches are useful in many aspects, they are largely subjective, and that makes team to team comparisons difficult. Therefore quantification is necessary to compare the results between investigators and for follow-up evaluation.

#### **2.3.4 Nailfold Capillary Morphology Pattern Classification, A Literature Review**

Current identification of nailfold capillary patterns is based largely on qualitative and subjective characteristics, which makes accurate classification difficult. Several different nailfold capillary patterns both in healthy and diseased subjects have been reported by the researchers [Gibson et al. 56, Norris and Chowning 63, Andrade et al. 90, Houtman et al. 86]. Presence of a certain capillary pattern or a collection of patterns is correlated with a disease as a partial determinant factor together with other capillaroscopic measures. The classification protocols of these findings to correlate the relevant diseases are beyond the scope of this study. The main interest of this study is to quantify the subjective classification criteria of nailfold capillary morphology patterns.

An attempt was made to set up a standard for measurement of capillary structure by Wertheimer and Wertheimer [55]. In their work, they evaluated the length, and thickness of loops in three grades, twistedness of loops in four grades, and plexus in five grades. The thinnest loops were rated “1” on the scale; the thickest “3”. The same rating system was applied to length of loops. Predominant rates of length, thickness, twistedness and plexus, were appointed to the whole population. The degree of twistedness, however, was determined by the density of twisted loops in whole population. A rating of “0” was given, if loops were twisted only rarely. As the number of twisted loops increased, the rate was increased. In grade 3, practically all of the loops were expected to be twisted. The rating system of plexus is outside the interest of this study. They also encountered various rare structures that were excluded from the statistical work to correlate the structural capillary patterns to psychiatric diagnosis. “Bi-

lobed” or even “triple lobed” formations were one of these patterns. “stunted” capillary loop formation was reported as exhibiting extremely short, thin loop whose shapes could be determined only with difficulty. Another loop was shaped like a sprung hair pin, open at the lower end, and often impossible to recognize as a loop, therefore it was called “unformed”. “indeterminate” loops were very much like those “stunted” ones but with no visible plexus.

The capillary loop patterns described above were supported with exemplary photos and tracings of nail bed. However, these descriptions were highly subjective. There were no certain measurements to justify true length or thickness grade of a capillary loop.

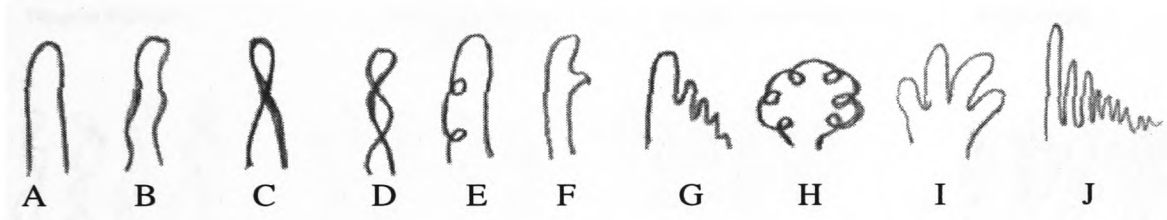


**Figure 2.2.** Ten basic morphological capillary loop patterns of Gibson et al.[56]

One year later, Gibson et al., [56] established ten basic morphological capillary loop patterns. These patterns are given in Figure-2.2. The patterns A and B, C and D, and E to J were, further grouped into three main capillary loop pattern groups “open”, “closed”, and “others”, respectively. **Pattern A** is represented by those capillaries that have no warpings or indentations of either of the limbs, and no twisting of either limb about itself or its opposite component. **Pattern B** has certain amount of warping or indentation of one or both limbs, and has no twisting of one limb around the other or itself. **Pattern C** is represented by the capillary loop shows single crossing. **Pattern D** has more than one crossing of the limbs around each other, and may show warpings, indentations, or dilation. **Pattern E** displays obscure twisting of one limb upon itself. This may be seen in either of afferent or efferent limbs. The patterns **F** to **J** are quite rare and their detailed descriptions can be found in the original article.

Although, capillary patterns were classified into a large selection of classes, their definitions were still qualitative. The “stunted” or “bi-lobed” capillary loops of Wertheimer and Wertheimer’s [55] classification system were not represented by any of the ten basic morphological patterns of Gibson et al. [56]. However in contrast to Wertheimer and Wertheimer 's [55]’s classification system, Ten basic patterns of Gibson et al. [56] represent directly the individual capillary loop’s shape, rather than overall appearance of the nail bed landscape.

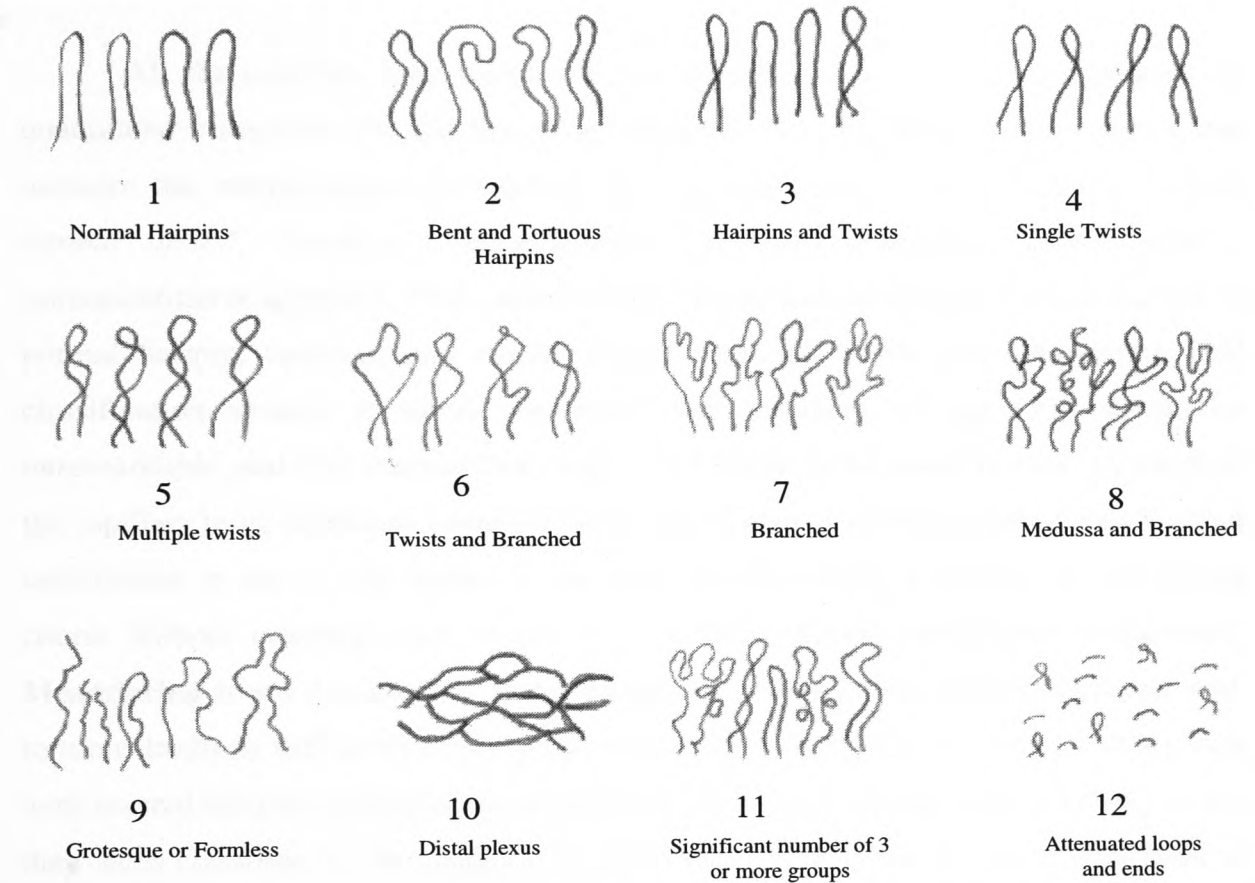


**Figure-2.3** *The capillary morphology of the nailfold by Norris and Chowning [63]*

By combining the previous investigators' classification systems, and adding encountered new classes, Norris and Chowning [63] developed their own classification system (Figure 2.3). They claimed that the classification groupings represent a continuum of abnormality. Thus group 1 represents normal hairpin configuration of a healthy capillary; following groups represents a gradual distortion until in group 10. The last two groups “mixed” and “attenuated loops and ends” were felt outside of the



continuum. Furthermore, they separated the classification groupings into three groups: (a) essentially normal (groups 1,2,3), (b) moderately abnormal (groups 4, 5, 6), and (c) remarkably abnormal (groups 7 through 12). Their qualitative classification system actually suggests eight individual capillary loop patterns, normal hairpin, bent hairpin, tortuous hairpin, twisted loop, branched loop, medusa loop, attenuated loop, and loop end. Excluding bent hairpin, medusa and attenuated loop configurations, the remaining five patterns have been widely used by other researchers.

All the capillary loop patterns so far described, have not been supported by quantitative measures. For the first time, Rouen et al., [72] attempted to classify and measure the morphological parameters of five basic capillary loop patterns, "*within normal limits*", "*tortuous*", "*meandering*", "*generally enlarged*", "*giant*" with a semiquantitative approach. Their definition of "within normal limits" is the collection of normal hairpin, tortuous, and single twisted loops of Norris and Chowning's [63] classification system. It should be noted that tortuosity of the loop should be *unremarkable*, and they claimed that single twist might be the result of viewing angle of the capillary loop. **Tortuous** capillary loops should display double crossing over without undulations in any of the limbs, or the limbs should follow a tortuous or undulating course without crossing over, or one of the limbs displays *remarkable* undulations. **Meandering** loops described as loops displaying double crossing over combined with tortuous limbs as well as the limbs cross over at three or more points. If a capillary loop with normal hairpin configuration is *substantially larger* than the other capillary loops, they were classified as "generally enlarged". These four basic patterns, regardless to Rouen and his co-workers' claim, have qualitative descriptions. There is not any defined tortuosity measure to compare being remarkable or unremarkable tortuous, or a critical ratio to decide on substantiality of the width. However, their definitions of "giant", as they claim, quantitatively evaluated. If the calculated area of generally enlarged capillary loop exceeds 20% of the total projected capillary area, it was classified as "giant".

The most serious attempt for standardization of terminology and quantification of capillary loop patterns has been made by Houtman et al., [86]. Twelve capillary loop

patterns are given in Figure 2.4. However, only those "enlarged" and "giant" patterns' critical values, 38.5 $\mu$ m and 76 $\mu$ m, respectively, were defined. The definitions of remaining patterns were made in a qualitative fashion. Furthermore, the patterns g through l reflects the abnormalities of width of the hair-pin shaped capillary loops. When only the morphological shape of the loops concerned, actually there are three basic patterns, hair-pin configuration, tortuous, and bushy or coiled, in Houtman's classification system. The whole set is completed with variations of these three basic patterns. Additional to the capillary loop patterns described above by various researchers, extremely long hair-pin capillary loops (longer than 300 $\mu$ m) have been further classified into class "elongated" by Kabasakal et al. [96]

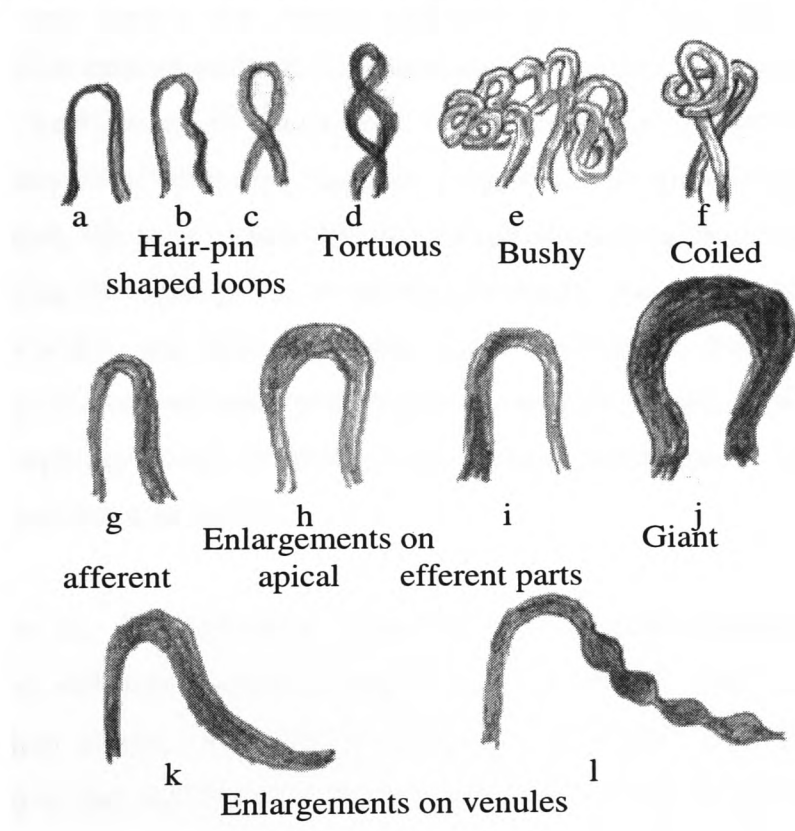


**Figure 2.4** Different patterns of nailfold capillary loops by Houtman et al. [86]

As a result, the literature review showed that several qualitative or semiquantitative nailfold capillary loop pattern classification systems had been developed, and diverse terminology had been used by the previous researchers. Although some of these capillary patterns, such as; "enlarged", "giant", "elongated",

"single twists", "coiled" had been introduced as basic patterns, actually they are variants of their fathers. These variants have importance as a class for certain diseases, but this does not change their status of being a variant not a basic pattern. In the following chapter, a discussion on the existing capillary loop pattern classes will be given, and actual basic patterns will be derived from the literature findings given in this section.

### **2.3.5 Quantitative Nailfold Capillary Microscopy**

Several different methods have been reported to measure the different morphological parameters of nailfold capillaries. Capillary loop density, diameters of the limbs, the loop length and width, tortuosity are the most commonly measured limited quantitative data of nailfold capillaroscopy. Measurement techniques vary from group to group. Lefford and Edwards [86], for example, took photomicrographs of the front row capillary loops with low magnification (50X). By projecting the photographs on to tracing paper, the most clearly focused image of each capillary loop was obtained. Then, by replacing the tracings on to millimetric paper, measurements of apex width, maximum limb width, and maximum loop width were made. Additionally they have used the tracings to measure inter-peak distance, capillary density in per millimeter and length of the capillary loops. However, this manual technique is long, tedious and difficult to use in clinical practice.

Rouen et al., [72] however, projected each photomicrographic slide upon a cardboard screen with total projected magnification of 1000X. They measured the total observed capillary length, the width of afferent, transitional and efferent limbs, and capillary density in per millimeter. The total observed length of the capillary loop was measured from first visible portion of the afferent limb to the last visible portion of the efferent limb following the center line of blood column. Transitional limb width was determined by the width of the mid point of apical part. Afferent and efferent limb widths were measured along perpendicular projections constructed at the three equidistant points along their respective lengths by taking the average. They also developed a formula, given in equation (6.13), to measure capillary loop area.

Studer et al. [91], used a video camera connected to a microscope (high magnification 270X) to perform quantitative capillaroscopy. Afferent and efferent limb width were measured from the point 100 $\mu$ m distant from the middle of the transitional segment. The largest loop width within this 100 $\mu$ m section was measured as the loop width. Carpentier and Maricq [90] performed morphometric study by means of a digitizing tablet on which photograph is projected. The lengths, areas and counts were determined with the help of a digitizing pen or of a mouse.

Lately, quantitative analysis of the nailfold capillaries are made on the images captured from video recordings of the nailfold area [Kabasakal et al. 96, Ohtsuka et al. 95]. By using commercially available image processing software, the visibility of the capillary loops is enhanced. The morphological parameters can be measured interactively by pointing and clicking the mouse on these enhanced images. Michoud et al., [94] attempted to develop an automated system for the calculation of morphological parameters. In his system, the user defines some points of the dermal edge to create a window. After improving interactively the visibility of the capillaries, and removing the 'haemorrhage structures' and the reflections within the window, the following parameters are calculated: the width and the length of the capillary loop (computed from a rectangle inscribing the capillary), capillary surface area, distance from capillary tip to the dermal edge of the nailfold, and distance between neighbouring capillary loops.

Involvement of the computerized systems, of course, improved the accuracy of the measurements. However, no one has reported a fully automated nailfold capillary analysis and classification system, yet. *This study is pioneering automated classifications of nailfold capillary patterns.* This, of course, clearly emphasizes the originality of this study.

# **CHAPTER 3**

## **Chapter 3 Proposing the Capillary Loop Pattern Classification Criteria**

### **3.1 Introduction**

In this chapter, first a discussion on the nailfold capillary loop patterns described by previous researchers, will be given. Some of the previous researchers attempted to set quantitative classification criteria for only "enlarged", "giant" and "elongated" loops. The importance of setting quantitative classification criteria will be emphasised throughout the chapter. Some of the existing loop classes will be criticized as being not a pattern but a loop's dimensional state indicator.

An experimental study that has been carried out with the participating clinicians, to be able to set quantitative classification criteria will be given in section 3.3. The urgent need for well defined nailfold capillary loop classification criteria will be demonstrated, and supported by analysing their classifications of some test images. The proposed class system, and the classification criteria will be given in detail in section 3.4. The proposed class system will consist of the most widely used capillary loop patterns, however these patterns will be combined to give as much information as possible about the loop's pattern and dimensions. The quantitative classification criteria will be given for the classes; cuticulis, "open" and "tortuous", and the anomaly classes; "elongated" and "giant". The classes "crossed", "bizarre" and "bushy" will be defined qualitatively and semi quantitatively by introducing a topological relation between the loop boundary and loop branches.

### **3.2 A Discussion on The Nailfold Capillary Loop Patterns Described By Previous Researchers**

As has been reviewed in the previous section, individual capillary loops show great morphological variability. All the capillary loop pattern definitions given in the previous chapter represent ideal examples of the relevant classes. Although Norris and Chowning [63] claimed that their classification groups represent a continuum of abnormality, there can not be an absolute continuum between the groups. A branched

capillary loop, in his classification system, may be gradually developed from normal hairpin shaped loop with increasing tortuosity until afferent, efferent or apical part of the capillary formed the branches. In this gradual distortion, in contrast to their claim, the branched capillary loop does not have to show a twisting phase. However, there is a transition between some of the pattern pairs; "cuticulis"- "open", "open"- "tortuous", normal length- "elongated", normal width- "enlarged", "enlarged"- "giant", "bushy"- "bizarre". A healthy capillary loop ("open" type), for example, may become a "tortuous" type with gradual distortion of its limbs' course, or, with increasing widening of loop width, a normal capillary loop gradually becomes an "enlarged" one. Qualitative definitions of these pattern pairs will always result in some misclassifications. The border line between the class pairs should be drawn quantitatively. The threshold points between normal length- "elongated", normal width- "enlarged" and "enlarged"- "giant" had been set to various values by previous researchers (for more information see section 3.4). However, none of them set the border lines between cuticulis- "open", "open"- "tortuous", "bushy"- "bizarre". Hence in addition to defining classes qualitatively, quantification is necessary to define actual borders of a pattern.

Another aspect is the selection of basic capillary loop patterns. Crucial features of the capillary loop morphology alterations should be evaluated carefully, before introducing it as a basic pattern. A basic pattern's features should be unique, and variants of a pattern should not be assigned as **basic pattern**. If afferent and efferent limbs of a capillary loop cross over each other once, it was called *single twist* in Norris and Chowning [63]'s classification system. Furthermore they introduced *multiple twists* as a basic pattern. The main characteristic of these capillary loops is having limbs twisted around each other. Hence the basic pattern should be twisted, and single twists, double, twists, multiple twists, etc., should be variants of the pattern twisted or "**crossed**". Particular amount of twisting(s) or the location of the twisting(s) in a capillary loop may have importance for a particular disease. Introducing such variants as a basic pattern after every study would soon result in tens of so called basic patterns.

Length and width are important morphological features of a capillary loop. If a capillary loop's width is larger than a certain amount of a healthy capillary loop's width, the capillary loop is called "enlarged", generally enlarged, mildly enlarged, moderately enlarged, ectatic loop, megacapillary, gigantic loop, giant capillary etc. If a certain part of the capillary is enlarged, it is called enlarged on afferent, on apical, on efferent part, or enlarged on venules (as in Houtman et al. [86]'s classification system). Both the amount and location of the enlargement are important. However, as it can be seen, there is no value in creating new patterns by emphasizing every important feature of a capillary loop.

### **3.3 An Experimental Study: The Classifications of the Test Images by Clinicians**

As it has been stated in Chapter 2, nailfold capillary loop pattern classification systems reported in the literature are mostly qualitative. In the last two decades, a few so-called semiquantitative classification systems have been reported. Capillary loop width, loop length, number of loops, and tortuosity index [Michoud et al. 94] are the capillary morphology parameters that are evaluated for classification of the loops. A review on the methods used for the calculations is given in section 2.3.4 and 2.3.5. However, while reviewing the literature, it has been noted that the researchers often emphasized that all the evaluations of nailfold capillary loops were made by same person. This assures the reader that the results are the product of only one observer's perception, and are free of classification errors due to interpreting the classification criteria differently from the co-workers. Therefore it can be concluded that even in a research group, interpretation of the classification criteria may vary from one person to another. Interpretation error is inevitable. Even one person carrying out the analysis, after working long hours, his perception and judgment will weaken, and this may result in error.

Apart from parameter dependent classes, such as "enlarged", "giant", elongated, etc., it was almost impossible to set quantitative criteria for "open", "tortuous", "bushy", etc., by reviewing the literature. To derive enough information to define border lines



between capillary patterns, on one hand, and to observe the classification errors mentioned above, on the another hand, some test images (Appendix A) were sent to Royal National Hospital for Rheumatic Diseases, Bath. Twelve clinicians, with different level of experience, were asked to classify six images, that contained a total of 217 capillary loops, into five basic patterns; cuticulis, "open", "tortuous", "crossed" and "bizarre". Six clinicians contributed to this project by replying our request, and their evaluation results can be found in Appendix-C. The clinicians suggested some other patterns; normal, "enlarged", "giant", elongated, "bushy", and mixed, additional to the five basic patterns.

The type of a capillary loop (consensus class) was determined by the majority of the classes that are assigned by the participating clinicians. The capillary loop (i1:N8) (The test image 1 of Appendix A, No:8), for example, was evaluated as follows;

Clinician 1: Enlarged	Clinician 2: Cuticulis	Clinician 3: Cuticulis
Clinician 4:Enlarged	Clinician 5: Enlarged	Clinician 6: Enlarged

The majority of the assigned classes is "enlarged", and the number of clinicians that reached the agreement are four. Therefore the capillary loop's consensus class is assigned to "enlarged", and the consensus value (CV) of the consensus class is set to 4.

If a clinician assigned more than one class to a capillary loop, his/her evaluation of the capillary loop was treated as if it was not evaluated at all, by the clinician. If the clinician did not assign a class to a loop, it is accepted that he/she was indecisive on the type of the loop. Multiple assignments are another form of indecisiveness, therefore, they should be evaluated as if they are left blank. The capillary loop (i1:N7), for example, was marked 'enlarged/giant?' by the clinician 4, and in Appendix-C, his/her classification of the loop (i1:N7) is entered as '\* '.

If, somehow, the majority could not be acquired, the capillary loop was assigned to more than one consensus class. The capillary loop (i3:N40), for example, was classified as "elongated", "normal", "open", "open", "enlarged" and "enlarged" by the clinicians 1 to 6, respectively. As it can be seen, the majority could not be acquired.

Both of the classes; "open" and "enlarged" have got the highest CV=2. If the capillary loop were to be eliminated from the analysis, 17% of the capillary loops must be discarded as well. Instead of discarding these loops all together, they were excluded from the data sets that are used to set the threshold values, but, were kept for performance analyses.

The evaluations on the participating clinicians' classifications are produced the following findings:

- 1) The clinicians were not unanimous on even a single capillary loop's pattern out of 217.
- 2) The class "enlarged" were assigned to 69 capillary loops of the test images by the consensus of the clinicians. 38% of these assignments are shared with another class(es) such as "open", cuticulis, etc., at the same time. Furthermore, the class "enlarged" was assigned, occasionally, to those "bizarre", "bushy" and "crossed" by the individual clinicians.
- 3) The clinician 2 is mainly concerned about the loop width. 60% of his/her overall assignments are either "enlarged" or "normal". S/He is the only clinician that assigned some of the loops as "normal".
- 4) The class "elongated". was assigned to the loops by only the clinicians 1 and 6.
- 5) The clinicians 1, 5 and 6 were assigned the individual capillary loops with "mixed". With few exceptions, "mixed" is assigned to only atypical loops.
- 6) None of the loops is assigned to "bushy", "normal" and "elongated" and only one loop is assigned to "giant" by the consensus of the clinicians.

The main reason not to be able to reach unanimity on the class of even a single capillary loop, is not only the subjectivity of existing qualitative classification criteria but also assignments of dimension information; enlargement, elongation as capillary loop class. This handicap can be avoided by using the proposed new class set in section 3.4. Although the clinicians have not been provided by the scale/magnification information, they have assigned several loops as "enlarged", and a few as "elongated" and "giant". The assignments of individual loops as "mixed" cannot be acceptable. In the literature, Kabasakal et al. [96], assigned the term "mixed pattern" to the capillary loops

of a finger lacking a single dominant pattern, not for individual loops. Therefore the participating clinicians' suggestion to use "mixed" as class is unacceptable, and the final classification system will not include so-called class "mixed".

By evaluating the clinicians' classifications, the borderlines between pattern pairs; cuticulis-"open", "open"- "tortuous", "enlarged"-giant, and 'within normal length'- "elongated" can be drawn quantitatively. Further evaluations of the clinicians' classifications for setting the threshold values will be given in section 3.4 and chapter 6.

### 3.4 The Classification Criteria

By reviewing the literature and evaluating the classifications of participating clinicians, six common patterns; cuticulis, "open", "tortuous", "crossed", "bushy" and "bizarre", are selected as basic morphology patterns of nailfold capillary loops. These six patterns have got *characteristic shapes*, will be called **Descriptive Classes (DC)**. Furthermore, descriptive classes can be divided into two main groups; parametric and non-parametric classes. The first three patterns; cuticulis, "open" and "tortuous", can be parametrically evaluated according to their length/width ratio and tortuosity measure, respectively. Therefore, they will be called **Parametric Classes** in general. The patterns; "crossed", "bushy" and "bizarre", on the other hand, can be evaluated, only, in a qualitative way. Hence they will be called as **Non-Parametric Classes** .

The classes; "enlarged", "giant" and "elongated", have not got a specific shape, they are the dimensional anomalies of capillary loops. An "elongated" capillary loop, for example, may have "open" or "tortuous" pattern. These classes give dimensional information about the capillary loop width and length, regardless of its shape. Therefore, they are excluded from the basic morphology patterns. However, the valuable dimension information they supply, should be preserved. Hence, they are considered as *Label Classes*, and will be attached to the descriptive classes. Furthermore, label classes can be divided into two sub groups **Width Anomaly Classes (WAC)**; "enlarged", giant and **Length Anomaly Class (LAC)** "elongated".

By combining primitive, descriptive and anomaly classes in the order of (WAC-LAC-DC), the full class name of a capillary loop can be obtained. By this way, the width and length information can be given as well as shape of the capillary loop within a class name. Three important features of the loop will be preserved by the proposed class name.

WAC and LAC are the optional labels of a loop's class. A capillary loop may not display any of the anomalies. So that none of WAC and LAC will be attached to DC. If an "open" loop is enlarged but not elongated than it will not possess LAC label. However if a loop displays anomalies in both width and length, then both of the WAC and LAC labels will be available. The classes "crossed", "bushy" and "bizarre" do not require any of the label classes, because width and length information are not available for them. However, in the survey some of these loops were assigned to "enlarged" by the participating practitioners, therefore, we accepted them in an implied enlarged state. Cuticulis capillaries cannot be "elongated" because they have got short limbs. They also cannot be giant because limb width information is not available for them. Therefore cuticulis loops can only have the LAC label "enlarged".

The nailfold capillary loops are proposed to be classified into the following 17 classes;

Open	(Op)	Tortuous	(To)
Enlarged Open	(EnO)	Enlarged Tortuous	(EnT)
Giant Open	(GO)	Giant Tortuous	(GTo)
Elongated Open	(EIO)	Elongated Tortuous	(EIT)
Enlarged Elongated Open	(EEO)	Enlarged Elongated Tortuous	(EET)
Giant Elongated Open	(GEO)	Giant Elongated Tortuous	(GET)
Cuticulis	(Cu)	Bizarre (Bzr)	Bushy (Bsh)
Enlarged Cuticulis	(EnC)	Crossed (Crs)	

### 3.4.1 Classification Criteria of Cuticulis Type

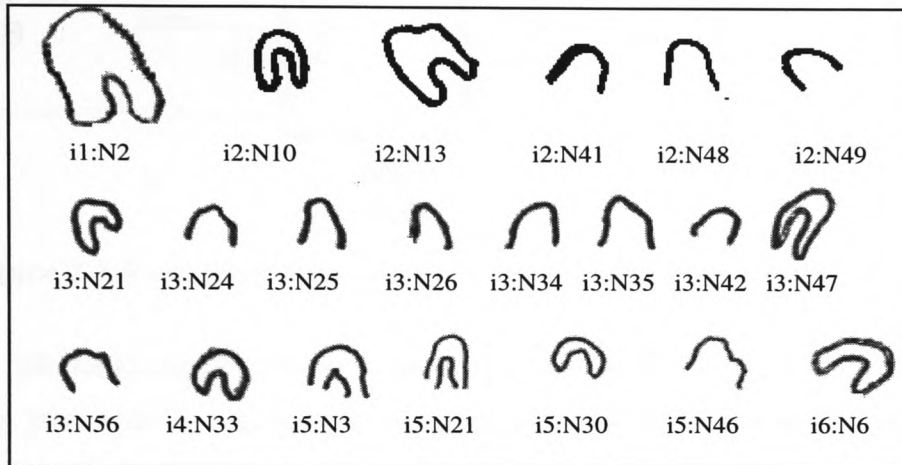
Andrade et al. [90], simply described "cuticulis" pattern as tiny red dots in high density. They are the tip points of capillary loops and the limbs are not visible. However, this qualitative definition proved not to be practical with the participating clinicians' classification results (Figure 3.1). Figure-3.1 is arranged to demonstrate that size of the "cuticulis" capillaries can vary in a large range, and the limbs can be visible in contrast to Andrade's definition. Additionally, the handicaps of the qualitative description is presented in Figure 3.1(b).

Some of the capillary loops, classified as "cuticulis" by the agreement of participating clinicians, are given Figure 3.1(a). The length and width of the "cuticulis" capillary loops display variations. As the apical part of the capillary loop enlarges, the size of the capillary "tip" becomes out of proportion. The capillary loop (i1:N2), for example, is far away being a "tiny red dot". However, it is certain that, (i1:N2) is the tip of an enlarged capillary loop. By comparing it with those "open" type capillary loops in Figure 3.1(c), it is even taller and larger than them. Therefore while describing a "cuticulis" capillary, the loop length cannot be restricted.

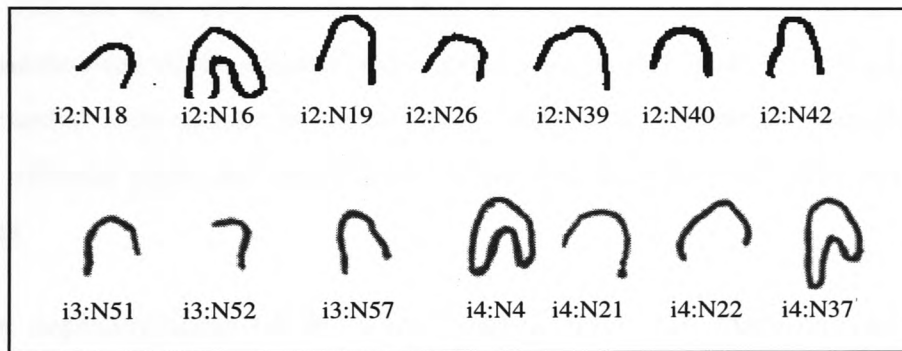
In contrast to Andrade et al. [90]'s definition, the limbs of the capillaries are visible in most of the cases, and their length vary in a large range. The limbs of the capillary loops (i2:N10), (i3:N47) and (i5:N21), for example, are not only visible but also long enough to create confusion to question them as "open" type. Since, nearly all of the capillary loops, classified as "cuticulis" type, present visible limbs, "cuticulis" pattern should be allowed having "short" limbs. In this case, the maximum allowed limb length of "cuticulis" type capillary loops has to be determined.

Although, the visible length of the limbs of (i1:N2) are proportionally short to be a "cuticulis" capillary, they are as long as those of (i2:N12), (i2:N13) and longer than of all the capillaries in group (b) (after taking away the apical parts). It should be noted that all of the capillary loops in Figure-3.1(b) and (c) (apart from (i1:N2) in (c)) are classified as "open" type. As the enlargement of capillary loop increases, actual length of the limbs increases as well. Proportionally the limbs can, still, be small enough to

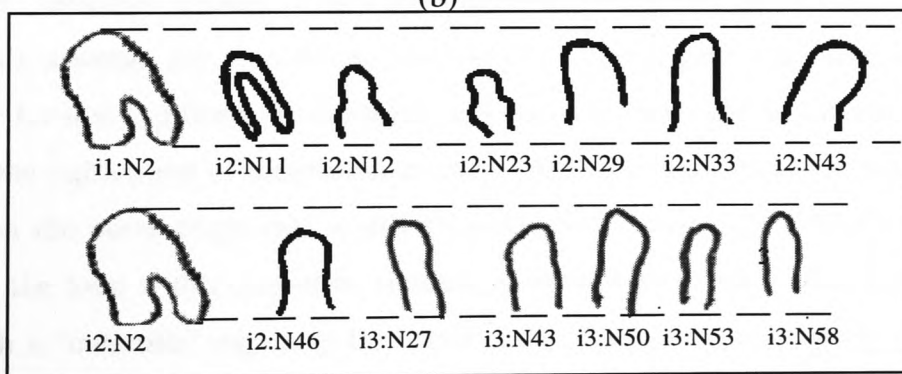
consider the loop a "cuticulis" one, but the limb length will no longer be "short". Therefore, instead of setting a threshold limb length, a threshold ratio between limb length and loop width must be used as a delimiter of "cuticulis" pattern.



(a)



(b)



(c)

**Figure 3.1.** (a) Some of the "cuticulis" type capillary loops in the test images (b) a collection of "cuticulis" loops mis-classified as "open" pattern (by the clinicians) (c) The "cuticulis" loop (i2:N2) is longer than several "open" type loops of the test images.

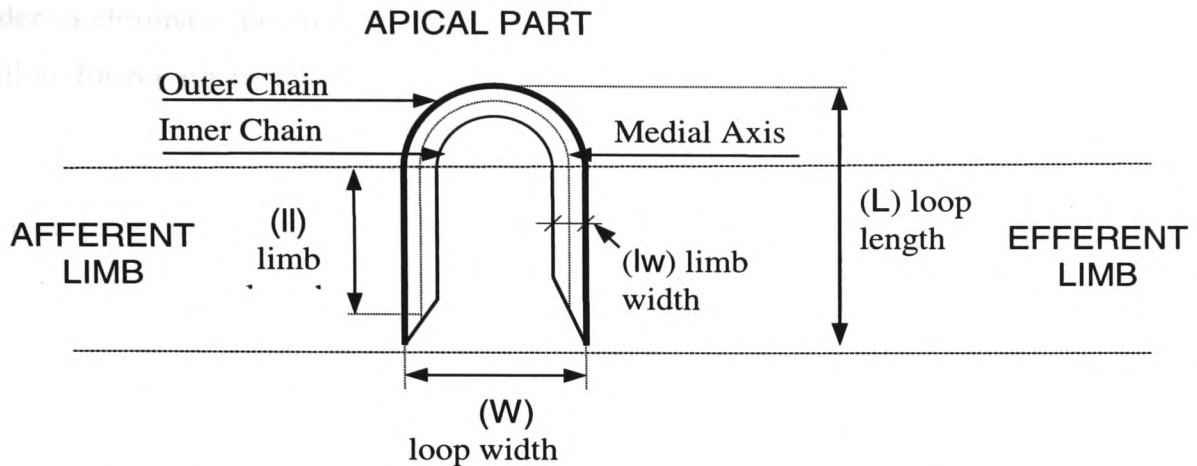


**Figure 3.2** A capillary loop and its morphological parameters.

An idealistic capillary loop is presented in Figure 3.2. The loop tip is ideally a semi circle. However, in real images of capillary loops demonstrate that apical part can be distorted and deviates from being a semi circle. It is practically difficult to locate where the afferent and efferent limbs join to the apical part. The inner chain is not always presented (as in the most of the capillary loops in Figure 3.1). Without the inner chain the medial axis cannot be determined. Therefore, instead of identifying afferent, apical and efferent parts, the outer chain of the capillary loop is taken into account for calculations.

The capillary loop (i5:N30) in Figure 3.1(a), has been chosen as an ideal example of "cuticulis" pattern. If any parts of both of its limbs are visible its difficult to locate. Let's assume, for a moment, that only the apical part (capillary loop "tip") is observable for this capillary. By knowing that not all of the capillary loops present inner chain, for the unification of measurement method for all capillaries, the calculations will be made on the outer chain that is always presented. Since, (i5:N30) does not display any limbs, the loop width cannot be measured. However, a width measure is necessary to establish a "cuticulis" capillary threshold ratio. The distance between end points of outer chain is assumed as loop width (LW). The line that connects these end points can be called a chord of an arc, since it is assumed that the outer chain is circular. The chord length, therefore, is equal to LW. Arc length is called (outer chain) loop perimeter, in

order to eliminate the possible confusion when the limbs are observable the outer chain will no longer appear an arc but a loop. A ratio between LW and loop perimeter:

$$\frac{LW}{\text{loop perimeter}} = \frac{\sin\theta}{\theta} = \text{sinc}\theta \quad (3.1)$$

proved to be useful to be a delimiter of "cuticulis" pattern. The solution of equation (3.1) produces a  $\theta$  value that half of the central angle sees the arc. The detailed analysis and justification of the ratio  $\text{sinc}\theta$  are given in section 4.2.5.6. A critical exclusive curvature angle  $\theta_{\text{CUTICULIS}}=131^\circ$  has been chosen after evaluating the clinicians' classifications of "cuticulis" type capillary loops. For computerized calculations, a "cuticulis" capillary loop's exclusive curvature angle  $\theta$  must be less than  $131^\circ$ . Equally, for manual computations visible length of the loop limbs must be less than 0.73 times of the loop width or loop length must be shorter than 1.23 times of the loop width.

Although, the capillary loops in Figure 3.1(b), are no different from those in Figure 3.1(a), they were classified as "open" type loops by the clinicians. They have got quite short limbs, and mostly apical parts of the loops are visible. Therefore they should have been classified as "cuticulis". However, they were mis-classified, due to the limited capabilities of human eye, poor judgment of the patterns, and using insufficient classification criteria. All of the mis-classified "cuticulis" capillary loops in Figure 3.1(b) have been correctly classified as "cuticulis" by the developed computerized classification system TANCCAS.

In summary, the qualitative and quantitative classification criteria of "cuticulis" will be given as follows; "cuticulis" pattern includes a range of capillary loops from tiny tip points to the loops with visible limbs up to 0.73 times of the loop width or with the loop length less than 1.23 times of the loop width..

### 3.4.2 Classification Criteria of Open and Tortuous Type

"open" and "tortuous" patterns are the most common capillary loop patterns in nailfold capillaroscopy observations. Gibson et al., [56] called both of the patterns "open", because of not showing any form of crossings on their limbs. Furthermore, they divided "open" pattern into pattern A and pattern B as given in section 2.2.4. In later



publications, pattern A has been called as “within normal limits” [Rouen et al. 72], “normal hair-pin” [Norris and Chowning 63], “open” [Andrade et al. 90], and pattern B has been called as “tortuous hairpin” [Norris and Chowning 63] or “tortuous” [Andrade et al. 90]. In this study, patterns A and B are called "open" and "tortuous" as in Andrade's classification system. In all of the classification systems, given in section 2.3.4, these two patterns were classified qualitatively.

An ideal "open" capillary loop has straight afferent and efferent limbs as given in Figure 3.2, however, in practice, the limbs' routes display slight distortions. As long as the routes of the limbs do not display significant tortuosity, the capillary loop is accepted within the limits of "open" pattern. Neither of the patterns are allowed to display any form of crossings of the limbs. The first row of the capillary loops in Figure 3.4, are the ideal examples of "open" pattern. The transitions between patterns have a single borderline in all of the capillary loop patterns, except "open" type. "open" pattern has got two transitions from "open" to "cuticulis", and from "open" to "tortuous".

The ratio between loop width and perimeter (equation 3.1) is a control parameter for the transition between "cuticulis" and "open" patterns, as it has been explained in section 3.4.1.1. Therefore, if the capillary loop does not display any form of crossings and any branchings, and if the exclusive curvature angle is larger than  $131^\circ$ , or the limb length is more than 0.73 times the loop width, or the loop length is more than 1.23 times the loop width, its pattern is a candidate to be an "open" or "tortuous" type. The borderline between "open" and "tortuous" patterns has a rather complex form. The number of segments of each limb, each segment's tortuosity value, significance of each segment on overall limb appearance are the controls of the transition between "open" and "tortuous" patterns. Either of the limbs has got 50% effect for deciding on the capillary loop's type. For example, while one of the limbs of the capillary loop is almost straight, the other one may display distortions on its course, as in the capillary loops (i2:N22), (i2:N31), (i3:N5), (i3:N45), (i3:N60) and (i5:N20). Therefore each limb will be analysed individually.

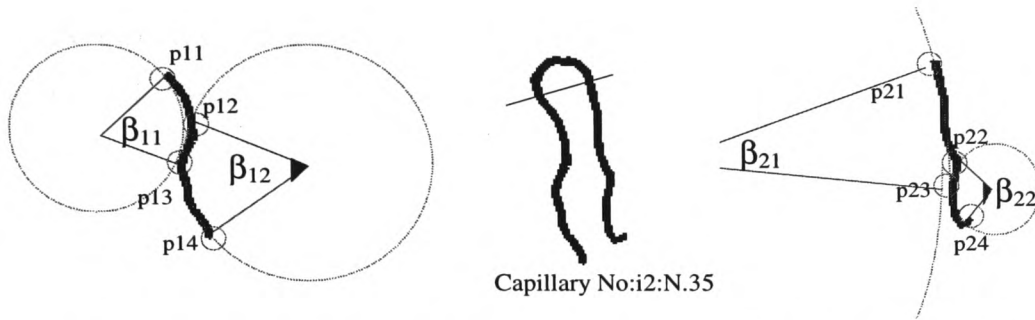


**Figure 3.3** Demonstration of dividing the capillary limbs into their segments and calculating the segmental curvature angles  $\beta_{ij}$ . (indices  $i$  and  $j$  represents the limb and the segment number, respectively) for (Image 2 capillary no 35)

By slicing off the semi circular apical part of the capillary loop, both of the limbs can be obtained individually for further analysis (Figure 3.3). A capillary loop's limb can be divided into its segments by controlling the direction changes of the limb route. The marked points "p<sub>ij</sub>" are the important points where the limb course changes direction. If the direction alteration is local and insignificant it can be ignored. The automated detection of important points is given in detail in section 5.4.3.2, however, for manual calculations, they are the beginning and end points of the concaves and convexes that form the limbs. The capillary loop (i2:N35), for example, has got one concave and one convex in each limb. By applying circular approximation (3.2), a measure of tortuosity ( $\beta_{ij}$ ) can be calculated for each concave or convex, and the justification of equation (3.2) is given in section (6.3). A set of  $\beta$ s will be obtained for each capillary loop to determine its class.

$$\{\beta\} = \{\beta_{11}, \beta_{12}, \beta_{13} \dots \beta_{1j} : \beta_{21}, \beta_{22}, \beta_{23} \dots \beta_{2j}\}$$

$\{\beta\}$  has to have a minimum of two elements (one for each limb). An "open" type capillary loop that has perfectly straight limbs, will have  $\{\beta\} = \{\beta_{11}=0^\circ : \beta_{21}=0^\circ\}$ . Each limb of the capillary loop (i2:N35), for example, has got two segmental curves (convex or concave), and naturally two segmental curvature angles  $\beta_{i, 1,2}$ . Therefore  $\{\beta\}$  of capillary (i2:N35) will be  $\{\beta_{11}=66^\circ, \beta_{12}=52^\circ : \beta_{21}=28^\circ, \beta_{22}=92^\circ\}$

$$\frac{\text{segment base length}}{\text{segment curve length}} = \frac{\sin(\beta_{ij}/2)}{(\beta_{ij}/2)} \quad (3.2)$$

where, segment base length is the projection distance between end points of the segment, and segment curve length is the actual length of the segment.

A critical segmental curvature angle  $\beta_{OPEN} = 56^\circ$  has been calculated by evaluating the clinicians classifications of "open" and "tortuous" type capillary loops. The details of the calculation of  $\beta_{OPEN}$  can be found in section (6.3).  $\beta_{OPEN}$  is the threshold angle to accept a segment as either an open or a "tortuous" segment. Any segment that has got  $\beta_{ij} \leq 56^\circ$  will be considered as an open segment, and any segment that has got  $\beta_{ij} > 56^\circ$  will be considered as a "tortuous" segment. For manual computations, if the depth of the curve, that is the length of the perpendicular line drawn from mid point of the segment base line, is equal or shallower than 1/8 of the segment base line, the segment is an "open" one, otherwise, it is a "tortuous" one.

$\beta_{11}$  and  $\beta_{22}$  of the capillary loop (i2:N35) are larger than  $56^\circ$ , therefore the relevant segments are "tortuous", and  $\beta_{12}$  and  $\beta_{21}$  smaller than  $56^\circ$ , therefore the relevant segments are "open". The loop (i2:N35) is classified as "open" type by the clinicians and TANCCAS. Let us consider a capillary loop with  $\{\beta\} = \{\beta_{11}=18^\circ, \beta_{12}=30^\circ, \beta_{13}=68^\circ, \beta_{14}=27^\circ : \beta_{21}=60^\circ, \beta_{22}=12^\circ\}$ . The loop has got 4 and 2 segments in each limb respectively. Although, only two of these segments ( $\beta_{13}$  and  $\beta_{21}$ ) are "tortuous", and the rest are "open" segments, the capillary loop does not have to be an "open" type. The "tortuous" segments might be proportionally larger than the "open" segments, and might be dominating the overall appearance of the loop (as in capillary loop i3:N44). In this case, the capillary loop must be classified as "tortuous" type. The capillary loops in Figure 3.5, were classified as "tortuous" and they are good examples of "tortuous" type. Each segment's effect on overall appearance should be taken into account. Percentage of the "open" segments in a limb ( $pOs_i$ ) and percentage of "tortuous" segments in a limb ( $pTs_i$ ) can be calculated as follows.

$$pOs_i = \text{total "open" segments length} / \text{total segments length}$$

$$pTs_i = \text{total "tortuous" segments length} / \text{total segments length}$$

The possibility of being an "open" type loop ( $pO$ ) and of being a "tortuous" type loop ( $pT$ ) can be calculated by adding both limbs'  $pOs_i$  and  $pTs_i$  respectively.

$$pO = pOs_1 + pOs_2$$

$$pT = pTs_1 + pTs_2$$

If  $pO \geq pT$ , the capillary loop is accepted as "open" type, otherwise it is classified as "tortuous" one. However, this is not always true.

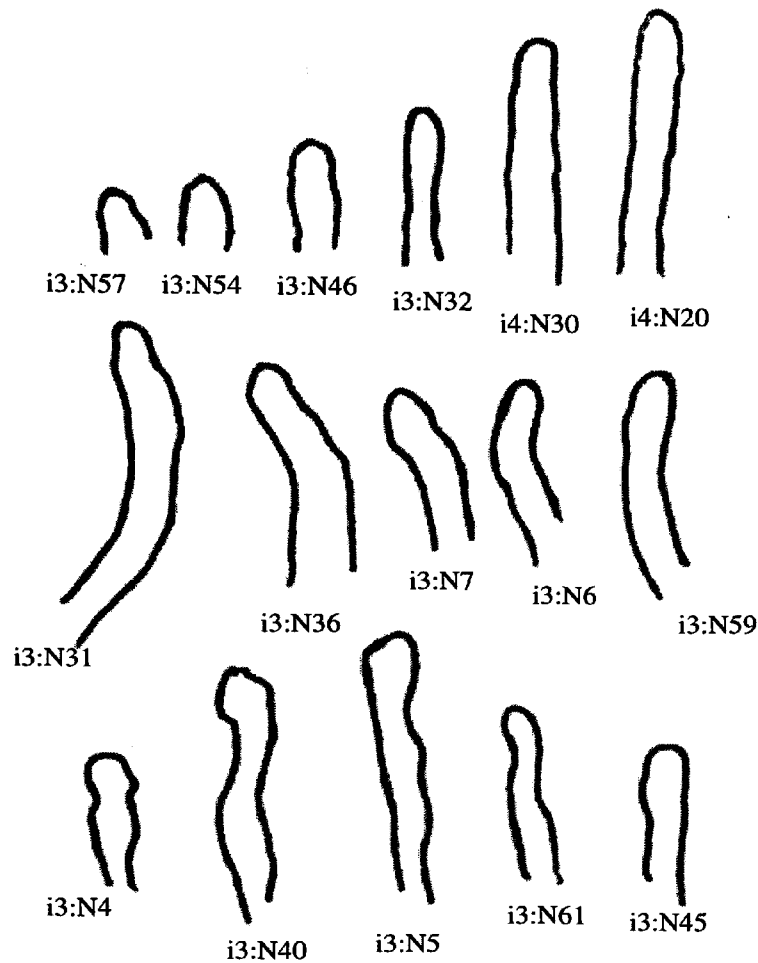


**Figure 3.4** A collection of open type capillary loops.

If a capillary loop's  $\{\beta\}$  contains only two elements, and  $\beta_{ij}$  values are wider than  $56^\circ$ , the capillary loop does not have to be a "tortuous" one. In such cases, the capillary loop's limbs are smooth and bent towards either of the sides. The second row of the capillary loops in Figure 3.4 are the closest examples of such cases. The capillary loop (i3:N36), for example, has  $\{\beta\}=\{\beta_{11}=50^\circ : \beta_{21}=50^\circ\}$ , and it is classified as "open" type. Let's assume that it is bent just a little bit more than it is. In this case  $\beta_{ij}$  values would be larger than  $\beta_{OPEN}$ . The human eye would not sense such a little change, and it still would be classified as "open" type by the clinicians. Having a smooth limb course makes us to accept it as an "open" one. However, if the bending was radical, then it has to be classified as "tortuous". Therefore, another critical segmental curvature angle  $\beta_{TORTUOUS}$  should be defined to control the "open" type capillary loop that has only two  $\beta_{ij}$  values in

{ $\beta$ } angle set and both of them are wider than  $\beta_{OPEN}$ . There could not be found any capillary loop that satisfies these conditions in the test images. Hence, a critical degree of bending ( $\beta_{TORTUOUS}$ ) could not be derived from the typical examples of this case. However,  $\beta_{TORTUOUS} = 98^\circ$  is proposed as a threshold. This value represents the mean segmental curvature angle of "tortuous" capillary loops. For manual calculations, if the depths of both of the limb curves are equal or less than 0.227 of the segment base length, the loop is still, an "open" one, otherwise it should be classified as "tortuous" type. Further investigations for  $\beta_{TORTUOUS}$  should be made to set a more accurate critical value. Therefore fine adjustment of  $\beta_{TORTUOUS}$  has been left as future work.

The classification steps of "open" and "tortuous" may seem too complex for manual evaluations, however, it is the first quantitative classification method ever proposed. If the researcher applies these rules whenever s/he is indecisive about the loop's pattern, it may speed up the process.

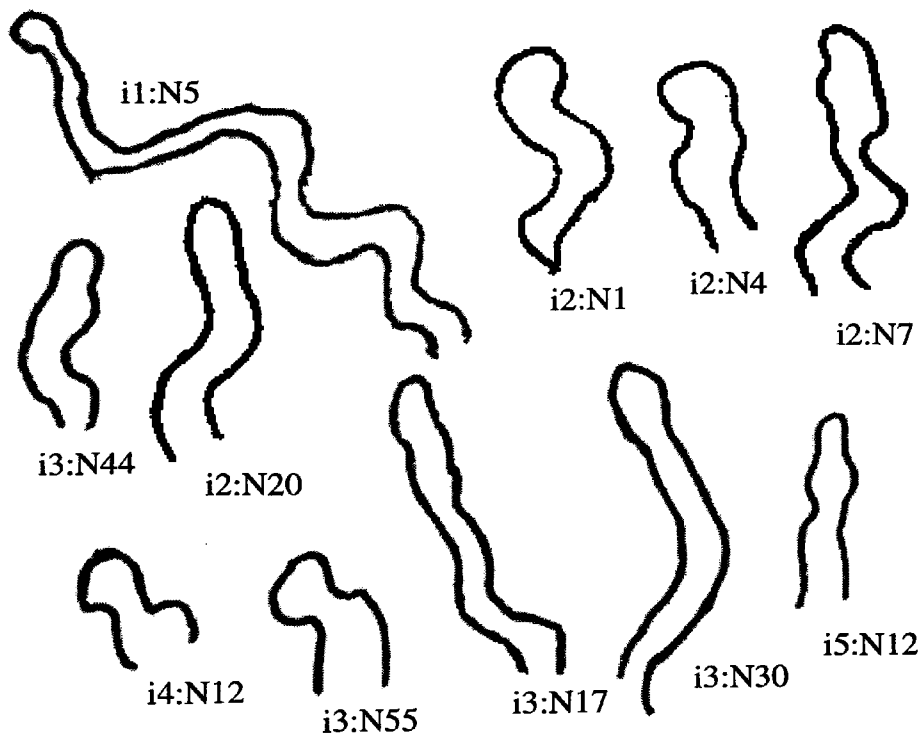


**Figure 3.5** A collection of tortuous capillary loops.

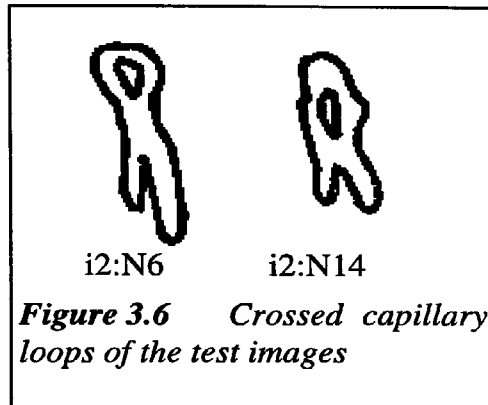
As a result, if a capillary loop does not show any form of branchings and crossings on its visible afferent, apical and efferent parts, and the loop length is longer than 1.23 times of the loop width, it can be classified as either "open" or "tortuous" type. The course of the limbs of a capillary loop, may display straight or/and "tortuous" segments. If the "tortuous" segment(s) are not dominating the overall appearance, the capillary loop is an "open" type, otherwise it is a "tortuous" one. If the depth of a segment is equal or shallower than 1/8 of the length of the segment's base line, the segment should be evaluated as an "open" segment, otherwise it is a "tortuous" one. Finally some "open" capillary loops may have smooth limb course (not showing any "tortuous" structure) and radically bent towards one side. The degree of bending may exceed the threshold value of being a "tortuous" segment. For such cases if both of the limbs segment depth are deeper than 1/4.4 times of the length of the limb segment base, the loop is no longer an "open" one, it should be classified as a "tortuous" type.

### **3.4.3 Classification Criteria of Crossed Pattern**

All of the classification systems given in section 2.3.4, except Houtman et al.'s [86] reported "crossed" pattern and its variants under many different pattern names and definitions. Rouen et al. [72], for example, called the "crossed" pattern "meandering" and only those capillary loops whose limbs display at least double crossing combined with "tortuous" course. The capillary loops whose limbs display single crossing were accepted as "within normal limits". Norris and Chowning [63], however, called "crossed" patterns as "twisted" and divided them into two groups; single twists and multiple twists. Furthermore, if the capillary loop limb curled upon itself, they called it "medusa". Gibson et al.'s [56] classification of "crossed" pattern (the patterns C, D, E) is not different from Norris and Chowning's [63]. Although, Houtman et al. [86], included the "crossed" patterns (c and d) in their classification system, they referred to them as hairpin shaped loop and "tortuous" respectively.

The characteristic feature of a "crossed" capillary is that limbs cross over each other. The number of crossings may have importance for a particular disease, therefore, "crossed" patterns can be divided into sub groups, such as; single twists, double twists,

twists on afferent limbs, twists on efferent limbs, etc. These sub groups are actually the variants of the "crossed" pattern. The capillary loops, showing single twisting, in Figure 3.6, are the only loops that were classified as "crossed" type by the agreement of the participating clinicians. Both of them are classified as "crossed" type by TANCCAS, as well.



The qualitative definition of "crossed" pattern is as follows; If a capillary loop does not display any form of branchings and "bushy" structure, and if the limbs are crossing over each other *at least once*, the capillary loop is a "crossed" type.

#### 3.4.4 Classification Criteria of Bushy and Bizarre Patterns

Parametric classes (cuticulis, "open", "tortuous") and "crossed" type capillary loops are finger like shaped. Their limbs do not show any form of branchings and budding. "Bushy" loops and "bizarre" structures, however, have got atypical morphology. Gibson et al.'s [56] patterns; from F to H and Houtman et al.'s [86] patterns; "bushy" and coiled display exceptional structures compared to normal capillary morphology. Andrade et al. [90], for example, classified the capillary loops that originate small and multiple buds on their limbs, as "bushy" type. They also defined "bizarre" pattern as the capillary structures having unusual distinctive morphology that cannot be included in any of the common patterns; "open", "tortuous", cuticulis, "crossed", "bushy" and "enlarged".

The classification results of the clinicians did not present any "bushy" capillary loops in the test images. However, the individuals; clinician-1 and 2, classified few loops into "bushy" pattern. The clinicians 5 and 6, used an indecisive term "mixed", for nearly all of the atypical capillary structures in the test images. Under these conditions, deriving a classification criterion from the clinicians evaluations proved to be almost impossible.

Some of the atypical capillary loops in the test images are presented in Figure 3.7. The capillary structures show enormous variations. All of the structures, apart from the capillaries (i1:N7), (i5:N28) and (i3:N48), display grotesque branchings of the limbs. However the limbs of the capillary loops (i5:N28) and (i3:48) of Figure 3.7, are about to form multiple branches. This formation is accepted as budding of the limbs, and Andrade et al.'s [90] definition of "bushy" patterns approves that these two capillary loops can be classified as "bushy" type. Therefore, any atypical capillary loop displaying small buddings on its limbs will be classified as "bushy", and any atypical structure that displays fully formed branches on its body will be classified as "bizarre" pattern.

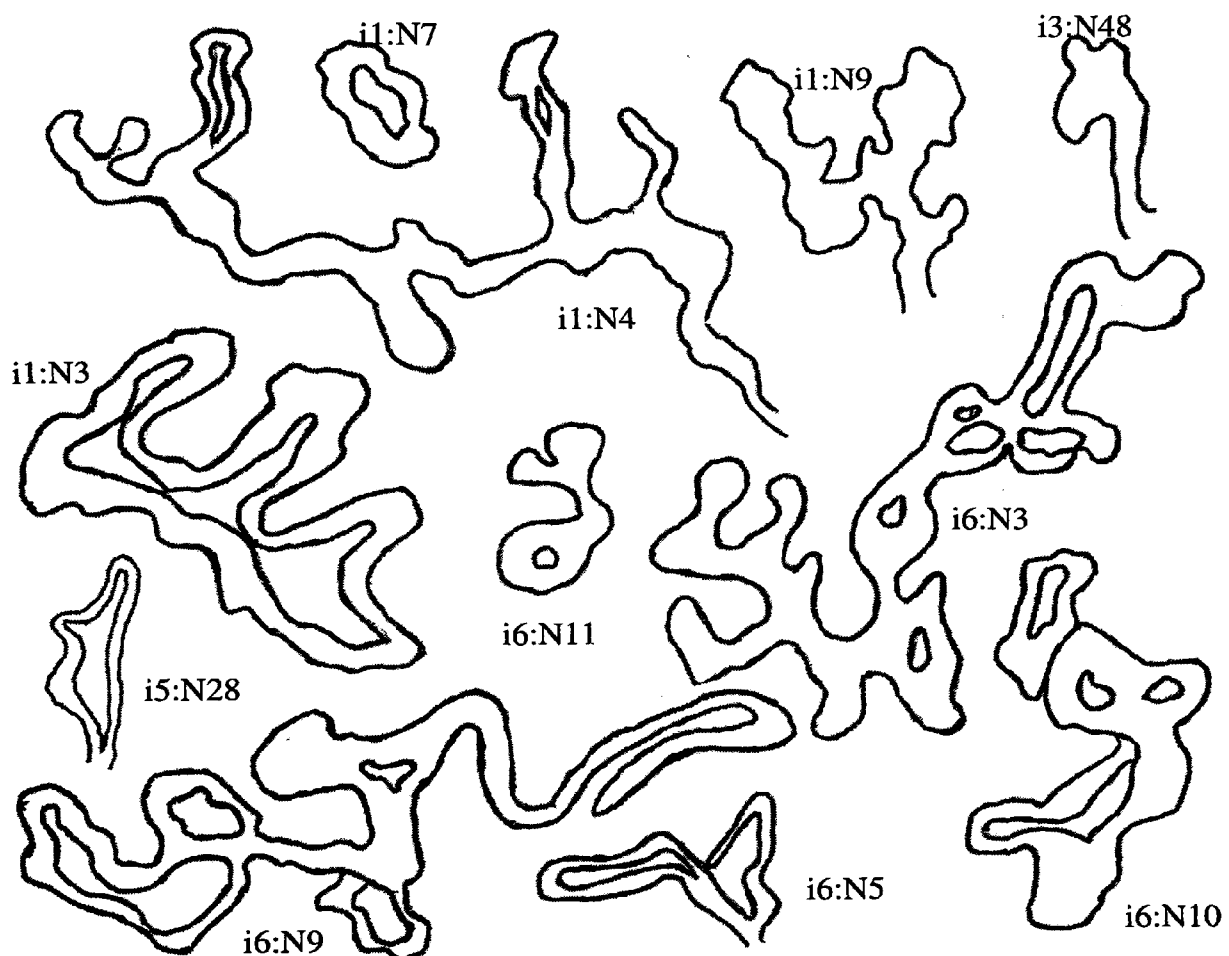


**Figure 3.7** Atypical capillary structures in the test images

In this case definitions of the atypical structure and fully formed branch must be clearly defined in order to prevent possible misclassifications. The "open" (i3:N22) and "tortuous" (i2:N20) capillary loops of Figure 3.8, are fine examples of typical capillary



morphology. Both of them display typical hairpin configuration of nailfold capillary loops. Their medial axis is a single line that passes through the points equidistant to the outer boundary of capillary wall. The medial axes of the capillary structures (i1:N3), (i1:N9), (i5:N28) and (i3:N48) of Figure 3.8, however, are formed by several line segments. If the limbs of a capillary loop start forming small branches (as in the cases of (i5:N28) and (i3:N48)), or form fully developed branches (as in (i1:N3) and (i1:N9)) the capillary will deviate from typical hairpin configuration. Therefore atypical capillary loops can be identified by examining their medial axes. If the medial axis is drawn with more than one line segment, the capillary is either "bushy" or "bizarre" pattern.

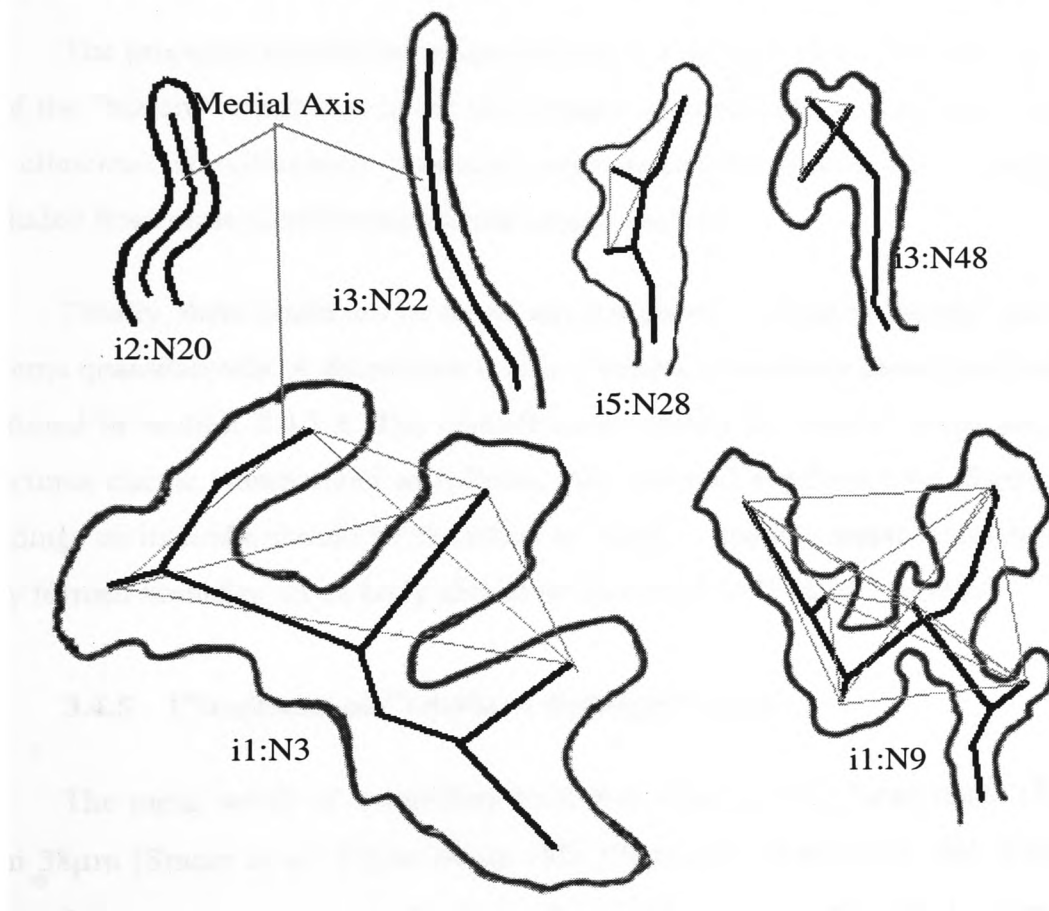


**Figure 3.8** Illustration of the classification mechanism of bushy and bizarre structures

There is, of course, a transition from the budding of a branch to fully developed branch. A decision mechanism should be constructed in order to eliminate misclassifications. The classification mechanism of "bushy" and "bizarre" structure is illustrated in Figure 3.8. First connect each "open" end of a medial axis segment to

another one's, with an imaginary line, except the bottom segment's end point. Then check whether all of the imaginary lines lie completely inside the outer boundary of a capillary loop, or not. If all of the lines are inside the capillary wall (as in (i3:N48) and (i5:N28)), it can be classified as "bushy" type. If the branches are fully developed, then some parts of the imaginary lines will be lying outside of the loop boundary (as in (i1:N3) and (i1:N9)). Buddings of the branches usually occur at the upper part of a capillary loop, as in (i3:N48). If the end point of bottom segment of the medial axis was connected to the other end points with imaginary lines, almost every budding loop would be mis-classified.

The proposed identification mechanism is used by TANCCAS and 71% (5 out of 7) of the "bizarre" capillaries in the test images are identified successfully. Note that, if the clinicians classifications produced joint consensus classes for a capillary it is excluded from class identification performance analysis.

Finally, there could not be found any parameter to identify "bushy" and "bizarre" patterns quantitatively. A discussion on the attempts to quantify their classifications can be found in section 5.4.3.3. The classification criteria of "bushy" loops and "bizarre" structures can be summarized as follows; Any atypical capillary loop displaying small buddings on its limbs should be classified as "bushy", and any atypical structure displays fully formed branches on its body should be classified as "bizarre" pattern.

### **3.4.5 Classification Criteria of Enlarged Loops**

The mean width of a capillary loop was reported in a large range (Table 7.6), from 38 $\mu$ m [Studer et al. 91] to 64 $\mu$ m (SD 17 $\mu$ m) [Michoud et al. 94]. The capillary loops whose loop widths are wider than a threshold value, are classified as "enlarged" in the literature [Zufferey et al. 92, Carpentier and Maricq 90, Kabasakal et al. 96]. Zufferey et al. [92], and Carpentier and Maricq [90], defined the threshold loop width for "enlarged" capillaries as 50 $\mu$ m. The capillary loops, that are thinner than 50 $\mu$ m, were accepted within normal limits. Kabasakal et al. [96], however, divided the capillary loops into 4 categories according to their loop width; to be of normal width (<25 $\mu$ m),

slightly widened (1-3 X normal), definitely widened (4-10 $\mu$ m X normal) and giant (>10 X normal). Maricq [81] and Andrade et al. [90], made similar categorization of the loop width. If the capillary loops enlarged about 4 and 10 times the normal width, Andrade et al. [90], classified them as ectatic and megacapillary loops, respectively. [Houtman et al. 86], on the other hand, controlled the limb width of the capillary loops. They classified the loops, that have wider limbs than 38.5 $\mu$ m, as "enlarged".

If the inner boundary of the capillary loop is visible, the majority of the clinicians displayed tendencies to classify the loop as "enlarged". The clinician 4 for example, classified the loop (i2:N11), that displays the inner boundary, and has 64.65 $\mu$ m loop width, as "enlarged", and classified the loop (i2:N22), that does not exhibit the inner boundary, and has 80.53 $\mu$ m loop width, as "open" type. Although (i2:N22) is larger than (i2:N11), the clinician was influenced by the presence of the inner boundary. The same attitudes were observed from the other clinicians as well. Furthermore, the clinicians 5 and 6, however, classified some of the loops, that do not exhibit the inner boundary, as "enlarged". Surprisingly, these two clinicians assigned "enlarged" to some of the loops, for example (i3:N2), (i3:N5), (i3:N11), (i3:N30), (i3:N31) that are, actually elongated, and their enlargements are not significant at all. Inappropriate use of class "enlarged" by the clinicians, resulted in not being able to set a threshold value for the detection of "enlarged" loops.

Although it is possible to adopt one of the threshold values reported in the literature, the majority of the clinicians' behaviour has been mimicked for the computerized classification. However, the program can be easily adapted to use a threshold value, that might be defined with a further study, for the classification of "enlarged" loops.

#### **3.4.6 Classification Criteria of Giant Loops**

A capillary loop, that has extremely widened limbs and loop width, are considered as abnormal, and often called megacapillaries [Andrade et al. 90] or "giant" capillaries [Kabasakal et al. 96, Houtman et al. 86, Rouen et al. 72, Carpentier and Maricq 90]. Giant capillaries can be identified quantitatively. Loop width [Andrade et

al. 90, Maricq 81, Kabasakal et al. 96] , limb width [Houtman et al. 86, Carpentier and Maricq 90] and limb surface area [Rouen et al. 72] were used to set a threshold to identify "giant" capillary loops. According to Andrade et al. [90], Maricq and Kabasakal et al. [96], the "giant" loop width must be more than ten times the normal loop width. Kabasakal et al. [96] for example, reported the normal loop width threshold as  $25\mu\text{m}$ , therefore, the "giant" loop width threshold value is set to  $250\mu\text{m}$ . Carpentier and Maricq [90], however, reported the threshold loop width as  $150\mu\text{m}$ . Houtman et al. [86], on the other hand, defined the threshold value of "giant" loops' limb width as  $77\mu\text{m}$  (or approximately "giant" loop width  $>231\mu\text{m}$ ).

According to the classification results of the clinicians, there is only one "giant" capillary loop (i5:N27) in the test images. The limb and loop width of the capillary loop (i5:N27) are calculated as  $48.48\mu\text{m}$  and  $167\mu\text{m}$ . None of the threshold values that were set by the previous researchers, are capable of detecting the only "giant" loop of the test images. Hence a threshold value,  $\text{LimbWidth}_{\text{GIANT}}=36.8\mu\text{m}$  was calculated and the details of its selection can be found in section 6.5. In addition to the capillary loop (i5:N27), three "giant" loops (i1:N1), (i5:N11) and (i5:N43) have limb widths wider than  $\text{LimbWidth}_{\text{GIANT}}$ . All of the "giant" loops of test images are given in Figure 3.9. The normal capillary loop (i3:N32) that has got  $44.26\mu\text{m}$  loop width and  $250.21\mu\text{m}$  loop length, is included in Figure 3.9, for visual comparisons.

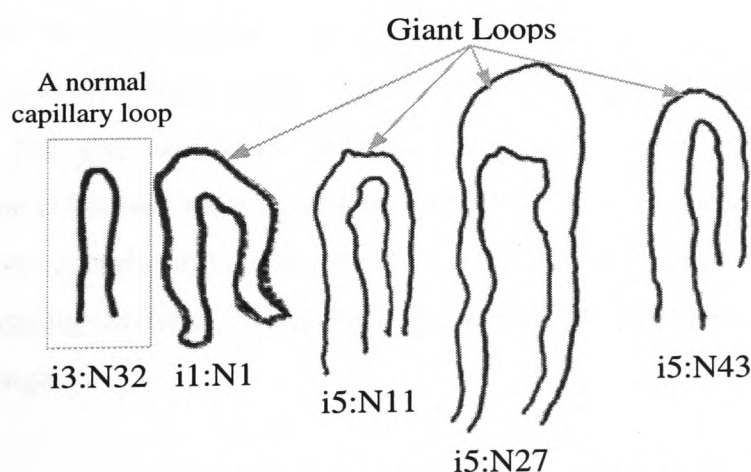


**Figure 3.9** Giant capillary loops of the test images.

The qualitative classification criteria of "giant" capillary loops can be given as follows; any "open" or "tortuous" pattern capillary loop, that has got limb width wider than  $\text{LimbLength}_{\text{GIANT}}=36.8\mu\text{m}$ , can be tagged with the label "giant".

### 3.4.7 Classification Criteria of Elongated Loops

Elongation of a capillary loop can be identified quantitatively by checking its loop length with a threshold value. Kabasakal et al. [96], classified the loops longer than  $300\mu\text{m}$  as "elongated" capillaries. This is the only critical length value found in the literature review. On the other hand,  $342.72\mu\text{m}$  is calculated as the critical loop length for "elongated" loops ( $\text{Length}_{\text{ELONGATED}}$ ) from the test images. Any "open" or "tortuous" capillary loop that has got observable length longer than  $342.72\mu\text{m}$  was tagged with the label "elongated", in this study. The selection of  $\text{Length}_{\text{ELONGATED}}$  can be found in section 6.4.

There are 44 capillary loops whose length are longer than threshold  $\text{Length}_{\text{ELONGATED}}$ , in the test images (Appendix A). Clinician-1 and 6 are the ones that classified some of the loops as "elongated". In clinician 1's classification result there are 41 "elongated" loops, and only 24 of them match with those 44 "elongated" loops, and clinician 6 assigned only one loop (i5:N20) with "elongated". The rest of the clinicians, however, concentrated on other morphological features of the loops such as, enlargement and the loop pattern ("open" or "tortuous"). Although, the critical length  $\text{Length}_{\text{ELONGATED}}$  is  $42.72\mu\text{m}$  longer than Kabasakal et al.'s [96] threshold value, the clinicians still felt that the other morphological features are more dominant than elongation. If the clinicians were aiming to find a link between a disease and the current nailfold capillary morphology, elongation of the capillary loops would be ignored. However, by tagging the label "elongated", the researchers will pay attention to the lost information elongation.

In conclusion; if the length of an "open" or "tortuous" capillary loop is longer than  $342.72\mu\text{m}$ , it can be tagged with the label class "elongated".

# **CHAPTER 4**

## Chapter 4 Image Processing Library of TANCCAS

### 4.1 Automation Strategy of The Classification Criteria

The important characteristics of nailfold capillary loops within a class have been highlighted in the proposed classification criteria in Chapter 3. Clinicians can identify some of these characteristics without making any analysis. Crossings of the capillary limbs over each other, long branchings, highly tortuous or straight loops, for example, do not require any calculations for clinicians. However, with no exception every capillary loop should be processed and analysed for automated recognition using various image processing and pattern recognition techniques. First of all, a capillary loop must be extracted from image to be able to identify its characteristics.

An image is a set of numbers stored in an array for a computer. While it is a very simple task to locate a capillary loop in an image for a clinician, a computer requires several calculations, transformations to decide which numbers represent objects and background. Furthermore, it has to be decided which foreground elements form a loop. *Thresholding* is a tool used for object background classification in an image array. Individual objects can be identified by *Labelling* that is assignment of a number to a group of foreground elements that are isolated by background. All the objects belong to same capillary loop are located inside the outer boundaries of the loop. Obtaining an enclosed area by connecting end points of outer boundary and assigning the same label to every object within enclosed area, a loop can be identified. This can be achieved by using geometrical and logical operations such as *Line Draw*, *Flood Fill*, *AND*, *OR*, *EXOR*, etc.

After identifying individual loops, they should be analysed to identify their important characteristics that are outlined by the proposed classification criteria. The thought process that is created the criteria is summarized in the following sub-sections.

#### 4.1.1 Atypical Loops.

Capillary loops can be decomposed into chains using medial axis transform (*skeletonization*). While decomposition of atypical loops, "bushy" and "bizarre" produce skeletons that have multiple chains, the skeletons of the remaining loop types have a single chain. This property can be used to filter out atypical structures from rest of the loops.

The popular shape descriptor *compactness* is the ratio between square of object boundary length and its area. It can be used to distinguish "bizarre" and "bushy" loops from one another. A circle is the most compact object in Euclidean space ( $compactness=1$ ). If a circular object is degenerated and become longitudinal, the object's compactness value will be higher than its circular formation's. Since the difference between "bizarre" and "bushy" loops is that "bizarre" structures has got fully developed longitudinal branches, compactness of "bizarre" structures is expected to be higher than "bushy" ones. However, some of the "bushy" loops that buddings occur without enlargement of the capillary body, are more compact than some of the "bizarre" structures that have got enlarged body and branches. Therefore the use of compactness as a delimiter of "bizarre" and "bushy" loops should be abandoned.

Another idea to differentiate "bizarre" and "bushy" loops is to measure *convex hulls* of a loop. Defining a critical ratio between convex height and convex base length, any loop that has a deep hull but narrow base can be identified as "bizarre" type. However if the long branches are far away from each other the "bizarre" structures will be mis-classified as "bushy" .

As it stated earlier on atypical loops have got multiple branches on their skeletons. Tip points of the long branches are located away from main loop body. Tip points of the buddings, on the other hand, are located close to the main body. If we can determine how far a branch's tip point is to main loop body, we can also identify "bizarre" and "bushy" loops. By connecting tip points of the branches that form skeleton



of the loop with lines, and checking whether they intersect with loop's outer boundary, we can determine geometrically how long branches are. If the lines do not intersect with loop's outer boundary, it is a "bushy" loop, otherwise it is a "bizarre" one. This classification method has produced the most satisfactory results, and has been proposed for identification of atypical loops.

#### **4.1.2 Crossed Loops**

"crossed" capillary loops have got the most distinguished characteristics, crossings of the limbs. "crossed" capillary loop boundary produces enclosed areas due to the limb crossings. Detection of such areas can be achieved by using image processing utility functions *Flood Fill*, *Color Replacer* and logical operation *NOT*. However, while experimenting with capillary loop tracings, this method proved not to be useful. In real capillary loop images it has been observed that a loop's boundary can form encircled areas, although the loop is not "crossed" type.

The skeleton of the "crossed" loops will have two long branches at the bottom, and the skeleton will be passing through the enclosed area that is formed by the crossing of the loop limbs. *Labelling* operations can be used to calculate the number of skeletal chains. The location of the branches can be determined relative to the *orientation and center of gravity* of the loop. By analysing the "crossed" loop's skeleton, automated recognition can be achieved.

#### **4.1.3 Open and Tortuous Loops**

An ideal "open" loop is almost straight, while a "tortuous" loop is snake-like. The first suggested method for the recognition of "open" and "tortuous" loops, was as follows. First, obtain the loop's skeleton and draw an imaginary line between the end points of the skeleton. If the skeleton crosses this line, it can be "tortuous" loop. However there are many "open" and "tortuous" loop formations that caused to abandon the use of this method.

The second method was to interpret the diagrams that were drawn as a function of the length of the *polygonally approximated* skeleton line segments and the angles between two consecutive segments. The segment groups that have either '+' or '-' angles represent a concave or convex on the skeleton. The line segments that have alternating signs represent the straight portions of the skeleton. The number of convexities and their significance on overall appearance was the key for "open" and "tortuous" loops' classification. However, "bi-lobed" shaped "tortuous" loops produce straight skeletons and they will be mis-classified by the use of this method. Of course this was not the only draw back. Recognition of the loops near to class border line was extremely difficult because of the large range of angles and their relative positions on a skeleton.

The third method is the improvement of the second method. This time the convexities are obtained from directly from skeleton rather than a diagram by checking the direction changes of the skeleton line segments. In the meantime the idea of approximating each convex to an arc, and representing each arc with a single numeric value *exclusive curvature angle* is put forward. Lower angle values are accepted as low tortuosity segments or vice versa. In order to eliminate misclassification of "bi-lobed" loops, tortuosity analyses are carried on both side chains that are obtained by slicing off the tip portion of a loop, instead of loop skeleton. By this final arrangement the proposed classification method has been developed, and its automation can be achieved.

#### **4.1.4 Cuticulis Loops**

Since a "cuticulis" capillary is the visible tip portions of a capillary loop, it is distinctively smaller than other capillary loop types. Therefore "cuticulis" loop boundary chain length should be short. However a critical chain length for the classifications of "cuticulis" loops can be inefficient for automation. Some of the enlarged "cuticulis" loops have longer boundary chain than some of the "open" loops (Figure 3.1(c)). *Surface area* of the loop cannot be useful for the same reasons. A ratio between loop length and width can be successfully employed as the delimiter of the "cuticulis" loops. Although, "cuticulis" *loop length* and *width* can be measured easily for manual computations, their

calculations are problematic for an automated system. The skeleton length of a loop can be accepted as loop length, and by dividing a loop's surface area with loop length, loop width can be obtained. However during the experiments, some "cuticulis" loops produced dis-oriented skeletons that cause mis-calculations. These mis-classifications were accepted as the pitfalls of the system, until the employment of *the circular arc approximation*.

Every loop can be represented with a single numerical value, exclusive curvature angle  $\theta$ . Theta is the central angle that sees the circular arc that is the approximation of a loop. In theory, theta value should be less than  $180^\circ$  for "cuticulis" loops. However, in practice, theta can exceed  $180^\circ$  for "cuticulis" loops. Defining a critical angle value, "cuticulis" loops can be successfully identified

## **4.2 Introduction To Image Processing Library of TANCCAS**

An image processing software is needed to carry out the experiments described in previous section and to implement the proposed classification criteria. Although it is possible to use commercially available image processing system development packages, for example Visilog4, the user is usually restricted by the packages' abilities. By using its C interpreter, it is possible to extend Visilog4's capabilities. However, the interpreter does not support *pointers, addresses* and some of the C operators such as; *switch, case, break, goto and continue*. Additionally, if the user wants to modify an existing library function, he may end up writing the whole function from the beginning. Therefore, instead of struggling to overcome the incapacibilities of a commercial package, it was decided to develop our own software independent from any other commercial package. The Automated Nailfold Capillary Classification and Analysis System (TANCCAS) had been developed using Borland C programming environment. The image processing library of TANCCAS consists of the following functions.

## **Shape Representation and Description Functions:**

### ***Boundary Descriptors;***

Polygonal Approximation

### ***Region Identification;***

Labelling

FCR Labelling

RS Labelling

### ***Region based shape representation;***

Region Skeleton by thinning,

Thinning by logical and arithmetical operations,

### ***Scalar region descriptors***

area,

height,

width,

compactness,

circular approximation,

orientation,

## **Mathematical Morphology Operations**

Erosion,

Dilation,

Opening,

Closing,

Pruning,

Boundary Extraction

## **Arithmetical Operations**

Addition,

Subtraction

Multiplication of an image with a constant

Addition,

Subtraction

Multiplication of two images.

## **Logical Operations**

NOT,

AND,

OR,

EXOR

## **Geometrical Tools**

Flood Fill,

LineDraw,

Conditional Line Draw

## **Miscellaneous Functions**

Image Allocate,

Image Display,

Image Copy,

Image Set,

Color Replacer,

Thresholding

In the following sections some of these functions will be briefly explained and their psuedocode will be given.

### 4.2.1 Thresholding

Thresholding, also known as binarization, is a popular tool used in image segmentation. It is the transformation of an input image  $f$  to an output binary image  $g$  as follows:

$$\begin{aligned}g(i,j) &= 1 \text{ for } f(i,j) \leq T \\ &= 0 \text{ for } f(i,j) > T\end{aligned}$$

where  $T$  is the threshold,  $g(i,j) = 1$  for image elements of objects, and  $g(i,j) = 0$  for image elements of the background. The choice of the  $T$  can be based on the image histogram. The thresholding techniques can be classified in two main groups as global [Pal and Bahandari 92, Angela et al. 82, Babaguchi et al. 90] and local thresholding methods [Hertz and Schafer 88], global thresholding can, further, be divided into point dependent and region dependent techniques [Wang and Haralick 84]. The type of global thresholding just described can be expected to be practical in highly controlled environments. Since the background and objects of the hand traced images of nailfold capillaries can be segmented simply by choosing a *Threshold* value, there is no need to employ or test any other thresholding method. An excellent survey of thresholding techniques can be obtained from Sahoo et al [88]. The details of some of these techniques can be found in the image processing books [Gonzales and Woods 92, Sonka et al. 94, Pitas 93]. Pseudocode of **Thresholding()** function of TANCCAS is given below;

```
Threshold(image array, threshold, number of rows, number of columns)  
begin  
  for every array element  
    if image arrayi,j ≤ threshold then image arrayi,j = 1;  
    else image arrayi,j = 0 ;  
end.
```

### 4.2.2 Mathematical Morphology Operations

**Mathematical Morphology (MM)** is a tool for extracting image components that are useful in the representation and description of region shape, such as boundaries,

skeletons. MM operations tend to simplify image data and preserve the main shape characteristics of objects. The language of MM is set theory. Sets in MM denote the shapes of objects in an image. The set of all black pixels in a binary image is a complete description of the image (the set in question is a member of 2-D integer space  $Z^2$  where each element of the set is a 2-D vector whose coordinates are the (x, y) coordinates of black pixel). Gray scale images can be represented as sets whose components are in  $Z^3$ . Two components of each element of the set refer to the coordinates of a gray pixel, and the third refers to its discrete intensity level. The tutorial paper of Haralick et al. [87] covers basic morphological transformations in both binary and gray scale images. Exact mathematical explanations of MM operations can be obtained from Wilson [92] and Bleau et al. [92a]. The basics of the MM are presented in most of the image processing books [Sonka 94, Gonzales and Woods 92, Pitas 93].

#### 4.2.2.1 Boundary Extraction

The boundary of a set X, denoted by  $\beta(X)$ , can be obtained by first eroding X by B (B is a suitable structuring element) and then performing the set difference between X and its erosion.  $\beta(X)$  can be given as follows;

$$\beta(X) = X - (X \ominus B)$$

The thickness of the boundary is related to the size of the structuring element B. While the most frequently used 3x3 structuring element of 1's produce one or two pixels thick boundary, 5x5 structuring element of 1's result in a boundary between 2 and 3 pixel thick. The pseudo code of boundary extraction is given below;

X	1	X
1	1	1
X	1	X

```

template array (B) =
B_Edge(array1,array2, template array, number of rows, number of columns)
begin
  for every active element of array1i,j
    if central element of template array1,1 is on the object
      for every element of template arrayk,l
        if template arrayk,l = array1i+k,j+l then array2i,j=0
        else array2i,j =array1i,j
end.

```

#### 4.2.2.2 Skeletonization

Object "skeleton" is an important topological shape descriptor [Rosenfeld 86] of a two dimensional binary or gray level images, and had been used extensively in various applications [Levine 85, Ogniewicz and Ilg 92]. Shape description by employing its skeleton was originated by Blum [67] who used the term medial axis. Medial Axis (MA) can be obtained by setting up a 'grass fire' [Xia 89, Wright and Fallside 93] simultaneously along the object boundary at  $t=0$ . MA is formed by the points where fire wavefronts intersects and extinguish. The term "skeleton" has been used in general to denote a representation of a pattern by a collection of thin (or nearly thin) arcs and curves [Shaked and Bruckstein 96], and the term "medial axis transform" is used to denote the locus of centers of maximal blocks that are also equivalent to the local maxima of chessboard distance. In this section, the term "skeleton" is used to refer to the result, *regardless* of the shape of the original pattern or the *method* employed.

Skeletonization is a powerful tool to reduce the amount of information to be processed to the minimum necessary for the recognition of patterns [Rom and Medioni 92]. Perhaps as a result of its central role in the preprocessing of data images, the design of thinning algorithms has been very active research area. Mathematical morphology is a powerful tool used to find the region skeleton [Jang et al. 90, Bleau et al. 92b] . Neural Networks and Voronoi diagram approach [Brandt and Algazi 92, Ogniewicz and Ilg 92] can also be applied to find the skeleton. In order to speed up computational time fast parallel algorithms [Hayat et al. 91, Guo and Hall 91] and architectures [Milgram and Pierre 90] are employed for thinning operations. A comprehensive survey on thinning methodologies can be found in Lam et al.[ 92].

Two different algorithm; skeleton by MM operation thinning (Skeleton()) and thinning by logical and arithmetical operations (Thinning()) are implemented in order to find the skeleton of capillary loops in this study. The function Skeleton() employs the mathematical morphology operation thinning by eight different structural elements that are listed in Figure 4.1. The conversion continues till there is no changed pixel found.

After the conversions, the resulting skeletons are 4-connected, in order to ensure the skeletons consist of one pixel thick chains, 4-connected skeletons are transferred to m-connected ones.

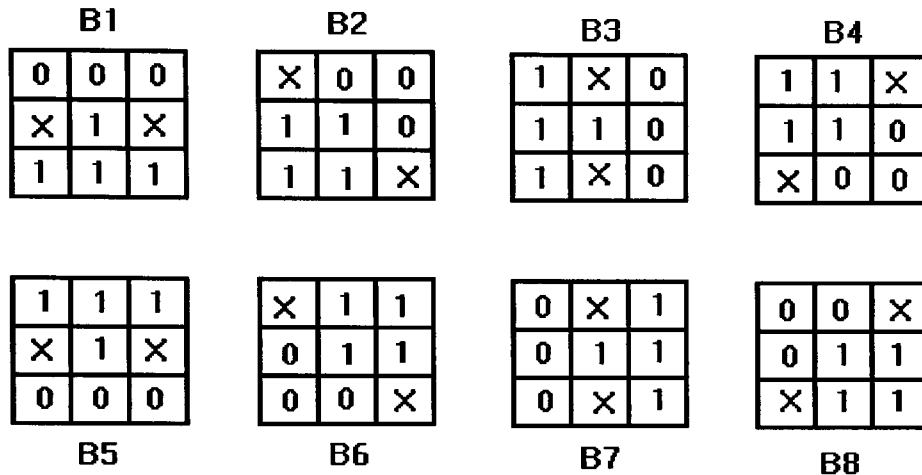


*Figure 4.1* The structural elements that used in *Skeleton()* function. X denotes “don’t care” condition

```

Skeleton(array1, array2, number of rows, number of columns)
begin
  repeat
    total+changed_pixels=0;
    B_Thinning(array1,array2,B1.rows,columns)
    B_Thinning(array2,array1,B2.rows,columns)
    B_Thinning(array1,array2,B3.rows,columns)
    B_Thinning(array2,array1,B4.rows,columns)
    B_Thinning(array1,array2,B5.rows,columns)
    B_Thinning(array2,array1,B6.rows,columns)
    B_Thinning(array1,array2,B7.rows,columns)
    B_Thinning(array2,array1,B8.rows,columns)
    calculate total_changed_pixels for one conversion
  until total_changed_pixels=0;
  {convert the 4-connected image into m-connected image}
end.

```



The function Thinning() consists of successive passes of two basic steps applied to the contour points of the object, where a contour point is any pixel with value 1 and having at least one 8-neighbour valued 0. With reference to the 8-neighbourhood definition, the contour points,  $p$ 's, are iteratively deleted until no further delation is possible, if the following conditions are satisfied:

(a)  $2 \leq N(p_1) \leq 6$ ;

(b)  $S(p_1) = 1$ ;

(c)  $p_2 \cdot p_4 \cdot p_6 = 0$ ;

(d)  $p_4 \cdot p_6 \cdot p_8 = 0$ ;

(c')  $p_2 \cdot p_4 \cdot p_8 = 0$ ;

(d')  $p_2 \cdot p_6 \cdot p_8 = 0$ ;

$p_9$	$p_2$	$p_3$
$p_8$	$p_1$	$p_4$
$p_7$	$p_6$	$p_5$

where  $N(p_1)$  is the number of nonzero neighbours of  $p_1$ , and  $S(p_1)$  is the number of 0-1 transitions in the ordered sequence of  $p_2, p_3, \dots, p_8, p_9, p_2$ . The conditions (c) and (d) are alternatively replaced by (c') and (d') for each iteration. The details of the method can be found in Gonzales and Wood [92] pp 492-5.

```

Thinning(array1, array2, number of rows, number of columns)
begin
  repeat
    total+changed_pixels=0;
    for every active element of  $array1_{i,j}$ 
      if ( $2 \leq N(p_1) \leq 6$ ) {it is a contour point} then calculate
        token1 =  $S(p_1)$  token2 =  $p_2 \cdot p_4 \cdot p_6$  token 3 =  $p_4 \cdot p_6 \cdot p_8$ 
        if (token1 · token2 · token3=1)  $array2_{ij} = 0$ 
      COPY(array2 to array1)
    for every active element of  $array2_{i,j}$ 
      if ( $2 \leq N(p_1) \leq 6$ ) {it is a contour point} then calculate
        token1 =  $S(p_1)$  token2 =  $p_2 \cdot p_4 \cdot p_8$  token 3 =  $p_2 \cdot p_6 \cdot p_8$ 
        if (token1 · token2 · token3=1)  $array2_{ij} = 0$ 
      COPY(array2 to array1)
    calculate total_changed_pixels for one conversion
  until total_changed_pixels=0;
  {convert the 4-connected image into m-connected image}
end.

```

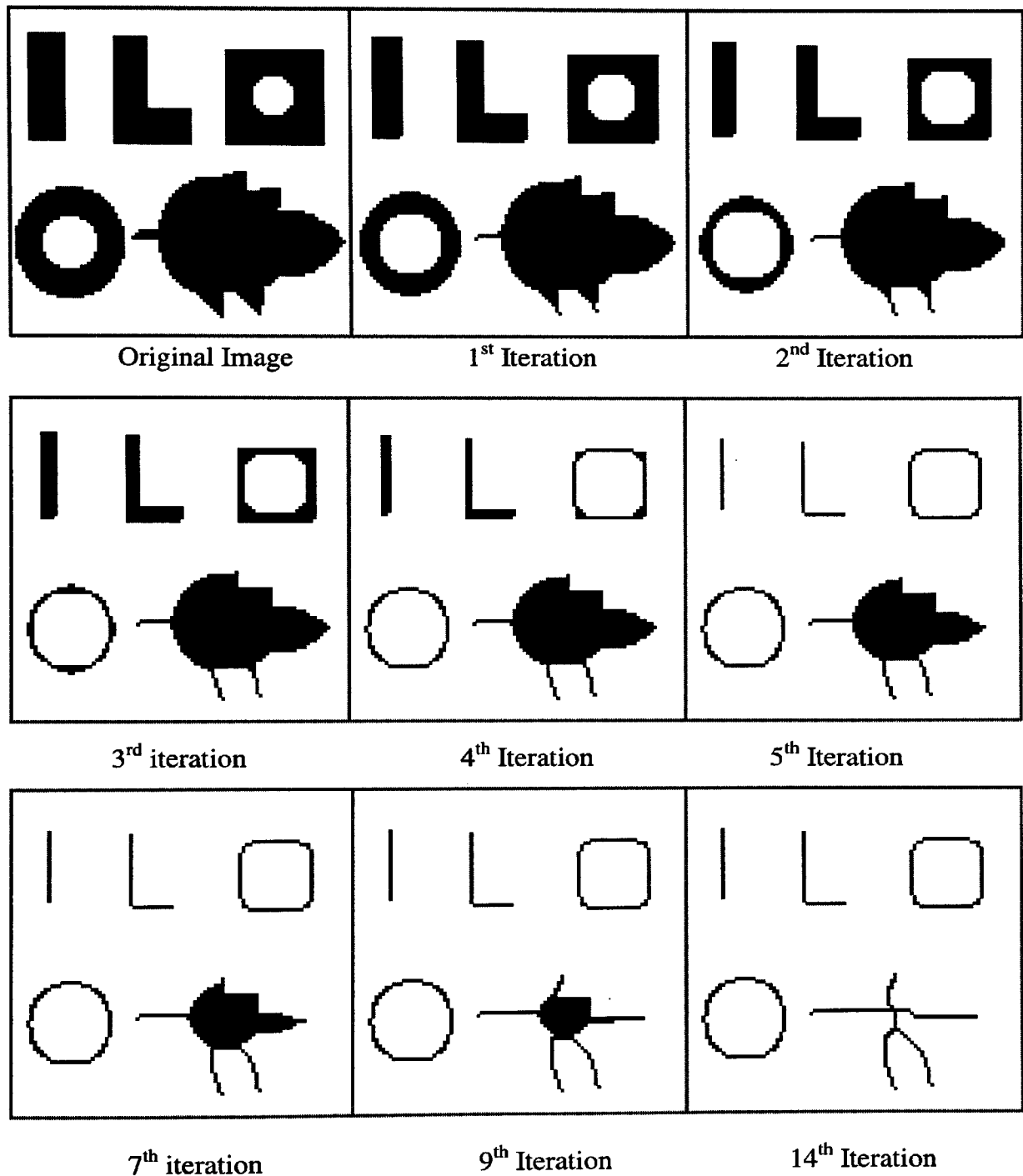


**Figure 4.2(a)** Thinning() operation on an artificial binary image by sequential logical and arithmetical operations . The function is insensitive to boundary corners and noise.

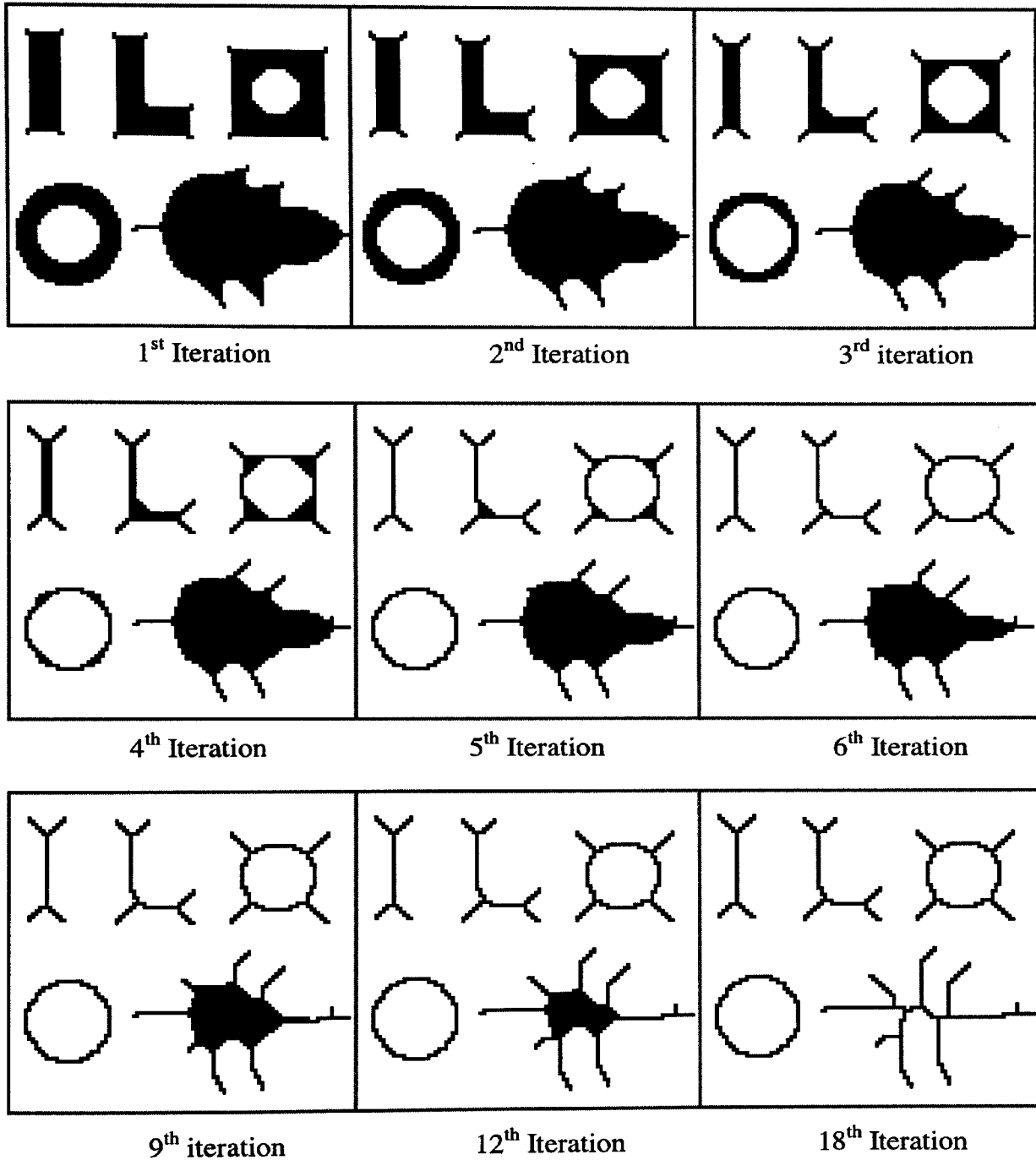


*Figure 4.2(b) Skeleton() operation on the artificial binary image by using sequential mathematical morphology operation thinning (structural element  $B^8$  is given in figure 4.1). The function is sensitive to boundary corners and noise.*

Thinning() function is less sensitive to the boundary noise and corners than Skeleton() (Figure 4.2(a) and (b)). The boundaries can be smoothed by the closing operation or polygonal approximation. By using various structuring elements, the sensitivity of the Skeleton() algorithm can be reduced or increased [Sonka et al 93]. Because of producing less 'spur' branches, the Thinning() algorithm is employed in order to obtain the skeleton of the enclosed capillary loops for the calculation of capillary loop length and classification of "bizarre"/"bushy" loops.

#### 4.2.2.3 Pruning

Pruning methods are an essential complement of thinning and skeletonizing algorithms, because these procedures leave parasitic components that need to be cleaned up by post processing. Gonzalez and Woods [91] suggest an algorithm to remove the spur branches that are less than 4 pixels, the formulation for this algorithm is:

$$\begin{aligned}
 X_1 &= A \otimes \{B\} \\
 X_2 &= \cup_{k=1} (X_k \otimes B^k) \\
 X_3 &= (X_2 \oplus H) \cap A \\
 X_4 &= X_1 \cup X_3
 \end{aligned}$$

The explanation and application steps of these formulae can be found in Gonzales and Woods [91]. To complete three pixel pruning the algorithm needs scan the whole image 18 times, but the algorithm presented below, that uses labelling for pruning, need to scan 8 times.

**Prune(*image array*, *size*, *number of rows*, *number of columns*)**

**begin**

label=2

**repeat**

**for** every active element of *image array*<sub>*i,j*</sub>

total\_active\_neighbours=0

**for** every neighbour

**if** neighbour<sub>*k,l*</sub>=1 **then** increment total\_active\_neighbours

*-continues on the next page-*

-continued-

```

    else if neighboursk,l=label then set total_active_neighbours=10
    if total active neighbours=2 it is an end point then image arrayi,j=label
increment label
until label=size+2

    { size number pixel elements from end points are labeled, if the pixel has
      got more than 2 active neighbour, any label has been assigned }
label=size+1
repeat
    for every active element of image arrayi,j
        if the biggest label assigned by label+1 is not in neighbourhood
            then delete the current pixel of image arrayi,j
            else preserve the neighbour label+1 for restoration
    decrement label;
until label=0

    { All the successive labels are deleted apart from label=2, and longer
      branches than size are restored in image array. }
for every image arrayi,j element labeled to 2
    if image arrayi,j is isolated point then delete it
    else restore it
end.
```

The function of Prune() is illustrated in Figure 4.3. The algorithm iteratively searches for the tip point of chains that consists of active elements '1's or 'n's ('n's could be the labels previously initialized). If the current pixel is a tip point then replace it with the label '2', '3' or '4' in 1<sup>st</sup>, 2<sup>nd</sup> or 3<sup>rd</sup> iterations, respectively, for three pixels pruning. Label '4' will not be assigned to the adjoining point of upper right two branches of middle object in Figure 4.3(b), although it appears to be an end point. because end points are searched by taking into account every nonzero element. In 4<sup>th</sup> iteration, the label '5' is assigned to approve restoration or deletion of labels '4' in 5<sup>th</sup> passing. If any image element that has label '4' has a neighbour labelled by '5', restore the neighbour,

otherwise remove the current pixel labelled by '4' (Figure 4.3(c)). Removal of label '4' will result the current pixels that have label '3' not having neighbours labelled '4'. Therefore propagation of pruning or restoration of the branches will be from adjoining points to the tip points. As it can be seen from Figure 4.3(d) Pruning() function not only removes the 'spur' branches that are less than 4 pixels in length but also filters out the small chains that are shorter than 7 pixels in length.

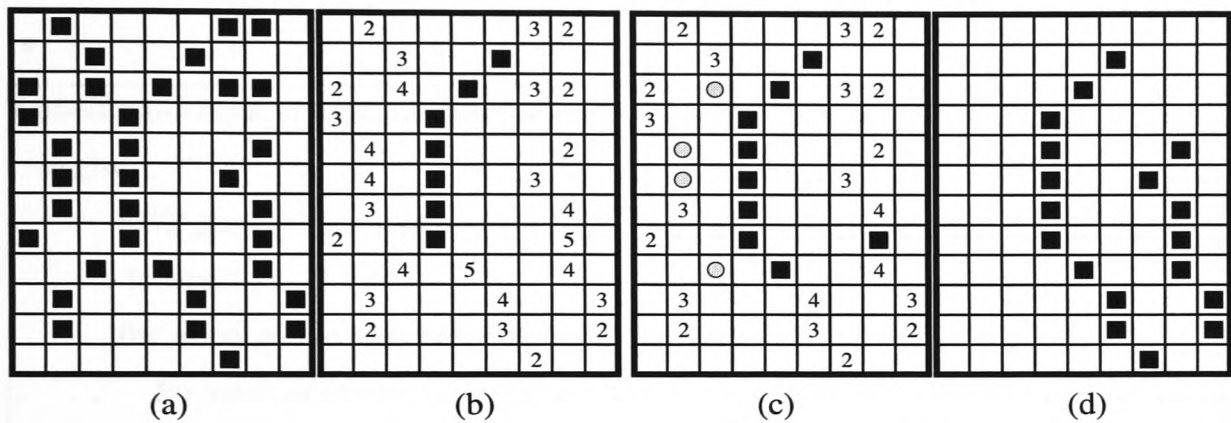


**Figure 4.3** Pruning by labelling (a) binary image to be pruned by 3 pixels (b) labelling of chains' end points (3+1 iteration) (c) Deletion of the pixels labelled 4 that have not got a neighbour that is labelled by 5, and restoration of pixels labelled 5 (in the next iteration deletion will be made on the pixels labelled 3 and restorations on the pixels labelled 4) (d) Prune() output of image (a)

### 4.2.3 Labelling

Connected component labelling (simply **labelling** or colouring) is a necessary process to give a unique (integer) identity number to each region for image understanding. The largest label (identity number) is, usually, the number of isolated regions in an image. In some methods, however, a small number of labels (usually four) are used to label the regions that any of two neighbouring regions have got different labels. Labelling algorithms can be divided into two classes; local neighborhood algorithms and divide-and-conquer algorithms. The algorithms belonging to the first class perform local operations. A unique label can be assigned recursively to each region (object) by scanning the image in a row-wise manner until the first pixel of the object's

boundary is hit, and setting a "grass fire", that propagates to all pixels belonging to 4 or 8-neighbourhood of the current pixel, until all pixels of the object are "burnt out". **FCR Labelling()** (Four Connected Recursive object Labelling) and **RS Labelling()** (8-connected Recursive *Segment* Labelling) functions of TANCCAS use such kind of method. However, the 'fire' is set only on the tip points of the chain for RS Labelling(), and extinguishes at the adjoining points of the chain segments. The output of RS Labelling and FCR Labelling can be found in Figure 5.19 and Figure 5.12, respectively.

```
Labelling(array1, array2, number of rows, number of columns)
```

```
begin
```

```
  SET_(array2,0,rows,cols)
```

```
  label=2;
```

```
  for every active element of array1i,j
```

```
    for west, north-west, north, and north-east neighbours of array1i,j
```

```
      if array1i,j is not labeled then
```

```
        array1i,j=0
```

```
        array2i,j=label;
```

```
        increment label
```

```
      else find the smallest label in neighbourhood
```

```
        array1i,j=0;
```

```
        array2i,j=smallest label;
```

```
    create a list[label] to hold the equalities
```

```
    Organize(list, label)
```

```
    for every labeled element of array2i,j
```

```
      array1i,j=new label {assigned by list[array2i,j ]}
```

```
  end.
```

Another local labelling algorithm [Ballard and Brown 82, Embrechts at al 93] that is described below, has been used for the **Labelling()** (8-connected *object* Labelling) function of TANCCAS. This algorithm scans the image twice. In the first

scan, the labels are assigned to object pixels by checking west, north, west-north and east-north neighbors of the current pixel. If at least one of the neighbors has been labelled in previous operations (label collision), then the current pixel is assigned by the smallest label of the labelled neighbors, and the collided labels are stored in a label equivalence list. If there is not any labeled element in the neighborhood then it assigns a new label number to the current pixel. After the first scan, the raw labeled image is obtained (Figure 4.4(b)). Then the function calls the Organize() function to define which label numbers are associated to each other, for example in Figure 4.4, the association list is {2=1, 3=1, 4=3, 5=1, 6=7}. Function Organize() creates a dynamic list to hold these equalities, however, for some images a label number does not indicate its root label. So that, the function Sorts() is called by Organize() in order to label every element of the chain with the same (root) label. Then, the number of unique labels is calculated by Organize(), accordingly the root labels are exchanged with new label numbers. For example in Figure 4.4(c), before this exchange the small chain and the large chains would be labeled 6 and 1 respectively. After organization of the labels, resulting image will be as shown in Figure 4.4(c).

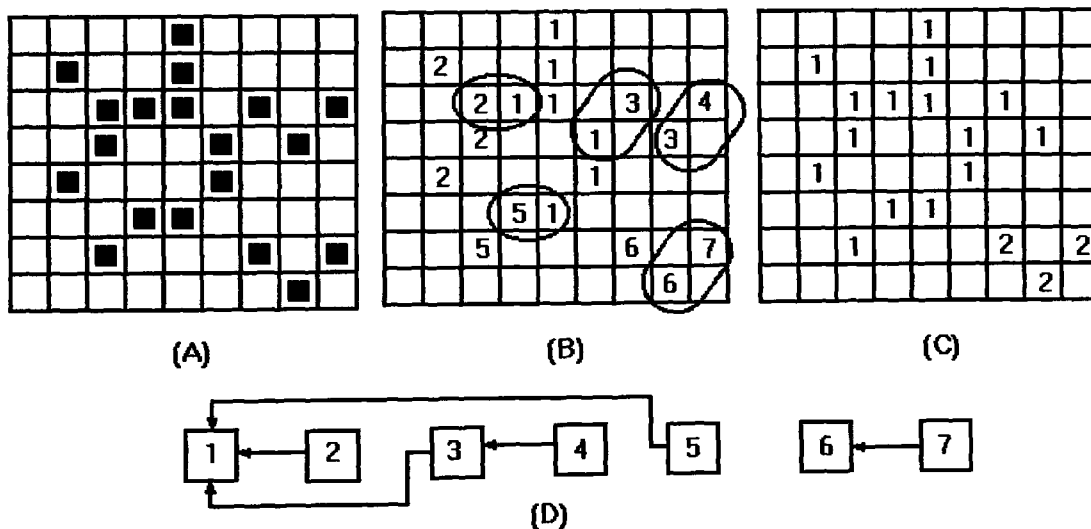


**Figure 4.4** The stages of the labelling algorithm; (a) Original image (b) After raw labelling (c) Labeled image (d) Equality list



#### **4.2.4 Polygonal Approximation**

In the applications that digital boundary (or curve) information carries vital information for identification of an object, approximation of the boundary to specified segments; lines [Lowe 87, Rosin and West 89], circular arcs [Rosin and West 89, Saund 93, Dori 95, Worring and Smeulders 95], elliptic arcs [Rosin et al. 95] or  $\beta$ -splines [Ikebe and Miyamoto 82, Lee and Pavlidis 88], to generate a representation scheme is an option for shape description. The goal of polygonal approximation is to capture the essence of the boundary shape with the fewest possible segments. The approximation can be achieved by recursively splitting the curve into its segments by fulfilling a preset criterion. A simple procedure for splitting starts by drawing an imaginary line between two end points of a curve. The next step searches all the curve points for the point with the largest distance from the imaginary line. If the point is within a preset distance between the line and itself, the curve can be represented by the line. Otherwise, the point is a new vertex, and the process recursively applied to both resulting segments (end\_point\_1, vertex) and (vertex, end\_point\_2). Similar splitting procedure can be applied to approximate the curves with 2<sup>nd</sup> or higher order polynomials. However, the specification of an circular or elliptical arc, or  $\beta$ -splines, requires more parameters as they have more degrees of freedom than a line.

#### **4.2.5 Scalar Descriptors**

##### **4.2.5.1 Area**

The simplest property of an object is its area, by counting the number of pixels that the object consists of in a rectangular raster, the area can be obtained.

##### **4.2.5.2 Length**

The length of a capillary loop is an important property for the classification of elongated loops. It can be easily calculated from the rectangle that bounds the loop.

However, with the increasing undulation of a loop, this measure cannot be acceptable. Instead, by polygonally approximating the loop's skeleton and calculating the total curve segments' length, LoopLength can be obtained. However, the **skeleton length** may not be the total loop length (Figure 4.5). The length of the gaps ( $G_{top}$  and  $G_{bottom}$ ) between skeleton tip points and the loop should be taken into account as well. By stretching the skeleton tip segments without changing their directions, until they intersect with the loop boundary,  $G_{top}$  and  $G_{bottom}$  can be calculated. Therefore total loop length will be

$$\text{LoopLength} = L_{\text{Segment 1}} + L_{\text{Segment 2}} + \dots + L_{\text{Segment n}} + G_{\text{top}} + G_{\text{bottom}}$$

#### 4.2.5.3 Width

Two different methods had been applied to calculate LoopWidth of a capillary loop. The first method, that was abandoned later on, is illustrated in Figure 4.5(a). The loop's width was calculated by averaging the loop segments' normalized widths. By drawing two lines that are perpendicular to a skeleton segment, from segment tip points, a loop slice can be obtained. Loop width, then, can be calculated by using the following formula:

$$\text{LoopWidth} = \frac{\sum_n \text{Area\_of\_Slice}_n}{\sum_n \text{Length\_of\_Segment}_n}$$

While this method producing accurate results for the loops like in Figure 4.5(b), because of the polygonal approximation, a loop might be sliced inappropriately (the first three bottom segment slices of the loop in Figure 4.5(a) are good examples of such cases). Naturally, such defects will cause calculation errors. Therefore for the calculation of LoopWidth, the following method is used; Assume that a loop can be approximated to a rectangle, since the loop total area and length are known, and these two parameters are also a rectangle's properties, then, loop width is

$$\text{LoopWidth} = \text{Area}/\text{LoopLength}$$

Semi circular tip point and irregular bottom segment may cause miscalculations, but their overall significancy are small. Although the calculation is not precise, it is safer than first method.

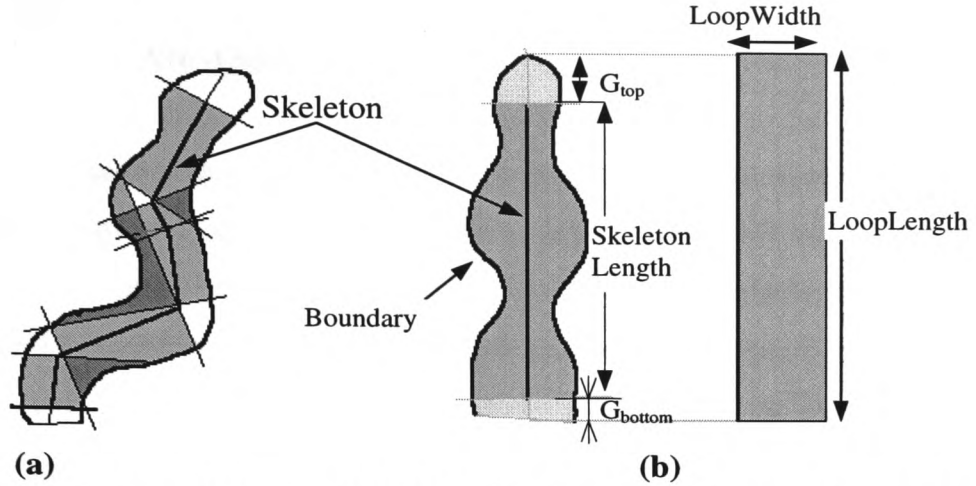


**Figure 4.5** Calculation of loop width by (a) 'slicing' method, (b) rectangular approximation.

#### 4.2.5.4 Orientation

Orientation is a property of elongated regions. If the shape moments are known the orientation  $\theta$  can be calculated as

$$\theta = \frac{1}{2} \tan^{-1} \left( \frac{2\mu_{11}}{\mu_{20} - \mu_{02}} \right)$$

where  $\mu_{pq}$  are central moments and can be calculated as

$$\mu_{pq} = \sum_{i=-\infty}^{\infty} \sum_{j=-\infty}^{\infty} (i-x_c)^p (j-y_c)^q f(i, j)$$

where  $x_c$  and  $y_c$  are the coordinates of the object's center of gravity which can be obtained by using the following relationships

$$x_c = \frac{m_{10}}{m_{00}} \quad y_c = \frac{m_{01}}{m_{00}} \quad m_{pq} = \sum_{i=-\infty}^{\infty} \sum_{j=-\infty}^{\infty} i^p j^q f(i, j)$$

#### 4.2.5.5 Compactness

Compactness is a popular shape description characteristic and independent of linear transformations. By using simple scalar descriptors, boundary length and area, it can be calculated as

$$compactness = \frac{(object\_boundary\_length)^2}{4\pi * Area}$$

The most compact object in a Euclidean space is a circle (compactness=1).

#### 4.2.5.6 Circular Arc Approximation

Circular arc approximation has been proposed to measure tortuosity of loop segments, and to represent capillary loops with a single numerical value, exclusive curvature angle  $\theta$ . An ideal "cuticulis" capillary loop (Figure 4.6) can be approximated to an arc of a circle. A critical ratio between LoopWidth and LoopLength can be used as a delimiter of "cuticulis" capillary loops. However, calculations of LoopWidth and LoopLength are proved to be difficult for "cuticulis" loops during the experiments. By measuring LoopPerimeter, and distance between loop end points, we can, still, define a delimiter, exclusive curvature angle( $\theta$ ), for "cuticulis" loops.  $\theta$  is the solution of

$$\sin c\theta = \frac{\sin \theta}{\theta} = \frac{\text{Distance\_Between\_Loop\_End\_Points}}{\text{LoopPerimeter}}$$

Capillary loop

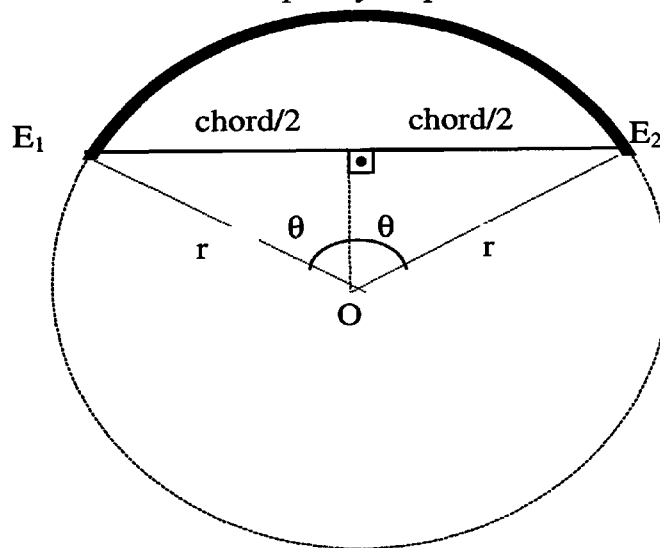


**Figure-4.6** Approximation of Cuticulis Capillaries to an Arc of Circle.

Assume that the capillary loop in question is an arc of the circle with radius  $r$  as in Figure-4.6. Projection distance between  $E_1$  and  $E_2$  (chord) and arc length can be easily calculated from the image. The central angle  $2\theta$  and radius  $r$  are unknown. The line, perpendicular to the chord passes through central point  $O$  and divides the chord into halves. Using one of the right-angled triangles

$$\text{chord}=2r \sin\theta \quad (4.1)$$

capillary loop length (arc\_length) is the length of the arc

$$\text{arc\_length}=2r \theta \quad (4.2)$$

The ratio between chord and arc\_length will be

$$\frac{\text{chord}}{\text{arc\_length}} = \frac{2r \sin\theta}{2r\theta} = \frac{\sin\theta}{\theta} = \text{sinc}\theta \quad (4.3)$$

From a look-up table  $\theta$  value can be obtained for each chord/arc length ratio. It should be noted that  $\theta$  is half of the central angle that sees the arc. The function  $\text{sinc}\theta$  is insensitive to small deformities on the capillary loop outer chain. It can be used as a tool to measure tortuosity of the loop segments, as well. The function produces the same output for the same shapes but in different scales. Therefore the enlargement of capillary loops will not affect the output.

When  $\theta$  approaches zero the arc approaches a straight line. The proof for this statement is as follows:

$$\lim_{\Delta\theta \rightarrow 0} \frac{\sin \Delta\theta}{\Delta\theta} \quad (\text{substitution gives } \frac{0}{0}) \quad (4.4)$$

From L'Hôpital rule, we can take derivatives of  $\Delta\theta$  of both numerator and denominator of equation (4.4)

$$\lim_{\Delta\theta \rightarrow 0} \frac{\frac{\partial}{\partial \Delta\theta}(\sin \Delta\theta)}{\frac{\partial}{\partial \Delta\theta}(\Delta\theta)} = \frac{\cos \Delta\theta}{1} = \frac{1}{1}$$

In the limit when the ratio chord/arc\_length is equal to 1, it can be said that the capillary loop is a straight line. In some "cuticulis" capillary loops, the central angle exceeds the ideal cuticulis margin. Could we still expect chord/arc\_length to be equal to  $\text{sinc}\theta$ ? In Figure 4.7, such an arc with its properties is given.

The ratio between base and the arc\_length for the arc in Figure 4.7

$$\frac{\text{chord}}{\text{arc\_length}} = \frac{2r \sin \beta}{2r(\pi - \beta)} = \frac{\sin \beta}{\pi - \beta} \quad (4.5)$$

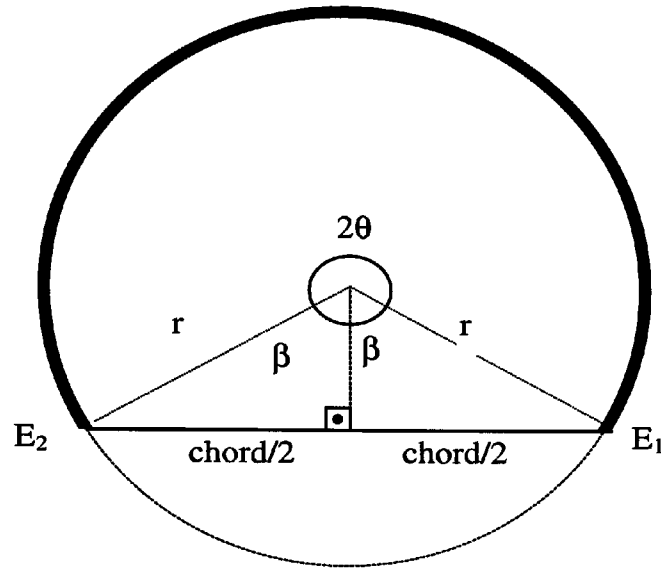


**Figure 4.7** An Arc With Central Angle  $\beta > \pi / 2$

It is also known that

$$\beta = \pi - \theta \quad (4.6)$$

By substituting (4.6) in (4.5),

$$\frac{\text{chord}}{\text{arc\_length}} = \frac{\sin(\pi - \theta)}{\pi - \pi + \theta} = \frac{\sin(\pi - \theta)}{\theta} \quad (4.7)$$

$\sin(\pi - \theta)$  can be re-arranged by using trigonometric equation (4.8)

$$\sin(\alpha - \beta) = \sin \alpha \cos \beta - \sin \beta \cos \alpha \quad (4.8)$$

Hence, 
$$\frac{\sin \pi \cos \theta - \sin \theta \cos \pi}{\theta} = \frac{\sin \theta}{\theta} = \frac{\text{chord}}{\text{arc\_length}} \quad (4.9)$$

Therefore  $\text{sinc}\theta$  function can be used for wide angles as well. When  $\theta$  is smaller than  $90^\circ$ , only the capillary loop's tip is visible and capillary loop is "cuticulis" type. When  $\theta$  exceeds  $90^\circ$ , the central angle exceeds  $180^\circ$  and the  $\text{sinc}\theta$  function treats the capillary loop as a circle, although it is finger like shaped.

Hence, regardless of its shape,  $\text{sinc}\theta$  approximates the capillary loop to an arc of a circle. The output of the function is a measure of concavity. For a "cuticulis" capillary loop, on the other hand, limbs will be short enough to be accepted as an arc of a circle.

As the limbs get longer, the shape of the capillary loop deviates from circular to longitudinal. Therefore, the smaller is the  $\theta$ , the more circular is the loop.

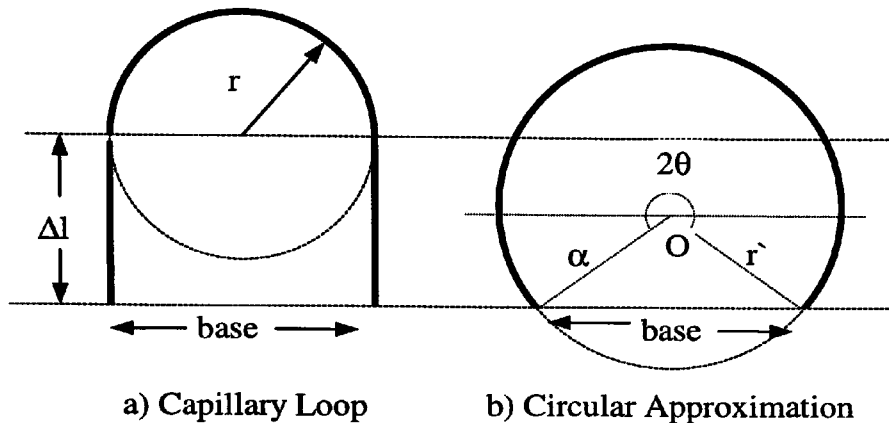


**Figure 4.8** (a) A capillary loop with  $\Delta l$  long limbs (b) Its circular approximation

The capillary loop in Figure-4.8(a), for example, can be approximated to an arc as in Figure-4.8(b). The capillary loop has  $\Delta l$  unit long limbs and width “base”. Since the capillary loop is artificial, its properties are known. But in practice, only the loop chain length and base are known. By using  $\text{sinc}\theta = \text{base}/\text{arc\_length}$ , the loop can be approximated to an arc with the central angle  $2\theta$  (Note that  $\text{base} = \text{chord}$ ). As the limbs get longer,  $\theta$  widens.

A function  $f(\theta, \Delta l/\text{base})$  can be written in order to monitor the effects of  $\theta$  changes on  $\Delta l$  limb length, and it is given as

$$\frac{\Delta l}{\text{base}} = \frac{1}{2} \left( \frac{\theta}{\sin \theta} - \frac{\pi/2}{\sin(\pi/2)} \right) \quad (4.10)$$

$f(\theta, \Delta l/\text{base})$  can be plotted as in Figure. 4.9. At  $\theta=90^\circ$ , the capillary loop has no limbs. As  $\theta$  increases, the limb length  $\Delta l$  increases non-linearly. For  $\theta$  angles closer to  $90^\circ$ ,  $\Delta l$  increases slowly. Contrary to this  $\Delta l$  increases rapidly as  $\theta$  gets closer to  $180^\circ$ . As it can be seen from Figure-4.9, a capillary loop with  $\theta=137.7^\circ$  has limbs that are long as its width.

Although  $f(\theta, \Delta l/\text{base})$  produces undesirably coarse results, for  $\theta$  values nearer to  $180^\circ$ , it can be successfully used to separate "cuticulis" capillary loops from the rest.

The aim was to segregate "cuticulis" capillary loops from rest, not to find their parameters. Since Exclusive-Curvature Angle proved to be useful to measure concavity of the loops, it has been employed to classify "cuticulis" capillary loops.

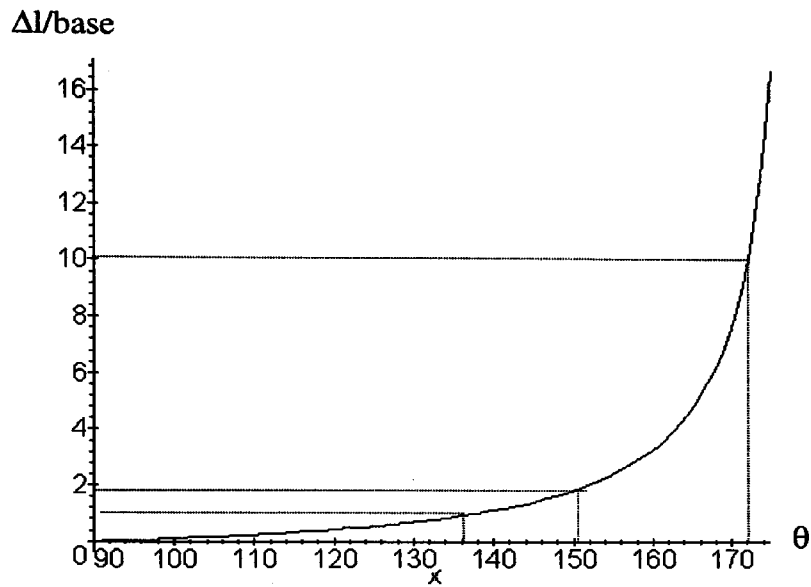


**Figure-4.9** The plot of the function  $f(\theta, \Delta l/base)$



# **CHAPTER 5**

## **Chapter 5 The Automated Classification and Analysis of Nailfold Capillaries**

### **5.1 Structure of The Automated Nailfold Capillary Classification and Analysis System (TANCCAS)**

The structure of the automated nailfold capillary classification and analysis system (TANCCAS) can be divided into 3 main sections (see Figure 5.1). These are the Pre-Processing Module (PPM), Main Classification Module (MCM) and Class Decision Unit (CDU). The nailfold capillary loops that were traced from the captured images, are reduced into m-connected chains in PPM. By identifying and cropping the chains belong to same capillary loop, a sub image file is created for each capillary loop. From this point forward all the capillary loops will be processed individually. Most of the "cuticulis" and "crossed" capillary loops are detected in PPM. The morphological parameter limb width can be calculated where it is available. Furthermore, a suggestion of the possible descriptive class of a loop will be noted in its data file.

MCM has got two inputs; the loop image file and its data file. The "cuticulis" loops that could not be detected in PPM are detected in the early stages of the MCM. By checking the number of chain segments that forms the loop's skeleton either Bushy-Bizarre Classification Unit (BBCU) or Open-Tortuous Classification Unit (OTCU) will be activated. Some of the "crossed" loops will be detected in MCM by checking the suggested class that was made in PPM, and the number of skeleton chain segments. BBCU applies the bushy and bizarre classification criteria as has been set in section 3.4.4. Similarly, by measuring the tortuosity level of the loops, "open" and "tortuous" loops will be detected in OTCU. The loop's preliminary class and the morphological parameters: loop width, loop length, tortuosity, can be determined in MCM.

The CDU is a logic unit that analyses the morphological parameters and the preliminary class of a loop that were determined in PPM and MCM. The output of CDU is the report file that contains the analysis and classification results for every capillary loop in the input image of PPM

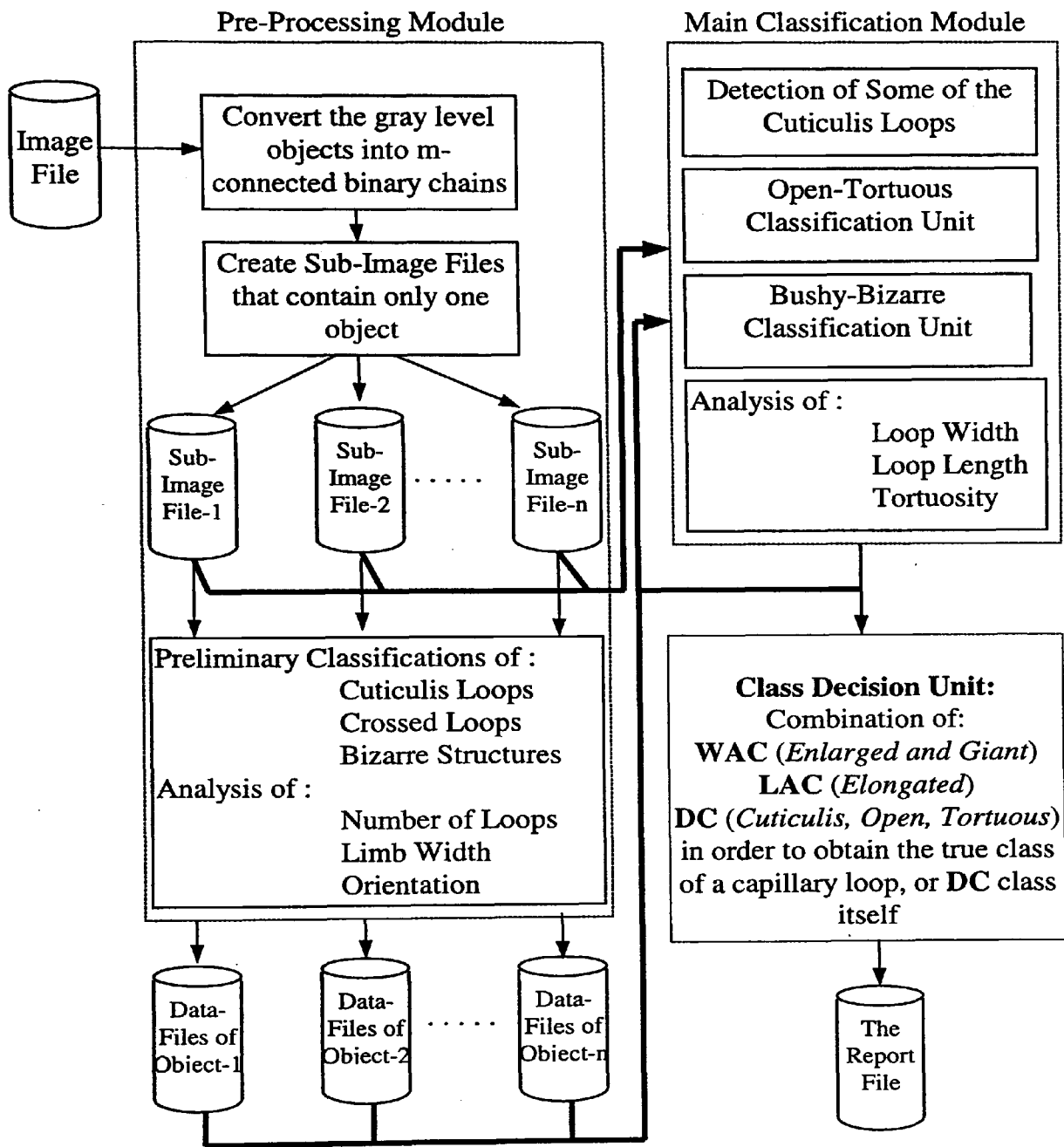
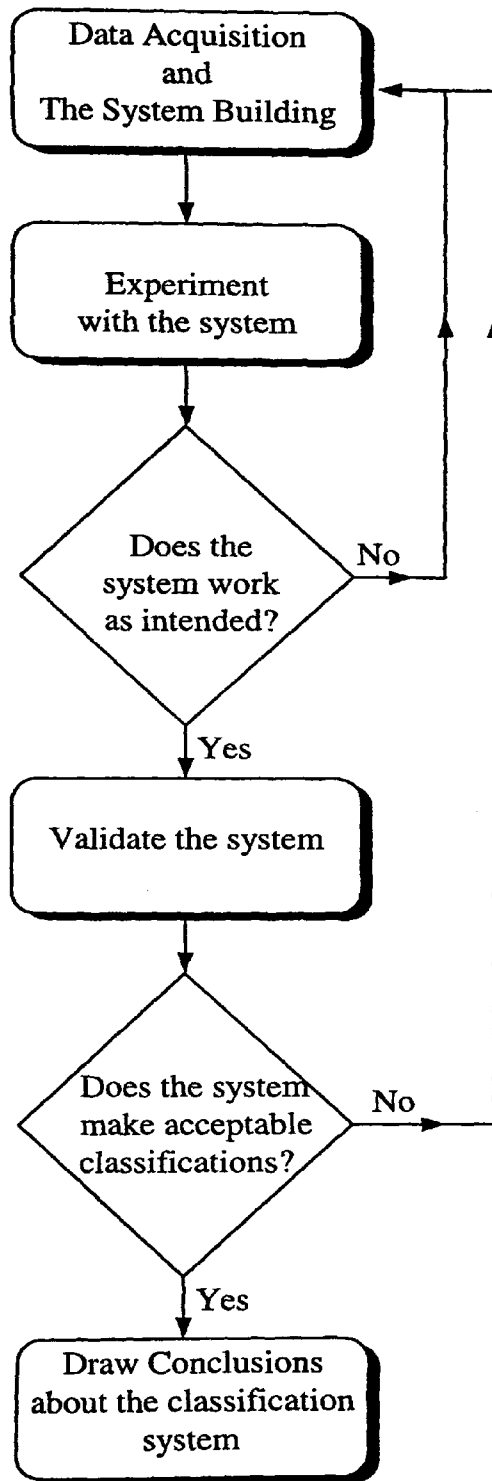


Figure 5.1 The structure of TANCCAS.

## 5.2 Development Methodology

The original aim of this study was to classify the nailfold capillary loops into four types: "cuticulis", "open", "tortuous" and "crossed" [Oral 96]. The first classifications and analyses were carried out with the synthetic drawings of the capillary

loops. By reviewing the literature, and with the suggestions of the participating practitioners the number of the capillary classes had grown to 17 at the end of the study. Figure 5.2 shows the development methodology of the classification and analysis system (TANCCAS).



*Figure 5.2 Development Methodology of the TANCCAS*

### 5.3 Data Acquisition

The capillary images were taken on the fourth finger of both hands, which usually offers the best capillary visibility. The optic microscope was connected to a video camera with enhanced red sensitivity (WV-CD 130/WVL) and 60-240 fold magnification. Incident lighting was provided by a Schott fiber optic illuminator. A U-MATIC video recorder provided the facility to repeatedly scan records. All observations were made after the epithelium was made more transparent by applying immersion or paraffin oil. The block diagram of the mechanism is shown in Figure 5.3.

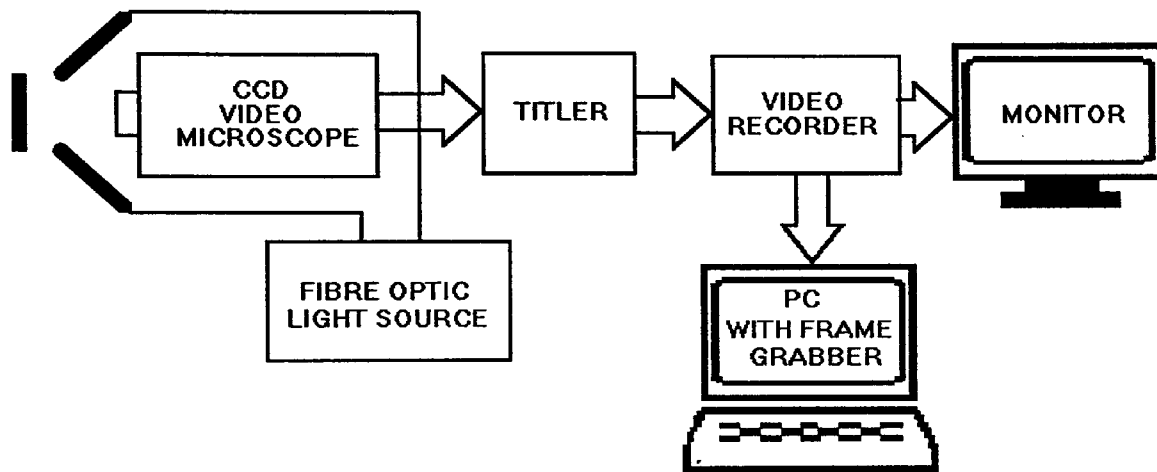


*Figure 5.3 The block diagram of the mechanism which takes images in the microvascular area.*

The video tape that contains nailfold capillary observations was supplied by Department of Clinical Measurements, Royal National Hospital for Rheumatic Diseases, Bath. This video tape was played back in a video player that connected to a PC. An image bank that provides several examples of the capillary types, was created by capturing the frames with Visilog 4.1.3(c) image processing software. These images, unfortunately, are of poor quality and have low contrast because of bad illumination and because they are captured from video recordings. Minimum and maximum gray levels of the image file "image\_1.tif", are given in Figure 5.4 together with its histogram; have the minimum and maximum gray levels are 17 and 127 respectively. Furthermore, the

picture is packed into a very narrow band with only 22 shades of gray (between 72 and 94) forming the picture. Image\_1.tif of Figure 5.4 is histogram equalized product of the original image, for display purposes.

Because of poor illumination, the corner areas of the images were expected to be darker than middle. The reflections of the light on the skin surface were, also, expected to create little bright white islands in the images. With the existing quality of the images, it is difficult to filter out the capillary loops for analysis and classifications. It should be remembered that *it is the aim of this study to demonstrate that computerized analysis and classification of nailfold capillaries can be achieved*. Because it is a difficult task, segmentation of the nailfold images were left as further study. In order to skip the segmentation processes, hand traced images of the nailfold capillaries from the original files were created and stored into TIFF and ASCII data formats.

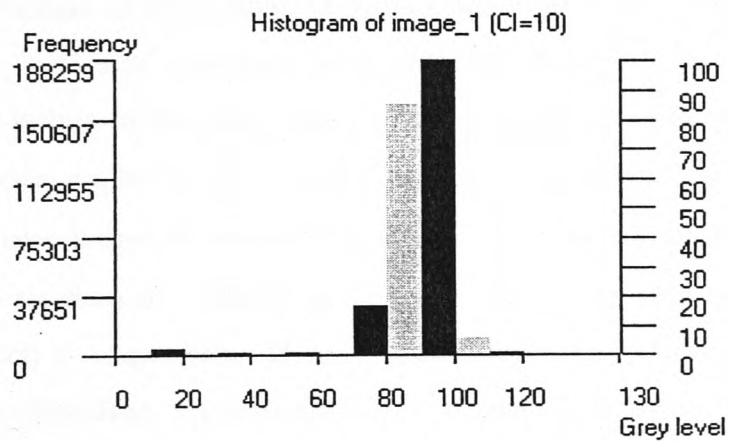
The hand traced, TIFF format, original images were converted into ASCII files, that are 4 bytes for each pixel and with no header information, by using export facility of Visilog4.1.3 image processing software. The ASCII format has been chosen to be able to easily visualize the outputs of the image processing functions in the development stage by using any text editor. With further development the system can be adopted to support common picture formats, such as bmp, pcx, gif, tiff, etc.[Rimmer 90] In addition to the captured images (Appendix A), some synthetic capillary images (Appendix B) are also included into the image bank, in order to test the special conditions of the classification and analysis processes.

#### **5.4 Implementation of The Classification Criteria**

The classification criteria of the six basic classes; "cuticulis", "open", "tortuous", "crossed", "bushy" and "bizarre", and the label classes; "enlarged", "giant" and "elongated", are given in section 3.4. In order to apply the classification criteria to the loops, first of all, each loop must be identified and extracted from the image. While



(a)



(b)

**Figure** (a) The original image of Image-1 of Appendix A (For better print quality, the original file is histogram equalized). (b) Histogram of the original image

tracing the capillary images, the investigator's tracing methods may vary. "Crossed" type capillary loops in the images T13.tif, T14.tif, T15.tif, and T37.tif of Appendix B, for example, display such kind of variations. (From now on, the loops in the images of Appendix B, will be called by the file name, for example, T13, T14, etc.) While the limb borders of T13, T14 and T15 are visible at the crossing points, they were not traced for

the loop T37. The bottom end of the limbs were enclosed for T37, but left unattached for T13 and T14, or, one limb's end was enclosed and the other one is left disclosed. Such variations make the pattern recognition difficult (some times impossible), therefore they have to be taken into account and to be reduced to a single style. The classification and analysis modules are designed to recognize the loops that are traced by the style of T37. Therefore, The loops T13, T14 and T15 must be adapted to the style of T37.

The tracing style is not the only problem. The "open" type capillary loop (i4:N28), for example, can be mis-classified as "cuticulis" if the cuticulis classification criteria are applied without any modification. The capillary loop width was assumed to be roughly the projection distance between the limb tip points. The loop length must be calculated before the loop width. The loop length is calculated by using the thinning algorithm. The algorithm generates disoriented skeletons for most of the "cuticulis" capillary loops because of their small size, and that makes the calculation of the actual loop width of a "cuticulis" capillary loop difficult. Therefore the projection distance between the end points of the outer body chain is assumed to be the loop length. The exclusive curvature angle  $\theta$  of (i4:N28), is less than  $\theta_{\text{CUTICULIS}}$ , although "open" capillary loops have larger  $\theta$  values than  $\theta_{\text{CUTICULIS}}$ . One of the limbs of (i4:N28) is considerably shorter than the other one, and that makes the loop width larger than the actual width which is impossible. If some other mechanisms are not been used, such loops will be mis-classified. Therefore another control mechanisms should be developed for automated classification.

Human perception may fail to classify the loops that are near to the borderlines of the classes (if the person knows the basic elements of the classification). For example, the loop (i4:N28), would not be questioned as a "cuticulis" by any practitioner, if s/he knows that a "cuticulis" capillary loop cannot have such long limb, although the other limb is not fully visible. The machine perception, on the other hand, has got many handicaps. The TANCCAS is allowed to mis-classify some of the loops that are near to borderline, because of the class borders (critical values) are not set precisely, but logical errors as in the loop (i4:N28) must be strictly avoided.



The implementation of the classification criteria will be given in the following section. Some modifications will be made on the classification criteria, given in section 3.4, because of the limited capabilities of the machine perception. These modifications do not affect the original criteria, because human perception is capable of eliminating such distractions. In order to demonstrate the classification and analysis processing steps of TANCCAS, the image file "collect.tif" (Figure 5.5) was created by collecting the capillary loops (i2:N6; Crossed), (i2:N7; Elongated Tortuous), (i2:N10; Enlarged Cuticulis), (i5:N11; Giant Open) and (i5:N28; Bushy) of Appendix A. The capabilities and the handicaps of TANCCAS will be demonstrated with some other images that contain the typical examples of the special cases. The synthetic (imaginary) capillary loops of Appendix B are designed for these purposes.

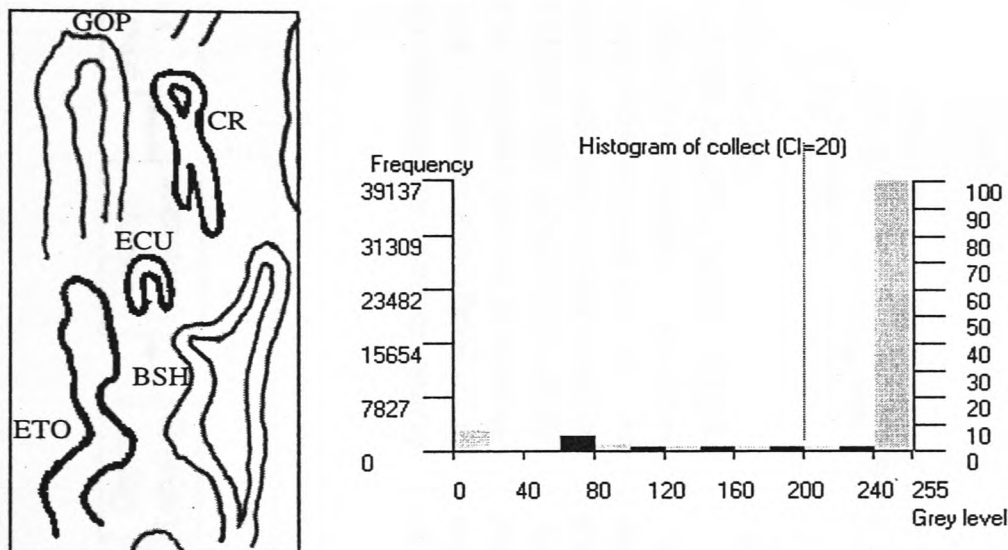
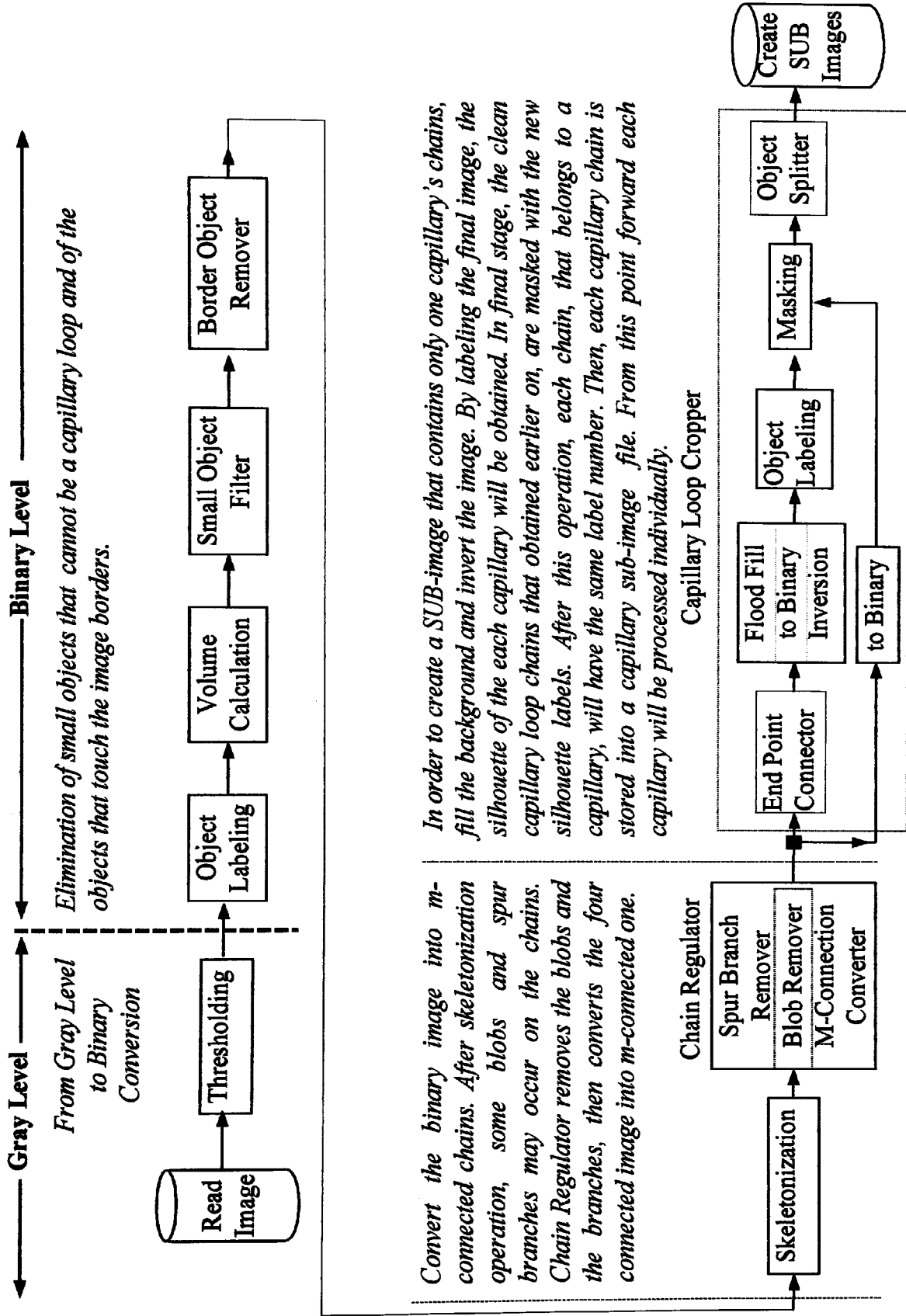


**Figure 5.5** The test file "collect.tif" and its histogram

#### 5.4.1 Pre-processing Module Part I (PPM-I)

The main function of PPM-I is to detect the capillary loops that are suitable for the analyses, from the input image, and store every one them, individually, into the sub-image files that hold the capillary loop chain(s). The block diagram of PPM-I is given in Figure 5.6. The gray level image (0-255) that contains the tracings of the capillary loops is the only input of the PPM-I. The image file "collect.tif" (Figure 5.5) will be processed to demonstrate the functions of PPM-I.



*Convert the binary image into m-connected chains. After skeletonization operation, some blobs and spur branches may occur on the chains. Chain Regulator removes the blobs and the branches, then converts the four connected image into m-connected one.*

*In order to create a SUB-image that contains only one capillary's chains, fill the background and invert the image. By labeling the final image, the silhouette of the each capillary will be obtained. In final stage, the clean capillary loop chains that obtained earlier on, are masked with the new silhouette labels. After this operation, each chain, that belongs to a capillary, will have the same label number. Then, each capillary chain is stored into a capillary sub-image file. From this point forward each capillary will be processed individually.*

**Figure 5.6** The block diagram of Pre-Processing Module (Part I)

After reading the input image to a dynamic array, it will immediately be converted into binary level by thresholding the gray level image with the intensity level 200. The gray levels [0-200] and [201-255] represent the objects and background respectively. The output of the thresholding operation for "collect.asc" is given in Figure 5.7(a). The capillary loops that are not fully visible (the remaining part of the loop is outside of the picture boundaries), must be removed from the picture, as well as the small objects that cannot be a capillary loop. **Border Object Remover (BOR)** deletes any object that has a picture element on the boundaries of the picture even if the capillary loop is completely visible, but touches the picture boundaries anywhere. **Small Object Remover (SOR)** gets rid of the objects that are less than 30 pixel in area. The critical area, 30 pixel, was set after the experiments. By labelling the output image of thresholding function, each object, that is surrounded by background, is detected and assigned with a label (Figure 5.7(b)). Then, the area of the each object is calculated and filtered by SOR. The output of SOR is fed into BOR, and the final binary image (Figure 5.7(c)) contains the capillary loops that are suitable for further analyses.

The next step is reducing the capillary loop boundaries into m-connected chains. This will be achieved by using the skeletonization algorithm and chain regulator (CR). The image processing library of TANCCAS is capable of both thinning and skeletonization operations. Although the **Thinning()** operation produces clean skeletons (it produces less spur branches than **Skeletonization()** algorithm), the medial axis of the object is located more accurately by the skeletonization algorithm. The output of the BOR is therefore fed into skeletonization unit. The algorithm produces the medial axis of the object in four connected mode (Figure 5.8(a)). The regions where the capillary loop tracing lines are somehow thicker than the neighbouring regions (marked with circles in Figure 5.7(c)), produce undesired spur branches (marked with circles in Figure 5.8(a)). Although skeletonization algorithm did not produce any blobs on the medial axis of the capillary loops of "collect.asc", in some cases, these blobs may occur, and cause misclassifications. Therefore, the output of the skeletonization algorithm must be re-organized.

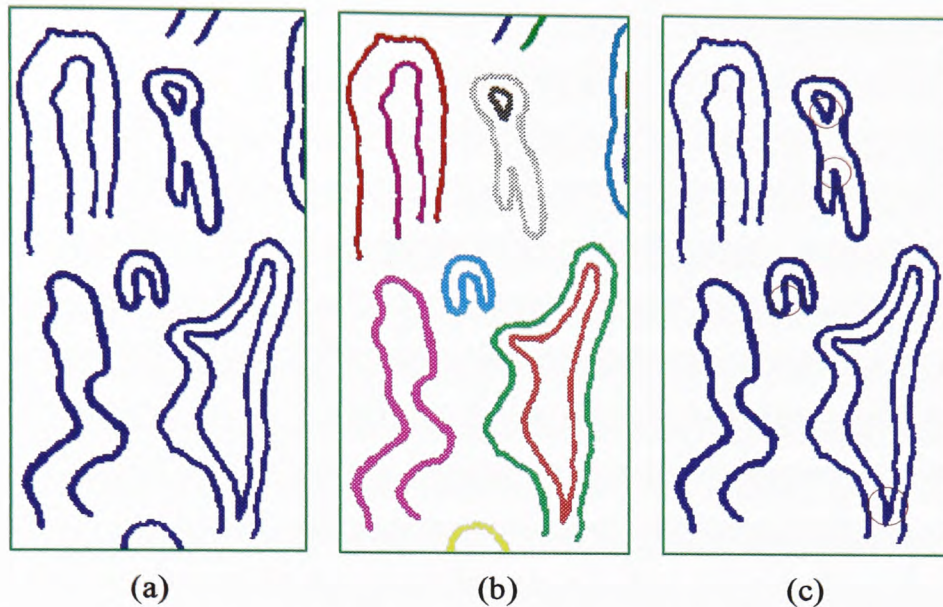


**Figure 5.7** (a) The Output of Thresholding function. (b) The labelled image. (c) The final image after removing the small objects and the objects that touch the picture borders

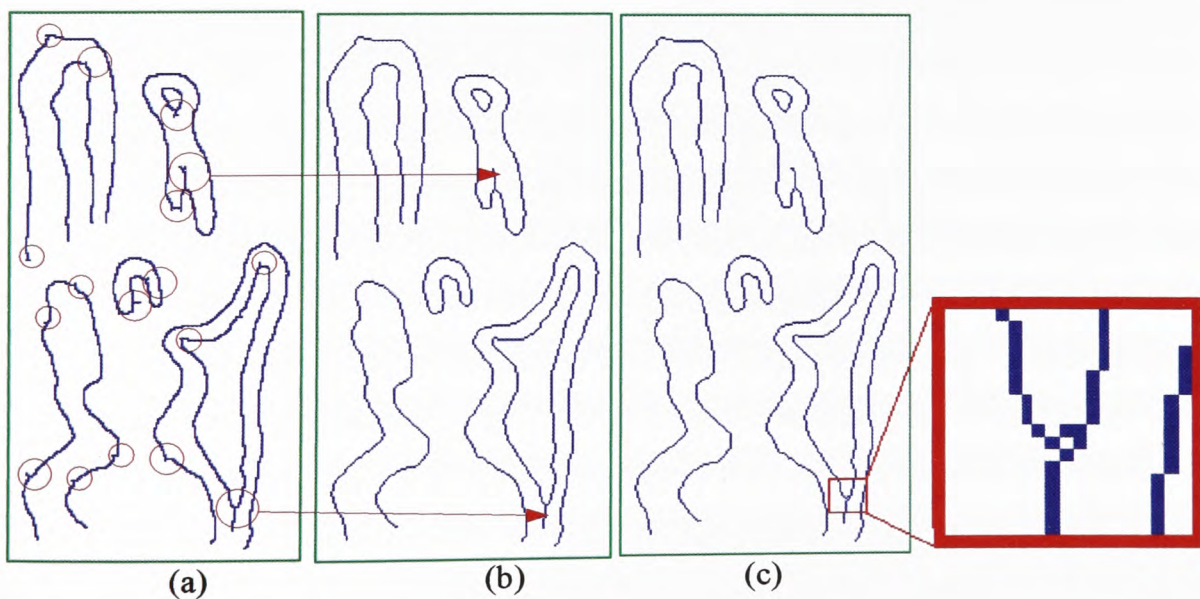


**Figure 5.8** (a) The output of skeletonization algorithm. (b) The input of Long Branch Remover (LBR). (c) Artificially created blob (The area of interest is magnified.)

#### 5.4.1.1 The Chain Regulator

The capillary loop chains, that are obtained by skeletonization algorithm, are four connected and may contain small blobs and spur branches. Many of the image processing library functions of TANCCAS require m-connected chains. The spur branches and the blobs on the loop chain must be cleaned in order to prevent misclassifications. **Chain Regulator (CR)** is employed to re-organize the output of the skeletonization algorithm, and produce m-connected clean chains. The block diagram of the CR is given in Figure 5.9. The output of the skeletonization algorithm displays many spur branches (marked with circles in Figure 5.8(a)). Although, most of these branches can be cleaned out by using pruning algorithm, the pruning algorithm is not capable of removing those two spur branches (marked with circles in Figure 5.8(b)). Only those branches that are shorter than 10 pixels in length can be wiped out by using the pruning algorithm of TANCCAS. Those marked two branches are longer than the pre-defined threshold length. However such undesired long branches will be controlled and filtered out in **Long Branch Remover (LBR)** unit. As it stated before, the output of skeletonization algorithm did not produce any blobs for "collect.asc". In order to demonstrate blob removing, one pixel of the "bushy" loop's skeleton chain was artificially changed, and a blob is created (Figure 5.8(c)).

The image that contains the four connected capillary loop chains that were produced by skeletonization algorithm is the input of the CR. First, the chains are converted to m-connected ones. Then, the pruning algorithm is applied twice to the image. The first application of the pruning algorithm clears those red branches in Figure 5.9, and the blue branch will be cleaned out in second pass. After the pruning operation, the adjoining points of the removed branches should be re-organized. Those points may not be m-connected, because of the deleting. Re-organization of the chains are achieved by refinement algorithm. At this point, the m-connected chains are supposed to be not having any spur branches, but small blobs.

The first step of blob removing is the filling operation. Flood fill starts from the most upper left corner of the image, and operates in four connected mode. Since the

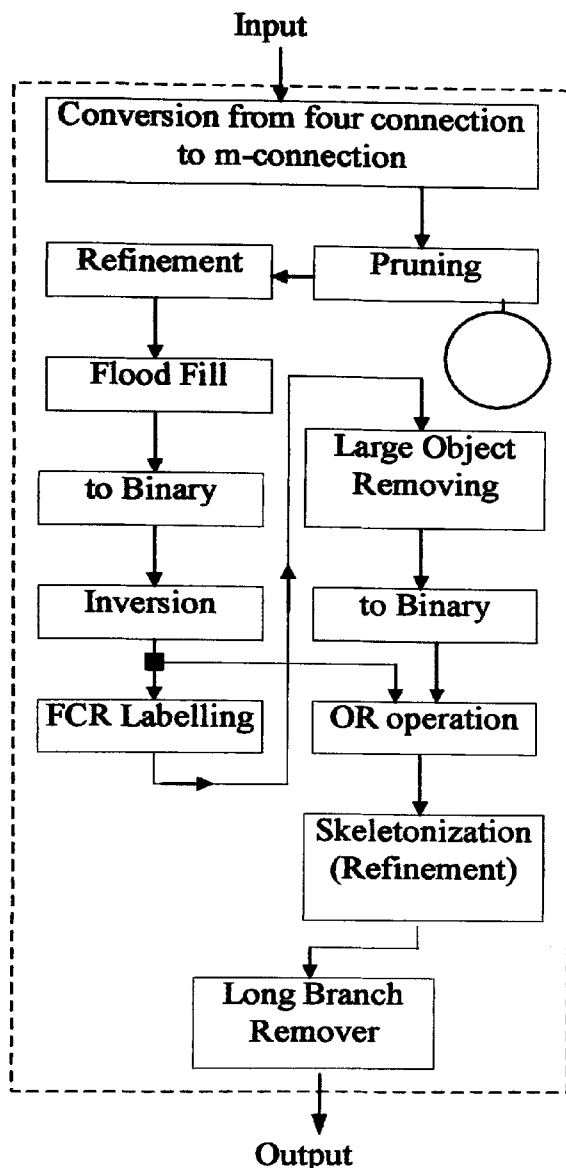


**Figure 5.9** The Block Diagram of Chain Regulator (CR)

capillary loop chains are m-connected, the four connection mode prevents the leakage into the enclosed areas. The output of the Flood Fill operation is given in Figure 5.10(a). Then, a conversion to binary is achieved by replacing any label of flood filled image, that is bigger than '0', with '1' (Figure 5.10(b)). By applying the logical NOT operation, the final image is inverted (Figure 5.10c)). That gives all the enclosed areas of the image, including the unwanted blobs. The enclosed area of a blob will be much smaller than those enclosed areas that are natural features of the capillary loops. Therefore, the blob(s), can be detected by checking the volumes of the enclosed areas. Each enclosed area is labelled by using **Four Connected Recursive Labelling** algorithm (FCR Labelling) of the image processing library function. Crossed capillary loop of "collect asc", has got two enclosed regions, one is encircled by the other one . Since the boundary line between these two regions is m-connected, these two regions may, actually, be touching each other. The labelling operation that was used earlier on to get rid of the small objects and objects at the border of image, operates in m-connected mode. Therefore FCR labelling is essential to detect every isolated object in the image. The output of FCR labelling is given in Figure 5.10(d). The area of interest is magnified to show that the area enclosed by the blob has got its unique label (purple). By measuring each object's area, and clearing out the objects larger than 30 pixels in area, all the objects will be deleted but the blob.

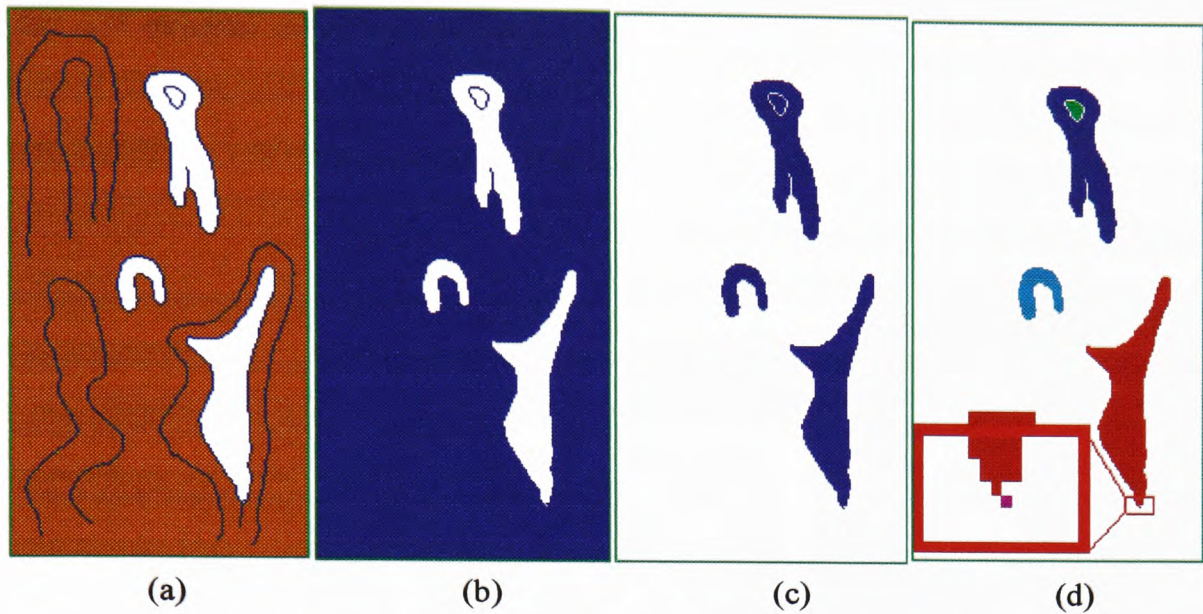


**Figure 5.10** (a) The output of Flood Fill algorithm, (b) Conversion to binary (c) Output of Logical NOT operation for 'b'. (d) The output of FCR Labelling. (The area of interest is magnified).

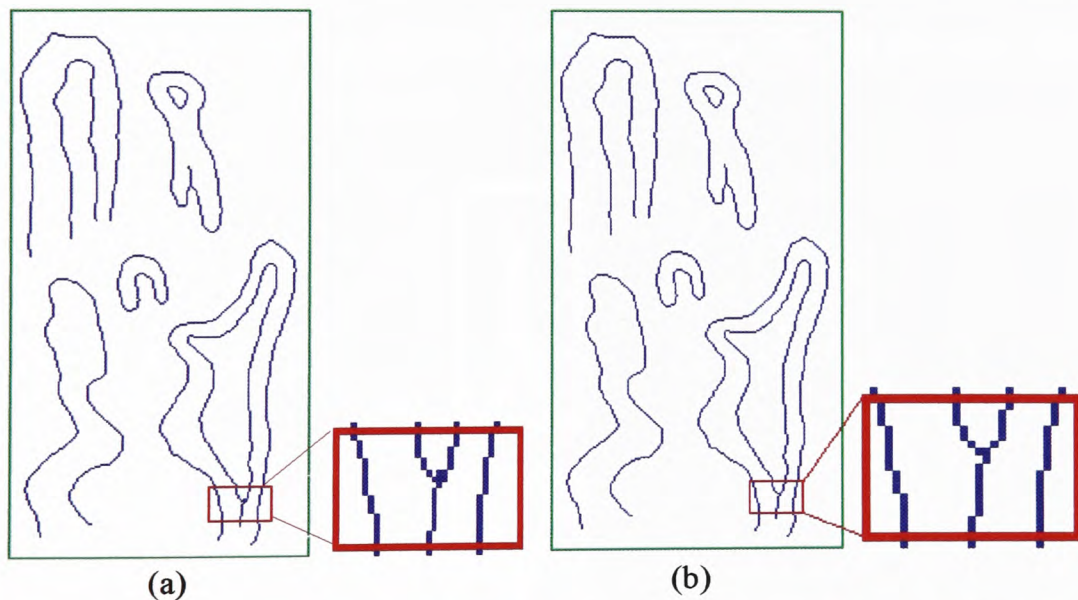


**Figure 5.11** (a) The output of OR operation (b) The input of Long Branch Remover (LBR) for artificially defected image "collect.asc".

The location of the blob on the skeletal chain is detected at this point. If the logical OR operation is applied between the skeletal image (Figure 5.8(c)) and the output image of large object remover, the blob will be filled (Figure 5.11(a)). Finally, by applying the skeletonization algorithm once more and refining its output for m-connection, the blob will be erased (Figure 5.11(b)). Apart from those long spur branches, the capillary loop chains are almost formed cleanly.

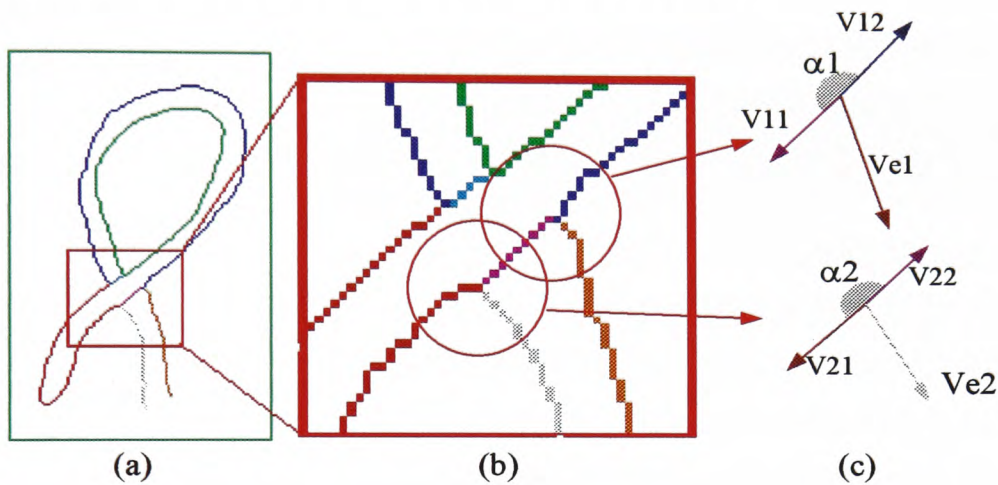


**Figure 5.12 (a)** The output of RS Labelling for the loop T11. **(b)** The area of interest **(c)** The vectors of the chain segments.

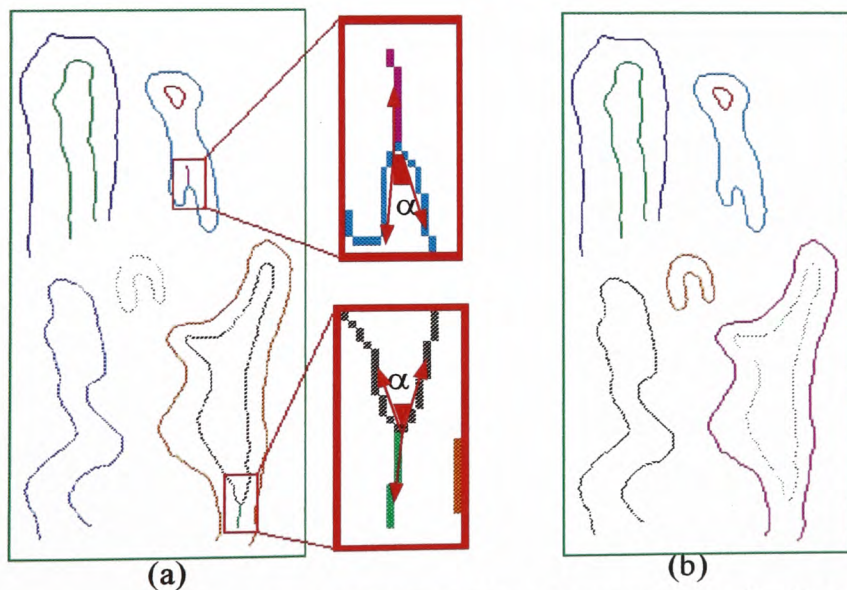


**Figure 5.13 (a)** The output of RS Labelling for the image "collect.asc", (Area of interest is magnified). **(b)** The output of Chain Regulator for the image "collect asc".



The long spur branches that could not be deleted by pruning algorithm, will be removed at the final stage of CR. While tracing the capillary loop borders, "V" turns should be avoided. Such sudden direction changes creates spur branches at the bottom of "V". The narrower the angle between the legs of "V", the longer the spur branch gets. If it is possible such corners should be traced "U" shaped that prevents any unwanted long branches. Those two unwanted long branches of skeletal chains are located at "V" turn points of the tracings of crossed and bushy loops of Figure 5.7(a). Fortunately, these long branches can be automatically detected and removed from the chains by using LBR.

A branch of a chain is the chain segment that is open at one end (not connected to any other segment), and closed at the other end (adjoined to another chain segment). A branch of a capillary loop chain does not have to be a spur branch. The capillary loops of Appendix B (from T11 to T15), for example, have got chain segments that are open at one end. Those segments are boundaries of the limb end points, and they must not be removed. The unwanted spur branches of Figure 5.8(b), on the other hand, must be removed. A decision mechanism should be employed to decide which branches must be kept or removed. As it stated earlier on, the long unwanted branches occur at those 'V' shaped corners. If the angle between two neighbouring chain segments that the branch is attached to can be measured, a decision can be made for removal of the branch. The capillary loop T11, for example offers two branches to be decided on (Figure 5.12(a)).

The first step of LBR is Recursive Segment Labeling (RS Labelling). RS Labelling function of the image processing library, assigns a label for each chain segment. The capillary loop T11 for example has got seven segments on its skeletal chain, and its RS Labelling function output is given in Figure 5.12(a). Then, each branch (the chain segment open at one end) and the chain segments that the branch is connected to, are approximated by the vectors (Figure 5.12(c)).

Approximation can be achieved as follows; from the intersection point, each of the segments are recursively traced, and the tenth pixel's location is assumed to be the end point of the vector. These vectors are assumed to be the direction vectors of the chain segments. If the angle  $\alpha_i$  between the vectors  $V_{i1}$  and  $V_{i2}$  is larger than  $30^\circ$ , the branch must not be removed (it is the boundary of a limb), otherwise it can be safely removed. The threshold angle had been set to  $30^\circ$ , after the experiments. The  $\alpha_i$  angles of the spur branches of Figure 5.13(a), on the other hand, are narrower than the threshold value and they can be removed. The output image of LBR, that is also the output of Chain Regulator for "collect.asc", is refined for m-connection, and RS

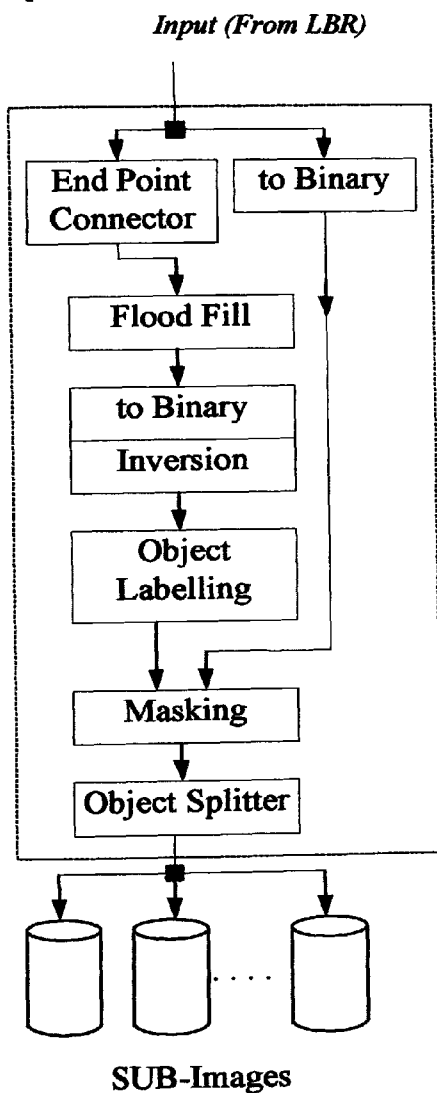


**Figure 5.14** The block diagram of Capillary Loop Cropper

Labelled. As desired, the output image of CR (Figure 5.13(b)) contains clean m-connected chains.

### 5.6.1.2 The Capillary Loop Cropper

A capillary loop may be traced by a single chain ("tortuous" and "cuticulis" loops of "collect.asc") or several individual chains. The "bushy", "crossed" and "giant open loops" of "collect.asc", for example, are formed by two individual chains. As the shape of the loop gets complex and bizarre, the number of chains may increase. The "bizarre" capillary loop (i6:N3), for example, was traced with six individual chains. Human perception, can easily detect which chains belong to which capillary loop, with no effort. For the machine, on the other hand, it is a difficult task. **The Capillary Loop Cropper (CLC)** identifies a capillary loop's chain(s), and crops them from the original image and stores into the sub-image files. A sub-image file holds only one capillary loop's chains.

The block diagram of CLC is given in Figure 5.14. The labelled image of CR's output is the input of **End Point Connector (EPC)**. Basically, EPC detects the end points of a chain, and encloses it by drawing a line between the end points. The idea is that if the outer boundary chain is enclosed, then the inner boundary chain(s) of the loop will be in this encircled area. Since it is not known which chains are the outer boundary chains, all of the chains have to be enclosed. The output of EPC for "collect.asc" is given in Figure 5.15(b). By flood filling (Figure 5.15(c)) and converting this image to binary followed by a NOT operation, individual capillary loops inner areas can be obtained (Figure 5.15(d)). By Object Labelling, each **capillary loop area** will be identified (Figure 5.15(e)). At this stage, it can be confidently said that any chain, that belongs to a capillary loop, overlaps with the capillary loop area. If the image that contains the output of LBR in binary level, is multiplied with the labelled capillary loop area image, the chains belonging to same capillary loop will have the same label number. As it can be seen from Figure 5.15(f), the chains belong to same capillary loop have got the same label. Finally, Object Splitter calculates the most upper, lower, right and left picture elements of an object, and defines the projectile boundaries of an objects. Then, it copies the object in a newly created sub-image file. From this point forward the operations will be carried out for individual capillary loops.

#### **5.4.2 Pre-Processing Module Part-II (PPM-II)**

The sub-image files that were created in PPM(I) contain m-connected capillary loop boundary chains. In the early stages of developments, TANCCAS was able to analyze and classify only those loops that had been traced with a single line. However, if the inner boundary of capillary limbs are visible, the number of chains increases. (This is not always true, while the capillary loops GOP, CR and BSH of "collect.asc" were traced with more than one chain, the enlarged cuticulis loop (ECU) has got only one boundary chain that surrounds the inner and outer boundary of the capillary limbs). The capillary loop T14 of Appendix B, for example has got fourteen chain segments in its sub-image file. The number of chains for this loop can be reduced to four without losing any shape information that is important for its classification. However, the input

of **Main Classification Module (MCM)** must be a sub-image file that contains only and only one chain. Furthermore, this chain must be a disclosed one, unlike ECU of "collect.asc". If a capillary loop's sub-image contains more than one chain, the loop must be pre-processed before inputting to MCM. This will be achieved in **Pre-Processing Module-Part II (PPM-II)**. The block diagram of PPM-II is given in Figure 5.16.

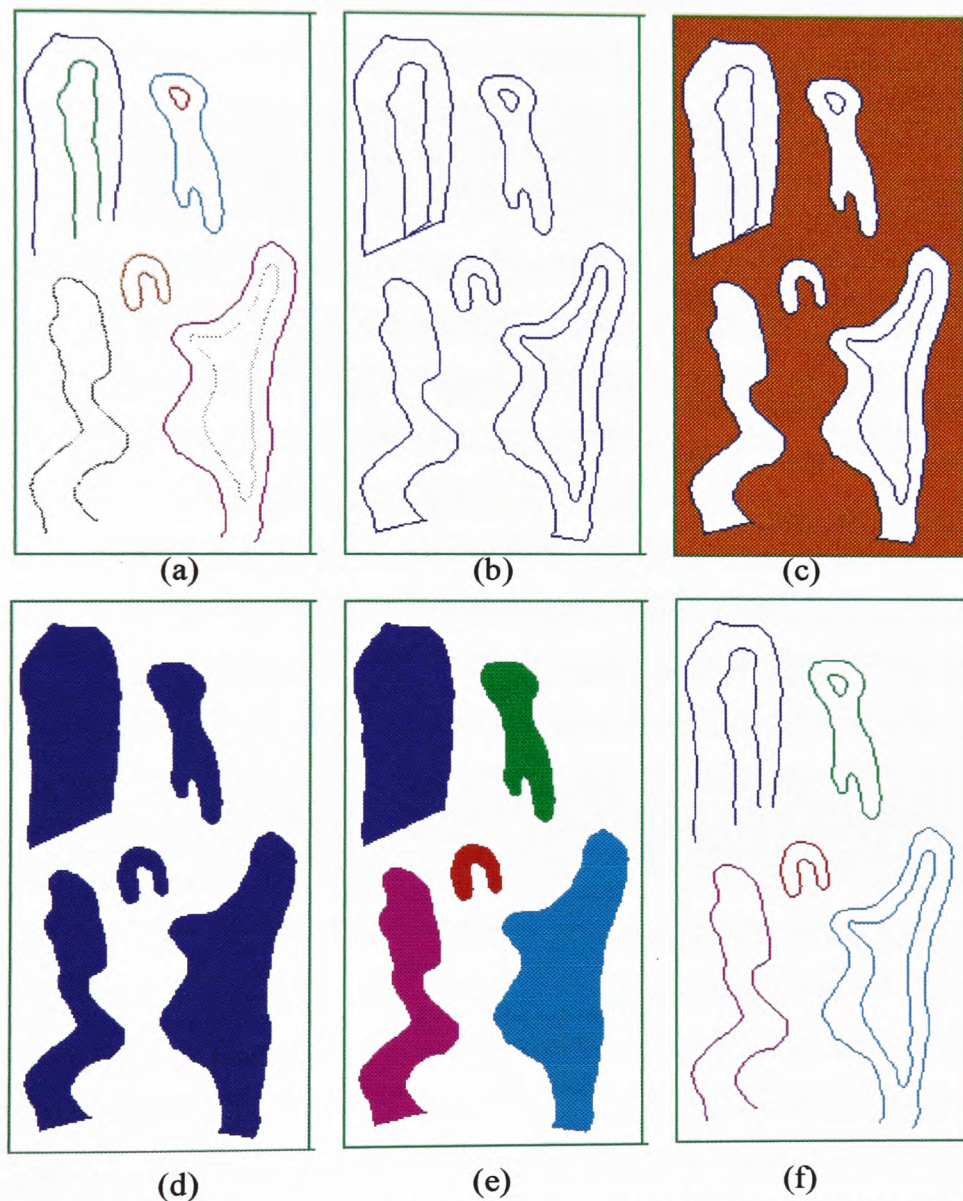


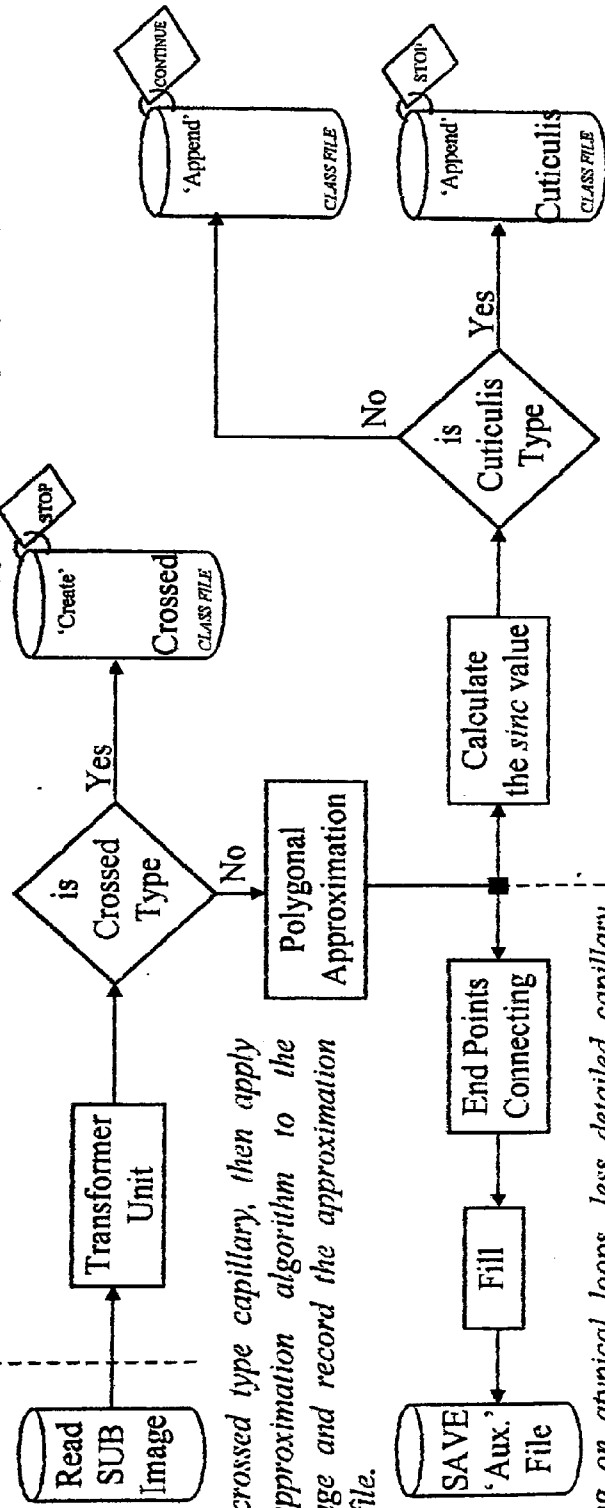
**Figure 5.15** The processing steps of Capillary Loop Cropper (CRC). (a) The input image (from LBR's output). (b) The output of End Point Connector, (c) Flood Fill operation, (d) Inversion output (e) Object Labelling output (f) The output of Masking operation.

The functionality of **Transformer Unit (TU)** will be given in next section. However, in general, TU reduces the number of chains in a sub-image file to a single chain, if possible, and predicts the loop's class in its **Auxiliary Classification Unit (ACU)**. Most of the "crossed" loops will be detected in ACU. The output of TU, therefore, will indicate whether the loop is a "crossed" one or not. If it is, then a class file for the loop will be created, and the loop will be classified as "crossed" type. Since the loop's class is determined, the loop must not be evaluated by MCM. Therefore, the class file should be tagged with "stop" label, in order to prevent further investigations on the loop.

If the output of TU is not "crossed" type, then possibility of the loop being a "cuticulis" one should be examined. The exclusive curvature angle  $\theta$  of a loop can be calculated from equation 3.1. According to "cuticulis" loop classification criteria (section 3.4.1), any loop that has  $\theta < \theta_{\text{CUTICULIS}}$  must be classified as "cuticulis" type. However, the enlarged open loop (i4:N28) has got  $\theta = 129^\circ$  that is less than  $\theta_{\text{CUTICULIS}} = 131^\circ$ . If the classifications of the loops were being made manually, this loop's  $\theta$  would not be calculated, because it is quite obvious that the loop has got pretty long limbs to be classified as "cuticulis". For computerized classification, however, if a loop is not a "crossed" type,  $\theta$  must be calculated. Even "bizarre" structures will be analyzed for membership of "cuticulis" class. At this point, the calculation of loop width (Lw) causes problems.

The capillary loop width cannot be calculated without calculating the loop length. The loop length of the capillary loop will be measured on the medial axis of the capillary loop. Thinning algorithms of TANCCAS produces disoriented skeletons for most of the "cuticulis" type capillary loops. The width of the "cuticulis" loop may be longer than its length. Therefore the thinning algorithm produces horizontal skeletons rather than verticals. In such cases the loop length will be mis-calculated. Instead of calculating the loop length and width, for detection of the "cuticulis" loops, the projection distance between end points of a capillary loop chain is assumed to be, roughly, the loop width (Lw). This assumption speeds up the calculations of  $\text{sin}\theta$  value, but causes errors for the loops like (i4:N28). The loop (i4:N28) has got one limb

Read an image that contains only one capillary (Created in previous section). If the capillary loop has got more than one chain, the number of chains should be reduced to one. The Main Classification Module (MCM) accepts the sub-image files that contain disclosed single chain. Transformer Unit (TU) assures that the output image will contain only one chain. Beside transformation, some early predictions are made about the capillary class in this module. Most of the crossed ones are detected in TU. If the output of TU is crossed then create a class file indicating that it is crossed type, with the stop tag to stop further process.



If it is not crossed type capillary, then apply polygonal approximation algorithm to the resulting image and record the approximation points into a file.

While deciding on atypical loops, less detailed capillary chain is needed. So this part is a preparation for the classification of bizarre and bushy loops in Main Classification Module (MCM). The approximation is made with high error toleration, hence the resulting image is very rough sketch of the original capillary chain. By connecting the end points of the chain, and filling the enclosed area, the Auxiliary Image is created. Although atypicals are decided in MCM, obtaining auxiliary image in this stage, eliminates the re-use of polygonal approximation on capillary body chain in MCM.

Calculate the length of the capillary chain and distance between end points, in order to determine  $\theta$  (Exclusive Curvature Angle) value of the loop. If  $\theta < \theta_{cuticulis}$ , then the loop is most probably a cuticulis one. Before deciding on the type, check whether one of the loop limbs is significantly longer than the other. If it is not, the loop is a cuticulis one, otherwise further investigation is necessary by MCM. If the capillary is cuticulis, then append the suggested class to the class file indicating that it is a cuticulis, with the stop tag to stop further computations on this image. Otherwise just set the class file tag to continue.

Figure 5.16 Pre-Processing Module Part II (PPM-II)

significantly longer than the other one, and the projection distance between the end points of the limbs cannot be assumed to be the loop width. It is the same for the loops (i4:N5) and (i4:N6). Experiments showed that the capillary loop is not a "cuticulis" one if the distance between the long limb's end point and the loop's centre of gravity is 1.5 times longer than the distance between the short limb's end point and the loop's centre of gravity. Therefore, the control mechanism given above will prevent misclassifications of the loops that have got one limb significantly longer than the other. After detecting the loop is "cuticulis" type, further analysis should be prevented by tagging the class file with "stop" label. The class file of cuticulis capillary was already created in transformer unit. The anomaly class label "enlarged" or label "normal" was assigned to the loop and was noted in its class file. Therefore, if the loop is "cuticulis" type, descriptive class label "cuticulis" must be appended to the class file.

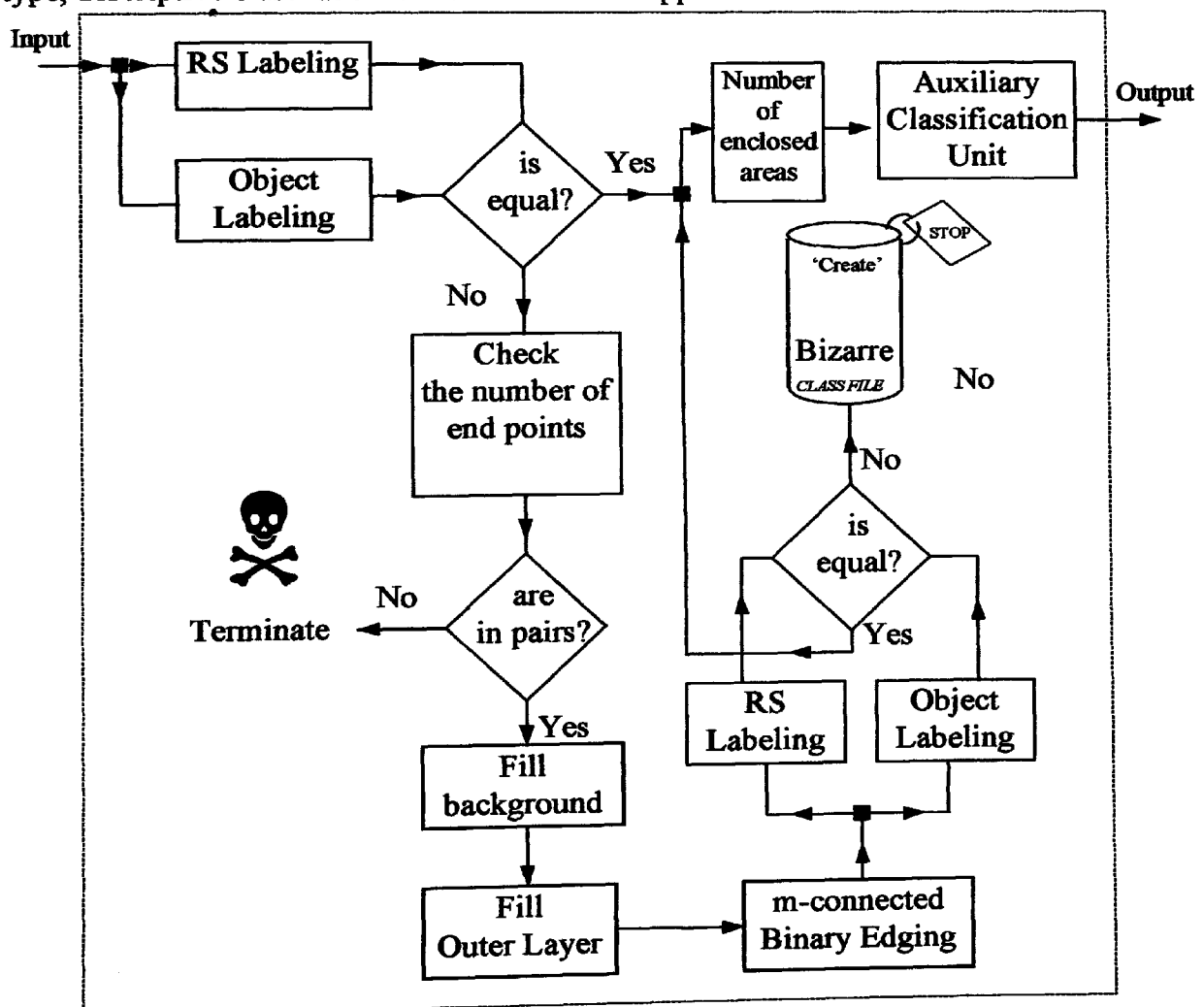
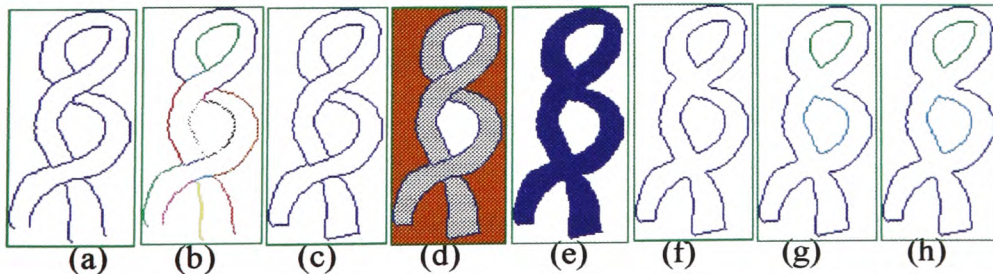


Figure 5.17 The block diagram of Transformer Unit (TU)

### 5.4.2.1 Transformer Unit (TU)

The main function of **Transformer Unit (TU)** is to transform the sub-image files that contain capillary loop chain(s), into the sub-image files that contain only and only one disclosed chain. Although, the EnC loop of "collect.asc" has got a single chain in its sub-image file, that chain should be processed and a disclosed chain must be obtained in order to be inputted to the MCM. The capillary loops having more than one chains, for example; GOP, BSH and CR of "collect.asc", will be reduced into a single chain. Most of the "crossed" capillary loops will be detected in this unit. The output of TU indicates whether the loop is "crossed" or not. Auxiliary Classification Unit (ACU) of TU predicts some of the loop's class, by analyzing the inner chains that will not be available for MCM. In another words ACU compensates the lost of some useful chains for MCM. The Block diagram of TU is given in Figure 5.17.

As stated earlier in this chapter, while tracing the capillary loops, the tracing style may vary from one person to another. The single twisted loops T11 and T35 of Appendix B, for example, are the product of two different styles. The loop T35 is the product of the desired style; the loop tracings are not touching each other, and tracing lines are the borders of object and background. TANCCAS should be able to process the loops that are traced with either of the styles. Therefore, the loops that have got chain segments where they are not bordering background should be eliminated. None of the loops in "collect.asc" needs such transformations. The loop T14 of Appendix B is selected to demonstrate elimination of unnecessary chain segments (Figure 5.18).



**Figure 5.18** (a) The input image to be transformed (b) The RS Labelled image (c) The output of end point connector (d) Flood Filled background (brown) and background controlled the most outer enclosed area filling (gray) (e) Thresholding output (f) Binary object edge detecting output (g) Object Labelling and (h) RS Labelling outputs.



The input image (Figure 5.18(a)), will be labelled by using object and RS Labelling. Object labelling function labels all of the chains that connected to each other anyhow, with the same label number. RS Labelling, on the other hand, labels each chain segment with a unique number. If the capillary loop chains are isolated from each other the number of chains and the number of chain segments will be equal to each other. It means that there is not any chain segment to be removed, therefore there is no need for transformation (For example, the sub-image files of "collect.asc"). The loop T14, however has fourteen chain segments (Figure 5.18(b)). All of these segments are connected to each other, therefore the number of chains is only one. Hence, the transformation must be proceeded.

First, check the numbers of chains' end points. The number of end points must be either two or four. Otherwise, either the loop was traced improperly by the observer, or the LBR failed to remove those unwanted long branches. Since the loop is not suitable for further computations, terminate the analysis. If the end points are in pairs then detect the end points that are belong to same limb, and connect them. The output of end point connection for T14 is given in Figure 5.18(c). Second, Flood Fill the background that is outside of the most outer chain (brown area in Figure 5.18(d)). Third, if a chain is bordering white background and brown background at the same time, then, Flood Fill white background with gray color (Figure 5.18(d)). By replacing brown with white, and thresholding this final image (Figure 5.18(e)), the most outer enclosed area of loop will be obtained. Finally, by applying binary edge detection algorithm, only the border chains will remain in the sub-image file (Figure 5.18(f)). Once more, checking the number of chain segments and the number of chains of the loop by applying RS Labelling and Object Labelling algorithms, respectively, the transformation result will be confirmed. As can be seen from Figure 5.18(g) and (h), both of the algorithms produced three labels for the loop T14. After the transformation, if the numbers of labels are still not equal, than it can be said that the loop's limbs forms quite complex shape. Therefore, without further computations, it should be classified as "bizarre" type.

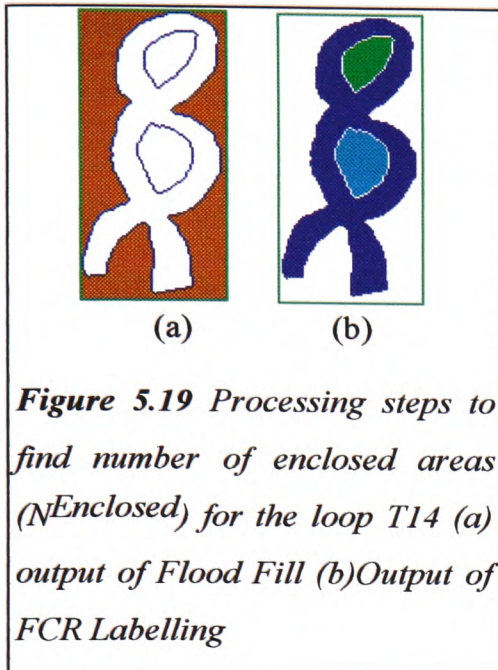


*Figure 5.19 Processing steps to find number of enclosed areas ( $N^{Enclosed}$ ) for the loop T14 (a) output of Flood Fill (b) Output of FCR Labelling*

Auxiliary Classification Module (ACM) requires three inputs; the sub image that contains single segmented loop chains, the number of chains ( $N^{Chains}$ ) and the number of enclosed areas ( $N^{Enclosed}$ ). The sub-image file and  $N^{Chains}$  are ready to be inputted to ACU. Therefore, the number of enclosed areas in the sub-image file must be calculated. The GOP and ETO loops of "collect.asc", for example, have two and one chains respectively. However, none of the chains form an encircled area. Therefore,  $N^{Enclosed}$  will be 0 for these two loops. As can be seen from Figure

5.18(g),  $N^{Chains}$  is three for the loop T14. The calculation of  $N^{Enclosed}$  is as follows; First Flood Fill the outside of the most outer enclosed area (Figure 5.19(a)). Second, threshold the image with  $object > 0$   $background = 0$ , then invert the image by applying logical NOT operation. Finally by labelling the objects with FCR Labelling algorithm (Figure 5.19(b)),  $N^{Enclosed}$  will be calculated as three.

#### 5.4.2.2 Auxiliary Classification Unit (ACU)

The Auxiliary Classification Unit (ACU) can predict some of the capillary loops' classes by checking ( $N^{Chains}$ ,  $N^{Enclosed}$ ) control pair. The output image of ACU will contain a single disclosed capillary chain that is required by MCM.

The most outer loop chain of the sub-image file will be the output of ACU. The loop chains that will be removed in ACU, of course, are important for the analysis and classifications. Therefore, as much information as possible should be computed before the removal of those chains that will not be present in MCM. Before explaining the functionality of ACU, a brief discussion about why the outer chain of a capillary loop is selected for output, should be given. A synthetic capillary loop given in Figure 5.20 has got two loop chains. The outer chain does not display any tortuosity on its course. Therefore, if the outer chain is selected as the input of MCM, the loop will be classified

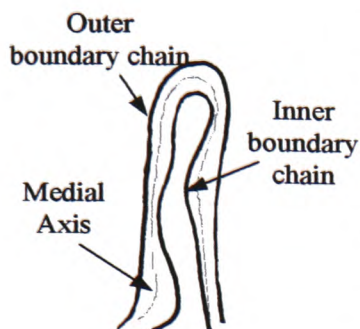


**Figure 5.20** *A problematic capillary loop*

as "open" type. The inner boundary of loop, on the other hand, has got high tortuosity, and MCM will classify it as "tortuous" type. Is this capillary loop, "open" or "tortuous" type? Which boundary chain should be selected as output? There may be a suggestion that the medial axis of the limbs may reflect the true nature of the limbs' course. This may be true for the loops like GOP of "collect.asc". However, if the inner boundary is an encircled chain, the medial axis of such loops' limbs, for example; (i2:N2), (i2:N9) and (i5:N26), will be totally different from overall appearance of the loop. Such cases also discourage the use of inner chain as the input of MCM. Therefore, the outer boundary is the only answer for the selection. Since the outer chain is available for all of the loops, the computations will be unified for all kind of loop tracings.

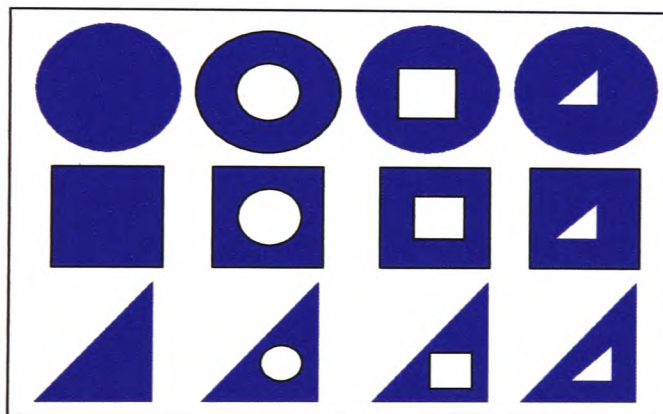


**Figure 5.21** *The objects to be classified one of the classes; Circular, Rectangular and Triangular.*

Additionally it is really safe to assume that basic shape of an object is dominated by its outer boundary. This can be demonstrated by classifying the blue objects on white background in Figure 5.21 into one of the classes; Circular, Rectangular and Triangular. Will any of the objects in top two rows be assigned to class Triangle? Since you are not allowed to suggest new classes, such as; Circular with triangular whole, Rectangular with triangular hole, etc., regardless to the shapes of the holes, the shape of the outer boundary will be the shape of the objects.

The output image of ACU, therefore, will contain only the outer boundary chain of the capillary loop. Bearing in mind that MCM requires disclosed chain, single boundary chains of the loops like T3 and T39 of Appendix B must be appropriately disclosed. By checking ( $N^{\text{Chains}}$ ,  $N^{\text{Enclosed}}$ ) control pair the following computations should be made.

**CASE (1,0):** There is only one disclosed loop chain in the image. Transformation is not needed.

**CASE (1,1)** The single boundary chain may be traced just for the outer boundary of a loop (Figure 5.22(a)), or for both inner and outer boundaries of the limbs (Figure 5.22(b)). In both cases a single disclosed chain is desired as output image. In the first case (Figure 5.22(a)) the loop is within normal width, and in the second case (Figure 5.22(b)), the loop is "enlarged". The first step of transformation and classification of these kind of loops is identifying their label classes.

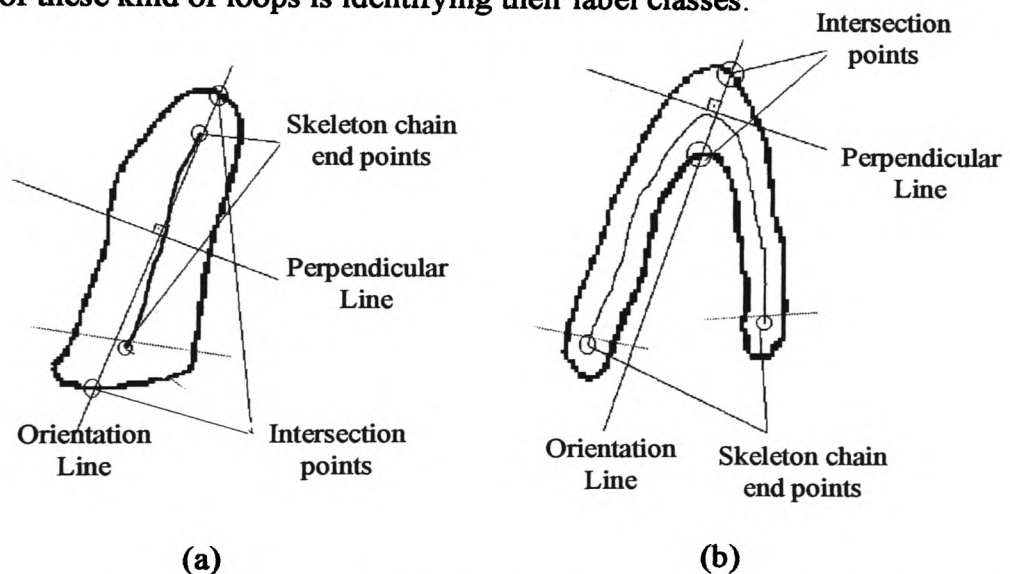


**Figure 5.22** Typical examples of case (1,1), (a) a capillary loop within normal width (b) "Enlarged" capillary loop.

First, find the orientation and center of gravity of the loop. Then find the medial axis of the limbs, and calculate the coordinates of its end points. Draw the orientation line of the loop (Figure 5.22). passing through the loop's center of gravity. Calculate the coordinates of top two intersection points between orientation line and capillary loop

chain. Then draw a perpendicular line that passes through middle point of the line that connects the intersection points. Calculate the numbers of medial axis end points that is located underneath and above of the perpendicular line. If one of the end points are underneath the perpendicular line, then the loop is within normal width. If both of the end points underneath the perpendicular line then it is "enlarged". Create a class file and write the loop's label class.

In order to obtain single disclosed capillary loop chain, depending on the loop's being within normal width or "enlarged", one or both of the capillary loop tip points must be cut from the dashed lines in Figure 5.22. If the loop is "Enlarged" both of the limb end parts must be cut by removing some of the pixels. Then case (2, 0) must be applied. Because by removing the limb end parts, the loop's ( $N^{\text{Chains}}$ ,  $N^{\text{Enclosed}}$ ) control pair has been transferred from (1,0) to (2, 0). Therefore, further transformation will be necessary for "enlarged" loop by applying case (2, 0). If the loop is within normal width, then only the bottom end point of loop will be removed. There is no need for further transformation for the loop.

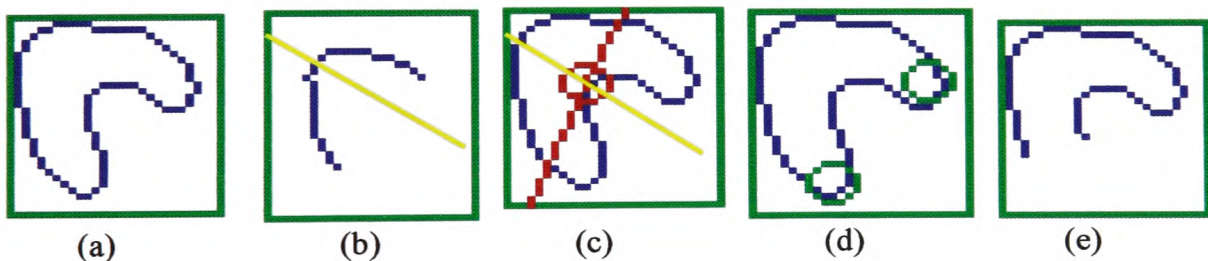


**Figure 5.23** Analysis steps of the loop (i3:N21) (a) the loop (b) its skeleton (c) Orientation line (red) (d) detected loop tip points (circled) (e) disclosed chain loop.

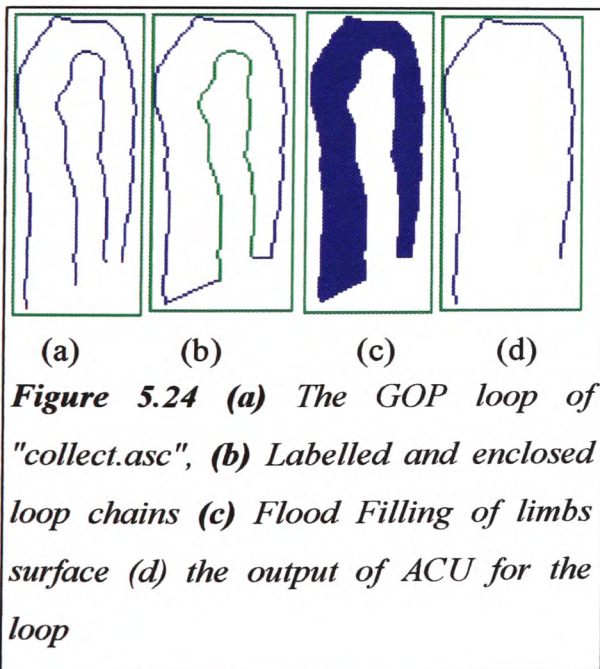
By using the method described above, the enclosed loop chain of (i3:N21) (Figure 5.23(a)) has been transformed to a disclosed one (Figure 5.23(e)). This capillary loop is specially selected to demonstrate the pitfall of the suggested transformation method. The loop limbs are so short, that the orientation line of the capillary loop (Figure 5.23(c) red line), will be disoriented from the desired direction (yellow line). Although the red orientation line has been calculated and drawn correctly, the deviation from the desired orientation line is due to the shape of the loop. Although the loop is

"enlarged", one of the skeletal chain end points will be underneath the perpendicular line (yellow line in Figure 5.23(b)). Therefore, TANCCAS will disconnect only one of the detected loop end points (Figure 5.23(d)). This disclosed single chain will be miss classified as "open" type in MCM. Unfortunately, There could not be found any method to correct this kind of transformation error. All of the test image loops that has (1,1) control pair, on the other hand, had been transformed successfully as well as the ECU loop of "collect.asc".

**CASE (1, $N^{Enclosed}>1$ )** Impossible condition. A single capillary loop chain that has not got any chain segments but itself, cannot create enclosed areas more than one.

**CASE (2,0)** The image that has (2,0) control pair, contains two chains; one for loop's outer boundary and another one for the inner boundary. By removing the inner boundary chain, the output image of ACU can be obtained. Since the labelling algorithm operates in top-down mode, the outer chain will have the label '1', if the image labelled. (It has been assumed that a capillary loop in the picture cannot be upside-down.) Therefore the loop chain that has label '2' must be removed. Before

removing the inner boundary chain, the limb surface area should be measured to calculate the limb width of the loop.



The processing steps will be demonstrated for the GOP loop of "colect.asc" (Figure 5.24(a)). In order to calculate the limb surface area, first detect the chains' end points. Then, find which end points should be connected to each other. Obtain an enclosed area by drawing lines between end point pairs (Figure 5.24(b)). Flood Fill the enclosed area and

measure its volume that is the limbs surface area (Figure 5.24(c)). This value will be used later on to calculate the limb width of enlarged capillary loops. Obtain the output

image by removing the loop chain that has label '2', (Figure 5.24(d)). Create a class file and note that it is "enlarged" type. Tag the class file with "continue" because further process is necessary to define the loops LAC and DC class label.

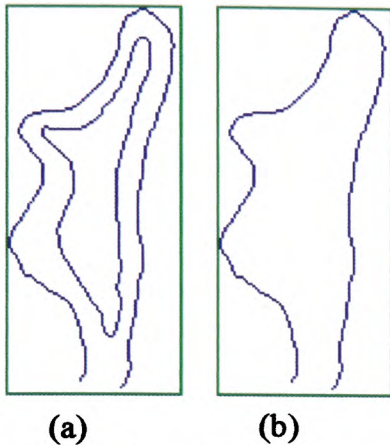


**Figure 5.25 (a)** The BSH loop of "collect.asc" as input image of ACU **(b)** The output of AUC for the loop

**CASE (2, 1)** The loop has got two chains and only one of them is encircled. The outer chain contains enough information to carry out the classification routines. Therefore encircled chain must be removed. A class file for the capillary should be created noting that it is "enlarged" type and further processes should be carried out. The BSH loop of "collect asc (Figure 5.25(a)), for example, is this kind of loop. The output image of ACU will be as in Figure 5.25(b), after removing encircled inner boundary chain. Although the loop is "enlarged", limb width cannot be calculated in this group.

**CASE (2, 2)** Most of the early suggestions on capillary loop's descriptive class will be made in this group. Some of the crossed and bushy type capillary loops will be identified, and they will be excluded from further analyses . Some of the bushy and bizarre structures, on the other hand, will be classified as "atypical" and by feeding their outer boundary chain into MCM, their classification will be completed.

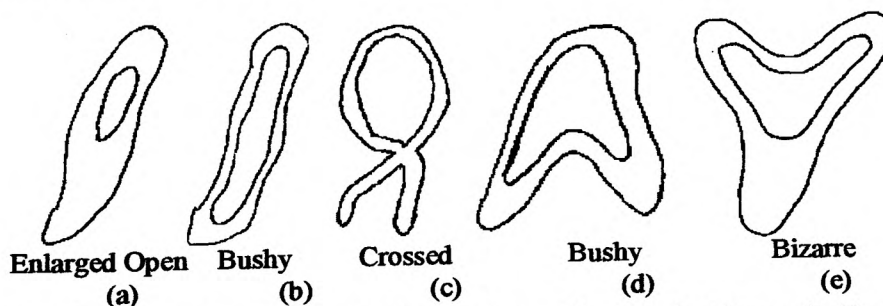


**Figure 5.26** The morphological variations of capillaries that have (2,2) control pair.

The capillary loops in this group display morphological variations (Figure 5.26). Different actions should be taken for each of these loops in order to complete their

transformation to be suitable for MCM (Figure 5.27). First, get the enclosed outer chain and Flood Fill the encircled area. Then, apply Thinning algorithm and obtain the loops skeleton. Calculate the number of chain segments of the skeleton by applying RS Labelling. If the number of chain segments  $N^{\text{segments}}$ ,

**( $N^{\text{segments}}=1$ )** The capillary type could be "open"/"tortuous", or "bushy" as in Figure 5.26(a) and (b). To differentiate them from each other, first, get the skeleton of outer chain and calculate its length. Then by masking skeleton chain with the inner enclosed area, calculate the percentage of the skeleton chain part that passes through inner section. If it is more than 50%, then the loop is bushy type. Create a class file and note that it is a "bushy" one and stop further process. If it is less than 50%, replace the original image file with the outer chain and repeat the condition (1,1).

**( $N^{\text{segments}}=2$ ) Impossible condition.**

**( $N^{\text{segments}}=3$ )** The capillary loops (c), (d) and (e) of Figure 5.26 are either atypical or "crossed" ones. Find the orientation line that passes through central point then draw a line that is perpendicular to the orientation line and passes through the adjoining point of the skeleton branches. Find the skeleton chains' end points. Calculate the number of end points that located underneath the perpendicular line. If it is '2' then it could be either "crossed" or "bushy" type. Find the percentage of skeleton chain part that passes through inner circle. If it is more than 60% of whole skeleton chain, it is an atypical loop. Create a class file indicating that it is "atypical" and further computation is required. Then replace the original image file with the outer chain and repeat case (1,1), If it is less than 60%, then it is "crossed" type and stop further process. if the number of end points that located underneath the perpendicular line is not '2', then create a class file indicating that it is "atypical" and further computations required. Replace the original image file with the outer chain and repeat condition (1,1).

**( $N^{\text{segments}} > 3$ )** It is a definite "atypical", create a class file indicating that it is "atypical" and further computations are required, then replace the original image file with the outer chain and repeat condition (1,1).



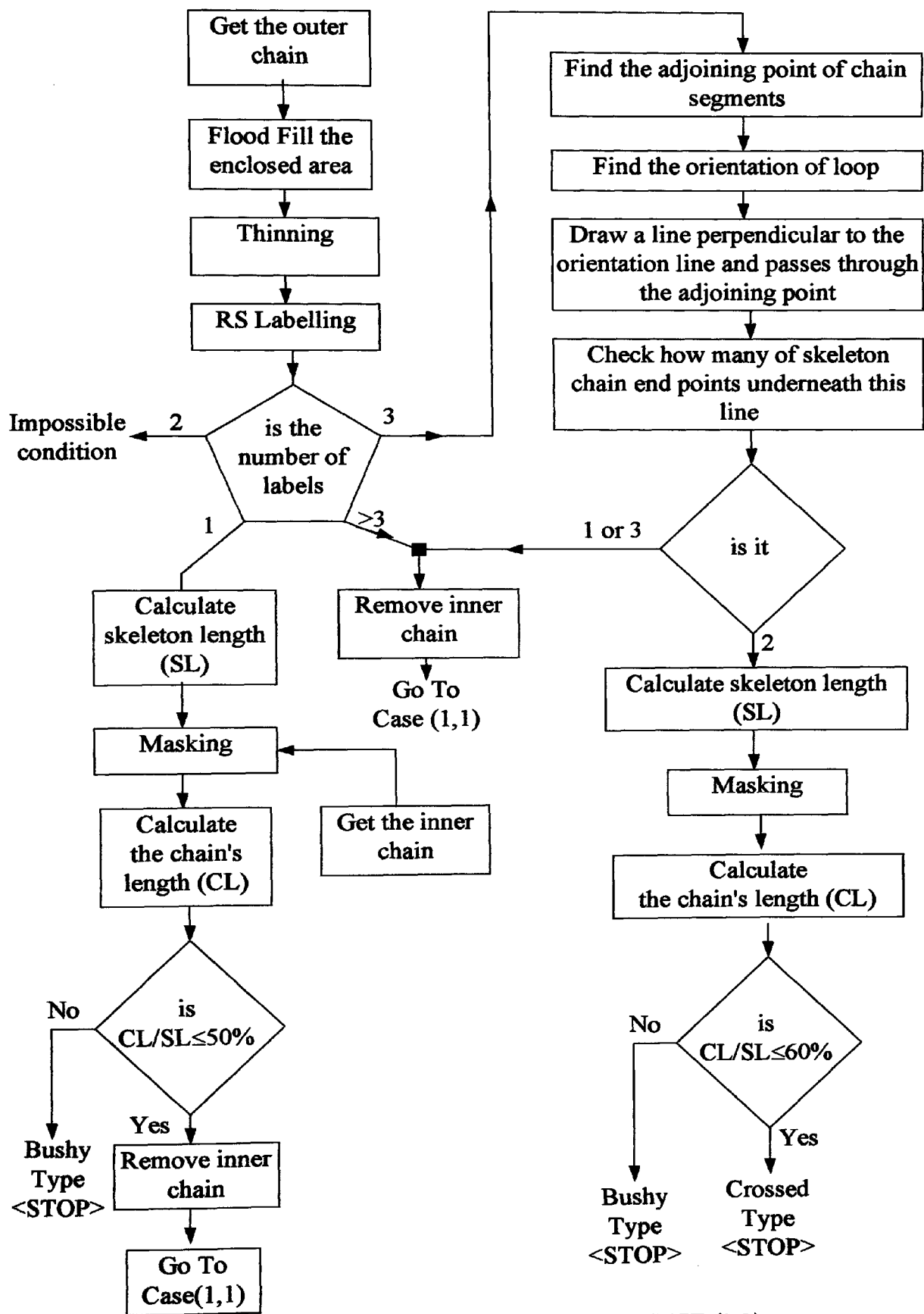
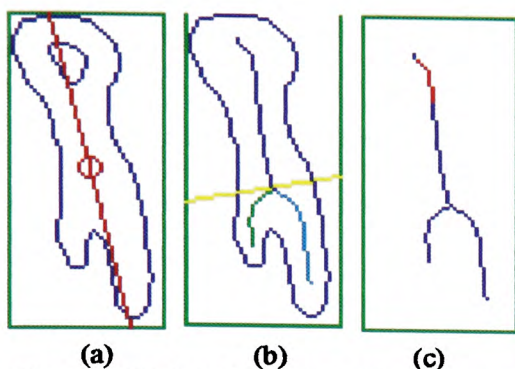
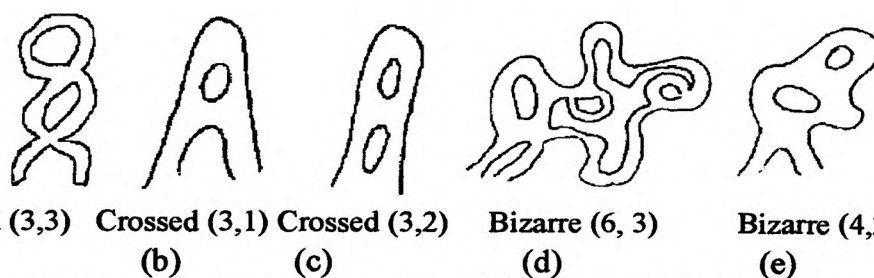


Figure 5.27 The analysis mechanism of CASE (2,2)



**Figure 5.28** (a) Crossed capillary loop of "collect.asc" and its orientation line. (b) The skeleton of the area encircled by outer chain and the perpendicular line (yellow) (c) the skeleton part that passes through the inner chains area (red).

The "crossed" loop of "collect.asc" (Figure 5.28(a)) has (2,2) control pair, and the number of skeletal chain segments  $N_{segments}$  is three (Figure 5.28(b)). Two of the end points of the skeletal chains are underneath the perpendicular line (yellow). Therefore the loop is either "bushy" or "crossed". The length of the skeletal that passes through the inner chain (red line in Figure 5.28(c)) is 10% of the total skeletal chain length. This value is less than 60%, therefore the loop is "crossed" type. No further computations are necessary.



Crossed (3,3) Crossed (3,1) Crossed (3,2) Bizarre (6, 3) Bizarre (4,2)  
 (a) (b) (c) (d) (e)  
**Figure 5.29** The possible inputs of CASE ( $N_{Chains} > 2, N_{Enclosed}$ ) (The numbers in parenthesis are ( $N_{Chains}, N_{Enclosed}$ ) control pair for the loop)

**CASE(2,  $N_{Enclosed} > 2$ ) Impossible condition.**

**CASE( $N_{Chains} > 2, N_{Enclosed}$ )** The morphological alterations of the loops in this group are even wider than case (2, 2) (Figure 5.29). However, descriptive class of a loop in this case can be either "crossed" or "bushy"/"bizarre". As in case (2, 2) some of the "crossed" and "bushy" type capillary loops will be identified, and they will be excluded from further analyses. Some of the "bushy" and "bizarre" structures, on the other hand, will be classified as "atypical" and by feeding their outer boundary chain into MCM, their classification will be completed. The transformations (and classifications) will be achieved as follows: Get the outer chain and Flood Fill from the coordinates (0,0). Threshold the resulting image and invert it. Apply Thinning operation to the final image. If there is no skeleton that means the outer chain is disclosed. The

capillary could be "crossed" or atypical. Create a class file and note that the loop's class is "UnDecided", and further process is required on the image that contains only the outer boundary chain. The capillary loops in Figure 5.29 (b), (c), (d) and (e) are such kind of loops. The loop (d) and (e) will be identified as "bizarre" in MCM. The loops (b) and (c), on the other hand will be classified as "open" (or "tortuous") in MCM, because of the shape of the outer chain. These two loops will be correctly identified as "crossed" in Class Decision Unit (CDU). The class files of loops (b) and (c) will have two labels; "UnDecided" and "open" when they were inputted to CDU. The label "UnDecided" will dominate the class label "open" and the loop will be classified correctly as "crossed". In loops (d) and (e)'s cases, however, CDU will ignore the label "UnDecided", because "bizarre" and "bushy" class labels has got priority over "UnDecided". If there is skeleton chain(s), then label the image by using RS Labelling. If the number of chain segments

**( $N^{Segments}=1$ )** It is a crossed type capillary, create a class file indicating that it is "crossed" and stop further computation.

**( $N^{Segments}=2$ ) Impossible condition**

**( $N^{Segments}=3$ )** The capillary loop is either atypical or crossed one. Find the orientation line that passes through central point then draw a line that is perpendicular to the orientation line and passes through the adjoining point of the skeleton branches. Find the skeleton chains' end points. Calculate the number of end points that are located underneath the perpendicular line. If it is '2' then the capillary is crossed type, create a class file indicating that the loop is "crossed" type, and stop computation. Otherwise, create a class file indicating that it is "atypical" and further computations are required. Replace the original image file with the outer chain and repeat condition (1,1).

**( $N^{Segments}>3$ )** It is a definite "atypical", create a class file indicating that it is "atypical" and further computations are required, then replace the original image file with the outer chain and repeat condition (1,1).

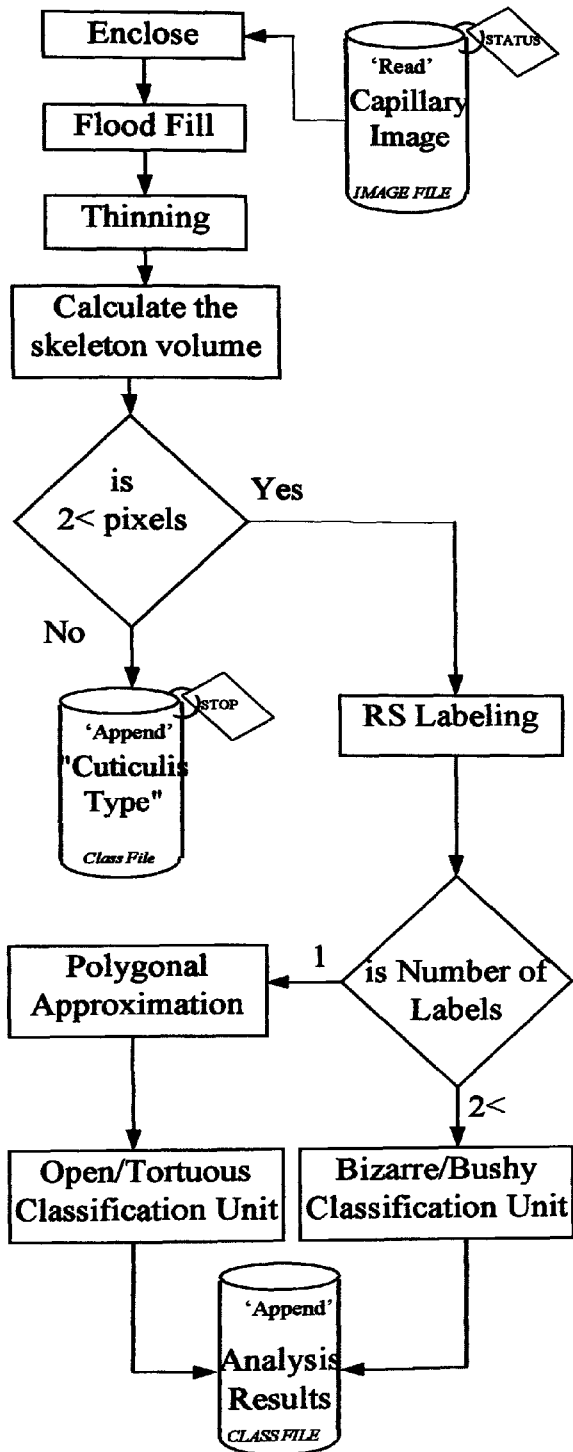


Figure 5.30 The block diagram of Main Classification Module (MCM)

### 5.4.3 Main Classification Module (MCM)

The capillary loops, whose outer chains display one of the descriptive class patterns; "open", "tortuous", "bizarre" and "bushy", will be identified in MCM by implementing the classification criteria given in section 3.4. **Open-Tortuous Classification Unit (OTCU)** is employed to recognize "open" and "tortuous" loops, as well as calculating their morphological parameters; loop width and length. "Bizarre" and "bushy" loops, on the other hand, are identified in **Bizarre-Bushy Classification Unit (BBCU)**. Furthermore, the loops that have exclusive curvature angle  $\theta > \theta_{\text{CUTICULIS}}$  but their loop skeleton areas are less than 3 pixels, will be exclusively classified as "cuticulis" type. Skeletons of such loops do not contain enough information to carry out analysis in OTCU or BBCU.

The image file that contains disclosed single capillary chain, is the input of MCM. If the 'status' of image file 'continue', that was defined in PPM-II, MCM analyzes the loop to find its descriptive class label. It should be

remembered that, in the Pre-Processing Module (PPM), it has been guaranteed that the input image file of MCM will contain only a single disclosed capillary chain.

First, find the loop chain's end points and connect them with a line. Then, fill the enclosed area and by thinning obtain the loop's skeleton chain. If the volume of skeletal chain is less than 3 pixels, neither OTCU nor BBCU are able to process the loop. Such a small chain can be produced for only those loops near to the borderline between "cuticulis" and "open" patterns. The loop (i5:N21), for example, is the only such kind of loop in the test images. Although, the loop's exclusive curvature angle  $\theta=132$  is wider than critical angle  $\theta_{\text{CUTICULIS}}=131$ , it will be classified as "cuticulis". TANCCAS must calculate "open" and "tortuous" loop's length and width. For this loop, these parameters cannot be measured because of insufficient skeleton information, therefore, the cuticulis classification criterion given in section 3.4.1 will be violated for such kind of loop. Actually, the thinning algorithm produces a skeleton chain that is longer than 2 pixels for almost every capillary loop (including (i5:N21)). After removing spur branches and re-arranging the resulting chain, the number of pixels remaining in the picture may be less than 3. Even if the loop is mis-classified, the classification error will not be so drastic, since this circumstance occur for the loops near to class boundaries.

If the skeletal chain is of acceptable length, then find the number of skeleton chain segments by applying RS Labelling. If it is a single chain(segment), then the loop cannot be an atypical loop. Therefore the loop should be processed in OTCU. If a chain has more than 2 segments it is atypical, and it is analysed in BBCU. Both of the classes that produced in PPM and MCM are only the suggested classes. In order to determine the final true class of a capillary loop, length and limb width should be processed in **Class Decision Unit (CDU)** as well as the suggested classes.

#### **5.4.3.1 Open-Tortuous Classification Unit (OTCU)**

The block diagram of Open-Tortuous Classification Unit is given in Figure 5.31 The function of the unit will be demonstrated by analysing the loop ETO of "collect.asc". The disclosed single loop chain (Figure 5.32(a)) were read as input of the MCM. The loop is enclosed by connecting the end points of the chain (Figure 5.32(b)).

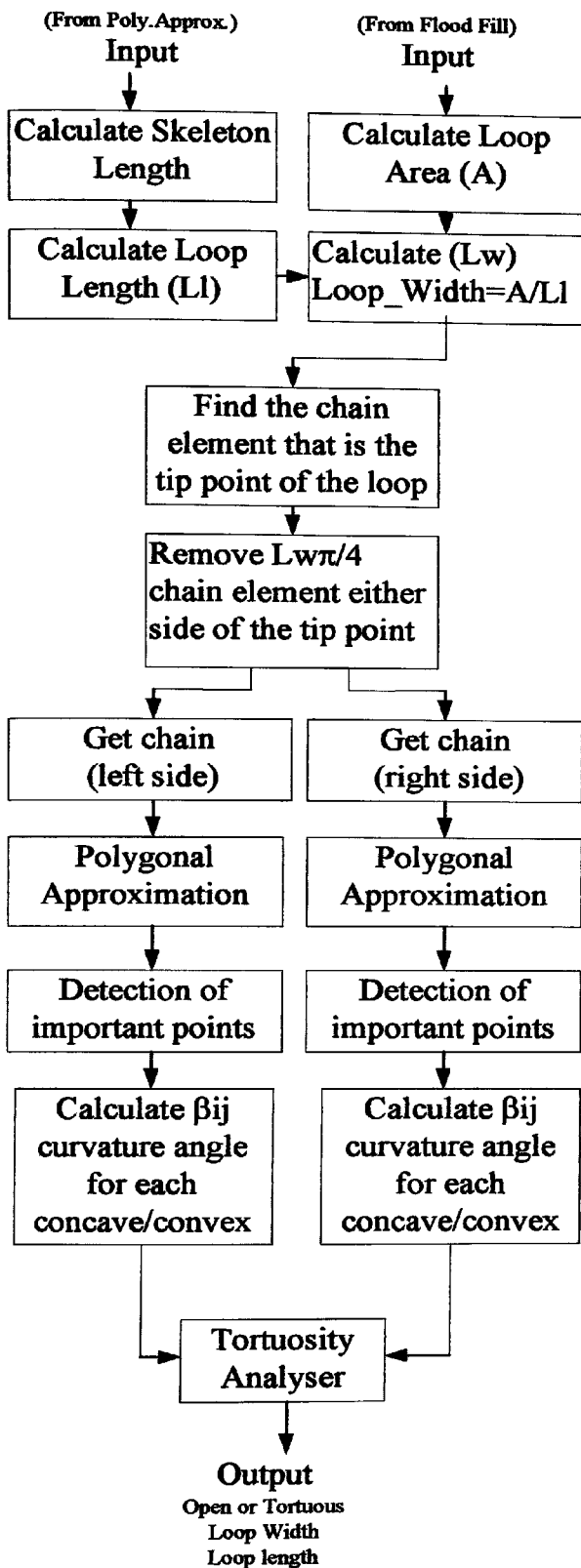


**Figure 5.31** The block diagram of Open-Tortuous Classification Unit (OTCU)

By Flood Filling the enclosed area, the loop's silhouette will be obtained (Figure 5.32 (c)). This image will be used for calculation of the loop width (Figure 5.31).

By applying Thinning() operation and removing the spur branches, the skeleton of the loop can be obtained (Figure 5.32(d)). Since the skeleton volume is more than 2 pixels, the loop will be RS labelled in order to find the number of skeleton chain segments. The loop ETO's skeleton has only one segment, therefore it will be analyzed by OTCU.

By applying polygonal approximation, obtain a skeletal chain that is drawn by line segments (Figure 5.32(e)). By measuring each line segment's length and adding them calculate skeletal chain's length. This measurement will be used to calculate loop length. As can be seen from Figure 5.32(f), the skeleton's length cannot be accepted as the loop length. Between skeleton tip points and loop chain there are gaps (yellow lines) that should be added to skeleton length in order to calculate the loop length accurately. By stretching the tip segments of polygonally approximated skeleton (segments' directions are preserved) and measuring the difference, the length of these gaps can be calculated.

The final length gives us the loop length (L). By counting the number of object elements in Figure 5.32(c), the capillary loop area (A) can be found. However, this measurement is not precise, and precise measurement is not essential. Dividing the area (A) by loop length (L), estimated LoopWidth (Lw) can be calculated.

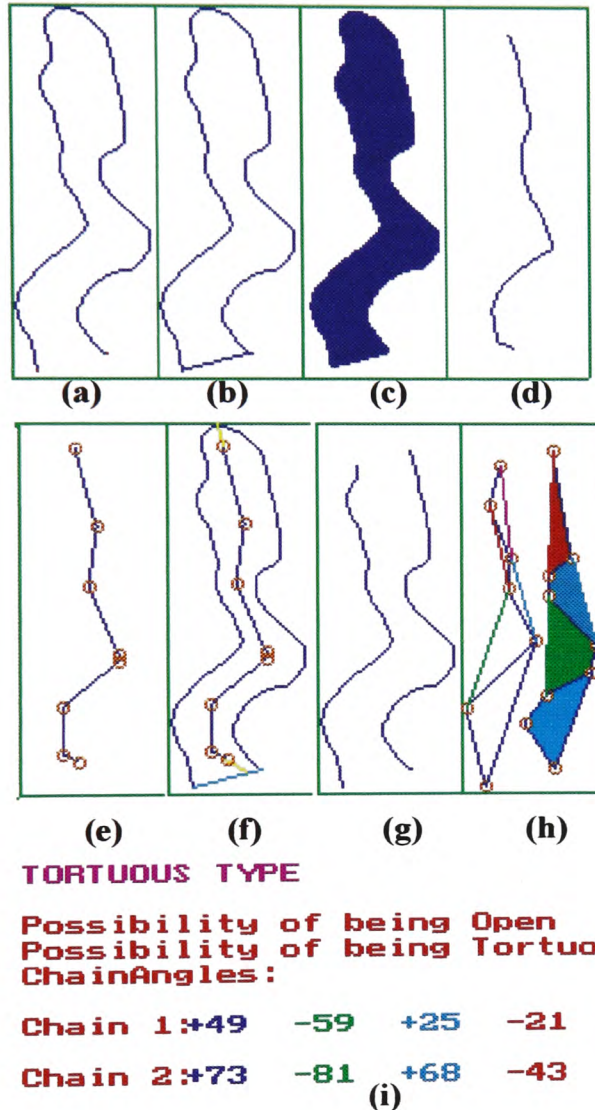


**Figure 5.32** The processing steps of MCM (a) The input image (The loop NET of "collect.asc", (b) Output of Enclose, (c) The loop's silhouette (d) Skeletal chain of the loop, (e) Polygonally approximated skeletal chain (f) Stretched skeletal chain tip segments (yellow lines) (g) The loop's side chains (h) Tortuosity analysis, (the detected concavities and convexities of chain 2, are flood filled for display purposes.) (i) Analysis result (given  $\beta_{ij}$  angle value belongs to the concave/convex that has got the same base line colour)

The intersection point of stretched skeleton tip segment and loop chain is accepted as the tip point of the capillary loop. Assuming that loop's tip is semi-circular and its radius is  $Lw/2$ ,  $(Lw\pi/4)$  chain element should be removed either side of the tip point, in order to obtain capillary loop side chains (Figure 5.32 (g)). By applying Polygonal Approximation, each side chains will be approximated to the line segments.

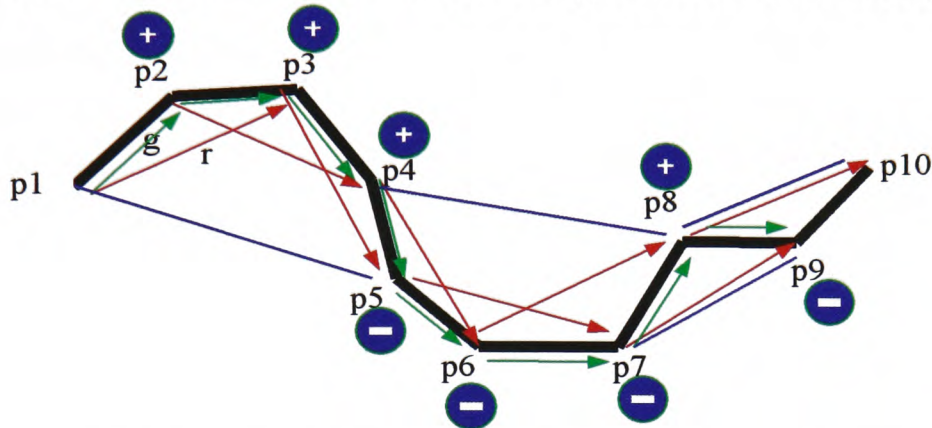


*Figure 5.33 Detection of concaves and convexes on a side chain.*

#### 5.4.3.2 Tortuosity Analyzer

Tortuosity analyzer detects the convexities and concavities on a polygonally approximated side chain, then, measures the curvature angle  $\beta_{ij}$  for each curve. The detection of curves (concavities and convexities) is illustrated in Figure 5.33. The polygonally approximated thick black line segments form four curves (curve end points connected with blue lines). The cross product of a red and a green vector pairs that have same application points is the key factor for detection. In a concave or convex, the sign of cross product  $\underline{r} \times \underline{g}$  must be same. The point, where the sign changes, is the end point of a concavity or convexity. The detected concavities and convexities of right hand side chain of the loop ETO are given in Figure 5.32(h) (Flood Filled areas).

After detecting each curve, the calculation of curve base length and curve perimeter is a simple task. By substituting these values in equation (3.2), the curvature angle  $\beta_{ij}$  can be calculated for each curve. A loop's class will be defined by its side chains' tortuosity levels. For each side chain, calculate the possibilities of being part of an open loop ( $pO_i$ ) and of a tortuous loop ( $pT_i$ ) as follows;



If the  $\beta$  angle of a curve is larger than  $\beta_{OPEN}$ , then increase the  $pT_i$  by the significancy amount ( $S_c$ ) of the curve on overall appearance, otherwise increase  $pO_i$  by  $S_c$ . Each curve's significancy in overall appearance ( $S_c$ ) is .

$$S_c = 100 * \text{curve\_base\_line\_length} / \text{total\_of\_curve\_base\_lines\_length}$$

By calculating the following parameters and checking the conditions in Table 5.1 for  $(n_1, n_2)$  control pair, the loop's class can be identified.

**$n_1$** : Number of curves on side chain1

**$n_2$** : Number of curves on side chain2

**$\beta$** : curvature angle

**$pO_1, pO_2$** : possibility of being "open" type for side chain1 and side chain2 respectively

**$pT_1, pT_2$** : possibility of being "tortuous" type for side chain1 and side chain2 respectively

$n_1$	$n_2$	CONDITIONS	CLASS
1	1	if $\beta_{11} > \beta_{TORTUOUS}$ and $\beta_{21} > \beta_{TORTUOUS}$ <otherwise>	Tortuous <Open>
1	2	if $\beta_{11} > \beta_{TORTUOUS}$ and $(\beta_{21}$ or $\beta_{22}) > \beta_{TORTUOUS}$ <otherwise>	Tortuous <Open>
1	$n_2 > 2$	if $pT_2 > 62.5\%$ <otherwise>	Tortuous <Open>
2	1	if $(\beta_{11}$ or $\beta_{12}) > \beta_{TORTUOUS}$ and $\beta_{21} > \beta_{TORTUOUS}$ <otherwise>	Tortuous <Open>
2	2	if $(\beta_{11}$ and $\beta_{12}) > \beta_{TORTUOUS}$ and $(\beta_{21}$ and $\beta_{22}) > \beta_{TORTUOUS}$ <otherwise>	Tortuous <Open>
2	$n_2 > 2$	if $(\beta_{11}$ and $\beta_{12}) > \beta_{TORTUOUS}$ <otherwise>	Tortuous <Open>
$n_1 > 2$	1	if $pT_1 > 62.5\%$ <otherwise>	Tortuous <Open>
$n_1 > 2$	2	if $(\beta_{21}$ and $\beta_{22}) > \beta_{TORTUOUS}$ <otherwise>	Tortuous <Open>
$n_1 > 2$	$n_2 > 2$	if $(pO_1 + pO_2) > (pT_1 + pT_2)$ <otherwise>	Open <Tortuous>

**Table 5.1** The conditions of being an open or tortuous loop by checking  $(n_1, n_2)$  control pair. ( $n_i$  number of curves on side chain-i,  $\beta_{ij}$  curvature angle,  $pO_i, pT_i$  possibility of being Open and Tortuous for side chain-i, respectively)

### 5.4.3.3 Bizarre-Bushy Clasification Unit (BBCU)

The capillary loops that have more than two skeleton chain segments, will be processed in BBCU. The classification criteria given in section (3.4.4) were implemented to develop BBCU. The attempts to introduce a quantitative classification

criterion by measuring the compactness of the loops, have been failed. Compactness of a loop can be calculated as  $Cmp = \text{loop\_perimeter}^2 / (4\pi * \text{loop\_area})$ . An "elongated tortuous" loop's compactness value, for example, can be as high as the "bizarre" loop's in Figure 5.34(b). Many "enlarged" open or tortuous loop's compactness, on the other hand, can be as low as the "bushy" loop in Figure 5.34(a). Some of the "bizarre" structures, that have got quite long limb branches, may have lower Cmp values than those "bushy" loops that display budding of the branches. The developed classification criteria, actually, had been formed after the attempts to employ compactness as a delimiter of atypical loops. The attempts to eliminate the pitfalls of the usage of compactness, helped to develop proposed the semi-quantitative classification criteria.

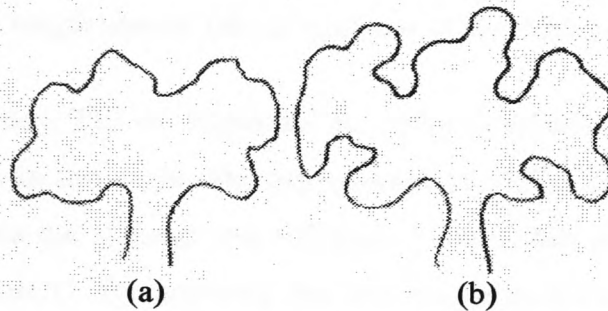


**Figure 5.34** The syntetic bushy (a) and bizarre (b) structures that had been used to test the efficiency of compactness as a delimiter of hemorrhage structures and open/tortuous loops in early development stages of TANCCAS.

While deciding on atypical loops, a less detailed capillary chain is needed. The Auxiliary Image, that was created in PPM-II, contains the silhouette of a very rough sketch of a capillary loop (The sketch was obtained after polygonal approximation with 10 pixels error tolerance). By thinning the rough silhouette of the loop and removing the spur branches in resulting image, get the new skeletal chain. The loop BSH of "collect.asc" (Figure 5.35(b)) produces three skeletal chain segments (Figure 5.35(a)). The silhouette of its rough sketch (Figure 5.35(c)), on the other hand, produces a single skeletal chain (Figure 5.35(d)). Since the loop is accepted by BBCU, there is nothing wrong, if the skeletal chain has got only one segment. Actually, the thinning algorithm had produced small chain segments for the budding of limbal branches, but they were so small as to be pruned in spur branch removing operation. Since there are no skeletal

branch end points, there is no need to control whether the lines, that were supposed to be connecting the end points of the skeletal branches, passes through the outside of the silhouette of the loop. The loop BSH of "collect.asc" is purely "bushy" type.

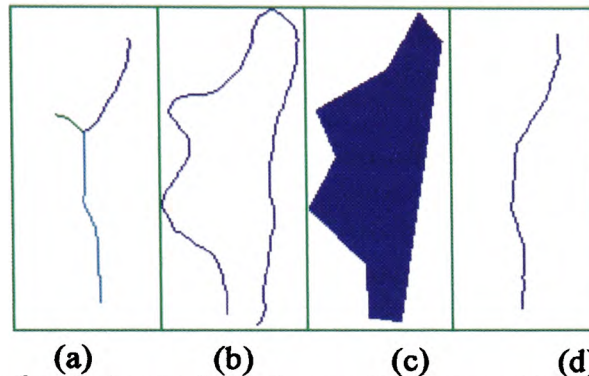


**Figure 5.35** (a) the skeletal chain of (b) the capillary loop BSH of "collect.asc", (c) the silhouette of the loop's rough sketch, (d) the skeleton of the silhouette.

The capillary loop T17 of Appendix B, will be processed to demonstrate the BBCU's analysis steps in full scale. The input image of MCM for the loop is given in Figure 5.36(a). Because the skeletal chain (Figure 5.36(b)) has got seven segments, it will be accepted to BBCU. By applying the thinning algorithm to the rough sketch silhouette of the loop (Figure 5.36(c)), its skeleton can be obtained (Figure 5.36(d)). While the BSH loop's two skeleton images were so different from each other, T17's silhouette produced very similar skeletal chain to original loop. This is due to the fully developed limbal branches of T17. By connecting the end points of skeletal branches, apart from bottom one (Figure 5.36(e)) and masking the line image with the silhouette of the loop (Figure 5.36(f)), it can be observed that the lines pass through the outer loop area. Therefore T17 is a "bizarre" loop.

#### 5.4.4 Class Decision Unit (CDU)

Class Decision Unit (CDU) is a logic unit where a loop's actual class is determined by analysing its morphological parameters LoopLength and LimbWidth, and preliminary classes that were suggested in PPM-II and MCM. The data files that contain analysis and classification results of a loop, are the input of CDU. CDU does not contain any image processing algorithm, since all the necessary data for the classification are produced in PPM and MCM. It combines Width Anomaly Classes

(WAC); "enlarged" and "giant", Length Anomaly Class (LAC) "elongated", and parametric Descriptive Classes (DC); "cuticulis", "open", "tortuous", and non-parametric DC; "crossed", "bizarre" and "bushy", in the order of *PC-AC-DC*. Non-parametric DCs does not require any anomaly label. Therefore the output of CDU will produce only DC class label for non-parametric classes; crossed (Crs), bizarre (Bzr) and bushy (Bsh).

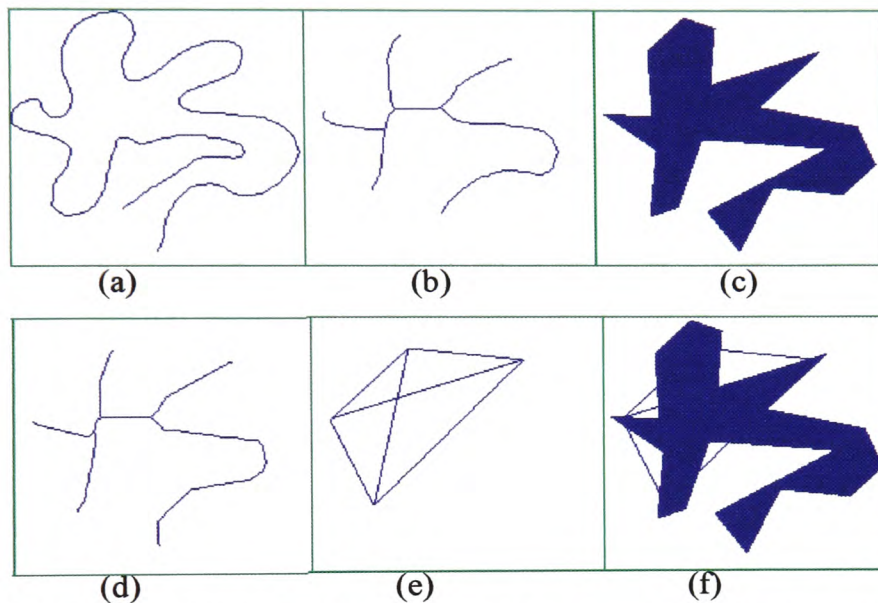


**Figure 5.36** (a) The sub-image of the loop T17 as input to MCM (b) The loop 17's skeleton, (c) The rough sketch silhouette of the loop (d) The silhouette's skeleton (e) Detected and connected skeletal branch end points. (f) Output of Masking operation.

The class decision mechanism of CDU is given in Figure 4.37. The (*italic and bold*) inputs are the findings from *PPM-II* and **MCM**, respectively. If a loop is identified as "bizarre" or "bushy" in either *PPM-II* or **MCM**, it is a positive identification and CDU assigns the relevant class to the loop as its true final class.

If a loop is identified as "*atypical*" in *PPM-II*, and "open" or "tortuous" in **MCM**, the actual class of the loop is "bushy". Such cases are the violations of the bushy classification criteria, because the outer boundary does not display budding of the limbal branches. However, the structures like T2, T7, T18, T19, T26, and T40 of Appendix B cannot be classified any other types but "bushy". Since bushy loops have

smoother outer boundaries than bizarre ones, their classifications as bushy loops will be reasonable regardless of the proposed classification criteria.

The loops that have been noted as "*UnDecided*" in *PPM-II* could be "crossed" types, as well as "bushy" and "bizarre" types. If the loop is "bushy" or "bizarre", they will be correctly identified in BBCU. However, if it is "crossed", it will be identified as "open" or "tortuous" in OTCU. Therefore, any loop that is noted as "UnDecided" and classified as "open" or "tortuous" will be identified as "crossed" in CDU, as well as those that are identified as "crossed" in PPM-II.

The capillary loops that were identified as "cuticulis" in *PPM-II* or *MCM*, are "cuticulis" type. However, their WAC label "enlarged" should be tagged if they are "enlarged". The presence of the loop's inner boundary chain is accepted as the sign of enlargement in section 3.4.5. During the transformations of multiple loop chains into a single disclosed chain in the Transformer Unit, if the inner chain was present, then WAC label "enlarged" had been noted in to the loop's class file. As it discussed in section 3.4.5, a threshold LoopWidth can be set to detect enlargement of loops, with further study rather than checking the presence of inner boundary chain. However, as was stated in section 5.4.2, calculation of loop width for some of the "cuticulis" loops whose orientation line intersects with the afferent and efferent limb walls, is almost impossible. In such cases, the distance between loop chain end points was assumed to be loop width during the analysis. If a threshold LoopWidth<sub>ENLARGED</sub> is desired to be used for detection of "enlarged" loops, then the WAC label that is read from the loop's class file should be ignored. Instead, it should be replaced with the result of a simple comparison between actual loop width and LoopWidth<sub>ENLARGED</sub>. Of course, the distance between end points of a "cuticulis" loop should be recorded as loop width into data file.

If a loop was identified as "open" or "tortuous" in *MCM*, and has been noted as neither "*UnDecided*" nor "*atypical*" in *PPM-II*, then the loop's DC label will be "open" or "tortuous". If the loop display any of the anomalies, then relevant labels should be tagged to DC label.

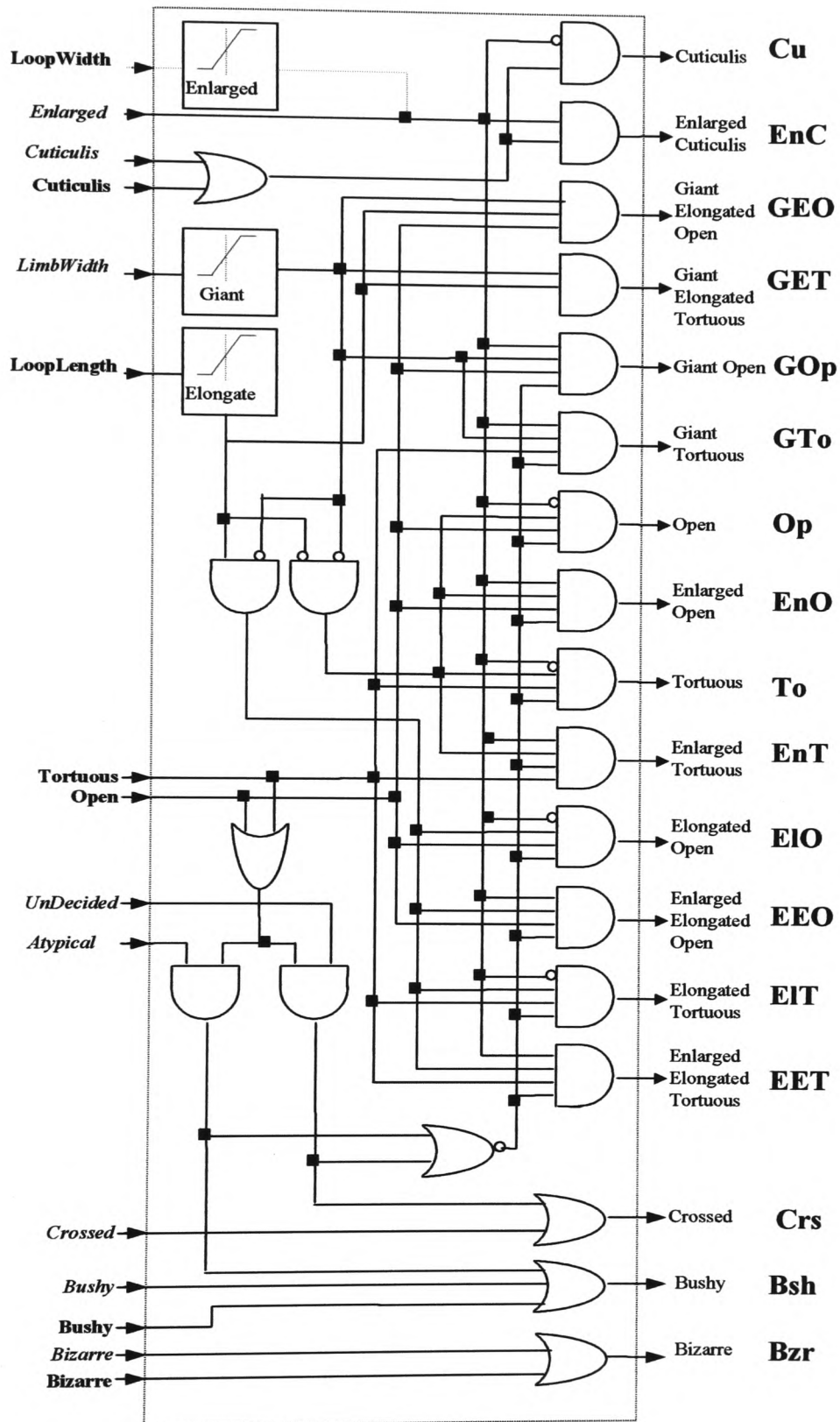


**Figure 5.37** Class Decision Mechanism of CDU

# CHAPTER 6

## **Chapter 6 Selection of The Critical Values**

### **6.1 Introduction**

The selections of the critical values of parametrical and anomaly classes will be given in this chapter. The critical exclusive curvature angle ( $\theta_{\text{CUTICULIS}}$ ) that is used for the classifications of cuticulis loops, and critical segmental curvature angles ( $\beta_{\text{OPEN}}$  and  $\beta_{\text{TORTUOUS}}$ ) that are used as the delimiters of "open" and "tortuous" loops, are the threshold values of parametrical classes. These values will be calculated by evaluating the practitioners' results.  $\text{Length}_{\text{ELONGATED}}$  and  $\text{LimbWidth}_{\text{GIANT}}$  are the threshold values of anomaly classes "elongated" and "giant" respectively. Although, the practitioners' evaluations do not provide sufficient data to set precise critical values for the anomaly classes,  $\text{Length}_{\text{ELONGATED}}$  and  $\text{LimbWidth}_{\text{GIANT}}$  will be set by using the practitioners' classifications evaluations under the guide lines of the findings from the literature.

### **6.2 Selection of Exclusive-Curvature Angle:**

#### **6.2.1 Preparation of Data Sets**

Exclusive-curvature angle  $\theta$  should be less than  $90^\circ$  for ideal "cuticulis" capillary loops. In practice, however, some of the capillary loops have limbs that are too small to be classified as anything but "cuticulis". Capillary loops with visible limbs will result in  $\theta$  values larger than  $90^\circ$ . Therefore a critical  $\theta_{\text{CUTICULIS}}$  should be selected to filter out "cuticulis" capillary loops.

Since "bizarre", "bushy" and "crossed" type loops have entirely different structure from "cuticulis" capillary loops, they cannot be used for the selection of  $\theta_{\text{CUTICULIS}}$ . "Cuticulis" loops can be mis-classified as either "open" or "tortuous" type. Therefore two different data sets should be prepared for calculation of  $\theta_{\text{CUTICULIS}}$ . The first data set is the collection of the exclusive-curvature angles( $\theta$ ) of capillary loops that are classified as "cuticulis" by majority of the six practitioners. The second data is the collection of  $\theta$  values of the capillary loops that are classified as "open" or "tortuous" by majority of the six practitioners, and it is called OP-TO population.



### 6.2.1.1 Arrangements of Sub-Data Sets

Exclusive-curvature angle ( $\theta$ ) distribution of both populations are given in Figure-6.1. Cuticulis and OP-TO populations contain 20 and 141 entries respectively. As it can be seen from Figure-6.1(b),  $\theta$  entries for OP-TO population are mainly accumulated in two regions, and  $\theta=125^\circ$  is the exclusive-curvature angle that separates these two regions. On the contrary, in a class the values should cluster in one region. Because these results are based on the practitioners' classifications, and the limitations of the human's eye perception, we can expect that there are some "cuticulis" loops that are mis-classified as "open" or "tortuous" type in OP-TO population. Similarly the cuticulis population contains some mis-classified "open" or "tortuous" loops. The existence of these mis-classified loops in cuticulis and OP-TO population can be observed in Figure-6.1(a) and (b).

Most of the "cuticulis" entries, 15 out of 20, are in the range of  $102^\circ \leq \theta \leq 132^\circ$ , and  $\theta=125^\circ$  divides the OP-TO population into two regions. Combining these two observations,  $\theta_{\text{CUTICULIS}}$  should be  $125^\circ \leq \theta_{\text{CUTICULIS}} \leq 132^\circ$ . or only slightly exceeding these limits.

On the other hand, apart from  $\theta=118^\circ$  there are no capillary loops with the same exclusive-curvature angle in cuticulis population. This is due to having few "cuticulis" entries. One way of increasing "cuticulis" samples is sending some new pictures to be analysed by the participant practitioners. However, remembering that the current six test pictures were sent twelve practitioners and only six of them responded to request and returned the results in four months time period, sending new pictures to practitioners will be included in future work. Fine adjustments of the critical values, that are found in this study, with a large cuticulis population data set is left as future work due to the time limitation.

Another way of increasing the population sizes is taking into account the Consensus Values (CV) of capillary loops while creating class populations. Consensus Value is the number of practitioners out of six that agreed on the capillary loop's class.

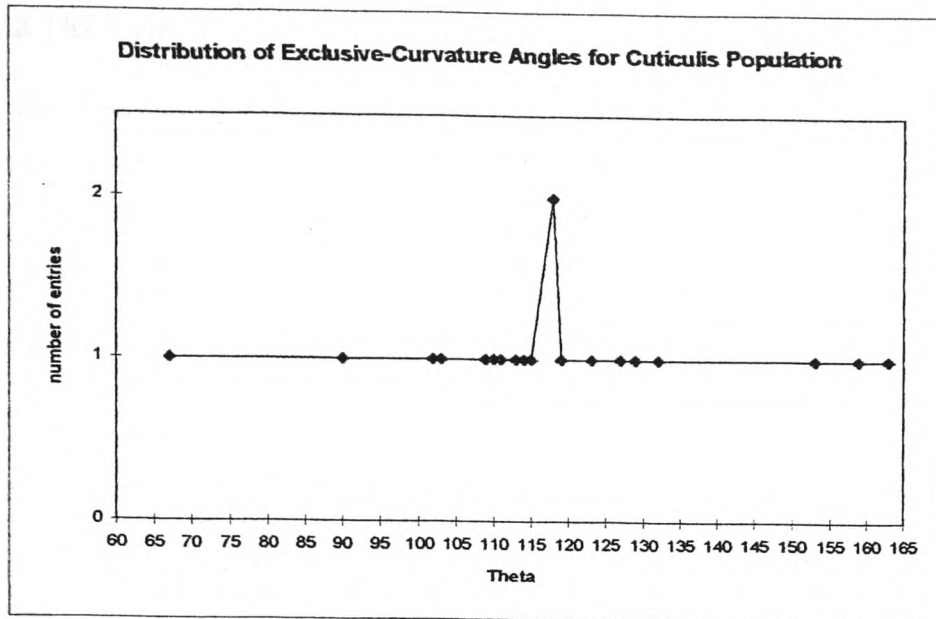
Two capillary loops with exclusive curvature angles  $\theta_1=110^\circ$  and  $\theta_2=150^\circ$ , for example, are assumed to be classified as "cuticulis" with  $CV_1=4$  and  $CV_2=2$ , respectively. Instead of adding one entry to corresponded  $\theta$  values in cuticulis population, four entries for  $\theta=110^\circ$ , and two entries for  $\theta=150^\circ$  should be made. In this way, the population size can be effectively increased, and in the mean time, corresponding  $\theta$  values will be strengthened according to their CVs.

Bearing in mind that the practitioners usually disagree on the class of capillary loops (the analysis results shows that they could not achieve agreement unity on the class of a single capillary loop out of 217), excluding one practitioner each time, new class populations can be obtained according to remaining five practitioners evaluations. In this way, additional to the class population that are created by taking into account the six practitioners classifications, six new class populations can be constructed.

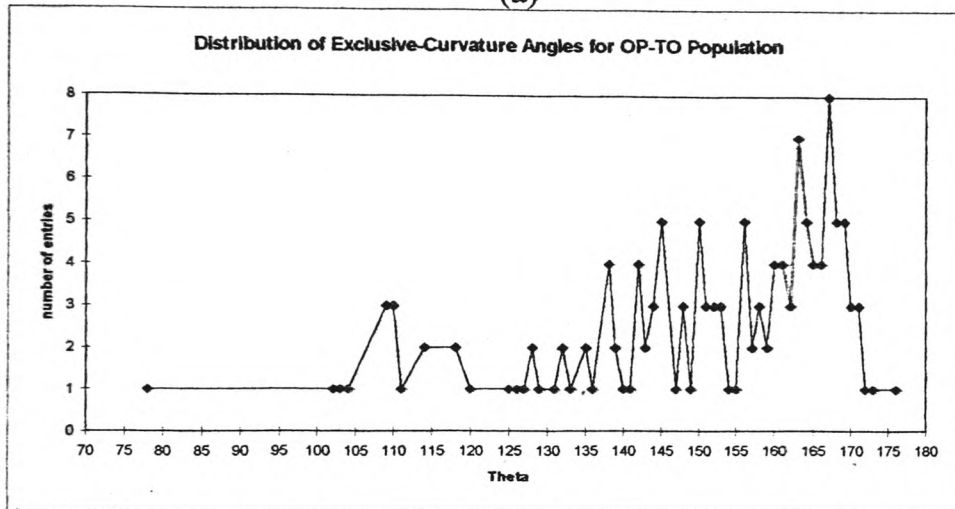
In Table 6.1, the effects of excluding a practitioner at a time on class agreement values are displayed. According to this table, excluding the 2<sup>nd</sup> or the 5<sup>th</sup> practitioners from the evaluations, 72% or 78% of the overall results will not change, respectively. Contrary to this, excluding the 3<sup>rd</sup> or the 4<sup>th</sup> practitioners' classifications from overall results will decrease the CVs. While the 5<sup>th</sup> practitioner's absence provides the least and the lowest decrease, the 2<sup>nd</sup> practitioner's absence results in the lowest increase on CVs. The 3<sup>rd</sup> practitioner's absence creates similar effects to the exclusion of the 4<sup>th</sup> practitioner on overall CVs.

The most important result could be drawn from this table is the importance of the 4<sup>th</sup> practitioner on overall results. It is his absence that causes the biggest decrease and increase on classification agreement rates. Therefore his classification results alone are worth evaluating in a separate class population data set.

By creating new sub-data sets from the six practitioners' classification results, eight different class populations are produced, overcoming the difficulty of having limited amount of data.



(a)



(b)

**Figure-6.1(a)** Distribution of exclusive curvature angles ( $\theta$ ) (a) for cuticulis population and (b) for OP-TO population.

	PR1	PR2	PR3	PR4	PR5	PR6
Decrease	52	23	69	71	12	50
No Change	42	72	19	15	78	39
Increase	6	5	12	13	11	11
Dec-Inc	45	18	56	58	1	40

**Table 6.1.** The effects on the overall class agreement in the cases of absence of each practitioner

## 6.2.2 The Critical Values Selection Methods

For the calculation of  $\theta_{\text{CUTICULIS}}$ , a set of critical  $\theta$  values are calculated by using two different methods. The first method uses cumulative frequency distribution and produces  $\text{OPTIMAL}_\theta$ . The second method uses normal distribution (ND) and produces  $\text{ND}_\theta$  suggested critical  $\theta_{\text{CUTICULIS}}$  angles. The mean value of all suggested critical angles  $\text{OPTIMAL}_\theta$  and  $\text{ND}_\theta$  is accepted as final  $\theta_{\text{CUTICULIS}}$ . The analysis results can be found in Table 6.2

### 6.2.2.1 Calculation of $\text{OPTIMAL}_\theta$

In section 6.2.1.1, it has been predicted that  $\theta_{\text{CUTICULIS}}$  should be  $125^\circ \leq \theta_{\text{CUTICULIS}} \leq 132^\circ$ . Suppose that the lower limit of  $125^\circ$  is accepted as  $\theta_{\text{CUTICULIS}}$ . In this case, 88% of OP-TO population and 70 % of cuticulis population will be classified in their actual classes. 86% of the overall capillary loops will be in their actual classes. However, if the upper limit  $\theta=132^\circ$  is accepted as  $\theta_{\text{CUTICULIS}}$ , 82% of OP-TO population, 85% of cuticulis population and 82% of overall capillary loops will be classified in their actual classes. As  $\theta_{\text{CUTICULIS}}$  decreases, more and more "open"- "tortuous" type capillary loops are classified in their actual classes. Correspondingly, less and less "cuticulis" type capillary loops will be in their actual classes. Mis-classifying only one of the entry of both OP-TO and cuticulis populations decrease the populations' actual classification rates by 0.7% and 5% respectively. This is due to the influence of OP-TO population that is approximately seven times larger than cuticulis population size on overall population.

While selecting  $\theta_{\text{CUTICULIS}}$ , it is the aim to find an optimal  $\theta$  value that satisfies both of the populations, although it does not produce the lowest overall mis-classification rate.

$\text{OPTIMAL}_\theta$  can be calculated by using cumulative frequency distributions of both populations. For discrete distributions, the function  $P(X=x)$  is often represented by  $p(x)$  and is called the *probability mass function, or pmf*. If the probability distribution is a population distribution,  $p(x)$  is the relative frequency of  $x$  in the population, or the

probability of the value  $x$  occurring if an observation is drawn at random from the population. In general,  $p(x)$  is the probability of obtaining the value  $x$  in an experiment. Symbolically,

$$p(x) = P(X = x) = \text{probability that } X=x$$

$X$  refers to the general variable, and  $x$  to a particular occurrence of it. The discrete variable  $X$  can take on only integer values of  $x$ :  $x=0, 1, \dots, n$ . Then

$$p(x) > 0 \text{ for } x=0, 1, 2, 3, \dots, n$$

and

$$p(x) = 0 \text{ for all other values of } x.$$

Also

$$\sum_{x=0}^n p(x) = 1 \quad (6.1)$$

**Cumulative distribution function cdf** is the probability that the outcome of an experiment will be less than or equal to a particular value, say 'a'. Symbolically,  $F(a)$  is used as the cdf, and it is

$$F(a) = P(X \leq a) = \sum_{x \leq a} p(x) \quad (6.2)$$

where

$F(a) = 0$  for  $a < \min x$  where  $\min x$  is the minimum value of  $X$  and

$F(a) = 1$  for  $a > \max x$  where  $\max x$  is the maximum value of  $X$ .

Both, probability mass function and cumulative frequency distribution of the populations are given in Figure 6.2 and 6.3.

**Reverse cumulative distribution function rcdf**, is the probability that the outcome of an experiment will be more than to a particular value, say 'a'. Symbolically

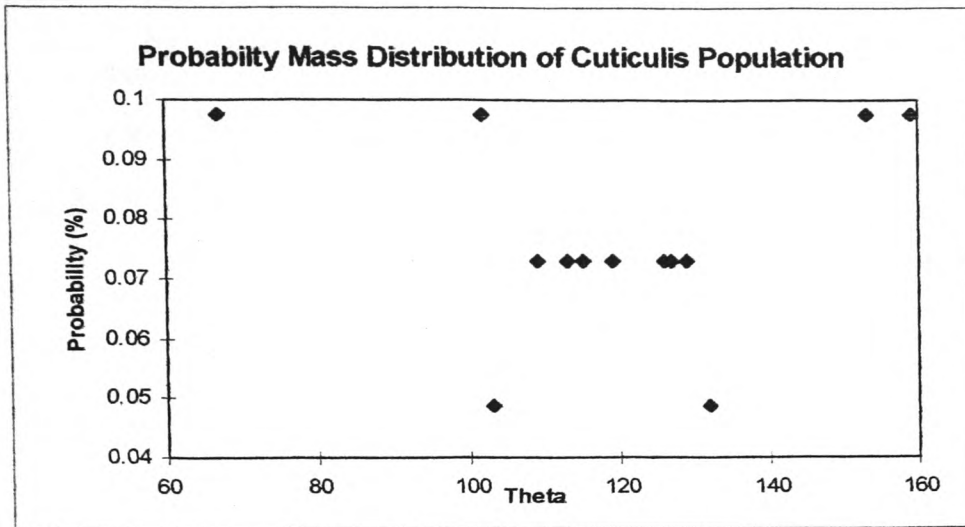
$\bar{F}(a)$  is used as the rcdf, and it is

$$\bar{F}(a) = P(X > a) = \sum_{x > a} p(x) \quad (6.3)$$

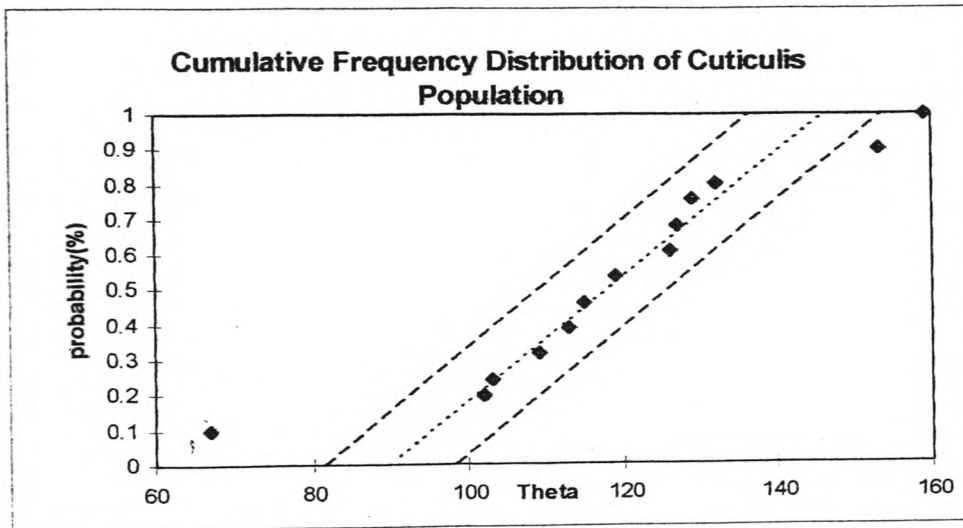
where

$\bar{F}(a) = 1$  for  $a < \min x$  where  $\min x$  is the minimum value of  $X$  and

$\bar{F}(a) = 0$  for  $a > \max x$  where  $\max x$  is the maximum value of  $X$ .



(a)

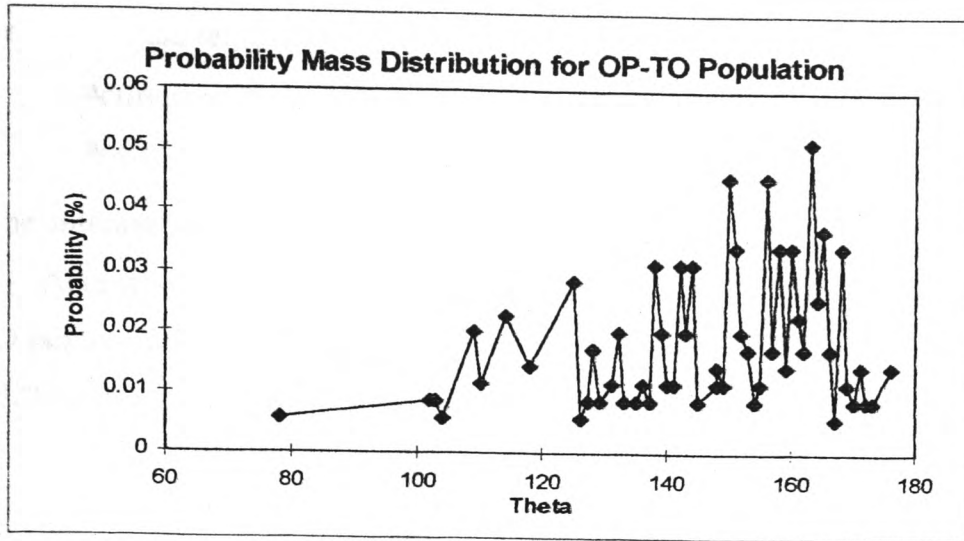


(b)

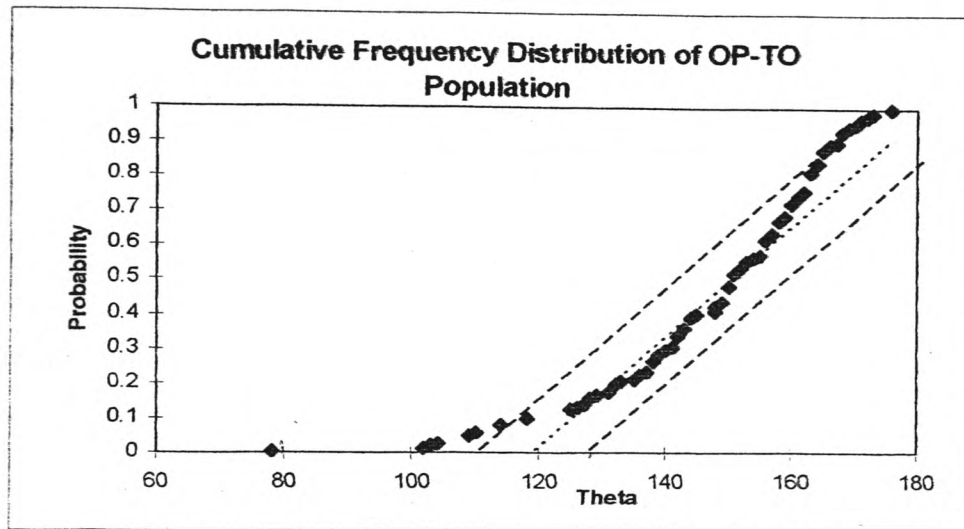
**Figure-6.2 (a) Probability mass distribution of cuticulis population**

**(b) cumulative frequency distribution of cuticulis population.**

Both the cumulative distribution function and reverse cumulative distribution functions are given in Figure-6.4. Note that both of the functions are perfectly straight lines. In practice, these functions can be approximated to a straight line by using regression lines. In Figure-6.5, for example, cumulative distribution frequency of cuticulis population and reverse cumulative distribution function of OP-TO population are plotted together with their regression lines.



(a)



(b)

**Figure-6.3** (a) Probability mass distribution of OP-TO population  
(b) Cumulative frequency distribution of OP-TO population

By employing *the least squares method*, the parameters of a regression line  $p(\theta)'=a+b\theta$  can be calculated from equations (6.4) and (6.5).

$$an + b \sum_{i=1}^n \theta_i = \sum_{i=1}^n p'_i(x) \quad (6.4)$$

$$a \sum_{i=1}^n \theta_i + b \sum_{i=1}^n \theta_i^2 = \sum_{i=1}^n \theta_i p'_i(x) \quad (6.5)$$

where

$n$  : population size

$p'(x)$  : cdf for cuticulis population and rcdf for OP-TO population

The parameters of the regression lines can be calculated as

$$\begin{aligned}
 a_{\text{CUTICULIS}} &= -93.45 & b_{\text{CUTICULIS}} &= 1.227 \\
 a_{\text{OP-TO}} &= 239.457 & b_{\text{OP-TO}} &= -1.256
 \end{aligned}$$

The intersection point of these two regression lines gives a value of  $134^\circ$  for  $\theta_{\text{CUTICULIS}}$ . Accepting this  $\theta$  value as critical exclusive curvature angle  $\theta_{\text{CUTICULIS}}$ , 82% of OP-TO population and 85% of cuticulis population could be classified in their actual classes. 82% of the overall population will also be in their actual classes.

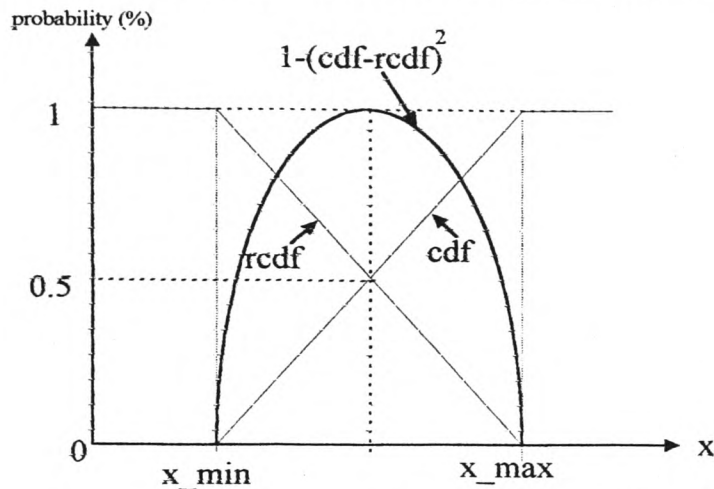


**Figure 6.4** Cumulative and reverse cumulative frequency distribution functions in continuous space.

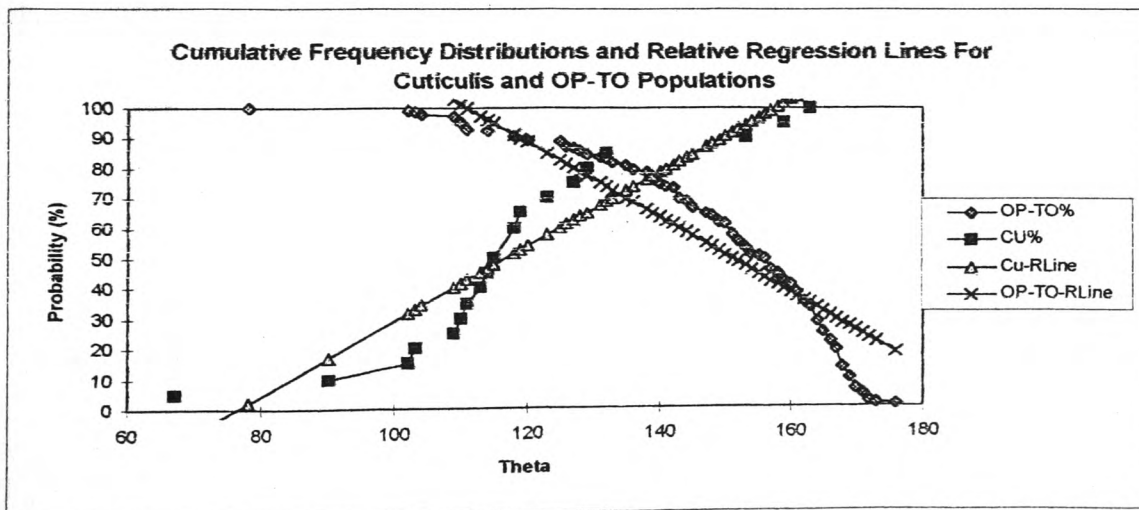


**Figure-6.5** Cumulative and reverse cumulative frequency distribution functions and their relative regression lines for Cuticulis and OP-TO Populations in discrete space.



The entries with high residual have a strong influence on the regression line. Therefore instead of approximating the population cdf to a regression line, we can employ a flexible method by using *powered bi-cumulative distribution functions (PB-CDF)*. The advantage of **PB-CDF** is that the population frequency distribution is not forced to approximate to any model. Therefore approximation errors will be reduced.

**Powered bi-cumulative distribution function PB-CDF** is the normalized and squared differential of both cumulative and reverse cumulative distribution functions. It can be written as:

$$\text{PB-CDF} = 1 - (\text{cdf-rcdf})^2 \quad (6.6)$$

When both populations' PB-CDF functions are plotted against their probability, they will be intersecting at a  $\theta$  value (Figure 6.6). This  $\theta$  value is the optimal solution for  $\theta_{\text{CUTICULIS}}$ , and symbolically, it is

$$\text{OPTIMAL}_{\theta} = \min [(\text{PB-CDF}_{\text{CUTICULIS}} - \text{PB-CDF}_{\text{OP-TO}})^2] \quad (6.7)$$

where

$$\mu^{\theta}_{\text{CUTICULIS}} < \theta < \mu^{\theta}_{\text{OP-TO}}$$

In Figure 6.7 the plot of  $(\text{PB-CDF}_{\text{CUTICULIS}} - \text{PB-CDF}_{\text{OP-TO}})^2$  is given for Cuticulis and OP-TO population. The  $\text{Optimal}_{\theta}$  is the  $\theta$  value where  $\min[(\text{PB-CDF}_{\text{CUTICULIS}} - \text{PB-CDF}_{\text{OP-TO}})^2]$  and  $\mu^{\theta}_{\text{CUTICULIS}} < \theta < \mu^{\theta}_{\text{OP-TO}}$

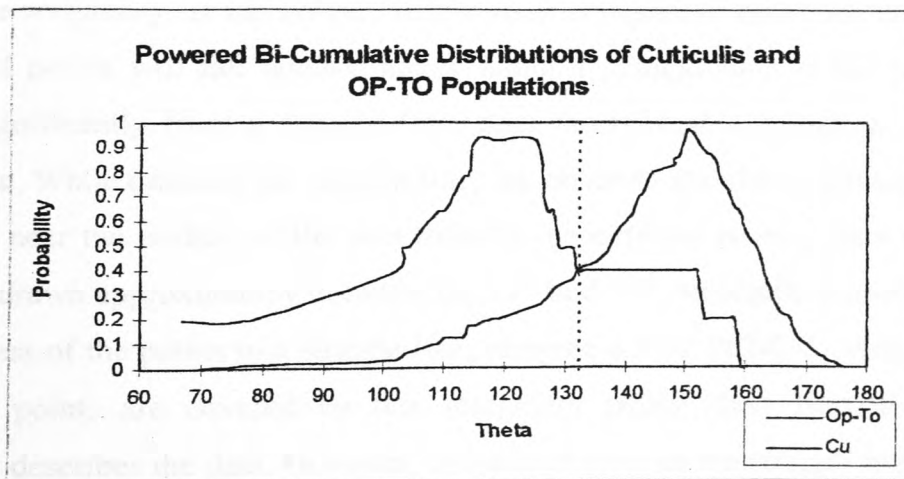


**Figure-6.6** *Powered Bi-Cumulative Distributions of Cuticulis and Op-TO populations*

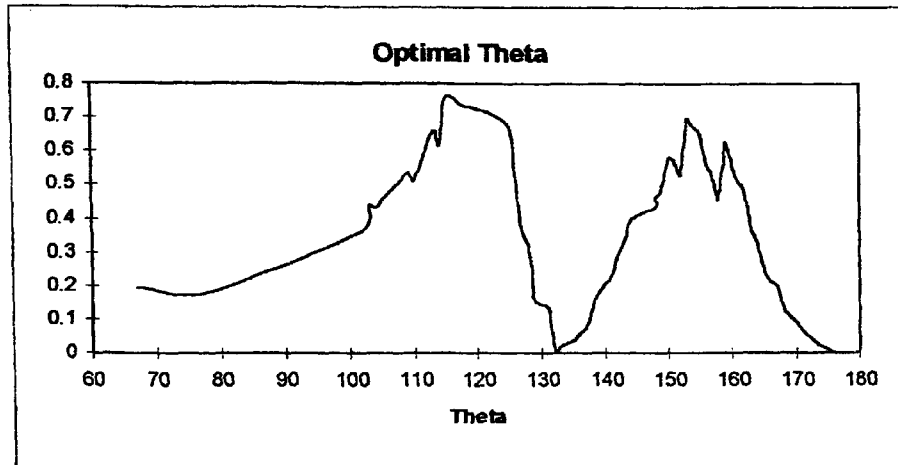


**Figure-6.7** *OPTIMAL  $\theta$  calculation from PB-CDFs of cuticulis and OP-TO populations*

#### 6.2.2.2 Fat Pencil Method

Before going any further, the distribution models of the population should be decided. In many engineering applications, the Normal Distribution model usually satisfies the distribution of the sample population. **FAT PENCIL** method [Montgomery and Runger 94] can be used to validate that normal distribution model can be safely used for the population.

To construct a probability plot, the entries in the population are first ranked from smallest to largest. The ordered entries of the population are, then, plotted against their cumulative frequency. If the normal distribution adequately describes the population, the plotted points will fall approximately along a straight line; if the plotted points deviate significantly from a straight line, then the normal distribution model is not appropriate. While drawing the straight line, the observer should be influenced more by the points near the middle of the plot than by the extreme points. As a rule, the line should be drawn approximately between the 25<sup>th</sup> and 75<sup>th</sup> percentile points. In assessing the closeness of the points to a straight line, imagine a FAT PENCIL lying along a line. If all the points are covered by this imaginary pencil then Normal Distribution adequately describes the data. However, at the both ends of the straight line, few entries may have high residuals. These entries are most likely to be the outliers of the population and they do not modify the population's normal distribution model.

If the outliers are eliminated from the class population, the model fits better to the population. Therefore additional to the eight population sets, another eight population sets can be created by eliminating the outlier entries.

### 6.2.2.3 Calculation of Suggested $\theta_{\text{CUTICULIS ND}_\theta}$ from Normal Distribution Functions.

The discrete distribution having the density

$$F(x) = \frac{1}{\sqrt{2\pi\sigma}} e^{-\frac{1}{2}\left(\frac{x-\mu}{\sigma}\right)^2} \quad (6.8)$$

is called the *normal distribution* or *Gauss distribution*. A random variable having this distribution is said to be normal or normally distributed. Many random variables of practical interest are normal or approximately normal or can be transformed into normal random variables in a relatively simple fashion. Furthermore, the normal distribution is a useful approximation of more complicated distributions. In (6.9) and (6.10)  $\mu$  is the mean and  $\sigma$  is the standard deviation of the distribution, and they are defined by

$$\mu = \sum_j x_j f(x_j). \quad (6.9)$$

$$\sigma^2 = \sum_j (x_j - \mu)^2 f(x_j) \quad (6.10)$$

In Figure-6.8, Normal Distribution of OP-TO and Cuticulis populations are given. The intersection point of these two normally distributed populations is accepted as the suggested  $\theta_{\text{CUTICULIS ND}_\theta}$ . For two normal distributed populations that have means of  $\mu_1$  and  $\mu_2$  and standard deviations of  $\sigma_1$  and  $\sigma_2$ , the intersection point  $x_i$ , can be calculated from quadratic equation  $ax^2 + bx + c = 0$ . The coefficients a, b and c, can be written as;

$$a = -(\sigma_2^2 - \sigma_1^2)$$

$$b = 2(\mu_1\sigma_2^2 - \mu_2\sigma_1^2)$$

$$c = -\left(\sigma_2^2\mu_1^2 - \sigma_1^2\mu_2^2 - \sigma_1^2\sigma_2^2 \ln \frac{\sigma_2}{\sigma_1}\right)$$

The intersection point  $x_i$  is one the roots of this quadratic equation in the range of

$$\mu_1 < x_i < \mu_2$$

Table 6.2 contains the analysis results to choose critical exclusive curvature angle  $\theta_{\text{CUTICULIS}}$  for the segregation of "cuticulis" capillary loops. The mean of all suggested critical  $\theta$ s that are calculated by  $\text{ND}_{\theta}$  and  $\text{OPTIMAL}_{\theta}$ , is  $131^{\circ}$  and is accepted as  $\theta_{\text{CUTICULIS}}$ . By using this critical value, 82% of OP-TO population and 85% of cuticulis population could be classified in their actual classes. 82% of the overall population will be in their actual classes, as well. Therefore 18% of the capillary loops are mis- classified as "open", "tortuous" and "cuticulis" by the practitioners. Since, TANCCAS's classification success rate will be calculated by comparing its output with the class that was assigned by the overall agreement of the six practitioners, 13% overall classification error can be expected. This is due to classification errors of the participant practitioners.

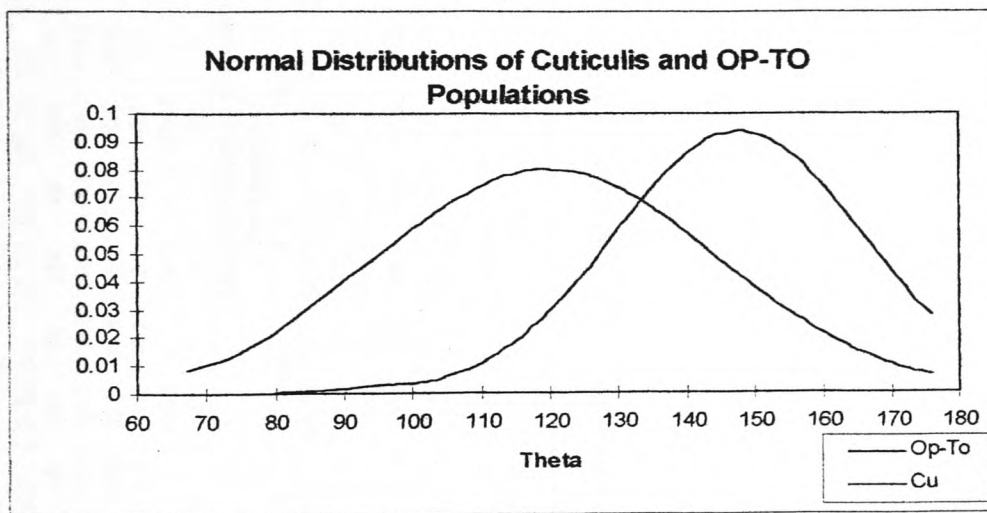


**Figure-6.8** Normal Distributions of Cuticulis and OP-TO Populations.

By using this  $\theta_{\text{CUTICULIS}}$  threshold angle we may define that a "cuticulis" type capillary may have limbs that are up to 1.46 times longer than the radius of the capillary tip.

		In The Absence of												Only							
		Pr-1			Pr-2			Pr-3			Pr-4			Pr-5			Pr-6			Pr-4	
		OP-TO	CU	OP-TO	CU	OP-TO	CU	OP-TO	CU	OP-TO	CU	OP-TO	CU	OP-TO	CU	OP-TO	CU	OP-TO	CU	OP-TO	CU
<b>Overall</b>		41	292	20	357	16	224	45	230	47	371	43	315	25	150	8					
<b>n</b>		147.6	119.7	147.8	117.6	146.1	118.8	148.8	118.6	149.1	118.8	149.7	119.6	150.1	118.1	148.7	124.5				
<b>μ</b>		18.1	24.7	19.1	30.9	21.2	33.4	15.8	20.8	15.2	20.2	17.8	24.1	17.5	32.0	20.4	31.2				
<b>σ</b>		-0.9	-0.4	-1.0	-0.2	-1.6	-0.2	-0.7	-0.3	-0.7	-0.3	-1.1	-0.4	-1.1	-0.2	*	*				
<b>Skewness</b>		133.4	131.9	141	143	130.1	134.3	134.7	134.8	134.0	143	135	143	134.0	134.0	*	*				
<b>ND 0</b>		132	141	143	130.1	134.3	134.7	134.8	134.0	143	135	143	134.0	134.0	*	*					
<b>OPTIMAL 0</b>																					
<b>After the Elimination of Outliers</b>																					
		In The Absence of												Only							
		Pr-1			Pr-2			Pr-3			Pr-4			Pr-5			Pr-6			Pr-4	
		OP-TO	CU	OP-TO	CU	OP-TO	CU	OP-TO	CU	OP-TO	CU	OP-TO	CU	OP-TO	CU	OP-TO	CU	OP-TO	CU	OP-TO	CU
<b>Overall</b>		29	292	14	357	10	224	39	230	41	371	35	315	17	150	5					
<b>n</b>		147.6	117.0	147.8	101.1	146.1	96.5	148.8	112.8	149.1	113.4	149.7	111.3	150.1	100.2	148.7	104.2				
<b>μ</b>		18.1	10.1	19.1	21.4	21.2	21.3	15.8	15.8	15.2	15.3	17.8	18.4	17.5	22.6	20.4	21.1				
<b>σ</b>		-0.9	-0.1	-1.0	-0.4	-1.6	-0.3	-0.7	-1.7	-0.7	-1.8	-1.1	-1.4	-1.1	-0.2	*	*				
<b>Skewness</b>		129.6	125.3	125.3	121.3	121.3	130.8	130.8	131.3	131.3	130.7	128	128	127.3	126.7	126.7	*				
<b>ND 0</b>		128	125	125	125	125	128	128	127	127	128	128	128	128	128	*	*				
<b>OPTIMAL 0</b>																					
<b>SUGGESTED 0</b>			131.2																		

**Table 6.2** The analysis results to choose a  $\theta_{CUTICULUS}$  critical angle for the classification of cuticulis type capillaries.

### 6.3 Selection of Critical Segmental Curvature Angles $\beta_{\text{OPEN}}$ and $\beta_{\text{TORTUOUS}}$

The segmental curvature angle(s) set  $\{\beta\}$  of an "open" or "tortuous" capillary loop can be obtained as it has been explained in Chapter 5. The  $\beta_i$  angle of a curve can be calculated by using sinc $\theta$  function (4.3). Instead of capillary loop length, this time the curve length will be used as *arc\_length*. Therefore

$$\text{sinc } \beta = \frac{\sin \beta}{\beta} = \frac{\text{base}}{\text{curve\_length}} \quad (6.11)$$

A set of segmental curvature angles  $\{\beta\}$  can be obtained for every "open" or "tortuous" capillary loop.

$$\{\beta\} = \{\beta_{11}, \beta_{12}, \dots, \beta_{1n}, \beta_{21}, \beta_{22}, \dots, \beta_{2n}\}$$

The indices 1 and 2 indicate that  $\beta$  angle belongs to side chain-1 and side chain-2 respectively. A side chain may have multiple  $\beta$  angles as in side chain-1 in Figure 6.9, or a single  $\beta$  value as in side chain-2. Therefore, in any case,  $\{\beta\}$  contains at least two angle values. The higher the  $\beta$  value the deeper the curvature and higher the tortuosity of the capillary. An "open" type capillary may have some segments with high tortuosity levels. The significance of these segments in overall appearance may be negligible, therefore the capillary can still be an "open" type. The opposite is also true for some "tortuous" capillary loops. They may have almost straight segments. Hence, in  $\beta$  populations of both types, an overlap is expected and this is not due to misclassification. Normal and powered bi-cumulative distributions of "open" and "tortuous" segmental curvature angles  $\beta$  for overall population, that are collections of six practitioners' evaluation without eliminating the outliers, are given in Figure-6.11 and Figure 6.12, respectively.

The methods that have been used for the selection of critical exclusive curvature angle  $\theta_{\text{CUTICULIS}}$ , are applied to the segmental curvature angles  $\{\beta\}$  population of "open" and "tortuous" type capillary loops, for the selection of critical angle  $\beta_{\text{OPEN}}$ . Sixteen data sets for "open" and "tortuous" type capillary loops are created in the same fashion as in section 6.2.1. The analysis results are given in Table-6.3 and critical tortuosity level  $\beta_{\text{OPEN}}$  has been determined as  $28^\circ$ .

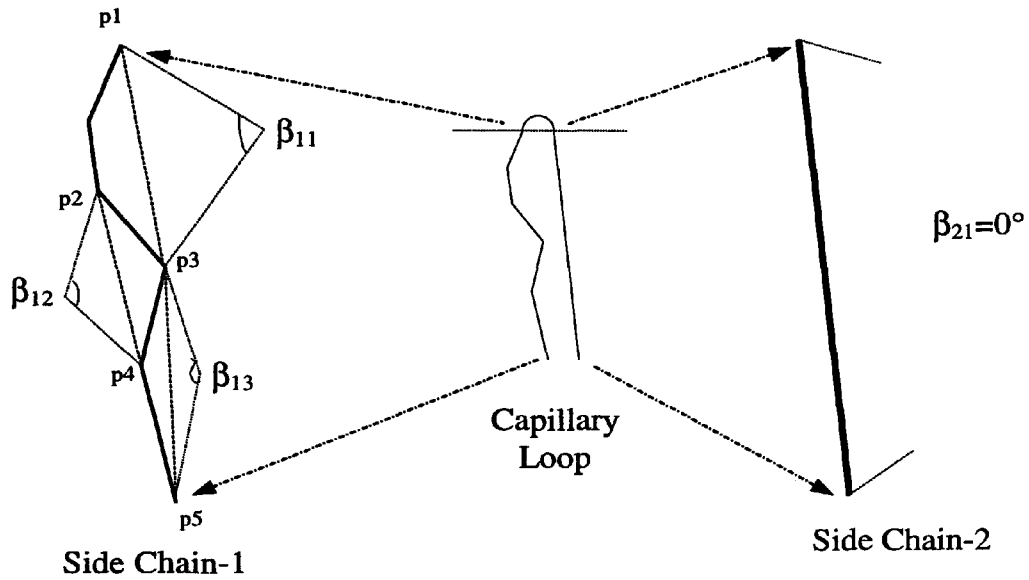


**Figure 6.9** A capillary loop and its side chains.

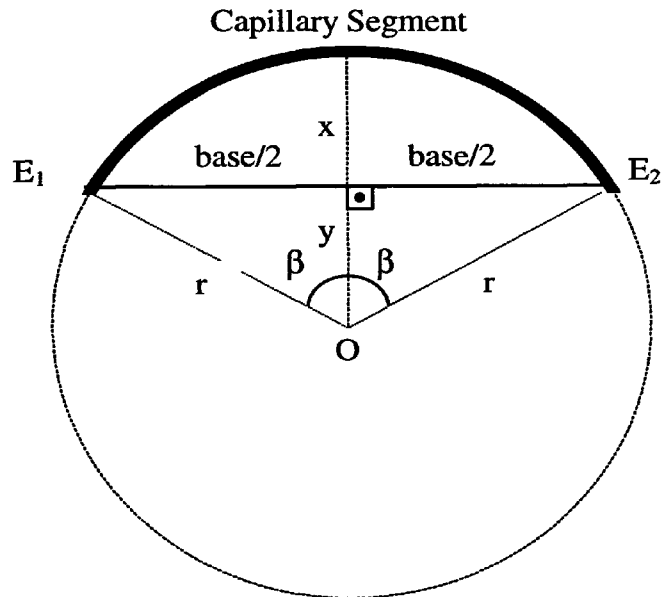


**Figure 6.10** A capillary segment and its properties

For a computerized system, calculation of  $\beta$  can be achieved as explained in Chapter 5, section 5.6.3.2. A ratio between curve base and its depth can be used for manual classification, instead of calculating the  $\beta$  angle. The depth of the curve can be measured by drawing a line that passes through the deepest point of the curve and perpendicular to curve base line. Although, in practice, not all curves are perfectly circular as displayed in Figure 6.10, they can be assumed as an arc of a circle. The depth of the curve ( $x$ ) can be written as;

$$x = r - y = \frac{base}{2} \left( \frac{1 - \cos \beta}{\sin \beta} \right) \quad (6.12)$$

where

$$r = \frac{base}{2 \sin \beta}, \text{ and } y = \frac{base}{2 \tan \beta}$$

By substituting  $\beta_{OPEN}=28^\circ$  in equation (6.12),

$$x \approx \frac{base}{8}$$

Therefore, any capillary side chain curve segment that has depth deeper than  $base/8$ , can be accepted as a "tortuous" segment.

The segmental curvature angle set  $\{\beta\}$  of an "open" or "tortuous" capillary loop should consist at least two  $\beta$  angle values, one for side chain-1 and another one for side chain-2. The number of curve segments in both chains can be represented in pairs as

$$SS\{\text{number of curves in side chain-1, number of curves in side chain -2}\}$$

The capillary loop given in Figure 6.9 has four  $\beta$  angles in its  $\{\beta\}$  set. They are distributed as three for side chain-1 and only one for side chain-2. Therefore  $SS\{\}$  segment size pair will be  $SS\{3,1\}$ . The distributions of the segment size pair  $SS\{\}$  of "open" and "tortuous" overall population is given in Figure 6.13. "open" type capillary loops have less curve segments in their side chains than "tortuous" ones. 90% of the open population have  $SS\{1, *\}$  segment size pair. Contrary to this, there is not a single capillary that has only one  $\beta$  angle in one of its side chains, in tortuous population. Additional to  $\beta_{OPEN}$ ,  $SS\{\}$  segment size pair should also be a classification criterion of "open" and "tortuous" capillary loops.

Having  $SS\{1,1\}$  segment size pair strongly indicates that capillary loop is an "open" type. 71% of the open population have  $SS\{1,1\}$  segment size pair. However,  $SS\{1,j>1\}$  pairs add up to 20% of the open population, while  $SS\{i>1, j>1\}$  pairs cover only 9%. Therefore, a capillary loop that has only one segmental curvature angle in both side chains, is most likely to be an "open" type capillary.



Although we have not come across such a capillary loop that is radically bent towards one side, classifying it as an "open" type will not be sensible. Critical degree of bending  $\beta_{TORTUOUS}$  should be evaluated in order to classify the loop in to either of the classes. Since, there is not any such capillary loop in the test images, an assumption should be made for  $\beta_{TORTUOUS}$  critical value. Although, critical segmental curvature angle  $\beta_{OPEN}$  could be used as  $\beta_{TORTUOUS}$ , it does not contribute being "radically bent".

The mean of all mean segmental curvature angles  $\mu_p$  of tortuous populations will be used as  $\beta_{TORTUOUS}$ , and it has been calculated as  $49^\circ$ . Since,  $\beta_{TORTUOUS}$  is almost twice large as  $\beta_{OPEN}$ , its usage is safer than  $\beta_{OPEN}$ . However, further investigations for  $\beta_{TORTUOUS}$  should be made to set a more accurate critical value. Therefore fine adjustment of  $\beta_{TORTUOUS}$  has been left as future work.

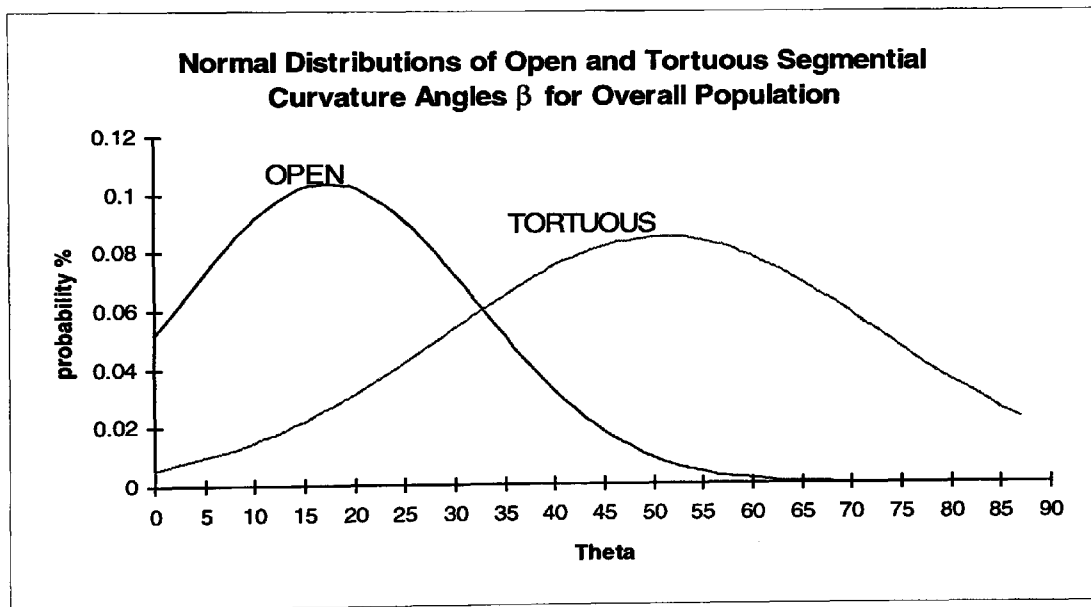


*Figure-6.11 Normal Distributions of Open and Tortuous Segmental Curvature Angles  $\beta$  for Overall Population.*

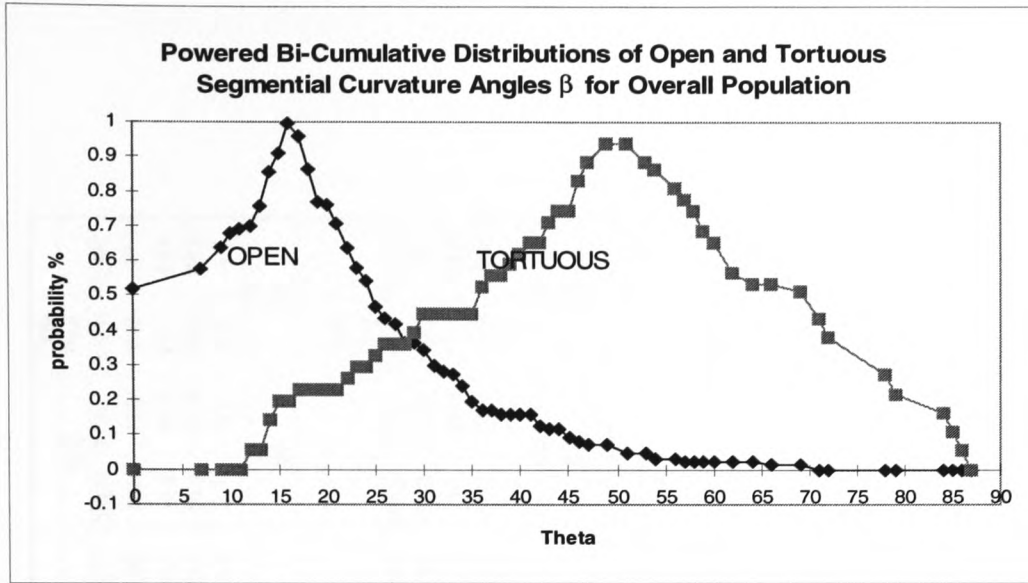


**Figure-6.12** Powered Bi-Cumulative Distribution of Open and Tortuous Segmental Curvature Angles  $\beta$  for Overall Population.

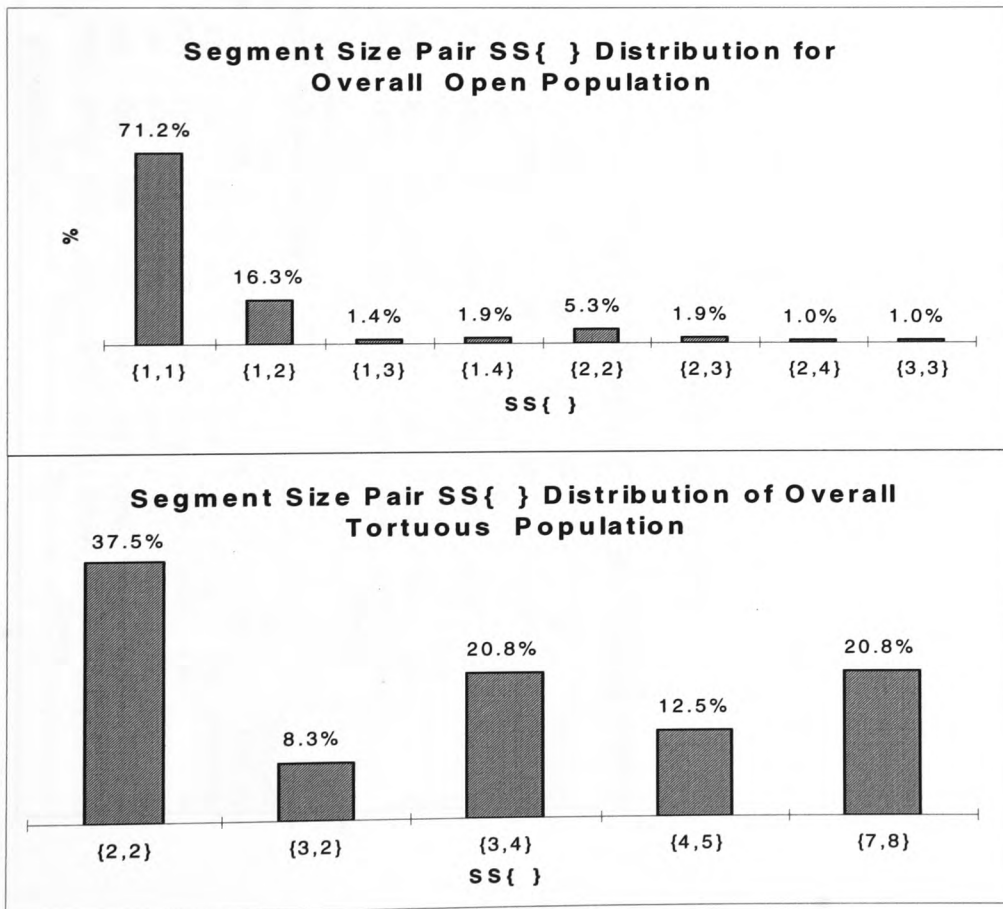


**Figure 6.13** Segment size pair distributions of open and tortuous populations in overall data sets

		In The Absence of																		Only			
		Pr-1			Pr-2			Pr-3			Pr-4			Pr-5			Pr-6			Pr-4		Only	
Overall		OPEN	TORT.	OPEN	TORT.	OPEN	TORT.	OPEN	TORT.	OPEN	TORT.	OPEN	TORT.	OPEN	TORT.	OPEN	TORT.	OPEN	TORT.	OPEN	TORT.	OPEN	TORT.
n		502	183	456	138	520	173	329	126	316	150	630	199	548	183	280	51						
$\mu$		17.4	51.1	17.5	51.3	17.4	50.5	17.2	52.4	16.2	50.0	17.9	46.1	18.2	46.0	21.7	42.6						
$\sigma$		14.8	21.9	14.2	22.1	14.6	22.1	15.7	22.3	14.7	22.7	13.8	22.6	14.0	23.5	15.9	23.3						
Skewness		0.8	-0.1	0.9	-0.1	0.8	0.0	1.0	-0.2	0.9	-0.1	0.3	-0.6	0.7	0.1	0.8	0.3						
ND Beta		33	33	33	33	33	33	33	33	32	31	31	31	31	31	33	33						
OPTIMAL		28	28	28	27	27	29	29	25	25	25	25	25	25	25	26	26						
After the Elimination of Outliers																							
		In The Absence of																		Only			
		Pr-1			Pr-2			Pr-3			Pr-4			Pr-5			Pr-6			Pr-4		Only	
Overall		OPEN	TORT.	OPEN	TORT.	OPEN	TORT.	OPEN	TORT.	OPEN	TORT.	OPEN	TORT.	OPEN	TORT.	OPEN	TORT.	OPEN	TORT.	OPEN	TORT.	OPEN	TORT.
n		441	170	416	124	459	160	271	116	266	136	581	191	510	183	245	51						
$\mu$		13.6	53.9	14.5	55.5	13.7	53.5	11.6	56.0	11.4	54.0	15.3	47.7	15.8	46.0	17.4	42.6						
$\sigma$		10.5	20.0	10.6	19.2	10.4	20.2	9.6	19.4	9.5	19.9	10.7	21.7	11.1	23.5	11.2	23.3						
Skewness		0.0	0.0	0.0	0.0	0.0	0.0	0.0	0.0	0.0	0.0	0.0	-0.6	0.0	0.1	0.0	0.3						
ND Beta		29	31	31	29	29	28	28	28	27	24	28	28	28	28	29	29						
OPTIMAL		26	28	28	25	25	25	25	24	24	24	24	24	24	24	24	24						
Suggested Beta-Opte		28	Beta-Tortuous	49																			

**Table 6.3** The analyses results to select a  $\beta$  OPEN critical segmental curvature angle.

#### 6.4 Selection of Critical Length $\text{Length}_{\text{ELONGATED}}$

Any "open" or "tortuous" capillary loop that has got observable length longer than critical length  $\text{Length}_{\text{ELONGATED}}$  can be tagged with anomaly class "elongated". The value of  $\text{Length}_{\text{ELONGATED}}$  is reported in the literature as  $300\mu\text{m}$  [Kabasakal et al. 96]. However, as they stated, this value is just an estimation, it has not been calculated from an "elongated" capillary loops population. Therefore, OP-TO and elongated populations should be created. OP-TO population can be obtained by combining "open" and "tortuous" capillary loop lengths and elongated population should be "elongated" ones. However, there could not be found any single capillary loop whose elongation is approved by overall agreement of six practitioners. By eliminating a practitioner at a time, it has been found that only one capillary loop (i5:N20) was assigned as "elongated" in the absence of practitioner-4 and practitioner-5 sub data sets. This particular capillary loop's length is calculated as  $502.5\mu\text{m}$ . Bearing in mind that  $502.5\mu\text{m}$  is much bigger than Kabasakal's critical elongation length  $300\mu\text{m}$ , one may expect a total agreement for the loop amongst six practitioners. Unexpectedly, only two practitioners accepted it as "elongated". That is not because the rest of the practitioners disagree on its elongation; they are concentrating on other properties of the capillary loop, such as, being enlarged, "open", "tortuous", etc. Therefore, the existence of some "elongated" capillary loops in overall data set can be expected.

Temporarily accepting that  $502.5\mu\text{m}$  is the threshold length  $\text{Length}_{\text{ELONGATED}}$ , another four capillary loops with  $506.33\mu\text{m}$ ,  $551.19\mu\text{m}$ ,  $704.19\mu\text{m}$ ,  $1095.51\mu\text{m}$  length, in overall agreement data set, should have been assigned as "elongated". Hence, we can assume that *although they have not been classified as "elongated", there are some "elongated" capillary loops in the overall agreement data set.* It is also safe to assume that *the outliers of the open-tortuous data set are definite elongated capillaries.*

The problem of detecting the outliers of the open-tortuous data set arises in this point. There are two approaches to solve this problem, formal and informal detection of the outliers.

### 6.4.1 Formal Detection of Elongated Capillary Loops in Overall Data Set

Assume that there is only one outlier in the data set. If the longest capillary loop is suspect, we can define

$$T_n = (X_n - \mu) / \sigma$$

where  $T_n$  = extreme studentized residual

$n$  = Sample size

$X_n$  = single largest observation that is suspected to be an outlier

$\mu$  = mean value of entire data set

$\sigma$  = standard deviation of the entire data set

By comparing  $T_n$  value from critical values for the single outlier statistic table that produced by G.L. Tietjen [Schiff and D'Agostino 96], we can decide whether it is an outlier or not. If the  $T_n$  value that is calculated for the suspected outlier is more than the critical value that is set according to sample size and  $\alpha$  significance level, it can be discarded from open-tortuous data set, and can be add in to imaginary elongated data set. Subsequently, questioning a suspected outlier each time, and finding the relative  $\mu$ ,  $\sigma$  and  $T_n$  values for reorganized data set with sample size  $n$ , we can detect the outliers. After removing each outlier, we have to switch to a new critical values table specifically designed for the number of suspected outliers. In Table 6.4  $\mu$ ,  $\sigma$  and  $T_n$  values for the open-tortuous data set are presented for each suspected outlier.

n	Mean Length	Variance	Eliminate?	Tn
70	287.94	170.85	1095.51	4.73
69	270.16	123.09	704.19	3.53
68	264.34	113.12	551.20	2.54

**Table 6.4** Detection of the outliers by using formal method.

According to Table 6.4, the first suspected outlier's length is 1095.51 $\mu$ m.  $T_n$  value for the relative  $n$ ,  $\mu$  and  $\sigma$  is calculated as 4.72. When we check this value from critical values table, it can be accepted as an outlier. Hence, the new sample size became 69, and this new set's  $\mu$  and  $\sigma$  values are calculated as in Table 6.4. 704.19 $\mu$ m could be accepted as an outlier and it can be eliminated from our OP-TO data set. For the new set  $T_n$  value is found lower than the critical value, therefore, it can be said that 551.20 $\mu$ m is not an outlier.

By using formal detection of outliers, unfortunately, 704.19 $\mu\text{m}$  is defined as  $\text{Length}_{\text{ELONGATED}}$  threshold value. However, from Kabasakal's report, it is known that  $\text{Length}_{\text{ELONGATED}}$  value should be as short as 300 $\mu\text{m}$ , or some where around this value, It can be said that formal detection of outliers is much tighter than expected. Therefore informal detection of outliers should be considered.

#### 6.4.2 Informal Detection of Elongated Capillary Loops in Overall Data Set

Box and whisker plots can be used in an informal way to identify observations that may be outliers. This can be achieved by replacing the whiskers by a line of length 1.5 - 3 times interquartile range. Any observation beyond this length qualifies as a potential outlier. In Table 6.5, the outliers are assumed to lie above the critical length  $\text{Length}_{\text{ELONGATED}}$ .

$$\text{outliers} > Q3 + f * \text{IQR}$$

where IQR : interquartile range =  $Q3 - Q1$

Q1 : the first quartile (the boundary of 25% the total entries)

Q3 : the third quartile (the boundary of 75% the total entries)

f : multiplier factor

ITERATION	f=1.5	
	1	2
N	232	224
MIN	103.53	103.53
MAX	1095.50	551.20
RANGE	991.97	447.67
MEDIAN	246.53	239.98
C	58.5	56.5
Q1	182.03	182.03
Q3	355.91	330.25
IQR	173.88	148.22
OUTLIERS	-78.78	-40.29
	616.72	552.57

**Table 6.5** Informal detection of outliers by using 1.5\*IQR whisker.

In the second iteration  $\text{Length}_{\text{ELONGATED}}$  became bigger than the maximum length, hence, there are no more outliers. However,  $\text{Length}_{\text{ELONGATED}}$  is still much more than the expected threshold value, and doesn't include the only "elongated" capillary whose length is 502.55 $\mu\text{m}$ . As a result, it can be said that selecting  $f=1.5$  is quite high even for informal detection of outliers.

In this point, a new strategy should be developed to satisfy either or both of our goals; a  $\text{Length}_{\text{ELONGATED}}$  value detects the "elongated" capillary whose length is  $502.55\mu\text{m}$ , and a  $\text{Length}_{\text{ELONGATED}}$  threshold that is close to Kabasakal's threshold value  $300\mu\text{m}$ . The first goal guarantees that all the capillary loops beyond this point can be accepted as "elongated". So, it can be assumed that  $502.55\mu\text{m}$  is the outlier limit of the OP-TO data set.

$$502.553\mu\text{m} = f * \text{IQR} + Q3$$

and

$$f = (502.553\mu\text{m} - Q3) / \text{IQR}$$

from the first column of Table 6.5,  $Q3=355.90$  and  $\text{IQR}=173.87$ ,  $f$  can be calculated as **0.84**

ITERATION	f=0.84				
	1	2	3	4	5
N	232	218	210	196	190
MIN	103.53	103.53	103.53	103.53	103.53
MAX	1095.50	491.22	455.06	426.14	401.08
RANGE	991.97	387.69	351.53	322.61	297.55
MEDIAN	246.53	234.81	222.68	204.96	198.95
C	58.5	55	53	48.5	48
Q1	182.03	178.58	178.58	173.63	173.63
Q3	355.92	329.62	313.76	300.54	297.33
IQR	173.88	151.04	135.18	126.91	123.69
OUTLIERS	35.41	51.22	64.59	66.63	69.34
	502.53	456.98	427.74	407.55	401.63
After 4th Iteration					
MEAN LENGTH			STANDARD DEV.		
ELONG.	OP-TO	ELONG.	OP-TO	Length <sub>ELONGATED</sub>	
554.35	229.05	211.47	81.23	342.73	

**Table 6.6** Informal detection of outliers by using  $0.84 * \text{IQR}$  whisker

By using  $f = 0.84$ , elimination of outliers halts at the fifth iteration. At this point  $\text{Length}_{\text{ELONGATED}}$  has been defined as  $401.63\mu\text{m}$  by the calculations. It is safe to say that any capillary beyond this length, is an "elongated" capillary loop. Assigning imaginary class "elongated" to these capillary loops, we obtain two populations; open-tortuous, and "elongated". Applying "fat pencil" test to these collections, we can say that both of the populations are normally distributed.

Open-Tortuous population qualifies being normal distributed by satisfying “Fat Pencil” test (Figure 6.14). On the other hand, the last two entries of elongated population have large residuals and fall apart from the straight line. If there were some other entries scattered after the last third sample of this population, these points would have small residuals, and “fat pencil” test would be satisfactory. Hence, it can be said that although the last two entries lie far from the straight line, elongated population, can still have a normal distribution.

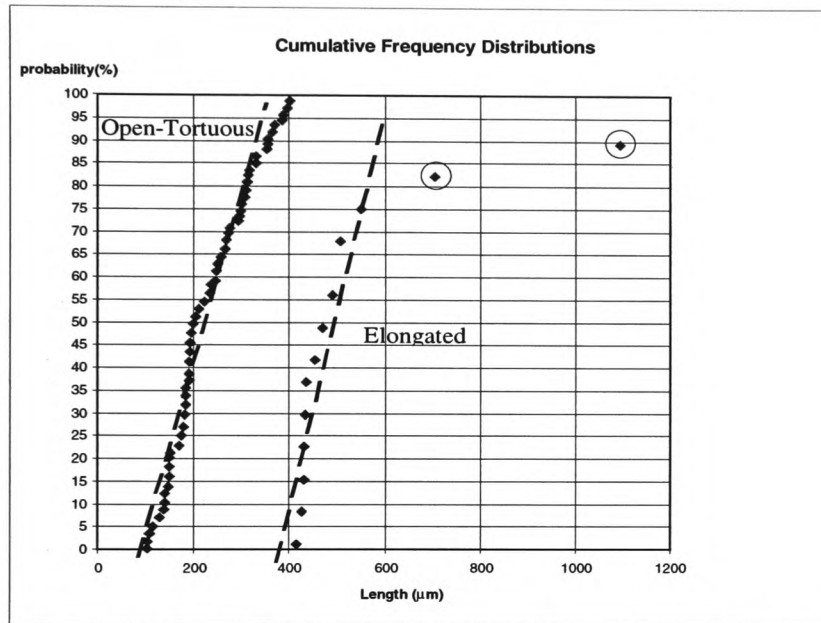


**Figure 6.14** Hypothesized distribution selection of the populations.

Accepting, both of the populations have normal distribution,  $\mu_{OP-TO}$ ,  $\sigma_{OP-TO}$ , and  $\mu_{ELONGATED}$ ,  $\sigma_{ELONGATED}$  have been calculated as in Table-6.6. The intersection point of two normal distributed populations  $342.72\mu\text{m}$  is accepted as  $\text{Length}_{ELONGATED}$  threshold point.

One may think that all the efforts to create an imaginary "elongated" capillary loop population and set a threshold  $\text{Length}_{ELONGATED}$  out of overall open tortuous data set, is nothing but speculation. Consider the cumulative frequency distribution of "open" and "tortuous" capillary loop lengths in the overall agreement data set that is given in Figure 6.15. According to the “Fat Pencil” test if the data set is normally distributed a “FAT” pencil, that locates on the line that influenced by the data between first and third quartiles, should cover all the data.



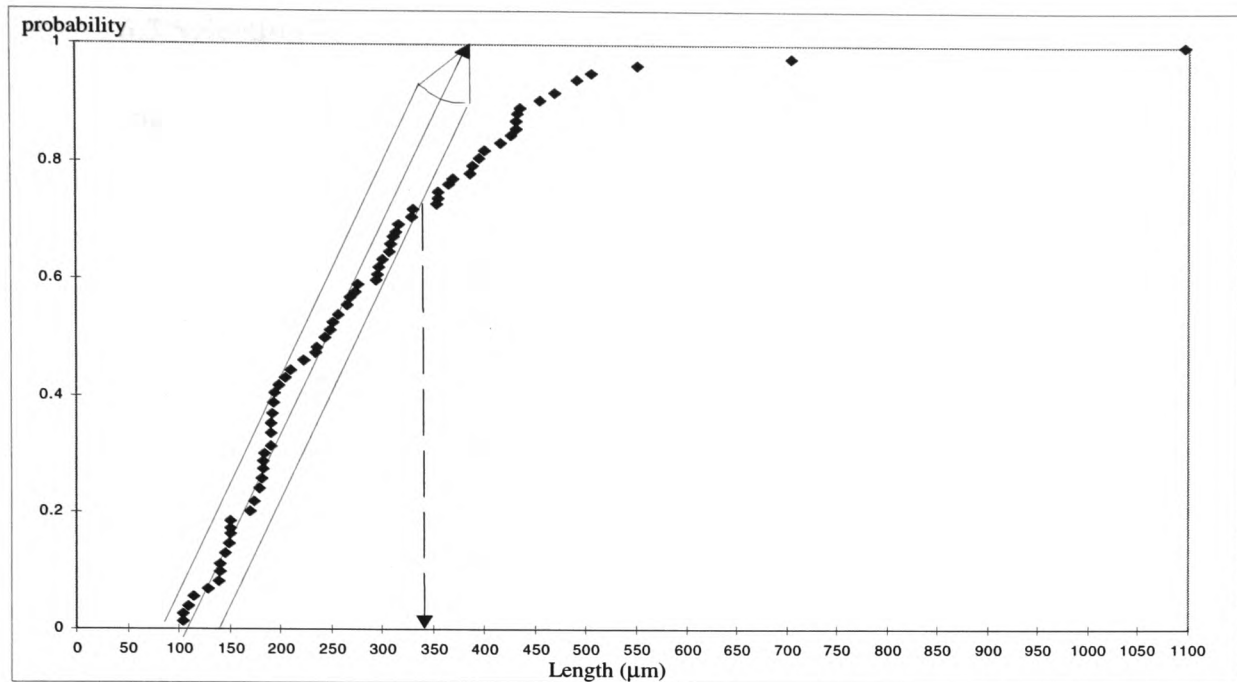


**Figure 6.15** Cumulative Frequency Distribution of Open and Tortuous Capillary Loop Lengths in Overall Agreement Data Set

After the loop length  $342\mu\text{m}$ , the entries are no longer covered by the “pencil” as can be seen in Figure 6.15. Note that the thickness of the pencil is influenced by the largest residual around  $200\mu\text{m}$ , and the smallest entry of imaginary elongated population that is  $416\mu\text{m}$  as can be seen in Figure 6.14. 92% of the open-tortuous capillary loops lie below the threshold value. Considering having only one capillary loop assigned as “elongated” in the data set, the final result is (quite surprisingly) on the target.

As a result, the “elongated” threshold value  $\text{Length}_{\text{ELONGATED}}=342.72\mu\text{m}$  is satisfactorily calculated by referring the Kabasakal’s estimation  $300\mu\text{m}$ . Also the mean length of the capillary loops is calculated as  $\mu=229.05\mu\text{m}$  and it is in agreement with those reported in literature  $215\mu\text{m}$  (SD 40) [Kabasakal et al.96]  $223.3\mu\text{m}$  (SD 51.9)[Maricq et al. 80], and  $234.9\mu\text{m}$  (SD 5.8)[Rouen et al.72]. However, further research with an elongated population is recommended to justify the critical length  $\text{Length}_{\text{ELONGATED}}$ .

## 6.5 Selection of Critical Limb Width $LimbWidth_{GIANT}$

The anomaly class "giant" can be tagged to any enlarged "open" or "tortuous" capillary loop that has wider limbs than critical **limb width**  $LimbWidth_{GIANT}$ . For the definition of the threshold value, loop width and limb area have been used in the literature by Kabasakal et al.[96], and Rouen et al.[72], respectively.

Kabasakal et al.[96], set the threshold value as  $LimbWidth_{GIANT} = 10 \times \text{threshold width of being normal}$  that is  $25\mu\text{m}$ . Therefore  $LimbWidth_{GIANT}$  should be set to  $250\mu\text{m}$ . However in the same report, they quoted a value at  $215\mu\text{m}$  the mean capillary loop length. Setting the threshold width to  $250\mu\text{m}$  that is even larger than the mean capillary loop length does not sound so realistic.

Rouen et al.[72], on the other hand, followed a rather different approach. First they measured afferent, efferent and transitional limb width of the capillary loops, then by using the following formula, they have calculated the area of a generally enlarged capillary loop;

$$Area = ALW \left( \frac{OL}{3} + TLW \right) + ELW \left( \frac{OL}{3} + TLW \right) + TLW \left( \frac{OL}{3} - \left( \frac{ALW}{2} + \frac{ELW}{2} \right) \right) \quad (6.13)$$

where ALW: Afferent Limb Width

ELW: Efferent Limb Width

TLW: Transitional Limb Width

OL: Observable Length

If the calculated area of generally enlarged capillary loop exceeded 20% of the total projected areas, the capillary loop classified as "giant". Note that the formula above is applicable to only those generally enlarged or "giant" capillary loops with transitional limbs almost as long as the visible lengths of the afferent or efferent limbs. If the lower boundary values of  $ALW=68.3\mu\text{m}$ ,  $ELW=95\mu\text{m}$ ,  $TLW=120.4\mu\text{m}$  and  $OL=780.3\mu\text{m}$  of giant population are replaced in equation (6.13) the area will be  $83,621\mu\text{m}^2$  (Note that ALW, ELW, TLW are obtained from the findings in Rouen et al.[72]). By dividing the

area with twice the observable length, an average limb width  $53.58\mu\text{m}$  can be obtained. Therefore,  $\text{LimbWidth}_{\text{GIANT}}$  should be near to  $53.58\mu\text{m}$ .

f=1.5				
iteration	1	2	Mean Limb Width	
n	83	73	Enlarged	Giant
min	18.73	18.73	27.64	46.27
max	48.48	33.70		
range	29.75	14.97		
median	28.75	28.43	<b>Standard Deviation</b>	
c	21.5	19	Enlarged	Giant
Q1	26.41	24.32	4.22	2.86
Q3	32.02	30.72		
IQR	5.62	6.40		
OUTLIERS	17.98	14.72	<b>LimbWidth<sub>GIANT</sub></b>	
	40.45	40.31	38.61	

Table 6.7 Detection of outliers by using  $1.5 \times \text{IQR}$  whisker.

In the overall agreement data set, only one capillary (i5:N27) is classified as "giant". The capillary loop has  $167\mu\text{m}$  loop width and  $48.48\mu\text{m}$  limb width. Neither Kabasakal's nor Rouen's threshold values will be able to detect this "giant" capillary loop. Therefore, a critical limb width for the selection of "giant" capillary loops, should be calculated by using enlarged capillary population in test images. The limb widths of capillary loops that are classified as enlarged by overall agreement of the practitioners, have been collected in a population and cumulative frequency distribution of this population is given in Figure 6.16.

By applying the "fat pencil" test to the distribution in Figure 6.16, the largest three entries can be visualized as the outliers of the population. By using box and whisker method with  $f=1.5$ , the outliers and possibly "giant" loops of the population can be detected. In Table 6.7, the analysis results are given. According to this table, in second iteration there are more outliers. These outliers are accepted as "giant" loop population. In Figure 6.17 cumulative frequency distributions of reorganized enlarged and the "giant" capillary loops populations are given. Note that both of the populations are normal distributed. The intersection point of these normal distributions,  $36.8\mu\text{m}$ , is the answer for the threshold limb width,  $\text{LimbWidth}_{\text{GIANT}}$ . Mean limb width and standard deviations of both populations can be found in Table 6.7.

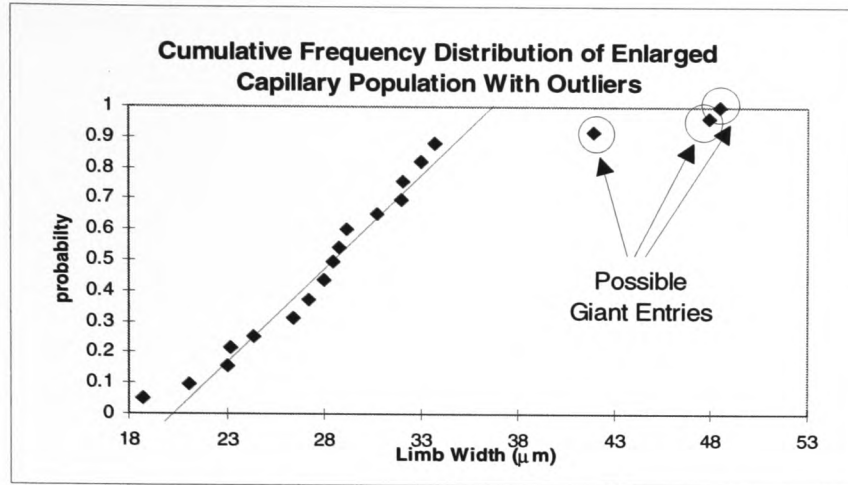


**Figure 6.16** Cumulative Frequency Distribution of Enlarged Capillary Population with Outliers that Possible Giant Entries

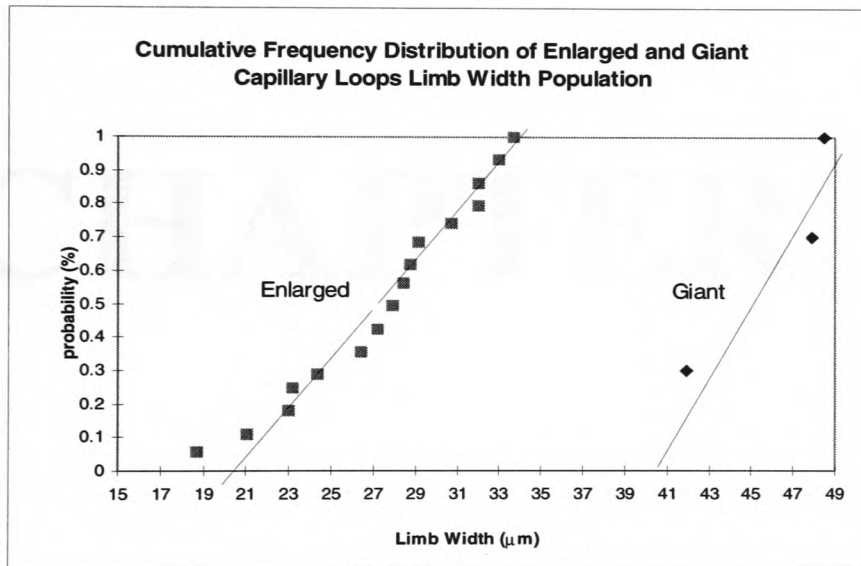


**Figure 6.17** Cumulative Frequency Distribution of Enlarged and Giant capillary Loop Populations.

As a result, neither limb surface area [Rouen et al. 72] nor loop width [Kabasakal et al. 96] but limb width of capillary loops is suggested for the classification of "giant" capillary loops. Assuming that loop width is 3\*limb width, Kabasakal's suggestion will be somewhere around 83 $\mu\text{m}$ , and Rouen's is 53.58 $\mu\text{m}$ . Neither of these thresholds can detect the only "giant" loop that is agreed by three of the practitioners in the test images. Alternatively a threshold value 36.8 $\mu\text{m}$  is calculated by creating an imaginary "giant" loop population out of enlarged capillary loop population.

# CHAPTER 7

## **Chapter 7 Validation of The System**

### **7.1 Introduction**

The Automated Nailfold Capillary Classification and Analysis System (TANCCAS) has been developed to satisfy the requirements of classification criteria given in Chapter 3. The validation of the automated system will be made comparing TANCCAS's and the participating clinicians' classifications of the test images. The clinicians had different levels of knowledge and experience in the field. Stereotype clinicians' evaluations may display similar outputs, but nailfold capillaroscopy has been studied all over the world by the researchers that have various background knowledge and experiences. Therefore, carrying out the tests with a mixed group of clinicians may display the clinicians' classification handicaps, especially individuals' concentration on some important characteristics of the capillary loops.

The performance of the system will be analysed for classification accuracy of individual classes and compatibility to the participating clinicians' evaluations in this chapter. The analysis capability of the system has been justified by comparing the mean length and width of the capillary loops, that are calculated in previous chapter, with the findings from the literature.

### **7.2 The Analysis Criteria**

TANCCAS's classification criteria had been gradually developed based on the findings of literature and outcome of the tests that carried out by the participant clinicians. The class set of the system differs from the clinicians' set, because of using combinational class set. Therefore a protocol should be established between these class sets to compare the results. The following rules are applied during the analysis.

1. Width Anomaly Class (WAC) set contains the labels "enlarged" and "giant".
2. Length Anomaly Class (LAC) set contains the label "elongated".
3. Descriptive Class (DC) set contains six basic patterns; "cuticulis", "open", "tortuous", "crossed", "bizarre" and "bushy".

4. Seventeen capillary classes of TANCCAS are created by combining the class sets WAC, LAC and DC, and they are:

Open	Tortuous	
Enlarged Open	Enlarged Tortuous	
Giant Open	Giant Tortuous	
Elongated Open	Elongated Tortuous	
Enlarged Elongated Open	Enlarged Elongated Tortuous	
Giant Elongated Open	Giant Elongated Tortuous	
Cuticulis	Crossed	
Enlarged Cuticulis	Bizarre	Bushy

5. The clinicians class set contains 11 classes, and they are:

"Cuticulis", "open", "tortuous", "crossed", "bizarre", "bushy", "enlarged", "normal", "giant", "elongated" and "mixed".

6. The so-called class "mixed" is accepted as either "bushy" or "bizarre", while comparing TANCCAS's and the clinicians' assignments. TANCCAS's class sets does not include so-called class "mixed". Therefore class "mixed", from clinicians' class set, has not got a real match except "bushy" or "bizarre". Instead of discounting "mixed" capillary loops, because they have been granted a class by the clinicians, the closest patterns "bushy" or "bizarre" are matched with "mixed". It has been observed that if the capillary loop is atypical and either the "bizarre" and "bushy" pattern is not dominant, the clinician assigned the class "mixed". It should be noted that in five cases out of 217 (i3:N44, i4:N10, i3:N12, i5:N38 and i5:N42), clinician-1 assigned the class "mixed" to non-atypical loops. In order to simplify the analysis, these cases ignored.

7. The unclassified capillary loops were not discounted during the analysis. Not being able to assign a class to a capillary loop, is incapability of a clinician. While measuring the individual's performance in order to compare with TANCCAS's performance, the handicap of human perception and indecisiveness should be taken into account. By the increasing numbers of unclassified capillary

loops, neither capillary loop class distribution nor the individuals' abilities will reflect the reality.

8. WAC and LAC anomaly classes are accepted in the sense of class in the clinicians' class set, not a label as in TANCCAS's class set. If clinician assigns a capillary loop with the one of anomaly classes, and TANCCAS tags this class as a label, an agreement will be granted between clinician and the TANCCAS. The agreement can not be granted between clinicians in such cases.
9. The classes "bizarre", "bushy", "crossed" always present an inner boundary that a sign of enlargement. If the capillary loop is classified one of these classes by a clinician, and "enlarged" by TANCCAS, an agreement is accepted between TANCCAS and clinician. On the other hand, this is not true for clinicians.
10. ConsensusClass is the class that is assigned to a capillary loop by the majority of the clinicians. Consensus Value (CV) is the number of clinicians that assigned the consensus class to the loop. Theoretically each capillary loop should be assigned with a single class, however this was not possible in some cases. Therefore, instead of eliminating those loops, more than one class (joint consensus classes) can be assigned to a capillary loop. If TANCCAS or a clinician has assigned one of these joint classes, its performance has been credited.

The following case is a good example of applications of the rules. The capillary loop (i6:N5) has assigned with the classes "bushy", "bizarre", "enlarged", "bizarre", "mixed", "mixed", by the clinicians and "bushy" by TANCCAS. By applying above rules, the CV's will be as follows;

Clinician-1 ("bushy" CV=0)	Clinician-4 ("bizarre" CV=2)
Clinician-2 ("bizarre" CV=2)	Clinician-5 ("mixed" CV=2)
Clinician-3 ("enlarged" CV=0)	Clinician-6 ("mixed" CV=2)
TANCCAS ("bushy" CV=6)	



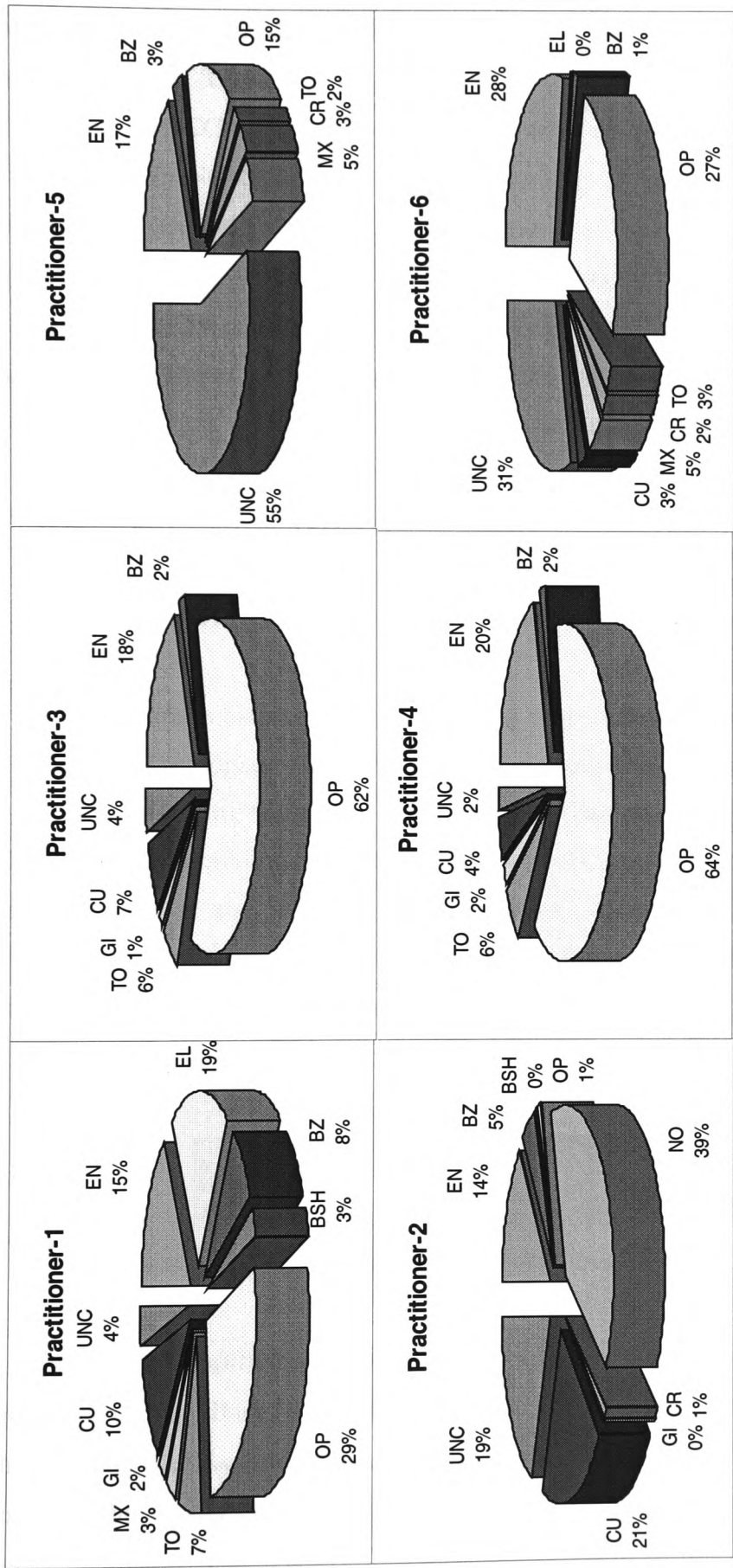


**Figure 7.1** The class distributions of the capillary loops in six test images by the practitioners

According to rule 10, the capillary loop will have two joint consensus classes "bizarre" and "mixed". If TANCCAS assigns either of these classes, success will be awarded. However, TANCCAS assigned the class "bushy". Therefore, a misclassification may be expected by TANCCAS. Nevertheless, according to rule 6, "mixed" classes are accepted as "bushy", and this over rules the misclassification. The maximum number of agreement (CV) is defined as two. Although these classes are accepted as "enlarged" (rule 9), failure is granted to clinician-3. Clinician-3 did not imply anything about being "bizarre" or "mixed", but enlargement. If the consensus class was "enlarged" then he would be granted with agreement. TANCCAS's consensus value, however, is set to four. According to rule six, a "mixed" capillary loop might be "bushy", that agrees with clinician-5 and 6. Rule 9, also, requires agreement between TANCCAS and clinician-3.

### 7.3 Justification of Proposed Combinational Class Set

Consensus class(es) of the capillary loop is defined by applying the tenth rule in section 7.2. The consensus class of a capillary loop has been accepted as loop's real type. In the case of failing to acquire majority, more than one consensus class (joint consensus class) has been assigned to the capillary loop, and if the clinicians or TANCCAS assigned one of the joint consensus classes, success has been granted. Consensus class(es) distribution of the capillary loops is given in Table 7.1. Seventeen percent of the 217 capillary loops have more than one consensus class. The capillary loop (i1:N2), for example, has got joint consensus classes; "cuticulis" (CV=2) and "enlarged" (CV=2).

	1 Class	2 Classes	3 Classes	4 Classes	5 Classes	6 Classes
n	180	33	2	1	1	0
%	82.95%	15.21%	0.92%	0.46%	0.46%	0.00%

**Table 7.1** Consensus class(es) distribution of the capillary loops

CV of a capillary loop is a way of measuring accuracy of the consensus class that assigned to a capillary loop. The higher the CV of a loop, the more clinicians agree on the consensus class, and vice versa. Having CVs more than 3 guarantees that capillary loop will have only one consensus class. Distributions of CVs of consensus classes and

CV of TANCCAS are listed in Table 7.2. It should be reminded that CV of a loop reflects the classification harmony amongst the clinicians. The table is arranged for TANCCAS and clinicians, in order to demonstrate both parties classification harmony with clinicians.

	CV 1		CV 2		CV 3		CV 4		CV 5		CV 6	
	TANCCAS	Cls	TANCCAS	Cls	TANCCAS	Cls	TANCCAS	Cls	TANCCAS	Cls	TANCCAS	Cls
n	5	7	15	48	43	77	70	41	42	17	15	0
%	3%	4%	8%	25%	23%	41%	37%	22%	22%	9%	8%	0%

**Table 7.2 Consensust Value Distributions for the clinicians and TANCCAS**

67% of the capillary loops are assigned with a class that satisfies more than three clinicians by TANCCAS. Contrary to this, only 31% of the capillary loops have CVs more than three. This proves that the combined class set of TANCCAS satisfies a wide range of clinicians. Another important result could be drawn from Table 7.2 is that *clinicians could not achieve unity on the consensus class*, not even for a single capillary loop. TANCCAS, on the other hand, is in unity with all of the clinicians in 15 cases that is 8 % of the capillary loop population. The capillary loop (i1:N8), for example, is assigned with the consensus class "enlarged" (CV=4). Class "cuticulis" is assigned by the remaining two clinicians. By assigning the class "Enlarged Cuticulis" (CV=6), TANCCAS achieved agreement with all of the clinicians.

#### **7.4 Classification Performance of TANCCAS**

Assuming that consensus class(es) of a capillary loop is its actual class, classification success rates of the parties can be determined. This analysis also demonstrates the individuals' harmony with the others while assigning a class to capillary loop. As it can be seen from Table 7.3, 88% of TANCCAS's classifications were in agreement with the majority of the clinicians.

TANCCAS's classification performance is better than clinicians 1, 2, 5 and 6 for the six populations. Clinicians 3 and 4 have better performances than TANCCAS for the image 2 and 4. Additionally, clinician 3 has better classifications than TANCCAS for

image 6. However, in overall evaluations TANCCAS has got the highest classification success rate.

	Clinician1	Clinician2	Clinician3	Clinician4	Clinician5	Clinician6	TANCCAS
Image 1	67%	44%	22%	67%	89%	67%	100%
Image 2	65%	18%	88%	84%	25%	67%	78%
Image 3	59%	21%	87%	87%	18%	52%	89%
Image 4	54%	21%	92%	95%	5%	77%	90%
Image 5	65%	43%	76%	93%	17%	52%	96%
Image 6	27%	64%	82%	45%	55%	64%	73%
Overall	59%	28%	83%	86%	22%	61%	88%

**Table 7.3 Classification Success Rates for the clinicians and TANCCAS**

According to Table 7.3, the participating clinicians can be divided into three groups. The clinicians 3 and 4 have got highest classification success rates amongst the clinicians 86% and 83% respectively. Their classifications of the test images (given in Figure 7.14) display great similarities. The clinicians 1 and 6's performances are average amongst the others, 59% and 61% respectively. The clinicians 2 and 5, on the other hand, have got the lowest success rates 22% and 28% respectively. The reasons of three different level of performances of the clinicians can be determined by checking the Table 7.4.

	Descriptive	Label	Unknown
pr1	56%	37%	7%
pr2	28%	53%	19%
pr3	77%	19%	4%
pr4	76%	22%	2%
pr5	23%	17%	59%
pr6	36%	29%	35%

**Table 7.4 Descriptive or label classes usage rates of the clinicians**

The clinicians' class set (given in section 7.2 rule 5) is divided in three groups; descriptive classes, label classes and unknown. Descriptive classes are same with TANCCAS's descriptive classes. Label classes are TANCCAS's anomaly label classes. Unknown capillary loops are the unclassified and "mixed" ones. Clinicians 3 and 4 achieved better results than the others, because they have mostly used the descriptive classes. Clinician 2 and 4 have the lowest successes, because they mostly assigned the

loops to the label classes or uncertainty. This is quite significant in Table 7.4. Therefore it can be said that by assigning a descriptive class to a capillary loop, a universal classification will be achieved. Contrary to this, by assigning label or uncertain classes (in clinician 2's and 3's cases respectively) the universal agreement will be disrupted.

#### 7.4.1 Class Identification Performance of TANCCAS

In previous section, TANCCAS's overall classification performance is analyzed. In this section, TANCCAS's classification performance of individual classes will be analyzed. If the class assigned by TANCCAS includes the common class of the capillary loop success is granted on account of TANCCAS. Table 7.5 displays the class identification success rates of TANCCAS. Note that the classes "elongated", "bushy" and "normal" are not included in the table, because none of these classes is assigned as consensus class by the clinicians. Therefore a comparison could not be made.

	EN		BZ		OP		TO		CR		GI		CU	
	MATCH	TOTAL	MATCH	TOTAL	MATCH	TOTAL	MATCH	TOTAL	MATCH	TOTAL	MATCH	TOTAL	MATCH	TOTAL
n	43	45	5	7	86	103	5	8	2	2	1	1	11	13
%	96%		71%		83%		63%		100%		100%		85%	

**Table 7.5** *Class Identification Success Rates of TANCCAS*

Largely populated classes; "enlarged", "open" and "cuticulis" are successfully identified, these are the classes determined the TANCCAS's overall performance. The lowest identification rates 63% and 71% belong to "tortuous" and "bizarre" capillary loops respectively. Their population however is quite small. The mis-classification of a single loop has great effect on the output or vice versa. This is, of course, true for "crossed", "mixed" and "giant" type loops that have 100% identification success rates. The identification success rates of the classes with small population, are deceptive. Therefore, apart from identification success rates of the "enlarged", "open" and "cuticulis", the other successes should not be credited. However, this does not mean that the developed algorithms are not reliable. Their performances could not be successfully measured by using the test images. Therefore, further analyses should be performed on largely populated different capillary loop patterns by both TANCCAS and the clinicians in the future.

The future analysis that should be carried out by the clinicians who should be fully informed of the classification system may increase the classification accuracy rate of TANCCAS.. Although the classification methods of TANCCAS and the clinicians differ, TANCCAS achieved 88% classification accuracy rate. If the clinicians use the proposed classification system, TANCCAS's and the clinicians' classification accuracy rate, obviously, will improve because of evaluating the loops in the same fashion. Therefore, the present analysis are sufficient to prove that TANCCAS is capable of making reliable classifications.

#### **7.4.2 TANCCAS's Agreement With Individuals**

By assuming that actual class of a capillary loop, regardless to other clinicians' opinion, is the class that assigned by the individual clinician, the agreement of each clinician with TANCCAS is measured. The analysis results are given in Appendix D.

The lowest agreement 46% is resulted with clinician-5. This is largely because of this clinician's low performance on overall success that is 22%. Although, clinician-2 scored pretty low overall performance that is 28%, he has got the highest agreement rate 88%. That is due to this clinician mostly assigned the width informative classes; normal and "enlarged" to the capillary loops. However, the agreement rates of TANCCAS with rest of the clinicians, are more than 70%. The agreement rates of TANCCAS with the most successful clinicians 3 and 4 are scored as 77% and 76%, respectively.

#### **7.4.3 Validation of Capillary Loop Analysis Capability of TANCCAS**

The analysis capability of TANCCAS can be justified by comparing the analysis parameters mean capillary loop length and width that have been calculated while selecting the critical values in chapter 6, with the findings from the literature. In Table 7.6, these findings are summarized.

The previous researchers' results can be divided into two main groups. Lefford and Edwards [86], Carpentier and Maricq [90] and Studer et al.[91] reported the mean

capillary loop width around 40 $\mu$ m. Maricq et al. [80], Michoud et al. [92] and this study reports a mean capillary loop width some where around 63 $\mu$ m. Mean loop length has been reported in the range of 215 $\mu$ m-234 $\mu$ m by previous researchers. In this study the mean loop length has been calculated as 229 $\mu$ m which is in the reported range.

	This Study	Maricq	Michoud	Lefford	Carpentier	Studer	Kabasakal	Rouen
Loop Width	63.96 $\pm$ 15.92 $\mu$ m	62 $\pm$ 9 $\mu$ m	64 $\pm$ 17 $\mu$ m	40 $\pm$ 10 $\mu$ m	41 $\pm$ 3 $\mu$ m	38 $\mu$ m	*	*
Loop Length	229.46 $\pm$ 81 $\mu$ m	223.3 $\pm$ 81 $\mu$ m	*	*	*	*	215 $\pm$ 40 $\mu$ m	234.9 $\pm$ 5.8 $\mu$ m

**Table 7.6** Capillary morphometry (Mean  $\pm$  SD), comparisons with the literature

It should be emphasized that in Michoud’s and this study, the measurements are carried out by computer systems that were developed for automated nailfold capillary loop analyses. The outputs of both systems are almost identical for mean loop width calculations. However, they have not reported a mean loop length to be able to compare our result with an automated analysis system.

## 7.5 Summary

The analysis results proved that the developed system TANCCAS is capable of performing accurate classifications and analyses. It can be used as a reliable diagnostic tool for nailfold capillaroscopy by clinicians. The proposed combinational class set results better classifications, and provides harmony between individual's classifications.

# CHAPTER 8



## **Chapter 8    General Conclusions and Recommendations for Future Research**

### **8.1 The Strengths and The Weaknesses of the Proposed Classification System and TANCCAS**

The **strengths** of the proposed classification system and TANCCAS are outlined below.

- 1)     By setting quantitative classification criteria for parametric classes: "cuticulis", "open" and "tortuous", anomaly classes: "giant" and "elongated", and setting semiquantitative classification criteria for "bizarre" and bushy types, the loops near to border lines are identified successfully. By using the proposed classification protocol, the harmony between the research groups will be established. This, of course, will increase the researchers' benefits from other research groups' findings.
  
- 2)     The proposed class system offers more information about the loops than the existing classes by combining the shape and anomaly information. Therefore the researchers may establish new links, which have not been available with the existing class systems, between the diseases and the nailfold capillary loop shape patterns.
  
- 3)     The computerized system TANCCAS is able to reduce the classification error not only by using the quantitative classification criteria, but also processing each individual loop with the same accuracy. The analysis and classification error due to the weaknesses of human perception and interpretation are eliminated. If the researcher feels that existence of a certain type of loop may have a connection with a certain disease, s/he may have tendencies to classify the loops near to border line into the relevant class(es). However, with a computerized system such inclinations will be avoided. During the analysis of the clinicians classifications, it has been observed that some of the capillary loops, that are almost identical, are classified into different classes.

This is because of either lack of concentration or the effects of the neighbouring loops on the clinician's perception. TANCCAS is free of such errors.

4) TANCCAS does not require a user that is expert in the field, since the classifications and the analysis are made with no user interaction.

5) TANCCAS proved to be more accurate than the clinicians with 88% classification success rate. The success rate is calculated by granting success for correctly identifying each loop's consensus class that is assigned to a loop by the consensus of the participating clinicians. The lowest and highest classification success rates of the clinicians are 22% and 86%, respectively. Therefore TANCCAS's classifications are reliable.

6) The agreement rates between TANCCAS's and the individual's classifications are calculated as 70%, 88%, 77%, 76%, 46% and 70% for clinician 1, 2, 3, 4, 5 and 6, respectively. Apart from clinician 5, TANCCAS sufficiently satisfies the clinicians' individual expectations. Therefore, practicality of TANCCAS's classifications will be approved by the individuals.

7) The analysis parameters LoopWidth, LoopLength and tortuosity value are calculated more precisely than those reported in the literature. The capillary loop length for example is calculated directly from the loop skeleton. In the literature, however, the projection distance between capillary tip point and the lowest end point of the limbs is accepted as loop length. If the capillary loop has high tortuosity level, such measurement's accuracy is questionable. [Michoud et al. 94], for example defined a tortuosity value as the ratio between loop skeleton length and the projection distance between end points of the skeleton. Such measurement will not reflect the real tortuosity of the loops that has got limbs that are symmetrical to the orientation line axis. Such a loop will have the lowest possible tortuosity value, 1, and will be classified as perfectly "open". However, carrying out the measurements on the limb boundaries

and by dividing them into smaller segments the tortuosity of the loops is measured accurately.

8) The hierarchical programming structure and image processing library of TANCCAS allow the future researchers to modify the classification criteria or increase its capabilities by adding new classes and analysis parameters. As an example of these future developments, the width and length measurements of afferent, efferent and apical parts of the loops, the ratio between afferent and efferent limbs can be given. The location of the loop tip point, loop width, limb surface area and limbs' skeleton length are already calculated. By using these data, more detailed analysis of the capillary loops is possible.

The **weaknesses** of the proposed classification system are outlined below. Some of these deficiencies can be overcome by further developments where this is the case suggestions are made as to how this can be achieved.

1) The threshold values  $\beta_{\text{TORTUOUS}}$ ,  $\text{Length}_{\text{ELONGATED}}$ , and  $\text{LimbWidth}_{\text{GIANT}}$  are selected hypothetically. Although they proved to be sufficient, these values should be selected from their actual populations that contain enough samples to set more precisely the threshold values. In general, the calculations of all of the threshold values from their actual populations that have large amount of samples, will increase the accuracy and the reliability.

2) The qualitative classification criteria for "enlarged" type should be set quantitatively. Unfortunately, the "enlarged" capillary loops population of the test images contains many 'within normal width' loops that prevent setting a critical  $\text{Width}_{\text{ENLARGED}}$  value. Although it is possible to adopt one of the values reported in the literature, TANCCAS mimics the clinicians' classifications. However, with further tests, a critical  $\text{Width}_{\text{ENLARGED}}$  can be calculated. By replacing the label "enlarged", that is identified in Pre-Processing Module (PPM), with the outcome of a simple comparison between the critical value and  $\text{LoopWidth}$  in Class Decision Unit (CDU), quantitative classification of "enlarged" can be achieved.

- 3) The classification of some 'haemorrhage' structures as "bushy" type creates mis-classifications. However, there is not any existing class(es) that such structures can be classified into. As [Maeda et al. 97] stated in their report, there is a need for new haemorrhage classes.
- 4) TANCCAS is capable of processing only those hand traced images of capillary images. Because of the low quality of the images and the time limitations the development of Segmentation Module (SM), that extracts the loop boundaries from the original images is left as future work.
- 5) PolygonalApproximation() and Pruning() algorithms, unfortunately, require the input parameters error tolerance threshold and spur branch threshold length, respectively. These parameters are pre-set in the header file. The change in microscope's magnification rate does not alter the present threshold values. However, by experimenting with the scale of the image a scale coefficient that alters the threshold parameters of PolygonalApproximation() and Pruning(), can be calculated.
- 6) The orientation line of some of the "cuticulis" loops that are wide and have small limbs, naturally intersects the loops' limbs horizontally where a vertically orientated line was expected. The orientation of the loop is used for the transformations of the enclosed loops' boundary chains. Disorientation of the line may cause mis-classification of "Enlarged Cuticulis" loop as "tortuous". The capillary loop may be a hook shaped "tortuous" loop, as well as a "cuticulis" one. The exclusive curvature angle  $\theta$  cannot be used to obtain extra information, because the  $\theta$  is scale invariant. Setting a critical loop perimeter length for the "cuticulis" loop will result mis-classification of extremely "Enlarged Cuticulis" loops as "tortuous". There could not be found any solution to overcome this problem.

## 8.2 General Conclusions

### 8.2.1 Proposing A New Class Set

Nailfold Capillaroscopy (NFC) as a diagnostic tool, has growing importance to diagnose endocrine, cardiovascular and connective tissue diseases. The distributions of the capillary loops, their morphological parameters and deformity degree of capillary loops are used to establish the link between the disease and NFC in numerous studies that have been reported in the literature. The terminology has been used to describe the capillary loops varies from one author to another.

The capillary class names should be descriptive, as well as being informative. After reviewing the literature and carrying out a survey with six clinicians, six shape informative classes; "cuticulis", "open", "tortuous", crossed, "bizarre" and "bushy" have been accepted as **Descriptive Classes (DC)**. The width anomalies, enlargement of loop width and having extremely widened limbs are represented by **Width Anomaly Classes (WAC)** "enlarged" and "giant", respectively. The **Length Anomaly Class (LAC)**, "elongated", represents extremely long loops. By combining these three class groups in the order of (WAC-LAC-DC), three important characteristics of a capillary loop can be preserved within class name. It should be noted the descriptive classes, crossed, "bizarre" and "bushy" do not require to be tagged with WAC and LAC. The proposed class set contains following seventeen classes:

Open	Tortuous	Cuticulis
Enlarged Open	Enlarged Tortuous	Enlarged Cuticulis
Giant Open	Giant Tortuous	
Elongated Open	Elongated Tortuous	
Enlarged Elongated Open	Enlarged Elongated Tortuous	
Crossed	Bizarre	Bushy

## **8.2.2 Proposing the Classification Criteria**

Without a common classification criteria for nailfold capillary loops, the analysis results will differ from one researcher to another. In the literature, it is often stated that classification and the analysis of nailfold capillary loops are made by same clinician. This assures the reader that the results are the product of only one observer's perception. If the classification and analysis processes are carried out by more than one observer, the results might have been different. With the observer's perception playing so important role on the results, how can we expect that the reader will benefit from the findings? Six participant clinicians demonstrated this confusion quite well in the tests. For example, there was no consensus on even a single capillary loop's class out of 217. Each clinician suggested a different class for the 3% of the capillary population. At least four out of 6 six clinicians are agreed on the same class for 29% of the 217 capillary loops. If one observer's opinion on the classes is so strongly differing from others, the need for a classification protocol will be urged.

Proposing the classification criteria for nailfold capillary loops is the main contribution of this project to the existing knowledge. Seventeen capillary classes, combined from WAC, LAC and DC, are described in detail for the first time.

### **8.2.2.1 Descriptive Class Definitions**

Descriptive Classes can be divided into two main groups as parametrical classes; "cuticulis", "open" and "tortuous" and non-parametrical classes; crossed, "bizarre" and "bushy". The parametrical classes can be classified quantitatively. While definition of non-parametrical class crossed is purely qualitative, a classification mechanism, that is neither qualitative nor quantitative, is proposed for "bizarre" and "bushy" loops.

#### **8.2.2.1.1 Non-Parametrical Classes Definition (Crossed, Bushy, Bizarre)**

Non-parametric classes do not require any pre-set critical values to control whether the capillary loop is within the class or not. Qualitative classification criteria of crossed capillary loops is as follows; if a capillary loop does not display any form of

branchings of the limbs, and if the limbs are crossing over each other at least once, the loop is "crossed" type. 100% of the crossed capillaries in the test images are successfully identified by TANCCAS.

Generally, a capillary loop is finger like shaped. if a loop's limbs form budding of the branches or fully grown branches, it is accepted as atypical loop. "Bizarre" and "bushy" loops display atypical formations. Atypical loops can be identified by checking the number of lines that form the medial axis of a loop. The medial axis of an atypical loop can be drawn at least three line segments because of its atypical limb formations.

"Bizarre" structures have got fully developed branches. "Bushy" loops, on the other hand, display buddings of the branches, in other words, the branches have not been developed yet. A semiquantitative classification mechanism has been proposed for "bushy" and "bizarre" structures. The classification mechanism is based on geometrical relations of the loop's medial axis line segment end points and loop boundaries. Since the classification is based on measurements but not numerical, the criteria is called semiquantitative. The criteria is as follows; If a loop's medial axis is drawn by at least three line segments, it is either "bizarre" or "bushy" loop. If all the end points of the medial axis lines, apart from the bottom line segment's, are connected each other with lines, and these lines lie within the boundary of loop, it is "bushy" loop. If these lines anyhow intersects with the loop boundary, it is "bizarre" type. 71% of the "bizarre" capillaries are successfully identified using the criteria by TANCCAS.

#### **8.2.2.1.2 Parametrical Classes Definition (Cuticulis, Open, Tortuous)**

"Cuticulis" type includes a range of capillary loops from tiny tip points to the loops with visible small limbs. A critical value should be defined to distinguish the "cuticulis" loops that have long enough limbs to be mistaken as "open" type. The critical ratios,  $\text{limb\_length}/\text{loop\_width}$  and  $\text{loop\_length}/\text{loop\_width}$  are calculated from "cuticulis" and "open"- "tortuous" populations of the test images for the quantitative classifications of "cuticulis" loops. A "cuticulis" loop is allowed to have limbs upto 0.73

times of its loop width or to have loop length upto 1.23 of its width. The calculations of loop width and length for computerized classifications are proved to be difficult. Therefore, a critical exclusive curvature angle ( $\theta_{\text{CUTICULIS}}=262^\circ$ ), that is the solution of  $\text{sinc}\theta=\text{projection\_distance\_between\_loop\_end\_points}/\text{loop\_perimeter}$ , is proposed for automated classifications. TANCCAS successfully identified 85% of the "cuticulis" population in the test images.

If a capillary loop does not show any form of branchings and crossings on its visible afferent, apical and efferent parts, and the loop length is longer than 1.23 times of the loop width, it can be classified as either "open" or "tortuous" type. The course of the limbs of a capillary loop, may display straight or/and "tortuous" segments. If the "tortuous" segment(s) are not dominating the overall appearance, the capillary loop is an "open" type, otherwise it is a "tortuous" one. If the depth of a segment is equal or shallower than 1/8 of the length of the segment's base line, the segment should be evaluated as an "open" segment, otherwise it is a "tortuous" one. Finally some "open" capillary loops may have smooth limb course (not showing any "tortuous" structure) and radically bent towards one side. The degree of bending may exceed the threshold value of being a "tortuous" segment. For such cases if both of the limbs segment depth are deeper than 1/4.4 times of the length of the limb segment base, the loop is no longer an "open" one, it should be classified as a "tortuous" type. 83% of the "open" loops and 63% of "tortuous" loops are identified successfully by TANCCAS.

#### **8.2.2.2 Anomaly Classes Definitions (Enlarged, Giant and Elongated)**

Width Anomaly Classes, "enlarged" and "giant" can be identified by checking the loop width and limb width of the capillary loops, respectively. Inappropriate assignments of class "enlarged" by the participating clinicians have not allowed us to set a critical loop width for quantitative classifications of "enlarged" loops. Although, it is possible to adopt one of the critical widths reported in the literature, TANCCAS mimicked the participating clinicians' classifications. They assigned the class "enlarged" to the loops that have got visible inner boundary. However, the software is developed to



enable future modifications to use a critical loop width for quantitative classifications of "enlarged" loops. 96% of the "enlarged" loops in the test images are identified successfully by TANCCAS.

A critical limb width  $38.6\mu\text{m}$  is calculated for quantitative classifications of the "giant" capillary loops. The loops whose limbs are wider than  $38.6\mu\text{m}$  can be classified as "giant". The only "giant" loop of the test images is identified successfully. Although the critical value  $38.6\mu\text{m}$  is found effective, further researches should be made to get more precise results.

Length Anomaly Class; "elongated" can be classified by checking the capillary loop's length. Although there was not any "elongated" capillary assigned by the majority of the clinicians, the presence of the elongation was obvious for some of the capillaries due to having extremely long limbs. In literature, Kabasakal et al. [96] reported the mean length of the capillaries and the critical length as  $215\mu\text{m}$  and  $300\mu\text{m}$  respectively. Rouen et al. [72], on the other hand, reported the mean capillary length as  $235\mu\text{m}$ . Our findings, however, are  $229\mu\text{m}$  for mean capillary length and  $342\mu\text{m}$  for the critical length. Therefore, if the capillary length is longer than the critical length  $342\mu\text{m}$ , length anomaly class "elongated" should be tagged to the loop's descriptive class.

### **8.3 Recommendations For Future Research**

To set more precise threshold values for the classifications of nailfold capillaries, the capillary loop population size of each type should be increased. Therefore some new capillary images that contain sufficient amount of each capillary type, should be analysed by the clinicians. The critical values  $\text{LoopLength}_{\text{ELONGATED}}$  and  $\text{LimbWidth}_{\text{GIANT}}$  are selected hypothetically from the capillary loops of the test images. Since these loops are rare in the nailfold area, the new test loops can be either produced synthetically or collected from several images. For the classification of hook shaped "tortuous" capillary loops, the critical bending angle  $\beta_{\text{TORTUOUS}}$  should be calculated from their actual population. Although the enlargement of the loops are detected by

checking the presence of the loop's inner boundary, a threshold width value  $\text{LoopWidth}_{\text{ENLARGED}}$  can be set, if a healthy "enlarged" population is obtained from future test images. For future classifications, the clinicians should be advised to use the proposed class system, in order to obtain as much information as possible about a loop. Such classifications may result to find some other classification parameters. A critical tortuosity value  $\beta_{\text{ENLARGED\_ELONGATED\_OPEN}}$ , for example, may result in more accurate classifications than using the global  $\beta_{\text{OPEN}}$  tortuosity value for any "open" or "tortuous" loop.

A future analysis should be performed on further capillary loops that analysed by both TANCCAS and by the clinicians who have been fully informed of the proposed classification system, for fututre validation of the automated system.

The atypical structures that have not got the basic features of "bizarre" and "bushy" loops should be classified into a new class(es) classes rather than "bushy". Classification of such structures as "bushy", contrasts to the clarity of the "bushy" class, and creates confusion. Therefore further classes should be created for atypical structures, and their automation should be integrated to TANCCAS.

The image quality should be increased by using better light source and by capturing the images directly from the camera that is connected to the microscope. The quality of the video tape and the video player play important role for the quality of images. Therefore, elimination of these two factors will substantially increase the image quality. By developing a new Segmentation Module (SM), the capillary loop boundaries can be extracted from the original pictures. The development of SM opens a door to further investigations for future researchers. Since this study outlines the important features of the loops for the classifications and analysis, it will be a guide to the preservation of the important data in the images.

# REFERENCES

## REFERENCES

- [Andrade et al. 90] Andrade, L.E.C., Gabriel, A., Assad, Jr.RL., Ferrari, AJL., Atra, E. "Panoramic nailfold capillaroscopy: A new reading method and normal range" *Seminars in Arthritis and Rheumatism, Vol. 20, No:1 , pp 21-31, August (1990)*
- [Angela et al. 82] Angela, YW., Hong, TH., Rosenfeld, A. "Threshold selection using quadrees" *IEEE PAMI, Vol.4, No.1, January, (1982)*
- [Arvesen et al. 94] Arvesen, A., Rosen, L., Eltvik, LP., Kroese, A., Strandén, E. " Skin microcirculation in patients with sequelae from local cold injuries", *International Journal of Microcirculation-Clinical and Experimental, Vol.14, No.6, pp.335-34, (1994)*
- [Arman and Pearce 90] Arman, F. and Pearce, J.A. "Unsupervised classification of cell images using pyramid node linking" *IEEE Trans. On Biomedical Engineering Vol. 37, No:6, June (1990)*
- [Babaguchi et al. 90] Babaguchi, N. et al. "Connectionist model binarization", *Proceedings 10th ICPR, pp:51-56, (1990)*
- [Baer-Suryadinata and Bollinger 85] Baer-Suryadinata, Ch., Bollinger, A., "Transcapillary diffusion of Na-fluorescein measured by a 'large window technique' in skin areas of the forefoot." *Int. J. Microcirc.: Clin. Exp. 4, 217-228, (1985)*
- [Ballard and Brown 82] Ballard, DH. and Brown, CM. *Computer Vision, Prentice Hall, (1982)*
- [Basler 19] Basler A. "Über die Bestimmung der Stromungsgeschwindigkeit in den BlutKapillalen der menschlichen Haut." *Muench Med Wochenschr 13:347-348, (1919)*
- [Bleau et al. 92a] Bleau, A., Guise, J., LeBlanc, R. "A new set of fast algorithms for mathematical morphology: I Idempotent geodesic transforms" *CVGIP: Image Understanding, Vol.56, No.2, pp:178-209, September, (1992)*

- [Bleau et al. 92b]** Bleau, A., Guise, J., LeBlanc, R. "A new set of fast algorithms for mathematical morphology: II Identification of Topographic features on grayscale images" *CVGIP: Image Understanding, Vol.56, No.2, pp:210-229, September, (1992)*
- [Blum 67]** Blum, H. "A transformation for extracting new descriptors of the shape" in *Models for the Perception of Speech and Visual Form, Wathen-Dunn, W., ed., MIT Press, Cambridge, Mass. (1967)*
- [Bollinger et al. 74]** Bollinger, A., Butti, P., Barras, JP., Trachsler, H., Siegenthaler, W. "Red blood cell velocity in nailfold capillaries of man measured by a television microscopy technique. *Microvasc. Res. 7,61-72,(1974)*
- [Bollinger et al. 79]** Bollinger A., Jáger, K., Roten, A., Timeus, Ch., Mahler, F. "Diffusion, pericapillary distribution and clearance of Na- fluorescein in the human nailfold." *Pflugers Arch. 382,137-143,(1979)*
- [Bollinger 82]** Bollinger, A. "Transcapillary and interstitial diffusion of Na-fluorescein in chronic venous insufficiency with white atrophy." *Int. J. Microcirc. Clin. Exp. Vol.11:pp.5-17, (1982)*
- [Bollinger et al. 82]** Bollinger, A., Frey, J., Jáger, K., Furrer, J., Siegenthaler, W. "Patterns of diffusion through skin capillaries in patients with long term diabetes." *New Engl. J. Med.307, 1305-1310, (1982).*
- [Bollinger et al. 86]** Bollinger, A., Frey, J., Jáger, K. "Fluorescence Video Microscopy techniques for the evaluation of human skin microcirculation." *Prog. Appl. Microcirc. 11, 77-97, (1986)*
- [Bollinger and Fagrell 90]** Bollinger, A., Fagrell, B. "Clinical Capillaroscopy -a guide to its use in clinical research and practice." *Stuttgart. Hogrefe and Huber, (1990).*
- [Bonacci et al. 96]** Bonacci, E., Santacroce, N., Damico, N., Mattace, R. "Nailfold capillaroscopy in the study of microcirculation in elderly hypertensive patients." *Archives of Gerontology and Geriatrics, No.s5, pp:79-83, (1996)*

- [Brandt and Algazi 92]** Brandt, JW. and Algazi, VR. "Continuous skeleton computation by Voronoi diagram" *CVGIP: Image Understanding, Vol.55, No.3, pp:329-338, May, (1992)*
- [Brånemark and Jonsson 63]** Brånemark, PI., Jonsson, I. "Determination of the velocity of corpuscles in blood capillaries." *Biorheology 1,143-146, (1963).*
- [Brånemark 64]** Brånemark, PI. "The contribution of microscopes to the study of living circulation: Contributions and limitations of refined classical methods." *J. Royal Microscopic. Soc. 83,29-35,(1964)*
- [Bruckstein et al. 93]** Bruckstein, AM., Holt, RJ., Netravali, AN., Richardson, TJ. "Invariant signatures for planar shape recognition under partial occlusion" *CVGIP: Image Understanding, Vol.58, No.1, pp:49-65, (1993)*
- [Carpentier and Maricq 90]** Carpentier, PH., Maricq, HR., "Microvasculature in Systemic Sclerosis", *Rheu. Dis. Clin. of North America, Vol.16, No.1, pp.75-91, (1990)*
- [Carski et al. 78]** Carski, TR., Staller, BJ., Hepner, G., Banka, VS., Finney, RA. "Adverse reactions after administration of indocyanine green." *J.Am. Med. Ass. 240, 635, (1978)*
- [Cash and Hatamian 87]** Cash, GL. and Hatamian, M. "Optical character recognition by the method of moments" *CVGIP, Vol.39, pp:291-310, (1987)*
- [Chang et al. 97]** Chang, CH., Tsai, RK., Wu, WC., Kuo, SL., Yu, HS. "Use of dynamic capillaroscopy for studying cutaneous microcirculation in patients with diabetes mellitus." *Microvascular Research, Vol.53, No.2, pp.121-127, (1997)*
- [Cromwell and Kak ]** Cromwell, RL. and Kak, AC. "Automatic generation of object class descriptions using symbolic learning techniques" *Vision and Sensor Interpretation*
- [Dayhoff and Dayhoff 88]** Dayhoff, RE. and Dayhoff, JE. "Neural networks for medical image processing: a study of feature identification" *12<sup>th</sup> Annual Symp. on Computer Appl. in Medical Care, pp:271-75, (1988)*

- [Dori 95] Dori, D. "Vector based arc segmentation in the machine drawing understanding system environment" *IEEE PAMI*, Vol.17, No.11, November, (1995)
- [Embrechts et al. 93] Embrechts, H., Roose, D., Wambacq, P. "Component labelling on a MIMD multiprocessor" *CVGIP, Image Understanding*, Vol.57, No.2, pp:155-165, March, (1993)
- [Enzmann and Ruprecht 82] Enzmann, V., Ruprecht, KW. "Zwischenfalle beider Fluoreszenzangiographieder Retina. Symptomatik, Probhylaxe und Therapie." *Klin. Mbl. Augenheilk.* 181, 235-239, (1982).
- [Fagrell et al. 77a] Fagrell, B., Fronek, A., Intaglietta, M. "A microscope television system for studying flow velocity in human skin capillaries." *Am. J. Physiol.* 233, H318-H321, (1977)
- [Fagrell et al. 77b] Fagrell, B., Fronek, A., Intaglietta, M. "Capillary blood flow velocity during rest and post-occlusive reactive hyperemia in skin areas of the toes and lower." *Bibl. Anat.* 16, 159-161, (1977).
- [Fagrell et al. 77c] Fagrell, B., Fronek, A., Intaglietta, M.:Capillary flow components and reactive hyperemia studied by clinical microscopy. *Bibl. Anot.* 16, 112-115, (1977)
- [Fagrell et al. 88] Fagrell, B., Eriksson, SE., Malmstrom, S., Sjolund, A., "A Computerized Data Analysis of Capillary Blood Cell Velocity" *Int. J. Microcirc. Clin. Exp.* 7:276, (1988)
- [Fagrell 90] Fagrell, B. "Peripheral vascular diseases, in Shepherd AP. Oberg A (eds): Laser Doppler Flowmetry." *Boston Kluwer Academic*, pp 201- 214, (1990)
- [Gibson et al 56] Gibson, WC., Bosley, HJ., Griffiths, RS. "Photomicrographic studies on the nail bed capillary networks in human control subjects", *J. Nerv. Ment. Dis.*, Vol.219, pp219-231, (1956)
- [Gonzales and Woods 92] Gonzales, RC. and Woods, RE. *Digital Image Processing*, Addison-Wesley Publishing Company, Inc. (1992)

- [Guo and Hall 92]** Guo, Z. and Hall, RW. "Fast fully parallel thinning algorithms" *CVGIP: Image Understanding, Vol.55, No.3, pp:317-328, May, (1992)*
- [Gupta et al. 93]** Gupta, AK., Chauhury, S., Parthasarathy, G. "A new approach for aggregating edge points into line segments" *Pattern Recognition, Vol. 26, No.7, pp-1069-1086, (1993)*
- [Haenggi et al. 95]** Haenggi, W., Linder, HR., Birkhaeuser, MH., Schneider, H., "Microscopic findings of the nailfold capillaries - dependence on menopausal status and hormone replacement therapy", *Maturitas, Vol.22, No.1, pp37-46, (1995)*
- [Haralick et al. 87]** Haralick, RM., Sternberg, SR., Zhuang, X. "image analysis using mathematical morphology" *IEEE PAMI-9, No.4, July, pp:532-550, (1987)*
- [Hayat et al. 91]** Hayat, L., Naqvi, A., Sandler, MB. "Parallel implementation of a fast thinning algorithm using image compression" *IEE Proceedings-I, Vol.138, No.6, pp:615-620, (1991)*
- [Hertz and Schafer 88]** Hertz, L. and Schafer, W. "Multilevel thresholding using edge matching" *CVGIP, Vol.44, pp:279-295, (1988)*
- [Houtman et al. 86]** Houtman, PM., Kallenberg, CGM., Fidler, V., Wouda, AA., "Diagnostic Significance of Nailfold Capillary Patients with Raynaud's Phenomenon" *The Journal of Rheumatology, 13:3, pp:556- , (1986)*
- [Ikebe and Miyamoto 82]** Ikebe, Y. and Miyamoto, S. "Shape design, representation and restoration with splines" *Picture Engineering -Conf-. Fu, KS. and KU, NII. (eds) (1982)*
- [Jäger et al. 80]** Jäger, K., Geser, A., Bollinger, A. "Videodensitometrische Messung der transkapillaren Passage und Gewebsverteilung von Na-Fluoreszein in menschlichen Hautkapillaren." *VASA 9, 132-136, (1980)*
- [Jang and Chin 90]** Jang, BK. and Chin, RT. "Analysis of thinning algorithms using mathematical morphology" *IEEE PAMI, Vol.12, No.6, pp:541-551, June, (1990)*
- [Jorneskog and Fagrell 96]** Jorneskog, G., Fagrell, B. "Discrepancy in skin capillary circulation between fingers and toes in patients with type 1 diabetes."



*International Journal of Microcirculation-Clinical and Experimental, Vol. 16, No.6, pp.313-319, (1990)*

**[Kabasakal et al. 96]** Kabasakal, Y., Elvins DM., Ring, EFJ., McHugh, NJ., "Quantitative nailfold capillaroscopy findings in a population with connective tissue disease and in normal healthy controls." *Annals of Rheumatic diseases Vol.55, pp.507-512, (1996)*

**[Kiryati and Maydan 89]** Kiryati, N. and Maydan, D. "Calculating geometric properties from Fourier representation" *Pattern Recognition Vol.22, No.5, pp:469-475, (1989)*

**[Klyszcz et al. 96]** Klyszcz, T., Bogenschutz, O., Junger, M., Rassner, G. "Morphological and functional alterations of nailfold capillaries in a patient with dermatomyositis." *Hautarzt, Vol.47, No.4, pp:289-293, (1996)*

**[Knoll and Jain 86]** Knoll, TF. and Jain, RC. "Recognizing partially visible objects using feature indexed hypotheses" *IEEE Journal of Robotics and Automation, Vol.RA-2, No.1, March, (1986)*

**[Lam et al. 92]** Lam, L., Lee, SW, Suen, CY, "Thinning methodologies - a comprehensive survey" *IEEE PAMI, Vol.14, No.9, September, (1992)*

**[Lee and Pavlidis 88]** Lee, D. and Pavlidis, T. "One-dimensional regularization with discontinuities" *IEEE PAMI, Vol.10, No.6, pp:822-829, November (1988)*

**[Lefford and Edwards 86]** Lefford, F., Edwards, JCW., "Nailfold capillary microscopy in connective tissue disease: a quantitative morphological analysis.", *Annals of the Rheumatic Diseases, Vol.45 pp.741-749, (1986)*

**[Leteurtre et al. 94]** Leteurtre; E., Hachulla, E., Janin, A., Hatron, PY., Brouillard, M., Devulder, B. "Dermatomyositis and polymyositis are thought to have a distinct pathogenetic mechanism." *Revue De Medicine Interne, Vol.15, No.12, pp:800-807, (1994)*

**[Levine 85]** Levine, MD. *Vision in Man and Machine, McGraw-Hill, New York, (1984)*

**[Lowe 87]** Lowe, DG. "Three dimensional object recognition from single two-dimensional images", *Artif. Intell. Vol.31, pp:355-395, (1987)*

- [Maeda et al. 95]** Maeda, M., Matubara, K., Kachi, H., Mori, S., Kitajima, Y., "Histopathological and capillaroscopic features of the cuticles and bleeding clots in ring or middle fingers of systemic scleroderma patients", *J. of Dermatological Science, Vol.10, pp.35-41, (1995)*
- [Maeda et al. 97]** Maeda, M., Kachi, H., Takagi, H., Kitajima, Y., "Hemorrhagic patterns in the cuticles distal to the proximal nailfolds of the fingers of patients with systemic scleroderma", *Eur. J. Dermatol. Vol.7, pp.191-196, (1997)*
- [Maricq et al. 80]** Maricq, HR., LeRoy, EC., D'Angelo,WA., Medsger, TA., Rodnan, Jr.GP., Sharp, GC., Wolfe, JF., "Diagnostic potential of in vivo capillary microscopy in Scleroderma and related disorders.", *Arthritis Rheumatism, Vol.23, No.2, pp.183-189, (1980)*
- [Maricq 81]** MARICQ, H.R. "Widefield capillary microscopy: technique and rating scale for abnormalities seen in Sceloderma and Related Disorders." *Arthritis Rheum. 24, pp:1159-1165, (1981)*
- [Maricq and LeRoy 73]** Maricq, HR. and LeRoy, E.C. "Patterns of finger capillary abnormalities in connective tissue disease by "Wide Field" microscopy" *Arthritis and Rheumatism, Vol:16. No:5, (1973)*
- [Meyer 79]** Meyer, F. "Interactive image transformations for an automatic screening" *Journal of Histochem. Cytochem. Vol.27, pp:128-35, (1979)*
- [Michoud et al. 92]** Michoud, E., Laurent, P., Carpentier, P., Franco, A., "An image processing system for mapping microvascular networks", *14<sup>th</sup> Annual Int. Conf. of the IEEE Engineering in Medicine and Biol. Soc. pp.1954-1955, Paris, (1992)*
- [Michoud et al. 94]** Michoud, E., Poensin, D., Carpentier, PH., "Digitized nailfold capillaroscopy", *VASA, Band 23, Heft 1, pp.35-42, (1994)*
- [Milgram and Pierre 90]** Milgram, M. and Pierre, TDS. "Boundary detection and skeletonization with a massively parallel architecture" *IEEE PAMI Vol.12, No.1, January, (1990)*
- [Montgomery and Runger 94]** Montgomery, DC. and Runger, GC. *Applied Statistics and Probability for Engineers, John Wiley and Sons, Inc. (1994)*

- [Netten et al. 96] Netten, PM., Wollersheim, H., Thien, T., Lutterman, JA. "Skin microcirculation of the foot in diabetic neuropathy" *Clinical Science, Vol.91, No.5, pp.559-565, (1996)*
- [Norris and Chowning 63] Norris, AS., and Chowning JR., "Capillary morphology of the nailfold in the mentally ill", *J. of Neuropsych. Vol.5, pp.225-234, (1963)*
- [Ohtsuka et al. 95] Ohtsuka, T., Yamakage, A., Tamura, T., "Image analysis of nailfold capillaries in patients with undifferentiated connective tissue syndromes.", *The Journal of Dermatology, Vol.22, pp.921-925, (1995)*
- [Ogniewicz and Ilg 92] Ogniewicz, R. and Ilg, M. "Voronoi skeletons: Theory and applications" *Computer Vision and Pattern Recognition Conference, pp:63-69, (1992)*
- [Oral 96] Oral, M. "Classification and analysis of nailfold capillaries by using image processing and neural nets", *Computer Studies Research Report, CS-96-1, University of Glamorgan, January (1996)*
- [Pal and Bhandari 92] Pal, NR. and Bhandari, D. "On object background classification" *Int. J. Systems Sci., Vol.23, No.11, pp:1903-1920, (1992)*
- [Pavlidis 72] Pavlidis, T. "Representation of figures by labelled graphs", *Pattern Recognition, Vol.4, pp:5-17, (1972)*
- [Pitas 93] Pitas, I. *Digital Image Processing Algorithms, Prentice Hall, London, (1993)*
- [Pries 88] Pries, AR. "A versatile video image analysis system for microcirculatory research." *Int. J. Microcirc.: Clin. Exp. 7, 327-345, (1988).*
- [Prasad et al. 95] Prasad, A., Dunnill, GS., Mortimer, PS., MacGregor, GA. "Capillary rarefaction in the forearm skin in essential-hypertension." *Journal of Hypertension, Vol.2, No.2, pp:265-268, (1995)*
- [Rimmer 90] Rimmer, S. *Bit-Mapped Graphics, Windcrest Books/McGraw-Hill, (1990)*
- [Rom and Medioni 92] Rom, H. and Medioni, G. "Hierarchical decomposition and axial representation of shape" *DARPA, Image Understanding Workshop, pp:607-613, January, (1992)*

- [**Rosenfeld 86**] Rosenfeld, A. "Axial representation of shape" *CVGIP*, Vol.33, pp:156-173, (1986)
- [**Rosin and West 89**] Rosin, PL., and West, GAW. "Segmentations of edges into lines and arcs" *Image and Vision Computing*, Vol.7, (1989)
- [**Rosin and West 95**] Rosin, PL., and West, GAW. "Nonparametric segmentation of curves into various representations" *IEEE Transactions on PAMI*, Vol.17, No.12, December, (1995)
- [**Rouen et al. 72**] Rouen, LR., Terry, EN., Doft, BH., Clauss, RH., Redisch, W., "Classification and measurement of surface microvessels in man", *Microvascular Res.* Vol.4, pp:285-92, (1972)
- [**Sahoo et al. 88**] Sahoo, PK., Soltani, S., Wong, AKC. "A Survey of thresholding techniques" *CVGIP*, Vol.41, pp:233-260, (1988)
- [**Saund 93**] Saund, E. "Identifying salient circular arcs on curves" *CVGIP: Image Understanding*, Vol.58, No.3, pp:327-337, November, (1993)
- [**Savini 88**] Savini, M. "Moments in image analysis" *Alta Frequenza* Vol.57, part 2, pp:142-152, (1988)
- [**Schiff and D'Agostino 96**] Schiff, D., D'Agostino, RB., *Practical Engineering Statistics*, John Wiley and Sons, Inc. Chapter 8, (1996)
- [**Sekita et al 92**] Sekita, I., Kurita, T., Otsu, N. "Complex Autoregressive model for shape recognition" *IEEE PAMI*, Vol.14, No.4, April, (1992)
- [**Shaked and Bruckstein 96**] Shaked, D. and Bruckstein, AM. "The curve axis", *Computer Vision and Image Understanding*, Vol.63, No.2, pp:367-379, March,(1996)
- [**Shiotani et al. 94**] Shiotani, S., Fukuda, T., Arai, F., Takeuchi, N., Sasaki, K., Kinoshita, T. "Cell recognition by image processing (Recognition of dead or living plant cells by neural network)" *JSME International Journal Series C*, Vol.37, No.1, pp:202-208, (1994)

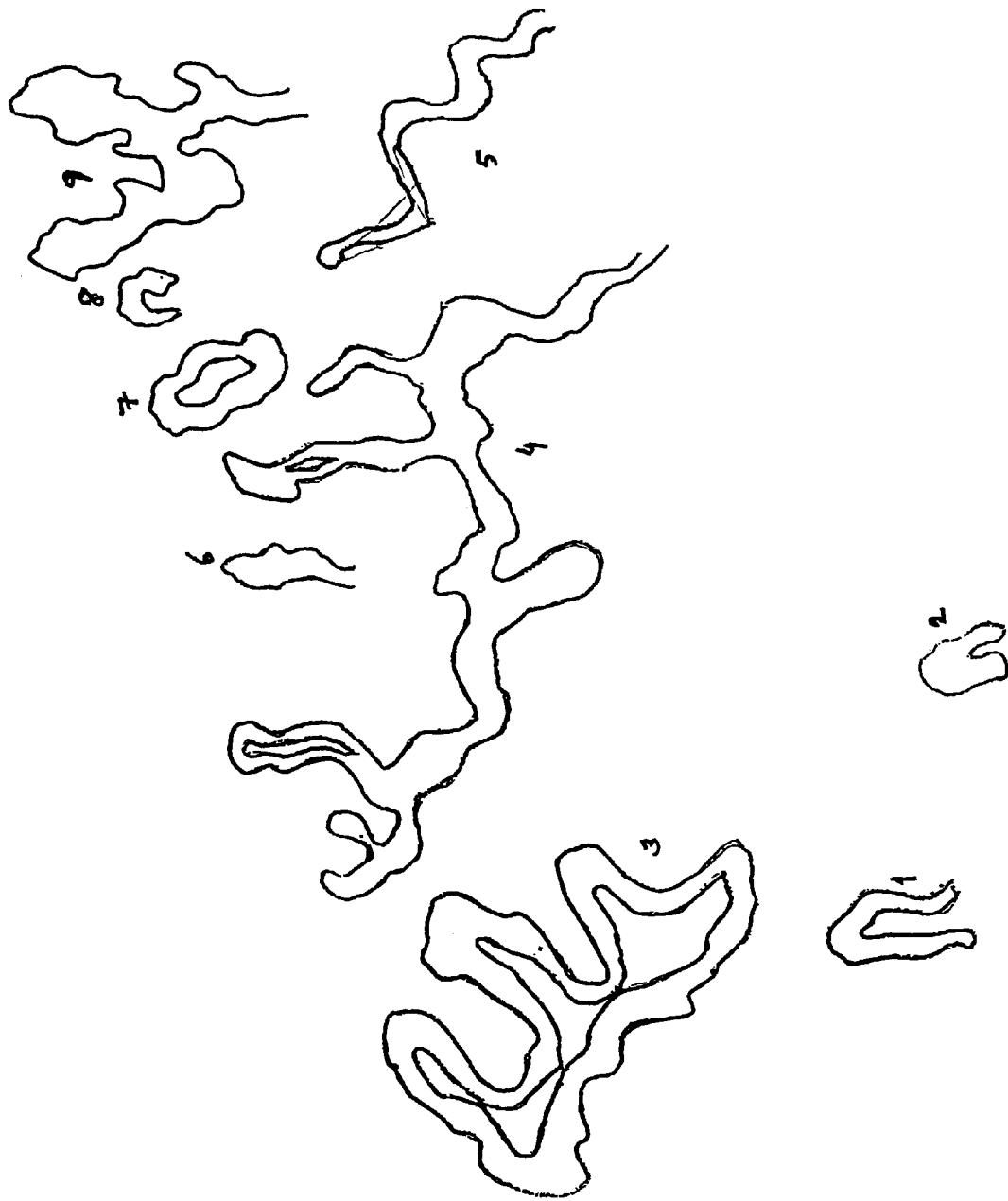
- [Simpson et al. ] Simpson, R., Culverhouse, P., Ellis, R., Williams, B. "Classification of Euceratium Gran. in neural networks",
- [Smeulders et al. 80] Smeulders, AWM., Vossepoel, AM., Vrolijk, J. "Some shape parameters for cell recognition" *Pattern Recognition in Practice E.S. Gelsema and L.N Kanal (eds.) North Holland Publishing Company, (1980)*
- [Sonka et al. 94] Sonka, M., Hlavac, V., Boyle, R. *Image Processing, Analysis and Machine Vision, Chapman and Hall Computing, London, (1994)*
- [Studer et al. 91] Studer, A., Hunziker, T., Lutolf, O., Schmidli, J., Chen, D., Mahler, F., "Quantitative nailfold capillary microscopy in cutaneous and systemic lupus erythematosus and localized and systemic scleroderma", *J. of Ame. Academy of Dermatology, Vol.24, No.6, Part.1, pp.941-945, (1991)*
- [Struijker-Boudier et al. 96] Struijker-Boudier, HAJ., Crins, FRL., Stolte, J., van Essen, H., "Assessment of the microcirculation in cardiovascular disease", *Clinical Science, Vol.91, pp.131-139, (1996)*
- [Tanaka et al. 85] Tanaka, HT., Ballard, DH., Tsuji, S., Curtiss, M. "Parallel polyhedral shape recognition" *IEEE, CH1245-1/85/0000/0491\$01.00© (1985)*
- [Thiel 94] Thiel, S. "The use of image processing techniques for the automated detection of blue-green algae" PhD Thesis, University of Glamorgan, Wales, (1995).
- [Waldhausen et al. 81] Waldhausen, E., Marquardt, E., Helms, U. "Erfahrungen aus 31 anaphylaktoiden Reaktionen." *Anesthesist 30, 47-51, (1981).*
- [Wang and Haralick 84] Wang, S. and Haralick, RM. "Automatic multithreshold selection" *CVGIP, Vol.25, pp:46-67, (1984)*
- [Wang and Pavlidis 93] Wang, L. and Pavlidis, T. "Detection of curved straight segments from gray scale topography" *CVGIP Image Understanding, Vol.58, No.3, pp:352-365, November, (1993)*

- [**Wertheimer and Wertheimer 55**] Wertheimer, N. and Wertheimer, M. "Capillary Structure: Its Relation to Psychiatric Diagnosis and Morphology" *J. Nerv. Ment. Dis., Vol.121, pp:14-27, (1955)*
- [**Wilson 92**] Wilson, SS. "Theory of matrix morphology" *IEEE PAMI, Vol.14, No.6, pp:636-652, June, (1992)*
- [**Worring and Smeulders 95**] Worring, M. and Smeulders, AW. "Digitized circular arcs: Characterization and parameter estimation" *IEEE PAMI, Vol.17, No.6, June, (1995)*
- [**Wright and Fallside 93**] Wright, W. and Fallside, F. "Skeletonisation as model-based feature detection" *IEE Proceedings-I, Vol.140, No.1, February, (1993)*
- [**Xia 89**] Xia, Y. "Skeletonisation via the realization of the fire front's propagation and extinction in digital binary shapes" *IEEE PAMI, Vol.11, No.10, October, (1989)*
- [**Young et al. 74**] Young, IT., Walker, JE., Bowie, JE. "An analysis technique for biological shape. I" *Information and Control, 25, pp:357-370, (1974)*
- [**Yu et al. 95**] Yu, HS., Chang, CH., Chen, GS., Yang, SA., "Dynamic capillaroscopy- a sensitive noninvasive method for the diagnosis of conditions with pathological microcirculation.", *Handbook of Noninvasive Methods and the Skin. Edt. Jorgen Serup GBE JEMEC, CRC Press Inc, pp.367-370, (1995)*
- [**Zauggvesti et al. 95**] Zauggvesti, BR., Franzeck, UK., Vonziegler, C., Furrer, J., Pfister, G., Yanar, A., Bollinger, A. "Skin Capillary aneurysms detected by indocyanine green in type 1 diabetes with and without retinal microaneurysms.", *Int. J. of Microcirculation-Clin. and Exp., Vol.15, No.4, pp.193-198, (1995)*
- [**Zimmer and Demis 64**] Zimmer JG, Demis DJ. "The study of the physiology and pharmacology of the human cutaneous microcirculation by capillary microscopy and television cinematography" *Angiology 15:232-235, (1964)*
- [**Zufferey et al. 92**] Zufferey, P., Depairon, M., Chamot, AM., Monti, M., "Prognostic significance of nailfold capillary microscopy in patients with Raynaud's phenomenon and Scleroderma-Pattern abnormalities A six-year follow up study" *Clinical rheumatology Vol.11, No.4, pp.536-541, (1992).*

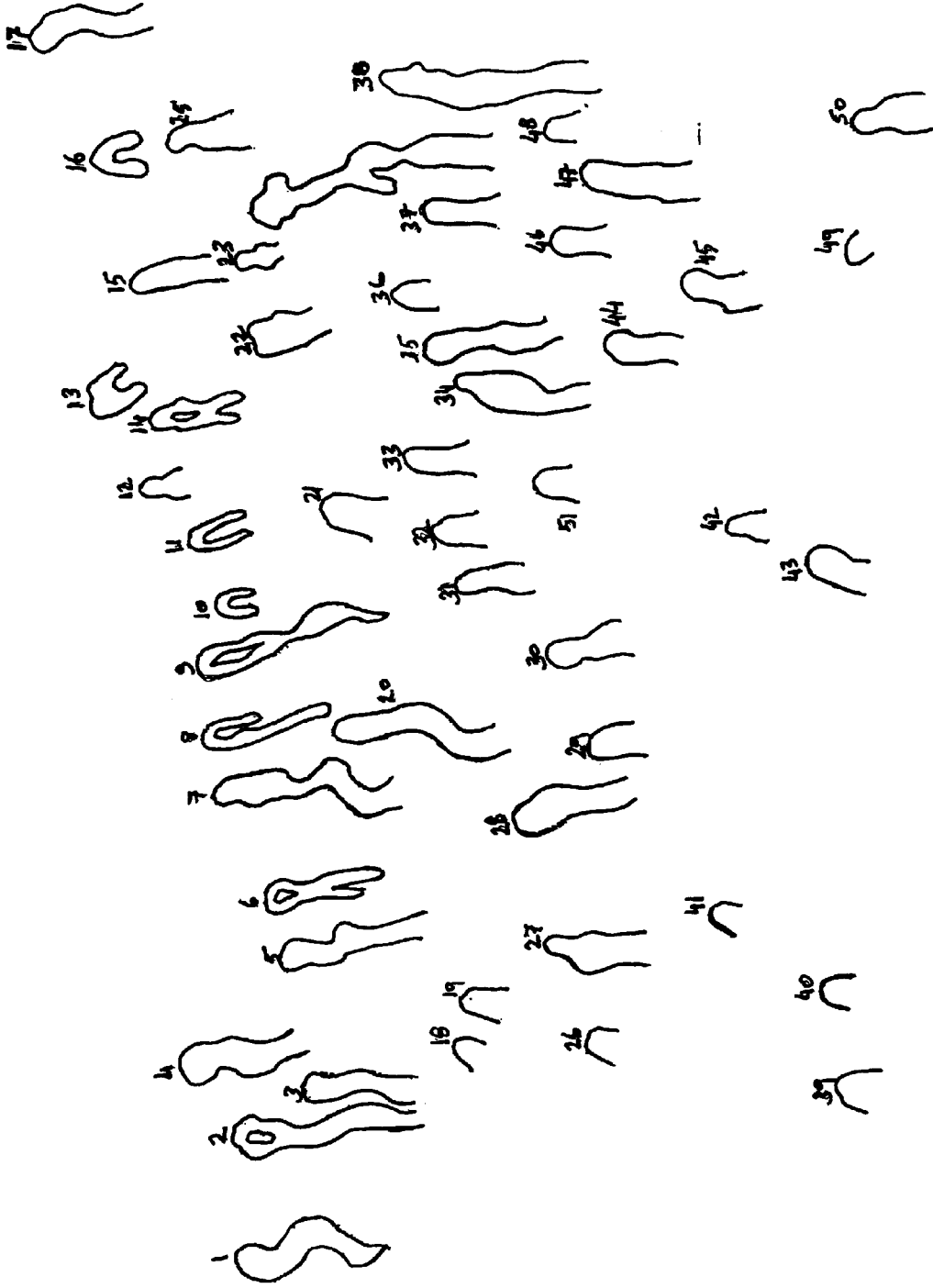
# **APPENDICES**

## **Appendix A    The Nailfold Capillary Loop Test Images**

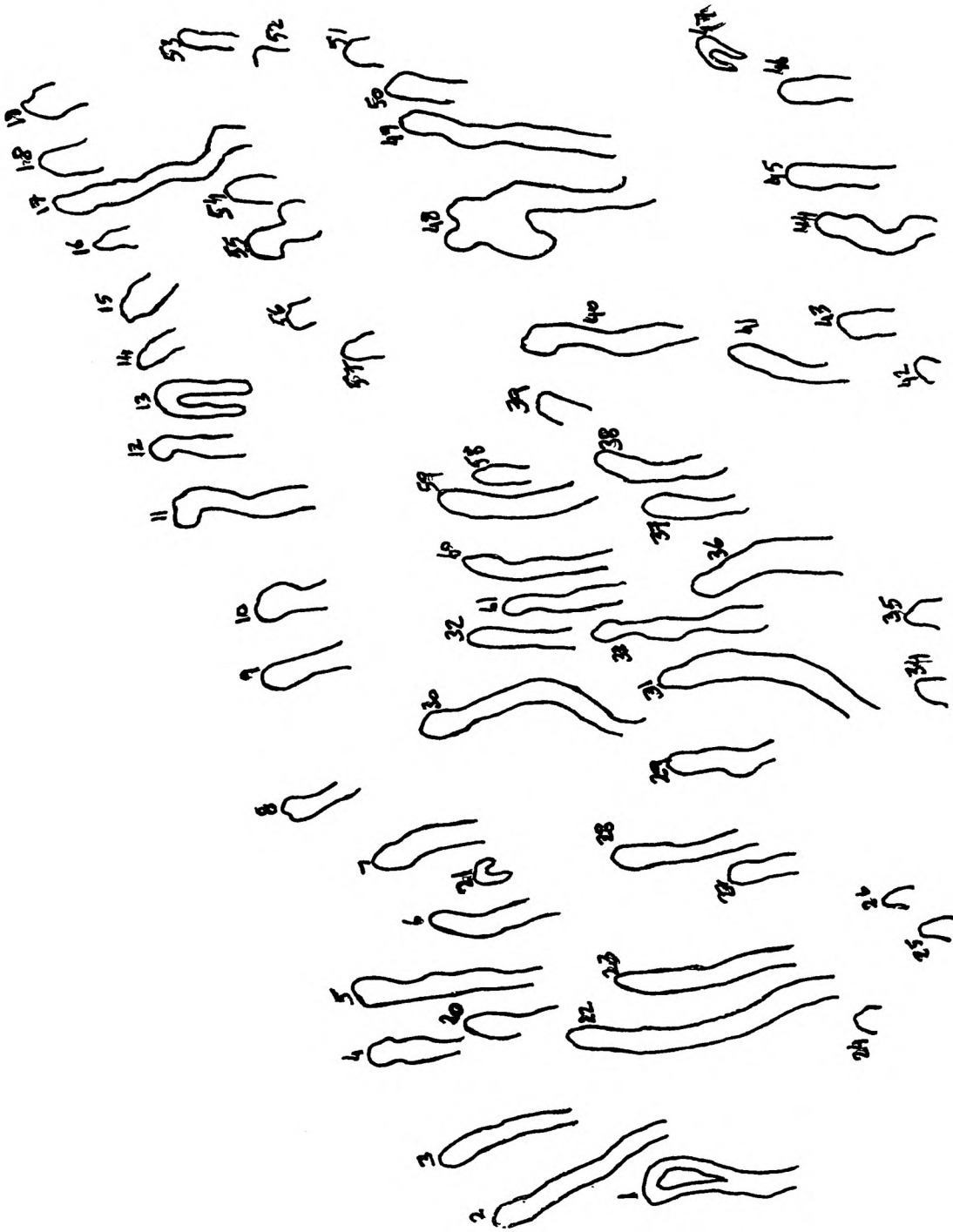




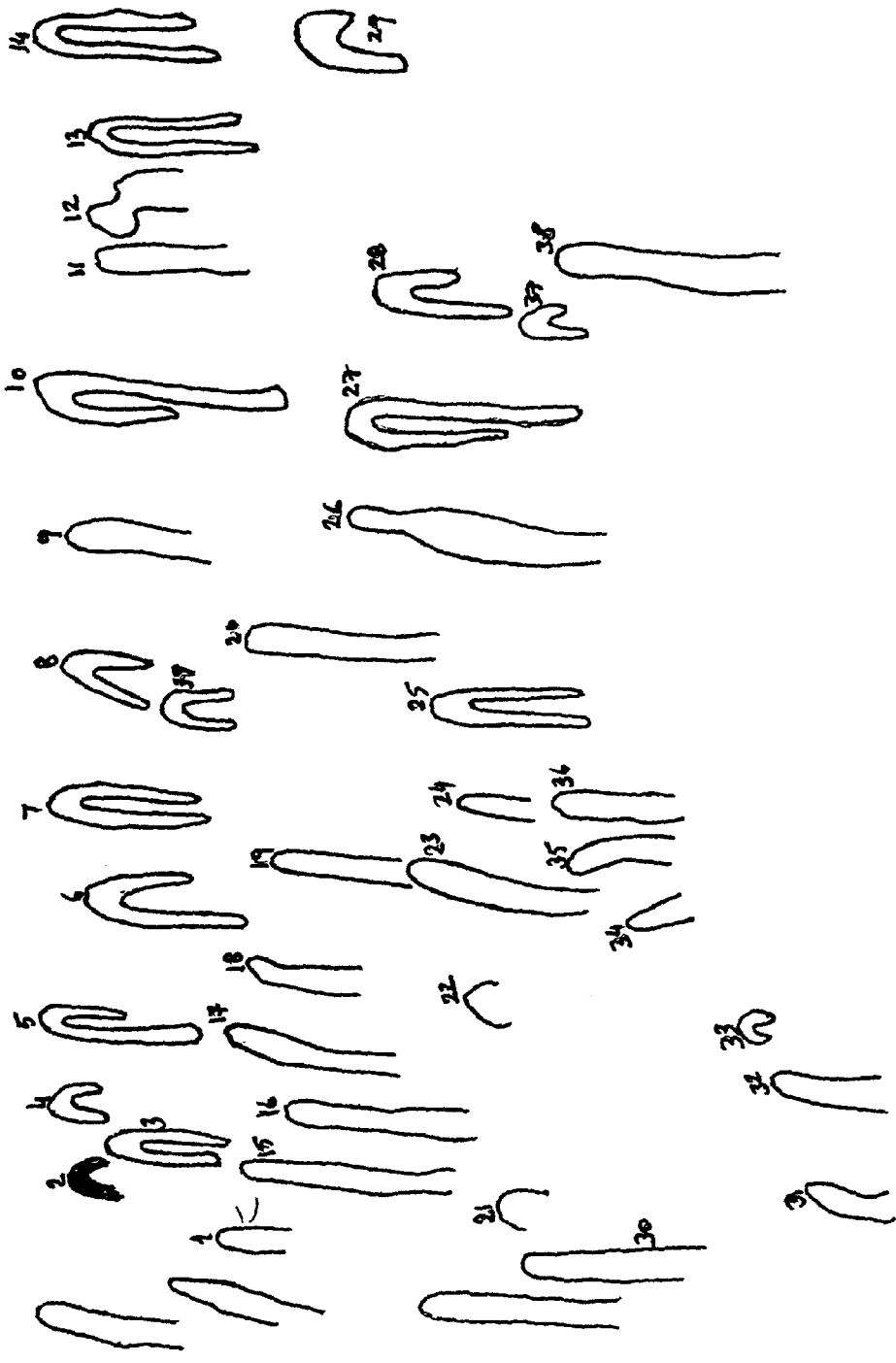
The Test Image 1



The Test Image 2



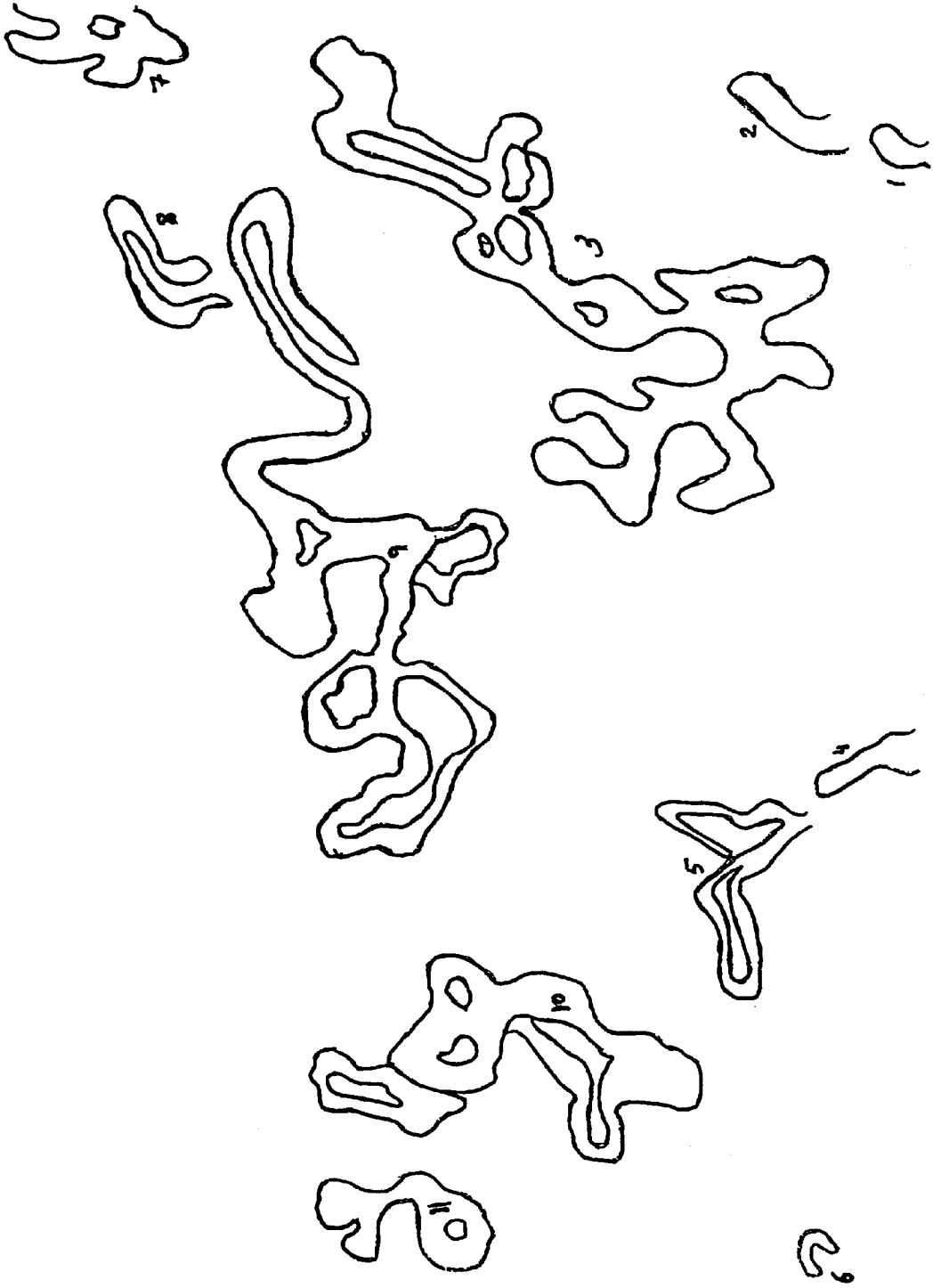
The Test Image 3



The Test Image 4

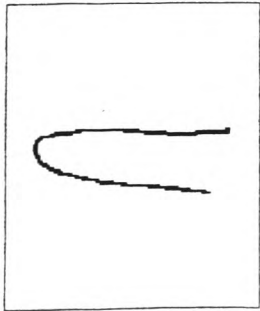


The Test Image 5

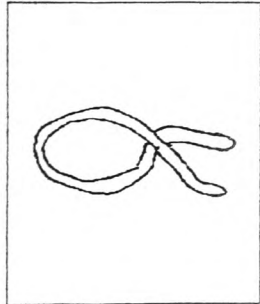


The Test Image 6

## **Appendix B    The Synthetic Capillary Loop Images**



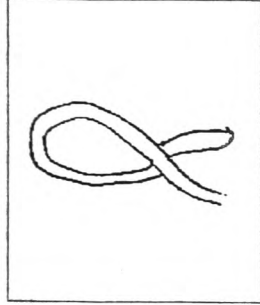
t1.tif



t10.tif



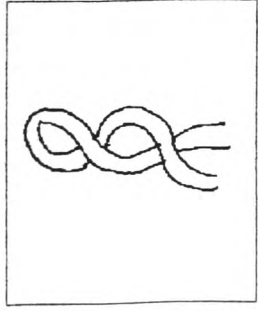
t11.tif



t12.tif



t13.tif



t14.tif



t15.tif



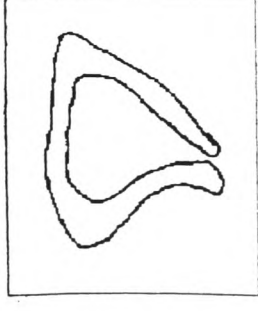
t16.tif



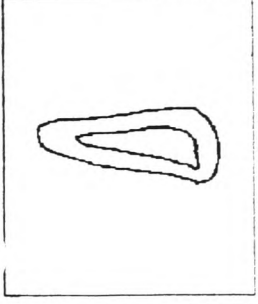
t17.tif



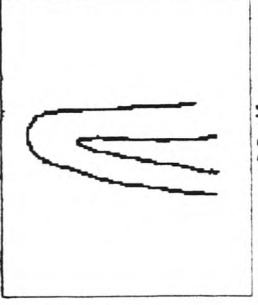
t18.tif



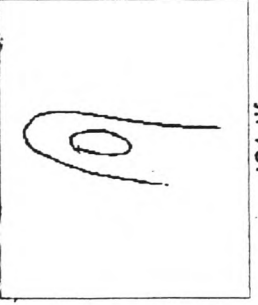
t19.tif



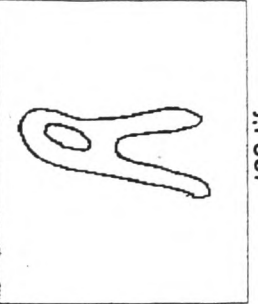
t2.tif



t20.tif

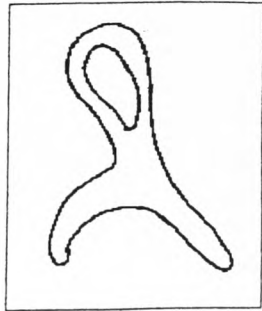


t21.tif

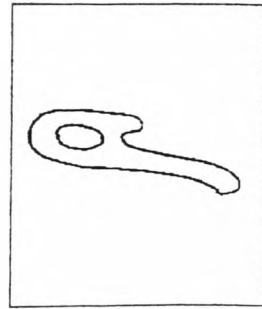


t22.tif

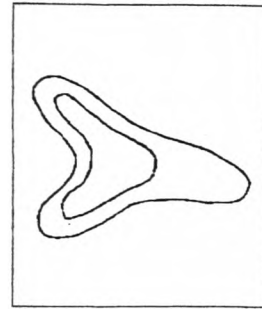




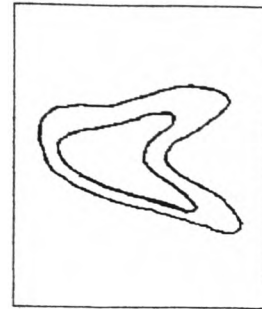
t23.tif



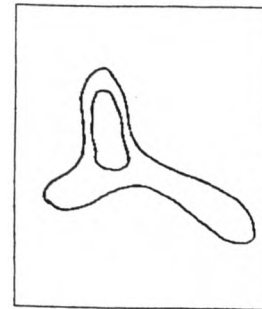
t24.tif



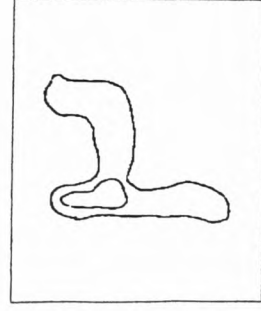
t25.tif



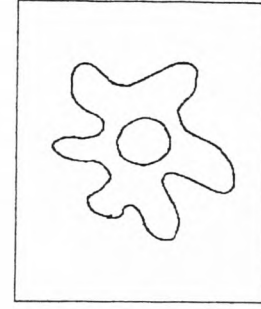
t26.tif



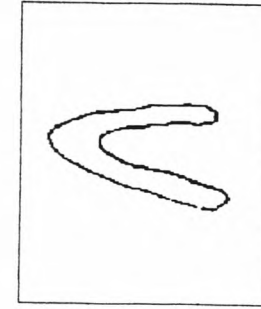
t27.tif



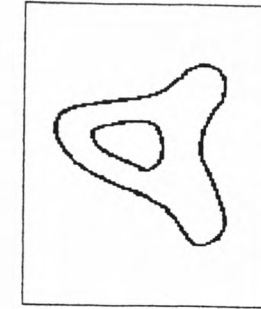
t28.tif



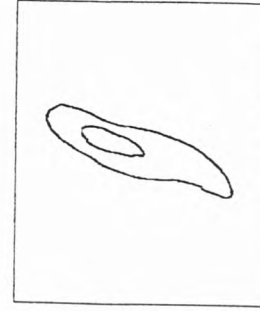
t29.tif



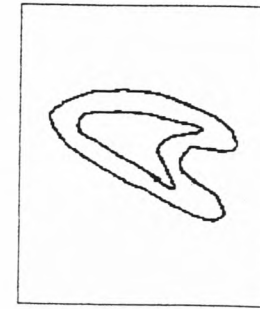
t30.tif



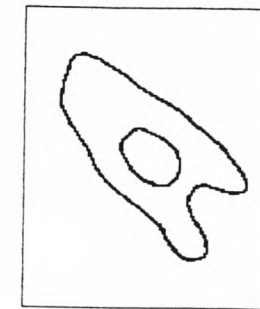
t31.tif



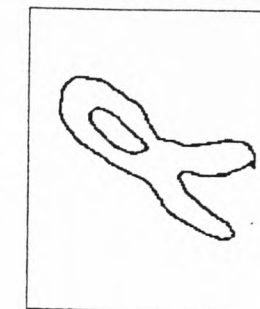
t32.tif



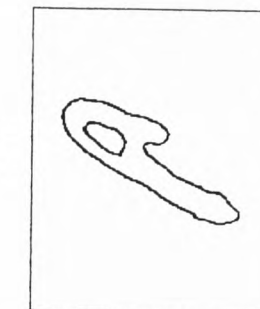
t33.tif



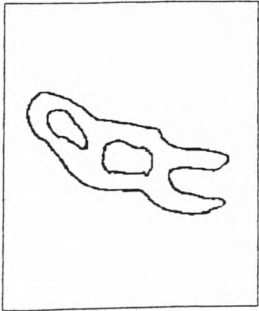
t34.tif



t35.tif



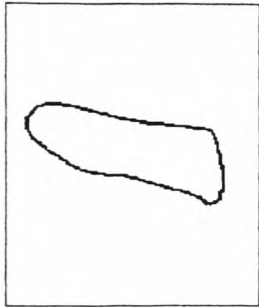
t36.tif



t37.tif



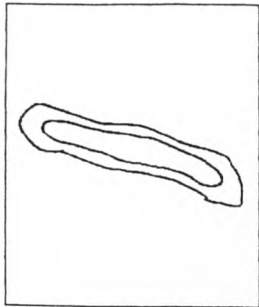
t38.tif



t39.tif



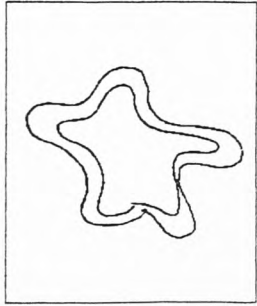
t4.tif



t40.tif



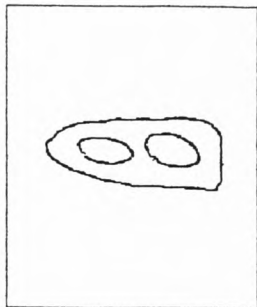
t41.tif



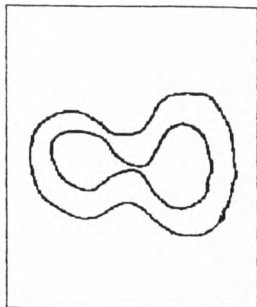
t42.tif



t5.tif



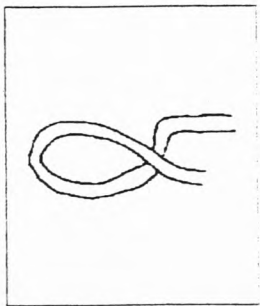
t6.tif



t7.tif



t8.tif



t9.tif

**Appendix C    The Classification Results of the Practitioners  
and TANCCAS for the Test Images**

Table AD -1 The classification results of the practitioners and TANCCAS for the test Image-1.

THE TEST IMAGE 1							
Capi. No	Pr 1	Pr 2	Pr 3	Pr 4	Pr 5	Pr 6	TANCCAS
1	Enlarged	Enlarged	Cuticulis	Enlarged	Enlarged	*	Giant Open
2	Giant	Cuticulis	Cuticulis	Enlarged	Enlarged	*	Enlarged Cuticulis
3	Bushy	Bizarre	Giant	*	Mixed	Mixed	Bizarre
4	Bizarre	Bizarre	Giant	Bizarre	Mixed	Mixed	Bizarre
5	Tortuous	Open	Tortuous	Tortuous	Tortuous	Tortuous	Elongated Tortuous
6	Open	*	*	Open	Open	Open	Open
7	Mixed	Bizarre	Open	*	Enlarged	Enlarged	Bushy
8	Enlarged	Cuticulis	Cuticulis	Enlarged	Enlarged	Enlarged	Enlarged Cuticulis
9	Bizarre	Bizarre	Enlarged	Tortuous	Bizarre	Bizarre	Bizarre

Table AD -2 The classification results of the practitioners and TANCCAS for the test Image-2.

THE TEST IMAGE 2							
Capi. No	Pr 1	Pr 2	Pr 3	Pr 4	Pr 5	Pr 6	TANCCAS
1	Tortuous	Enlarged	Tortuous	Open	*	*	Elongated Tortuous
2	*	Enlarged	Enlarged	Open	Crossed	Enlarged	Enlarged Elongated Open
3	Elongated	Normal	Open	Open	*	*	Open
4	Elongated	*	Tortuous	Open	Tortuous	Tortuous	Open
5	Elongated	*	Open	Open	*	*	Elongated Open
6	*	Crossed	Enlarged	Open	Crossed	Crossed	Crossed
7	Tortuous	*	Tortuous	Tortuous	Tortuous	Tortuous	Elongated Tortuous
8	Tortuous	Open	Enlarged	Enlarged	*	*	Crossed
9	Bizarre	Enlarged	Enlarged	Enlarged	Crossed	Crossed	Enlarged Open
10	Enlarged	Cuticulis	Cuticulis	Enlarged	*	*	Enlarged Cuticulis
11	Enlarged	Cuticulis	Cuticulis	Enlarged	*	Enlarged	Enlarged Open
12	Open	Cuticulis	Open	Open	*	*	Open
13	Enlarged	Cuticulis	Cuticulis	Open	*	Enlarged	Enlarged Cuticulis
14	Bizarre	Crossed	Cuticulis	Enlarged	Crossed	Crossed	Crossed
15	Elongated	Normal	Open	Open	*	Open	Open
16	Enlarged	Cuticulis	Cuticulis	Enlarged	*	Enlarged	Enlarged Cuticulis
17	Tortuous	Normal	Open	Open	*	*	Open
18	Open	Cuticulis	Open	Open	*	*	Cuticulis
19	Open	Cuticulis	Open	Open	Open	Open	Cuticulis
20	Tortuous	*	Tortuous	Open	*	Tortuous	Elongated Open
21	Open	Cuticulis	Open	Open	Open	Open	Cuticulis
22	Elongated	*	Open	Open	*	Open	Open
23	Open	*	Open	Open	*	*	Open
24	Bizarre	*	Tortuous	Tortuous	Bizarre	Bizarre	Bizarre
25	Open	*	Open	Open	*	*	Open
26	Open	Cuticulis	Open	Open	*	Open	Cuticulis
27	Elongated	Normal	Open	Open	Tortuous	Tortuous	Open
28	Elongated	Normal	Open	Open	*	Open	Open
29	Open	Cuticulis	Open	Open	*	Open	Open
30	Open	Normal	Open	Open	*	Open	Open
31	Open	Cuticulis	Open	Open	*	Open	Open
32	Open	Cuticulis	Open	Open	Open	Open	Cuticulis
33	Open	Cuticulis	Open	Open	Open	Open	Open
34	*	Normal	Open	Open	Enlarged	Enlarged	Open
35	Elongated	Normal	Open	Open	Enlarged	Enlarged	Open
36	Open	Cuticulis	Open	Open	*	Open	Open
37	Open	Normal	Open	Open	*	*	Open
38	Tortuous	Normal	Open	Tortuous	Enlarged	Enlarged	Elongated Open
39	Cuticulis	Cuticulis	Open	Open	*	Open	Cuticulis
40	Cuticulis	Cuticulis	Open	Open	*	Open	Cuticulis
41	Cuticulis	Cuticulis	Open	Open	*	*	Cuticulis
42	Open	Cuticulis	Open	Open	*	*	Cuticulis
43	Open	Cuticulis	Open	Open	*	Open	Open
44	Open	Cuticulis	Open	Open	*	Open	Open
45	Open	Cuticulis	Open	Open	*	Open	Open
46	Open	Cuticulis	Open	Open	*	Open	Open

47	Elongated	Normal	Open	Open	*	Open	Open
48	Cuticulis	Cuticulis	Open	Open	*	*	Cuticulis
49	Cuticulis	Cuticulis	Open	Open	*	*	Cuticulis
50	Open	Cuticulis	Open	Open	*	Open	Open
51	Open	Cuticulis	Open	Open	*	*	Cuticulis

Table AD -3 The classification results of the practitioners and TANCCAS for the test Image-3.

Capi. No	Pr 1	Pr 2	Pr 3	Pr 4	Pr 5	Pr 6	TANCCAS
1	Bizarre	Enlarged	Enlarged	Enlarged	Crossed	*	Enlarged Elongated Open
2	Elongated	Normal	Open	Open	Enlarged	Enlarged	Elongated Open
3	Elongated	Normal	Open	Open	*	Enlarged	Elongated Open
4	Open	Normal	Open	Open	*	Enlarged	Open
5	Elongated	Normal	Open	Open	Enlarged	Enlarged	Elongated Open
6	Open	Normal	Open	Open	*	Enlarged	Open
7	Open	Normal	Open	Open	*	Enlarged	Open
8	Open	Normal	Open	Open	Open	Open	Open
9	Open	Normal	Open	Open	*	Open	Open
10	Open	Normal	Open	Open	Open	*	Open
11	Tortuous	Normal	Open	Open	Enlarged	Enlarged	Elongated Tortuous
12	Tortuous	Normal	Open	Open	*	Enlarged	Open
13	Enlarged	Enlarged	Enlarged	Enlarged	*	Enlarged	Enlarged Open
14	Open	Normal	Open	Open	*	*	Open
15	Open	Normal	Open	Open	*	Open	Open
16	Open	Normal	Open	Open	*	*	Open
17	Tortuous	Normal	Tortuous	Tortuous	Enlarged	*	Elongated Open
18	Open	Normal	Open	Open	*	*	Open
19	Open	Normal	*	Open	*	*	Cuticulis
20	Open	Normal	Open	Open	*	*	Open
21	Cuticulis	Cuticulis	Cuticulis	Cuticulis	*	*	Open
22	Elongated	Normal	Open	Open	Enlarged	Open	Elongated Open
23	Elongated	Normal	Open	Open	Enlarged	Open	Elongated Open
24	Cuticulis	Cuticulis	Open	Open	*	Cuticulis	Cuticulis
25	Cuticulis	Cuticulis	Open	Open	*	Cuticulis	Cuticulis
26	Cuticulis	Cuticulis	Open	Open	*	Cuticulis	Cuticulis
27	Open	Normal	Open	Open	*	*	Open
28	Elongated	Normal	Open	Open	Enlarged	Open	Elongated Open
29	Elongated	Normal	Tortuous	Open	*	*	Open
30	Tortuous	Normal	Tortuous	Open	Enlarged	Enlarged	Elongated Tortuous
31	*	Normal	Open	Open	Enlarged	Enlarged	Elongated Open
32	Elongated	Normal	Open	Open	*	Open	Open
33	Tortuous	Normal	Open	Open	*	Enlarged	Elongated Open
34	Cuticulis	Cuticulis	Open	Open	*	Cuticulis	Cuticulis
35	Cuticulis	Cuticulis	Open	Open	*	Cuticulis	Cuticulis
36	Elongated	Normal	Open	Open	Enlarged	Open	Elongated Open
37	Elongated	Normal	Open	Open	*	Open	Open
38	Elongated	Normal	Open	Open	*	Open	Open
39	Open	Normal	Open	Open	*	*	Open
40	Elongated	Normal	Open	Open	Enlarged	Enlarged	Elongated Open
41	Elongated	Normal	Open	Open	*	*	Open
42	Cuticulis	Cuticulis	Open	Open	*	Cuticulis	Cuticulis
43	Open	Cuticulis	Open	Open	*	*	Open
44	Mixed	Normal	Tortuous	Open	*	Enlarged	Tortuous
45	Open	Normal	Open	Open	*	Open	Open
46	Open	Normal	Open	Open	*	*	Open
47	Enlarged	Cuticulis	Cuticulis	Cuticulis	*	*	Enlarged Cuticulis
48	Bizarre	Bushy	Tortuous	Tortuous	Bizarre	Bizarre	Bushy
49	Elongated	Normal	Open	Open	Enlarged	Enlarged	Elongated Open
50	Open	Normal	Open	Open	*	*	Open
51	Cuticulis	Cuticulis	Open	Open	*	Open	Cuticulis
52	Cuticulis	*	Open	Open	*	*	Cuticulis
53	Open	Normal	Open	Open	*	*	Open
54	Open	*	Open	Open	*	Open	Open

55	*	*	Tortuous	Open	Bizarre	*	Open
56	Cuticulis	Cuticulis	Open	Open	*	*	Cuticulis
57	Open	Cuticulis	Open	Open	*	*	Cuticulis
58	Open	Normal	Open	Open	*	*	Open
59	Elongated	Normal	Open	Open	*	Open	Elongated Open
60	Elongated	Normal	Open	Open	*	Open	Elongated Open
61	Elongated	Normal	Open	Open	*	Open	Open

Table AD -4 The classification results of the practitioners and TANCCAS for the test Image-4.

Capi. No	Pr 1	Pr 2	Pr 3	Pr 4	Pr 5	Pr 6	TANCCAS
1	Open	Normal	Open	Open	*	*	Open
2	*	*	*	Open	Open	Enlarged	Cuticulis
3	Enlarged	Enlarged	Enlarged	Enlarged	*	*	Enlarged Open
4	Enlarged	*	*	Enlarged	Open	Enlarged	Enlarged Cuticulis
5	Enlarged	*	Enlarged	Enlarged	Open	Enlarged	Enlarged Open
6	Enlarged	*	Enlarged	Enlarged	Open	Enlarged	Enlarged Open
7	Enlarged	Enlarged	Enlarged	Enlarged	Open	Enlarged	Enlarged Open
8	Enlarged	Enlarged	Enlarged	Enlarged	*	Enlarged	Enlarged Cuticulis
9	Elongated	Normal	Open	Open	*	Open	Open
10	Mixed	*	Enlarged	*	Open	Enlarged	Enlarged Elongated Open
11	Elongated	Normal	Open	Open	*	Open	Open
12	Mixed	Normal	Tortuous	Tortuous	Bizarre	Tortuous	Tortuous
13	Enlarged	Enlarged	Enlarged	Enlarged	Open	Enlarged	Enlarged Open
14	Enlarged	Enlarged	Enlarged	Enlarged	Open	Enlarged	Enlarged Elongated Open
15	Elongated	Normal	Open	Open	Enlarged	Open	Elongated Open
16	Elongated	Normal	Open	Open	Enlarged	Open	Elongated Open
17	Elongated	Normal	Open	Open	Enlarged	Open	Elongated Open
18	Elongated	Normal	Open	Open	*	Open	Open
19	Elongated	Normal	Open	Open	*	Open	Open
20	Elongated	Normal	Open	Open	Enlarged	Open	Elongated Open
21	Cuticulis	*	Open	Open	*	*	Cuticulis
22	Cuticulis	*	Open	Open	*	*	Cuticulis
23	Elongated	Normal	Open	Open	Enlarged	Open	Elongated Open
24	Open	Normal	Open	Open	*	Open	Open
25	Enlarged	Enlarged	Enlarged	Enlarged	*	Enlarged	Enlarged Open
26	Mixed	Normal	Open	Open	Enlarged	Enlarged	Elongated Open
27	Enlarged	*	Enlarged	Enlarged	Open	Enlarged	Enlarged Elongated Open
28	Enlarged	Open	Enlarged	Enlarged	Open	Enlarged	Enlarged Open
29	Giant	Enlarged	Enlarged	Giant	Open	Enlarged	Enlarged Cuticulis
30	Elongated	*	Open	Open	Enlarged	Open	Elongated Open
31	Open	Normal	Open	Open	*	*	Open
32	Open	Normal	Open	Open	*	*	Open
33	Cuticulis	Cuticulis	Cuticulis	Cuticulis	*	*	Open
34	Open	Normal	Open	Open	*	*	Open
35	Open	Normal	Open	Open	*	Open	Open
36	Open	Normal	Open	Open	*	Open	Open
37	Enlarged	Cuticulis	*	Enlarged	Open	Enlarged	Enlarged Cuticulis
38	Elongated	Normal	Open	Open	Enlarged	Open	Elongated Open
39	Enlarged	*	Enlarged	Enlarged	*	Enlarged	Enlarged Cuticulis

Table AD -5 The classification results of the practitioners and TANCCAS for the test Image-5.

Capi. No	Pr 1	Pr 2	Pr 3	Pr 4	Pr 5	Pr 6	TANCCAS
1	Bizarre	*	*	Cuticulis	*	*	Enlarged Cuticulis
2	Bizarre	*	*	Cuticulis	*	*	Cuticulis
3	Cuticulis	Cuticulis	Cuticulis	Cuticulis	*	*	Enlarged Cuticulis
4	Open	Normal	Open	Enlarged	*	Open	Open
5	Enlarged	Enlarged	Enlarged	Enlarged	Open	Enlarged	Enlarged Elongated Open
6	Enlarged	Enlarged	Enlarged	Enlarged	Open	Enlarged	Enlarged Elongated Open
7	Enlarged	Enlarged	Enlarged	Enlarged	Open	Enlarged	Enlarged Open
8	Enlarged	Enlarged	Enlarged	Enlarged	Open	Enlarged	Enlarged Elongated Open

9	Enlarged	Enlarged	Cuticulis	Enlarged	Open	Enlarged	Enlarged Open
10	Enlarged	Enlarged	Enlarged	Enlarged	Open	Enlarged	Enlarged Open
11	Giant	Enlarged	Enlarged	Enlarged	Open	*	Giant Elongated Open
12	Tortuous	Normal	Open	Tortuous	Enlarged	Enlarged	Open
13	Tortuous	Normal	Open	Open	*	Enlarged	Open
14	Tortuous	Normal	Open	Tortuous	*	Enlarged	Open
15	Elongated	Normal	Open	Open	Enlarged	Enlarged	Elongated Open
16	Bizarre	Enlarged	Enlarged	Enlarged	Mixed	Mixed	Bizarre
17	Elongated	Normal	Open	Open	Enlarged	Enlarged	Elongated Open
18	Enlarged	Enlarged	Enlarged	Enlarged	Open	*	Enlarged Open
19	Open	Normal	Open	Open	*	*	Open
20	Elongated	Normal	Open	Open	Enlarged	Elongated	Elongated Open
21	Cuticulis	Cuticulis	*	Enlarged	*	*	Enlarged Cuticulis
22	Elongated	Normal	Open	Open	Enlarged	Enlarged	Elongated Open
23	Enlarged	*	Cuticulis	Enlarged	Open	*	Enlarged Open
24	Bizarre	Enlarged	Enlarged	Enlarged	Crossed	Crossed	Crossed
25	*	*	Cuticulis	Enlarged	*	*	Enlarged Open
26	Bizarre	Enlarged	Enlarged	Enlarged	Crossed	Crossed	Enlarged Elongated Tortuous
27	Giant	Giant	Enlarged	Giant	Mixed	Mixed	Giant Elongated Open
28	Bushy	Enlarged	Enlarged	Enlarged	*	Enlarged	Bushy
29	Enlarged	*	Enlarged	Enlarged	*	*	Enlarged Tortuous
30	Cuticulis	Cuticulis	Cuticulis	Cuticulis	*	*	Enlarged Cuticulis
31	Open	Enlarged	Enlarged	Enlarged	Bizarre	Enlarged	Enlarged Open
32	Open	*	Open	Open	*	*	Open
33	Elongated	Normal	Open	Open	Enlarged	Enlarged	Enlarged Open
34	Open	*	Open	Open	*	Open	Open
35	Open	*	Open	Open	*	Open	Open
36	Enlarged	Enlarged	*	Open	Open	*	Enlarged Open
37	Tortuous	*	Open	Open	Enlarged	*	Open
38	Mixed	*	Open	Open	*	Open	Enlarged Tortuous
39	Open	*	Open	Open	Open	Open	Open
40	Enlarged	Enlarged	Enlarged	Enlarged	Mixed	Enlarged	Enlarged Open
41	Open	*	Open	Open	*	*	Open
42	Mixed	*	Open	Tortuous	Enlarged	Enlarged	Elongated Open
43	Giant	Enlarged	Enlarged	Enlarged	Open	Enlarged	Giant Elongated Open
44	Open	*	Open	Open	*	Open	Open
45	Open	*	Open	Open	*	Open	Open
46	Cuticulis	*	Open	Cuticulis	*	*	Cuticulis

Table AD -6 The classification results of the practitioners and TANCCAS for the test Image-6.

THE TEST IMAGE 6							
Capi. No	Pr 1	Pr 2	Pr 3	Pr 4	Pr 5	Pr 6	TANCCAS
1	Bizarre	*	Open	Tortuous	*	Open	Open
2	Bizarre	*	Open	Tortuous	Enlarged	Enlarged	Open
3	Bizarre	Bizarre	Bizarre	Bizarre	Mixed	Mixed	Bizarre
4	Bizarre	Normal	Open	Open	Enlarged	Enlarged	Open
5	Bushy	Bizarre	Enlarged	Bizarre	Mixed	Mixed	Bushy
6	*	*	Enlarged	Cuticulis	Open	*	Open
7	Bushy	Bizarre	Bizarre	Giant	*	Mixed	*
8	Enlarged	Enlarged	Enlarged	Giant	Open	Enlarged	Enlarged Open
9	Bizarre	Bizarre	Bizarre	Bizarre	Mixed	Mixed	Bizarre
10	Bushy	Bizarre	Bizarre	*	Mixed	Mixed	Bizarre
11	Bushy	Bizarre	Bizarre	*	Mixed	Mixed	Crossed

**Appendix D    The Tables that Display TANCCAS's  
Agreements with the Practitioners**



	EN		EL		BZ		BSH		OP		TO		NO		CR		MX		GI		CU		UNC		OVER ALL			
	MATCH	TOTAL	MATCH	TOTAL	MATCH	TOTAL	MATCH	TOTAL	MATCH	TOTAL	MATCH	TOTAL	MATCH	TOTAL	MATCH	TOTAL	MATCH	TOTAL	MATCH	TOTAL	MATCH	TOTAL	MATCH	TOTAL	MATCH	TOTAL	MATCH	TOTAL
Image 1	2	2	*	*	2	2	0	1	1	2	0	1	*	*	*	*	1	1	0	1	*	*	0	7	9			
Agreement	100%				100%		0%		50%		0%		*	*	*	*	100%		0%		*	*			78%			
Image 2	4	4	1	9	1	3	*	*	16	21	0	6	*	*	*	*	*	*	*	*	*	5	5	3	27	48		
Agreement	100%		11%		33%		*	*	76%		0%		*	*	*	*	*	*	*	*	*	100%			56%			
Image 3	2	2	12	17	0	2	*	*	22	22	0	5	*	*	*	*	0	1	*	*	*	9	10	2	45	59		
Agreement	100%		71%		0%		*	*	100%		0%		*	*	*	*	0%		*	*	*	90%			76%			
Image 4	13	13	7	11	*	*	*	*	7	7	*	*	*	*	*	*	0	3	0	1	2	3	1	29	38			
Agreement	100%		64%		*		*	*	100%		*	*	*	*	*	*	0%		0%		*	67%			76%			
Image 5	11	11	4	5	1	5	1	1	10	10	0	4	*	*	*	*	0	2	3	3	4	4	1	34	45			
Agreement	100%		80%		20%		100%		100%		0%		*	*	*	*	0%		100%		*	100%			76%			
Image 6	1	1	*	*	2	5	1	4	*	*	*	*	*	*	*	*	*	*	*	*	*	*	1	4	10			
Agreement	100%		*		40%		25%		*		*	*	*	*	*	*	*	*	*	*	*	*			40%			
Over All	33	33	24	42	6	17	2	6	57	61	0	16	*	*	*	*	1	7	3	5	20	22	8	146	209			
Agreement	100%		57%		36%		33%		93%		0%		*	*	*	*	14%		80%		91%				70%			

Table AD-1 The Clinician 1's evaluations of the test images and TANCCAS's agreement with his/her assignments

	EN		EL		BZ		BSH		OP		TO		NO		GR		MX		GI		CU		UNC		OVER ALL	
	MATCH	TOTAL	MATCH	TOTAL	MATCH	TOTAL	MATCH	TOTAL	MATCH	TOTAL	MATCH	TOTAL	MATCH	TOTAL	MATCH	TOTAL	MATCH	TOTAL	MATCH	TOTAL	MATCH	TOTAL	MATCH	TOTAL	MATCH	TOTAL
Image 1	1	1	*	*	*	*	*	*	*	*	*	*	*	*	*	*	*	*	*	*	*	*	*	*	*	*
Agreement	100%								0	1												2	2	1	6	8
Image 2	2	3	*	*	*	*	*	*	0	1																
Agreement	67%								0	1												15	28	8	30	43
Image 3	2	2	*	*	*	*	*	*	*	*																
Agreement	100%																					10	12	3	56	58
Image 4	7	7	*	*	*	*	*	*	1	1																
Agreement	100%								100%													1	2	10	28	29
Image 5	16	16	*	*	*	*	*	*	*	*																
Agreement	100%																					3	3	16	29	30
Image 6	1	1	*	*	*	*	*	*	*	*																
Agreement	100%																									
Over All	29	30	*	*	*	*	*	*	1	3												31	45	41	154	176
Agreement	97%								33%													69%				88%

Table AD-2 The Clinician 2's evaluations of the test images and TANCCAS's agreement with his/her assignments

	EN		EL		BZ		BSH		OP		TO		NO		CR		MX		GI		CU		UNC		OVER ALL			
	MATCH	TOTAL	MATCH	TOTAL	MATCH	TOTAL	MATCH	TOTAL	MATCH	TOTAL	MATCH	TOTAL	MATCH	TOTAL	MATCH	TOTAL	MATCH	TOTAL	MATCH	TOTAL	MATCH	TOTAL	MATCH	TOTAL	MATCH	TOTAL	MATCH	TOTAL
Image 1	1	1	*	*	*	*	*	*	1	1	0	1	*	*	*	*	*	*	*	*	*	*	1	4	8			
Agreement	100%								100%		0%									0%					50%			
Image 2	4	4	*	*	*	*	*	*	27	37	0	5	*	*	*	*	*	*	*	*	*	3	5	0	34	51		
Agreement	100%								73%		0%														67%			
Image 3	2	2	*	*	*	*	*	*	40	50	1	6	*	*	*	*	*	*	*	*	*	1	2	1	44	60		
Agreement	100%								80%		17%															73%		
Image 4	13	13	*	*	*	*	*	*	19	21	1	1	*	*	*	*	*	*	*	*	*	0	1	3	33	36		
Agreement	100%								90%		100%															92%		
Image 5	16	16	*	*	*	*	*	*	19	21	*	*	*	*	*	*	*	*	*	*	*	2	5	4	37	42		
Agreement	100%								90%																	88%		
Image 6	2	3	*	*	3	5	*	*	3	3	*	*	*	*	*	*	*	*	*	*	*	*	*	0	8	11		
Agreement	67%					60%			100%																	73%		
Over All	38	39	*	*	3	5	*	*	109	133	2	13	*	*	*	*	*	*	*	*	*	8	16	9	160	208		
Agreement	97%			0%		60%			82%		16%															77%		

Table AD-3 The Clinician 3's evaluations of the test images and TANCCAS's agreement with his/her assignments

	EN		EL		BZ		BSH		OP		TO		NO		CR		MX		GI		CU		UNC		OVER ALL		
	MATCH	TOTAL	MATCH	TOTAL	MATCH	TOTAL	MATCH	TOTAL	MATCH	TOTAL	MATCH	TOTAL	MATCH	TOTAL	MATCH	TOTAL	MATCH	TOTAL	MATCH	TOTAL	MATCH	TOTAL	MATCH	TOTAL	MATCH	TOTAL	
Image 1 Agreement	3	3	*	*	1	1	*	*	1	2	0	2	*	*	*	*	*	*	*	*	*	*	2	6	86%	7	
Image 2 Agreement	6	6	*	*	*	100%	*	*	28	42	0	3	*	*	*	*	*	*	*	*	*	*	0	34	51	67%	
Image 3 Agreement	2	2	*	*	*	*	*	*	41	55	0	2	*	*	*	*	*	*	*	*	*	1	2	0	44	61	72%
Image 4 Agreement	13	13	*	*	*	*	*	*	19	22	1	1	*	*	*	*	*	*	0	1	1	0	1	1	33	38	87%
Image 5 Agreement	19	20	*	*	*	*	*	*	18	17	0	3	*	*	*	*	*	*	1	1	5	5	0	41	46	89%	
Image 6 Agreement	*	*	*	*	2	3	*	*	1	1	0	2	*	*	*	*	*	*	0	2	0	1	2	3	9	33%	
Over All Agreement	43	44	*	*	3	4	*	*	107	138	1	13	*	*	*	*	*	*	1	4	6	9	5	161	212	76%	
	98%		*	*	76%		*	*	78%		8%		*	*	*	*	*	*	25%		67%						

Table AD-4 The Clinician 4's evaluations of the test images and TANCCAS's agreement with his/her assignments

	EN		EL		BZ		BSH		OP		TO		NO		CR		MX		GI		CU		UNC		OVER ALL	
	MATCH	TOTAL	MATCH	TOTAL	MATCH	TOTAL	MATCH	TOTAL	MATCH	TOTAL	MATCH	TOTAL	MATCH	TOTAL	MATCH	TOTAL	MATCH	TOTAL	MATCH	TOTAL	MATCH	TOTAL	MATCH	TOTAL	MATCH	TOTAL
Image 1	4	4	*	1	*	1	*	*	1	2	0	1	*	*	*	*	2	2	*	*	*	*	0	0	9	9
Agreement	100%			100%					50%		0%						100%								100%	
Image 2	0	3	*	1	*	1	*	*	2	4	0	3	*	*	2	4	*	*	*	*	*	*	36	5	15	15
Agreement	0%			100%					50%		0%				50%										33%	
Image 3	0	12	*	2	*	2	*	*	2	2	*	*	*	*	0	1	*	*	*	*	*	*	42	2	17	17
Agreement	0%			0%					100%						0%										12%	
Image 4	*	*	*	0	*	1	*	*	8	12	*	*	*	*	*	*	*	*	*	*	*	*	18	8	21	21
Agreement	*			0%					67%																38%	
Image 5	1	8	*	0	*	1	*	*	12	12	*	*	*	*	1	2	1	3	*	*	*	*	20	15	26	26
Agreement	13%			0%					100%						50%		33%								58%	
Image 6	0	2	*	*	*	*	*	*	2	2	*	*	*	*	*	*	4	5	*	*	*	*	2	6	9	9
Agreement	0%								100%								80%								67%	
Over All	5	37	*	6	*	6	*	*	28	33	0	4	*	*	3	7	7	10	*	*	*	*	118	45	97	97
Agreement	14%			33%					86%		0%				43%		70%								46%	

Table AD-5 The Clinician 5's evaluations of the test images and TANCCAS's agreement with his/her assignments

	EN		EL		BZ		BSH		OP		TO		NO		CR		MX		GI		CU		UNC		OVER ALL	
	MATCH	TOTAL	MATCH	TOTAL	MATCH	TOTAL	MATCH	TOTAL	MATCH	TOTAL	MATCH	TOTAL	MATCH	TOTAL	MATCH	TOTAL	MATCH	TOTAL	MATCH	TOTAL	MATCH	TOTAL	MATCH	TOTAL	MATCH	TOTAL
Image 1 Agreement	2	2	*	*	1	1	*	*	1	2	0	1	*	*	*	*	2	2	*	*	*	*	2	7	100%	7
Image 2 Agreement	4	7	*	*	1	1	*	*	15	20	0	4	*	*	2	3	*	*	*	*	*	*	16	22	73%	35
Image 3 Agreement	1	15	*	*	0	1	*	*	15	16	*	*	*	*	*	*	*	*	*	*	*	*	23	22	38	58%
Image 4 Agreement	14	16	*	*	*	*	*	*	14	14	1	1	*	*	*	*	*	*	*	*	*	*	8	29	31	94%
Image 5 Agreement	11	18	1	1	*	*	*	*	6	7	*	*	*	*	1	2	1	2	*	*	*	*	16	20	30	67%
Image 6 Agreement	1	3	*	*	*	*	*	*	1	1	*	*	*	*	*	*	4	6	*	*	*	*	1	6	10	60%
Over All Agreement	33	61	1	1	2	3	*	*	53	59	1	6	*	*	3	5	7	10	*	*	*	*	66	106	151	70%
	54%		0%		67%				90%		17%				60%		70%						100%			

Table AD-6 The Clinician 6's evaluations of the test images and TANCCAS's agreement with his/her assignments

	EN		EL		BZ		BSH		OP		TO		NO		CR		MX		GI		CU		OVER ALL		
	MATCH	TOTAL	MATCH	TOTAL	MATCH	TOTAL	MATCH	TOTAL	MATCH	TOTAL	MATCH	TOTAL	MATCH	TOTAL	MATCH	TOTAL	MATCH	TOTAL	MATCH	TOTAL	MATCH	TOTAL	MATCH	TOTAL	
Clinician 1	33	33	24	42	6	17	2	8	57	61	0	18	*	*	*	*	1	7	3	5	20	22	8	146	209
	100%		57%		35%		33%		93%		0%		*	*	*	*	14%		60%		81%			70%	
Clinician 2	29	30	*	*	6	10	1	1	1	3	*	*	83	84	2	2	*	*	1	1	31	45	41	154	176
	97%		*	*	60%		100%		33%		*	*	99%		100%		*	*	100%		69%			88%	
Clinician 3	38	39	*	*	3	5	*	*	109	133	2	13	*	*	*	*	*	*	0	2	8	16	9	160	208
	97%		*	*	60%		*	*	82%		15%		*	*	*	*	*	*	0%		50%			77%	
Clinician 4	43	44	*	*	3	4	*	*	107	138	1	13	*	*	*	*	*	*	1	4	6	9	5	161	212
	98%		*	*	75%		*	*	78%		8%		*	*	*	*	*	*	25%		67%			76%	
Clinician 5	5	37	*	*	2	6	*	*	28	33	0	4	*	*	3	7	7	10	*	*	*	*	118	45	97
	14%		*	*	33%		*	*	85%		0%		*	*	43%		70%		*	*	*	*		46%	
Clinician 6	33	61	1	1	2	3	*	*	53	59	1	6	*	*	3	5	7	10	*	*	*	*	6	106	151
	54%		100%		67%		*	*	90%		17%		*	*	60%		70%		*	*	100%			70%	
Overall	181	244	25	43	22	45	3	7	355	427	4	52	83	84	8	14	15	27	5	12	71	98	247	772	1053
%	74%		58%		49%		43%		83%		8%		99%		57%		56%		42%		72%			73%	

Table AD-7 The Clinicians' overall evaluations of the test images and TANCCAS's agreement with his/her assignments